Organisation structurale et fonctionnelle du métabolisme énergétique dans les cellules musculaires striées en conditions physiologiques et physiopathologiques

Rafaela Bagur Quetglas

UNIVERSITÉ DE GRENOBLE

THÈSE

Pour obtenir le grade de

DOCTEUR DE L'UNIVERSITÉ DE GRENOBLE

Spécialité : **Sciences du Vivant - PHYSIOLOGIE PHYSIOPATHOLOGIES PHARMACOLOGIE**
Arrêté ministériel : 7 août 2006

Présentée par

Rafaela BAGUR QUETGLAS

Thèse dirigée par le **Prof. François Boucher** et co-encadrée par le **Dr. Rita Guzun**

préparée au sein du **Laboratoire Techniques de l'Ingénierie Médicale et de la Complexité** et du **Laboratoire de bioénergétique fondamentale et appliquée**
dans **l'École Doctorale Chimie et Science du Vivant**

Organisation structurale et fonctionnelle du métabolisme énergétique dans les cellules musculaires striées en conditions physiologiques et physiopathologiques

Thèse soutenue publiquement le **28 Septembre 2015**, devant le jury composé de :

Mr. Jacques BODENNEC
Maître de Conférences, Université Claude Bernard Lyon 1, Centre de Recherche en Neurosciences de Lyon, Rapporteur

Mr. Jose-Antonio ENRIQUEZ
Professeur, National Center for Cardiovascular Research Carlos III, Madrid (Espagne), Président du jury

Mr. François BOUCHER
Professeur, Université Joseph Fourier, Grenoble (France), Membre

Mme. Rita GUZUN
Maître de Conférences – praticien hospitalier, Université Joseph Fourier et CHU, Grenoble (France), Membre

Mme. Tuuli KAAMBRE
Group leader, National Institute of Chemical Physics and Biophysics, Tallinn (Estonia), Membre

Mr. Uwe SCHLATTNER
Professeur, Université Joseph Fourier, Grenoble (France), Membre

Université Joseph Fourier / Université Pierre Mendès France / Université Stendhal / Université de Savoie / Grenoble INP

Acknowledgments

This work would not have been possible without the financial support of the Agence Nationale de la Recherche (SYBECAR project, nr RA0000C407) and the scientific support of my supervisor Dr. Guzun and my director of thesis Prof. Boucher. I would like to express my gratitude to them for their scientific guidance and enthusiasm in this work and for helping me to develop my background in heart physiology and cardiac energy metabolism. I would also like to thank Prof. Valdur Saks for being patient with me when I arrived to his team without knowing any bioenergetics and for taking his time to teach me all I know now. I also highly appreciate that he has showed me that you can live doing a work that you love and enjoy during all your life; you just need to never give up and always continue learning.

I am also very grateful to Prof. Uwe Schalttner for accepting me in his lab and giving me the access to the laboratory and research facilities and to Dr. Guzun, Prof. Boucher, Dr. Tanguy, Dr. Sanchez and Sarah Foriel for the great experience of working hand by hand with them during these 3 years. I also immensely thankful to my co-authors for their contribution to this work, in particular to Dr. Usson and Dr. Grichine for helping me with the confocal microscopy analysis and for their enthusiastic participation in this work. Moreover, I am grateful to all my labmates for their support, help and all the great moments that we shared during these years. More specially, to the PhDs of this lab who became good friends since the beginning. They have celebrated with me all the good moments of the thesis and supported me in the bad ones. It would have been a lonely lab and much harder experience without you.

Finally, I want to thank my family and Aitor for being always there for me. They have been my major support in the difficult moments. Therefore, this work would not have been possible to do without their unconditional support, patience and love.

Résumé

La stabilité métabolique des cellules cardiaques est dépendante d'une organisation fonctionnelle qui favorise le transfert des liaisons phosphate depuis les sites de synthèse de l'ATP (mitochondries) jusqu'aux sites d'utilisation de l'énergie. Au niveau mitochondrial, cette fonction est principalement assurée par l'Interactosome Mitochondrial, comprenant les complexes respiratoires, l'ATP synthasome fonctionnellement couplé à la créatine kinase mitochondriale et le pore de la membrane mitochondriale externe VDAC qui régit la diffusion des nucléotides adényliques sous le contrôle de protéines du cytosquelette. Il est communément admis que la situation d'ischémie/reperfusion (IR) du myocarde affecte l'organisation intracellulaire des cardiomyocytes, les phosphorylations oxydatives (OxPhos), ainsi que le transfert de l'énergie cellulaire.

L'objectif de ce travail était d'étudier les mécanismes de régulation de la fonction mitochondriale par les interactions entre la tubuline βII et la membrane mitochondriale externe (MME) d'une part et l'organisation de supercomplexes respiratoires (SCR) d'autre part. Différents types de muscles striés (cardiaque et squelettique) ont été utilisés pour étudier le lien entre la tubuline βII et la perméabilité de la MME pour les nucléotides adényliques. De plus, le rôle de la tubuline βII et de l'organisation des SCR ont été étudiés dans la situation physiopathologique de l'IR cardiaque.

Dans les cardiomyocytes, comme dans les cellules issues de muscles squelettiques oxydatifs de rats adultes, la tubuline βII est colocalisée avec les mitochondries et la perméabilité de la MME pour l'ADP est faible. A l'aide du système pyruvate kinase/phosphoénolpyruvate, destiné à piéger l'ADP extramitochondrial, nous avons montré que l'affinité apparente d'OxPhos pour l'ADP est directement liée à la perméabilité de la MME. Ainsi, dans le muscle cardiaque

comme dans les muscles squelettiques oxydatifs, un fort Km apparent pour l'ADP est associé à une faible perméabilité de la MME à l'ADP et à une forte expression de tubuline βII, présente sous une forme non-polymérisée. A l'inverse, dans les muscles glycolytiques, la très faible teneur en tubuline βII non-polymérisée est associée à une forte perméabilité de la MME aux nucléotides adényliques (faible Km apparent pour l'ADP).

Les effets de l'ischémie (20 ou 45 minutes) et de la reperfusion cardiaque (30 minutes) ont été étudiés sur un modèle de coeur isolé perfusé de rat. Les principaux résultats sont que la séquence d'IR induit un réarrangement de la tubuline βII, associé à une réduction du Km apparent pour l'ADP, une baisse du contrôle de la respiration par la créatine et une diminution de la capacité d'OxPhos. Les modifications observées étaient dépendantes de la durée de l'ischémie et variables d'un cœur à l'autre. De plus, le groupe soumis à 20 minutes d'ischémie était caractérisé par la présence de SCR incluant le complexe I et l'absence de perte de cytochrome c (suggérant l'absence d'apoptose cellulaire). A l'inverse, 45 minutes d'ischémie suivies de reperfusion ont conduit à une perte de cytochrome c et à un remodelage de l'ultrastructure mitochondriale, sans modification de l'organisation des SCR.

En conclusion, nos résultats soulignent l'importance des interactions mitochondrie-cytosquelette, et plus particulièrement celles impliquant la tubuline βII, dans la compartimentation intracellulaire des nucléotides adényliques et les transferts d'énergie dans les muscles striés oxydatifs. Par ailleurs, la séquence d'IR myocardique induit une désorganisation de la tubuline βII, qui contribue à la dysfonction mitochondriale. Enfin, l'absence de réorganisation des SCR quand la lésion d'IR est irréversible (45 minutes d'ischémie) suggère que le réarrangement des SCR observé après 20 minutes d'ischémie pourrait être l'un des mécanismes adaptatifs mis en jeu pour prévenir la dysfonction mitochondriale à la suite d'une séquence d'IR.

Mots clés: métabolisme énergétique, ischémie-reperfusion cardiaque, interaction cytosquelette-mitochondries, organisation de supercomplexes respiratoires, morphologie mitochondriale, analyse du contrôle métabolique.

Abstract

Cardiac metabolic stability is highly dependent on the intracellular functional organization which favors compartmentalized phosphoryl flux transfer between sites of mitochondrial ATP synthesis and sites of ATP hydrolysis (mainly myofibrillar ATPases). At the level of mitochondria, this function is provided by Mitochonrial Interactosome which includes respiratory complexes, ATP Synthasome coupled functionally to mitochondrial Creatine Kinase, Voltage-Dependent Anion Channel (VDAC) and cytoskeletal protein regulating ATP/ADP diffusion through VDAC. Cardiac ischemia-reperfusion (IR) injury alters intracellular organization, oxidative phosphorylation (OxPhos) and compartmentalized intracellular phosphoryl flux transfer.

The aim of this work was to study the regulation of mitochondrial activity by β tubulin II interaction with mitochondrial outer membrane (MOM) and by respiratory supercomplex (RSC) organization, under physiological conditions as well as in ischemia-reperfusion in striated muscles. For this purpose, Different types of striated muscles (cardiac and skeletal) were used for studying the link between β tubulin II and MOM permeability to adenine nucleotides. In addition, the role of β tubulin II and RSC organization was studied in the pathophysiological context of cardiac ischemia-reperfusion.

In cardiac and oxidative skeletal muscles from adult Wistar rats, β tubulin II is colocalized with mitochondria and associated with low MOM permeability to ADP. Using pyruvate kinase and phosphoenolpyruvate trapping system for ADP, we show that the apparent affinity of OxPhos for ADP can be directly linked to the permeability of MOM. High apparent Km for ADP in cardiac and oxidative skeletal muscle is associated with low MOM permeability to ADP and high expression of non-polymerized βII tubulin. Very low expression of non-polymerized β tubulin II

in glycolytic muscles is associated with high MOM permeability for adenine nucleotides (low apparent Km for ADP).

The effect of the IR-injury was studied by subjecting isolated and perfused Wistar rat hearts to total ischemia (for 20 min and 45 min) followed by 30 min of reperfusion (I20R and I45R groups, respectively). The IR-injury induced intracellular rearrangement of β tubulin II was associated with decreased apparent Km for ADP, creatine-control of respiration and reduced OxPhos capacity. Observed changes were dependent on the duration of ischemia and were heterogeneously present across hearts. Additionally, in the I20R group we evidenced an increase in the content of the RSC embodying complex I in the absence of cytochrome c release (evidencing the absence of apoptosis). Forty five minutes of ischemia followed by reperfusion resulted in increased cytochrome c release and mitochondrial cristae remodeling without alteration of RSC organization.

The results of this study highlight the importance of cytoskeleton-mitochondria interactions, and particularly that of β tubulin II, for adenine nucleotide intracellular compartmentalization and phosphoryl flux transfer in oxidative striated muscles. In addition, cardiac IR was shown to induce β tubulin II disorganization contributing to mitochondrial dysfunction. The absence of the RSC reorganization after irreversible IR injury (45 minutes of ischemia) suggests that the rearrangement of RSC observed after 20 minutes of ischemia could be an adaptive mechanism to overcome the IR-induced alterations of mitochondrial function.

Key words: energy metabolism, cardiac ischemia-reperfusion, cytoskeleton-mitochondria interaction, Respiratory Supercomplex Organization, mitochondria morphology, Metabolic Control Analisis

First author publications

Bagur R[1] , Varikmaa M[1] , Kaambre T, Grichine A, Timohhina N, Tepp K, Shevchuk I, Chekulayev V, Metsis M, Boucher F, Saks V, Kuznetsov AV, Guzun R. Role of mitochondria-cytoskeleton interactions in respiration regulation and mitochondrial organization in striated muscles. *Biochim Biophys Acta*. 2014 Feb; 1837(2):232–45.

Bagur R, Tanguy S, Foriel S, Grichine A, Sanchez C, Pernet-Gallay K, Kaambre T, Kuznetsov AV, Usson Y, Boucher F, Guzun G. The impact of cardiac ischemia/reperfusion on the mitochondria-cytoskeleton interactions. *Biochim Biophys Acta*. (Article under revision; manuscript number: BBADIS-15-333)

Respiratory supercomplex organization: an adaptive mechanism in cardiac ischemia/reperfusion? (Article in preparation)

[1] These authors contributed equally to this work.

Other publications

Beside the three papers introduced in the result part of this manuscript, during the three years of the thesis my work have contributed to a review article, a book chapter and other scientific articles with our collaborators.

1. Modular organization of cardiac energy metabolism: energy conversion, transfer and feedback regulation. Guzun R, Kaambre T, **Bagur R**, Grichine A, Usson Y, Varikmaa M, Anmann T, Tepp K, Timohhina N, Shevchuk I, Chekulayev V, Boucher F, Dos Santos P, Schlattner U, Wallimann T, Kuznetsov AV, Dzeja P, Aliev M, Saks V. *Acta Physiol (Oxf)*. 2015 Jan; 213(1):84-106

2. Systems Level Regulation of Cardiac Energy Fluxes Via Metabolic Cycles: Role of Creatine, Phosphotransfer Pathways, and AMPK Signaling. Valdur S, Schlattner U, Tokarska-Schlattner M, Wallimann T, **Bagur R**, Zorman S, Pelosse M, Dos Santos P, Boucher F, Kaambre T, Guzun R. In: Aon MA, Saks V, Schlattner U, editors. Systems Biology of Metabolic and Signaling Networks. *Springer Series in Biophysics* Volume 16, 2014, pp 261-320

3. Metabolic control analysis of respiration in human cancer tissue. Kaambre T, Chekulayev V, Shevchuk I, Tepp K, Timohhina N, Varikmaa M, **Bagur R**, Klepinin A, Anmann T, Koit A, Kaldma A, Guzun R, Valvere V, Saks V. *Front Physiol*. 2013 Jun; 4:151

4. Mysterious Ca(2+)-independent muscular contraction: déjà vu. Kuznetsov AV, Guzun R, Boucher F, **Bagur R**, Kaambre T, Saks V. *Biochem J*. 2012 Aug 1;445(3):333–6.

Table of contents

1. Background: theoretical basis of bioenergetics and cellular metabolism

More than 200 years ago it was discovered that respiration through oxidation of organic substrates is one of the main sources of energy for living cells. The discovery of oxygen in 1774 was almost simultaneously done by Joseph Priestley in England, Carl Scheele in Sweden, and Antoine Laurent Lavoisier in France. A couple of years later, Lavoisier in collaboration with Laplace discovered the process of biological oxidation which consists on the consumption of oxygen and the production of carbon dioxide by living organisms during respiration. Moreover, they developed the calorimetry technique in order to measure the quantity of heat produced during respiration, along with the simultaneous analysis of the changes in the air composition within the calorimeter. These studies led the authors to the remarkable conclusion that "respiration is a process similar to the burning of coal", this was later considered the discovery of the biological oxidation. These discoveries led to the birth of Bioenergetics: the science studying energy transformations within living cells, and how cells obtain energy to live and to perform work: mechanically (via motility and contraction), osmotically (via ion transport), or chemically (via biosynthesis).

1.1. Thermodynamic laws and the theoretical bases of cellular metabolism

The theory of thermodynamics was developed in the 19th century and explains the laws that govern energy transformations in the universe, between a system and its surroundings.

The first law of thermodynamics named the "*law of conservation of energy*" states that the total amount of energy in the universe is constant. Therefore, energy can be converted from one form to another, but it cannot be created or destroyed. The application of this statement to a system which undergoes some sort of transformation reveals that the change in the internal energy of this system (dU) is equal to the amount of heat supplied to the system (δQ) minus the amount of work done by the system on its surroundings (δW):

$$dU = \delta Q - \delta W$$

The second law of thermodynamics asserts that no natural process (i.e. non spontaneous reaction) can occur unless it is associated with an increase in the randomness or disorder of the universe. The measure of this change in the universe is referred to as the change in entropy (dS). The concept of entropy gives us a more quantitative way to predict the spontaneous direction of any given process. The entropy change of a system undergoing a process is described by:

$$dS \geq \frac{\delta Q}{T}$$

where dS is the entropy change in a system, δQ is the heat flow into or out of a system, and T is the absolute temperature in degrees Kelvin.

In 1873, the Gibbs free energy was introduced as a thermodynamic potential that predicts the direction of a chemical reaction under constant temperature (isothermal) and pressure (isobaric) conditions. The changes in the Gibbs free energy (dG) (i.e. capacity to do "useful" work) are described by the equation below, where dH is the change in enthalpy (i.e. maximal amount of exchangeable heat a system can produce).

$$dG = dH - T \cdot dS$$

Consequently, the application of the second law to this equation revealed that a reaction is spontaneous only when $dG < 0$, is in equilibrium when $dG = 0$, and is non-spontaneous when $dG > 0$. In conclusion, the thermodynamic laws dictate that all processes and reactions proceed only in the direction in which the Gibbs free energy decreases and entropy increases and thereby, in which disorder increases. This conclusion seems to be in contradiction with cell life since the cells present high structural and functional organization (low internal entropy).

In 1944 Erwin Schrödinger showed that the apparent contradiction is overcome if we consider that living cells are open systems (i.e. exchanging energy and mass with their surrounding medium), that by means of metabolism, decrease or maintain their low entropy state by increasing the entropy of the medium (also known as Schrödinger's principles of negentropy) (Schrödinger, 1944). In cellular metabolic systems, catabolic reactions (i.e. breakdown of substrates) through coupling to anabolic reactions (i.e. biosynthesis) maintain cell structure and organization as an expression of low internal entropy. Figure 1 shows that the processes of free energy conversion are central for coupling catabolism to anabolism, emphasizing the central role of bioenergetics in studies of integrated metabolism of the cells.

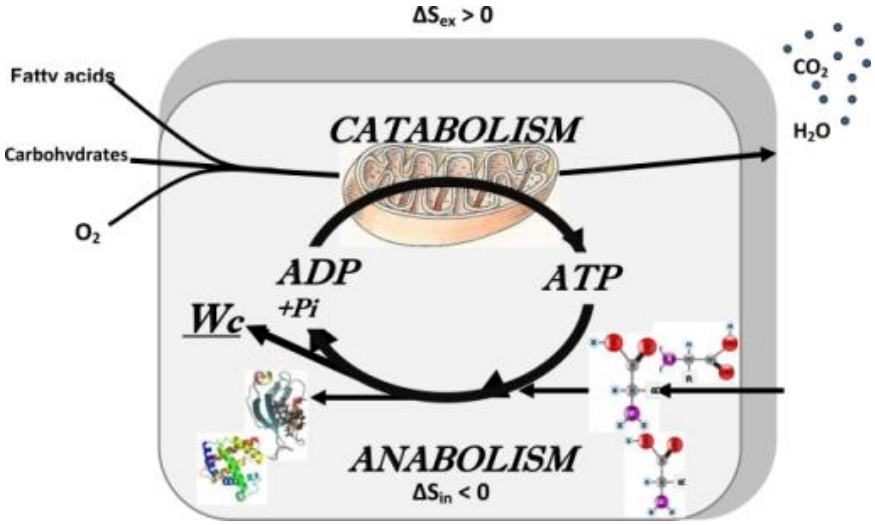

Figure 1. General scheme describing the cellular integrated metabolism as an open system exchanging both energy and mass with surrounding medium (Saks et al., 2007).

1.2.Metabolic substrates

Energy metabolism in living organisms is mostly supported by the degradation of carbohydrates (such as glucose) and fatty acids. In mammalian cells, glucose can be taken up by membrane glucose transporters (GLUT) and degraded via glycolysis pathway. This metabolic pathway converts one molecule of glucose to two molecules of pyruvate, generating two molecules of both ATP and NADH. The pyruvate and NADH produced are either converted to lactate and NAD^+ in the cytosol (lactic fermentation) or shuttled into the mitochondrial matrix, where pyruvate is converted to acetyl-CoA by pyruvate dehydrogenase (aerobic oxidative glycolysis). In the case of fatty acids, the mechanism to cross the plasma membrane depends on the length of the fatty acid chain. Short-chain fatty acids enter into cytoplasm via free diffusion, whereas long-chain fatty acids (LCFAs) cross the plasma membrane via protein-mediated mechanism, involving one or more LCFA-binding proteins (such as FATCD36 in striated muscles). Once in the cytoplasm, fatty acids are esterified to acyl-CoA to later be transported into the mitochondrial matrix by carnitine palmitolyltransferase (CPT) I and II. Inside the mitochondrion, acyl-CoA is converted to acetyl-CoA via the β-oxidation pathway. Fatty acid oxidation to acetyl-CoA also occurs in peroxisomes when the fatty acid chains are too long to be handled by mitochondria. Acetyl-CoA produced by glycolysis and β-oxidation is oxidized in the Krebs cycle generating NADH, $FADH_2$ and CO_2.

The breakdown of metabolic substrates leads to the release of energy, some of which is used to form high-energy compounds (e.g. ATP) and reduce electrons carriers (NADH, NADPH and $FADH_2$). Adenine dinucleotides (NADH and $FADH_2$) that are reduced during glycolysis and β-oxidation pathways are re-oxidized in the respiratory chain with final ATP synthesis. It is important to note that the redox power generated by these metabolic pathways is not the same and depends on the availability of oxygen. Under normoxic conditions, the net

yield of ATP produced per substrate consumed is 38 molecules for glucose and 128 molecules for palmitic acid (major fatty acid substrate). This difference is due to the higher content of nonoxidized -C—C— and —C—H chemical bonds in palmitic acid ($C_{16}H_{32}O_2$) compared to that in glucose ($C_6H_{12}O_6$). Compared to carbohydrate oxidation, fatty acid oxidation provides more free energy per unit of mass when oxygen is not a limiting factor (aerobic conditions). Under anaerobic conditions, fatty acid oxidation is inhibited due to its strict dependence on oxygen availability, whereas glucose can be converted into lactate (Lactic fermentation) producing 2 molecules of ATP per molecule of glucose. Lactic fermentation is a less efficient energy production metabolic pathway, which can support energy demands when oxygen availability is limited.

1.3. Electron Transfer and Respiratory Chain

Most of the energy released during substrates breakdown is transported by reduced adenine dinucleotides to the respiratory chain for ATP production. NADH and $FADH_2$ enter the respiratory chain via NADH–ubiquinone oxidoreductase (Complex I) and succinate–quinone oxidoreductase (Complex II), respectively. NADH molecules bind to Complex I and transfer its two high-potential electrons to the flavin mononucleotide (FMN) prosthetic group of this complex to give the reduced form, $FMNH_2$. These electrons are then transferred through the FMN via a series of iron-sulfur (Fe-S) centers to ubiquinone (Q). The reduction of Q to ubiquinol (QH_2) results in the uptake of two protons from the mitochondrial matrix. The flow of electron through complex I leads to a conformational change of the protein complex, causing the pumping of four protons out of the mitochondrial matrix. On the contrary, $FADH_2$ are generated during the Krebs cycle by the oxidation of succinate to fumarate via the succinate dehydrogenase (i.e. enzyme comprised in the complex II). As a result, the electrons are transferred from $FADH_2$ towards Q via Fe-S centers with absence of proton pumping across

mitochondrial inner membrane (MIM). Other substrates for mitochondrial dehydrogenases transfer electrons into the respiratory chain at the level of ubiquinone, but not through Complex II. These electron-transferring enzymes (such as acyl-CoA dehydrogenase or glycerol 3-phosphate dehydrogenase) are flavoprotein located on the outer face of the MIM, and like succinate dehydrogenase they channel electrons into the respiratory chain by reducing ubiquinone.

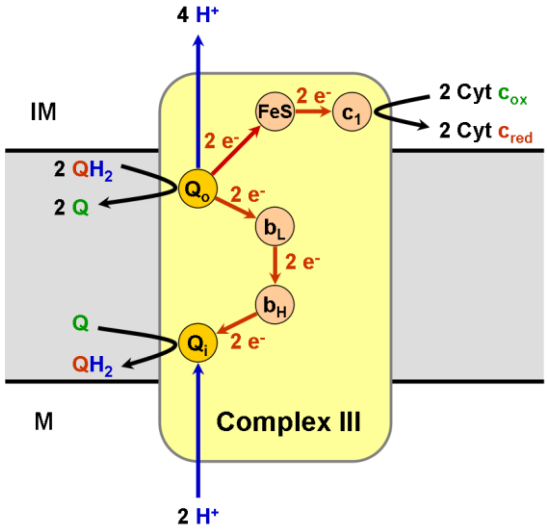

Figure 2. Schematic representation of the Q cycle (https://en.wikipedia.org/wiki/Q_cycle; consulted on 28.05.2015)

The electrons from QH_2 are transferred to cytochrome *c* through cytochrome bc1 (Complex III) following the mechanism known as Q cycle (Fig. 2). This mechanism also facilitates the switch from the two-electron carrier QH_2 to the one-electron carrier cytochrome *c*. The cycle starts with QH_2 binding to the Q_0 site of complex III and transferring its electron, one at a time. One electron flows first through the Rieske (2Fe-2S) cluster and cytochrome c_1 to an oxidized cytochrome *c* molecule (reduced cytochrome *c* is set free). The other electron is transferred through cytochrome b_L and cytochrome b_H to a Q bound in the Q_i site of complex III, resulting in the formation of a semiquinone anion. Once the electrons are transferred, oxidized Q in the Q_0 site is free to diffuse out into the Q pool, and its two protons are released at the cytosolic side of the membrane. In order to complete the cycle, another QH_2 is required to bind to the Q_0 site of complex III and transfer its electron. In this case, the second electron reduces the semiquinone bound in the Q_i site of complex III to QH_2 (uptake of two protons from the mitochondrial matrix), which is set free together with the Q from the Q_0 site (Gennis et al., 1993).

The last stage of the respiratory chain is the reduction of dioxide (O_2) to two molecules of water (H_2O) through cytochrome c oxidase (Complex IV) using four reduced cytochrome *c*. The first reduced cytochrome *c* transfers its electron to Cu_B and the second reduced cytochrome *c* transfers its electron to the iron (Fe) in heme a3. This Fe^{2+} center then binds to a molecule of O_2, which is transformed to peroxide by the transfer of the two electrons. The peroxide forms bridges between the Fe and Cu_B. The introduction of an additional electron by a third molecule of reduced cytochrome c cleaves the O-O bond and results in the uptake of a proton from the mitochondrial matrix. The introduction of a final electron and three more protons generates two molecules of H_2O, which are released from the enzyme to regenerate the initial state (Wikström, 1989).

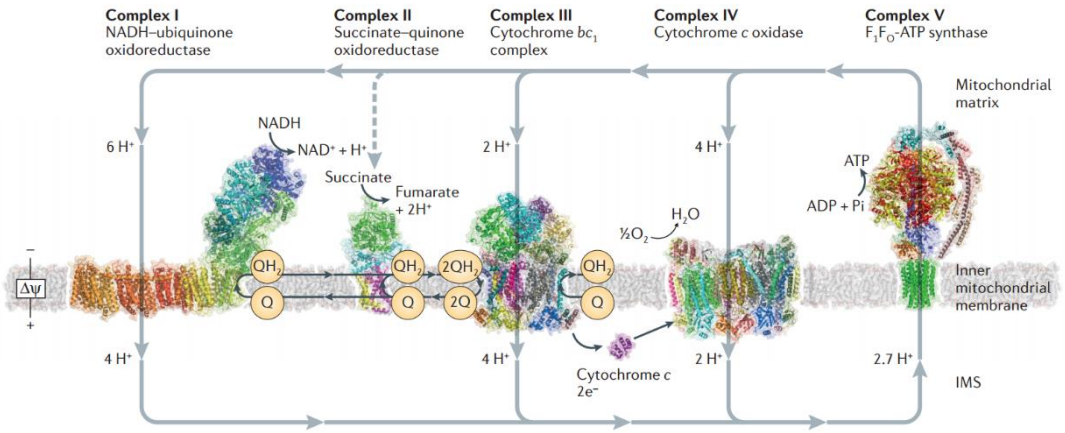

Figure 3. The respiratory chain components and the proton flow through electron transfer. Respiratory chain is comprised of three proton-pumping enzymes: complex I (NADH–ubiquinone oxidoreductase), complex III (cytochrome bc1) and complex IV (cytochrome *c* oxidase). These enzymes contribute in the generation of the proton motive force that in turn drives F_1F_O-ATP synthase. Electron transport between complexes is mediated by membrane-embedded ubiquinone and soluble cytochrome c. Complex I is the entry point for electrons from NADH, while the electrons from $FADH_2$ enters the respiratory chain via complex II (succinate–quinone oxidoreductase) (Sazanov et al., 2015).

1.4. Oxidative Phosphorylation and the Chemiosmotic Theory

The proton gradient generated by complexes I, III and IV (Fig. 3) is the result of the energy-yielding reactions of electron transport through the respiratory chain. Complexes I and IV transfer four protons across MIM per pair of electrons, as a result of conformational changes induced by electron transport. On the contrary, in complex III the protons are carried across the

membrane by Q, which accepts protons from the mitochondrial matrix at complexes I or II and releases them into the intermembrane space at complex III (Q cycle). In this case, two protons per pair of electrons are pumped across the membrane and another two protons per pair of electrons are combined with O_2 to form H_2O within the mitochondrial matrix. Consequently, the number of protons translocated across the MIM is 10 for each oxidized NADH molecule and 6 for each oxidized $FADH_2$ molecule. The difference in the number of protons translocated is because the electrons driven from $FADH_2$ oxidations enter the respiratory chain via complex II.

The transfer of protons from the mitochondrial matrix to the intermembrane space plays the critical role of converting the energy derived from the oxidation-reduction reactions of electron transport to the potential energy stored in a proton gradient (Mitchell, 1961; Mitchell, 1976; Mitchell, 1976(b); Mitchell, 1977). This proton gradient is composed by both a chemical gradient (ΔpH) associated to the different proton concentration between intermembrane space and mitochondrial matrix, and a transmembrane electrical potential ($\Delta\Psi_m$) created between the mitochondrial matrix (negatively charged) and the intermembrane space (positively charged due to the proton charge). Consequently, we can describe the proton gradient as:

$$\Delta\mu_{H^+} = 2.3RT \cdot \Delta pH + F \cdot \Delta\Psi_m$$

where *R* is the gas constant [1.987 cal/(degree·mol)], T is the temperature expressed in degrees Kelvin, and *F* is the Faraday constant [23,062 cal/ (V·mol)].

The restricted diffusion of ions through MIM triggers proton transport back to the mitochondrial matrix through a protein channel. Thus, the energy stored in the proton gradient will be used by the ATPSynthase to re-phosphorylate ADP to ATP. ATPSynthase is a complex comprised of two structurally distinct components, F_0 and F_1, which are linked by a slender stalk (Fig. 4A). The F_0 complex is comprised in the MIM and provides a channel through which protons are able to flow back from the intermembrane space to the mitochondrial matrix. The

energetically favorable return of protons to the mitochondrial matrix is coupled to ATP synthesis, catalyzed by the F_1 subunit. The mechanism of ATP synthase involves mechanical coupling between the F_0 and F_1 subunits. In particular, the flow of protons through F_0 drives the rotation of F_1, which acts as a rotary motor to drive ATP synthesis (Fig. 4B). In brief, the flow of four protons from the intermembrane space to mitochondrial matrix through F_0 is required to drive the synthesis of one molecule of ATP. Therefore, the oxidation of one molecule of NADH provides enough energy to synthesize three molecules of ATP, whereas the oxidation of $FADH_2$ yields only 2 ATP molecules (Boyer, 1993; Duncan et al., 1995; Zhou et al., 1996).

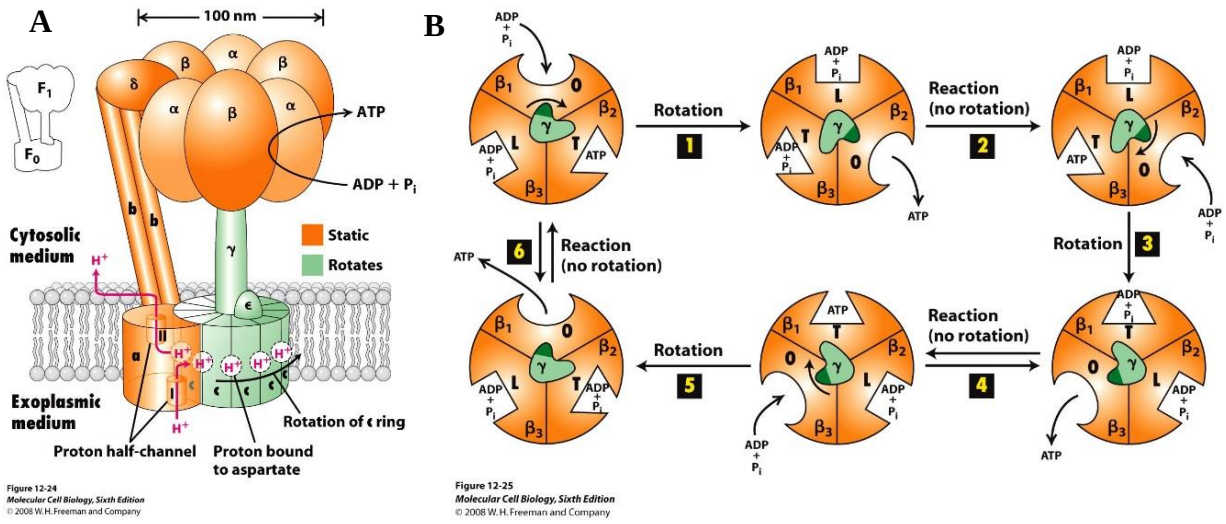

Figure 4. A) Scheme of ATP Synthase structure, which is comprised of two subunits: F_1 (peripheral domain) and F_0 (transmembrane domain). F_1 subunit consists of 3 α subunits and 3 β subunits, one δ subunit, and a central shaft (γ subunit). F_0 includes multiple copies of c subunits, one a subunit and 2 b subunits. F_0 provides a transmembrane channel through which about four protons are pumped (pink arrows) to synthesize one ATP molecule in the β subunits of F_1. B) Schematic representation of the ATP synthesis mechanism. The binding change mechanism involves the active site of a β subunit's cycling between three states. In the "open" state, ADP and phosphate (P_i) enter the active site (half circle shape). The protein then closes up around the molecules and binds them loosely — the "loose" state (half square shape). The enzyme then undergoes another change in shape and forces these molecules together, with the active site in the resulting "tight" state (half triangle shape) binding the newly produced ATP molecule with very high affinity. Finally, the active site cycles back to the open state, releasing ATP and binding more ADP and P_i, ready for the next cycle of ATP production (Molecular Cell Biology, 4th edition, 2000, W.H. Freeman and Company).

ATP produced from oxidative phosphorylation (OxPhos) is transported from the mitochondrial matrix to the intermembrane space via adenine nucleotide translocase (ANT). ANT is a transporter protein that catalyzes ADP/ATP exchange across the mitochondrial inner

membrane. This transporter protein is one of the most abundant mitochondrial proteins, and, in energy demanding tissues such as heart, it represents up to 10% of the protein content of the inner membrane (Fiore et al., 1998; Klingenberg et al., 1980). ANT drives ATP out of the mitochondrial matrix into the intermembrane space in exchange for ADP entering into the mitochondrial matrix. The flux of ATP/ADP through MIM cannot occur spontaneously due to the large negative membrane potential across the inner mitochondrial membrane (about –180mV) and the much higher ATP/ADP ratio present in the cytosol compared to that of mitochondria (Klingenberg et al., 1980). Once in the intermembrane space, ATP can either across mitochondrial outer membrane (MOM) via voltage dependent anion channel (VDAC) or transfer its phosphoryl group to creatine in the MtCK reaction to produce phosphocreatine (PCr) which will be exported from the mitochondria. Once in the cytoplasm, both high-energy phosphoryl compounds (ATP and PCr) can be used as the principal energy currency of the cell to power thermodynamically unfavorable (non-spontaneous) reactions. The resulting products of ATP and PCr hydrolysis are transported back into the mitochondrial matrix to be re-phosphorylated.

1.5. Respiratory chain complex organization

The organization of respiratory chain (RC) complexes in the inner membrane has been an object of intense debate. Two alternative models have been proposed: random collision model (RC complexes are individual and independent units) and solid-state model (RC complexes form a unique unit called respiratory supercomplex) (Schematic representation of both models in Fig.5).

According to the random collision model, RC complexes and electrons carriers (ubiquinone and cytochrome c) are in constant and independent diffusional motion in the inner membrane. Therefore, electron transfer depends on the random and transient encounter of the

individual RC complexes with the electron carriers (i.e. diffusion-based random collision process). Consequently, in this model electron transport is basically controlled by diffusion. In a remarkable study published in 1986, Hackenbrock et al., proposed five fundamental postulates upon which the random collision model is founded (Hackenbrock et al., 1986): 1) all redox components are independent lateral diffusers; 2) cytochrome *c* diffuses primarily in three dimensions; 3) electron transport is a diffusion-coupled kinetic process; 4) electron transport is a multicollisional, obstructed, long-range diffusional process; and 5) the rates of diffusion of the redox components have a direct influence on the overall kinetic process of electron transport and can be rate limiting, as in diffusion control. Finally, the authors confirmed that the random collision model offered better explanation for the structural organization of the respiratory chain than the solid-state model.

The solid-state model was proposed in 1955 by Chance and Williams and it states that RC components are closely packed to permit the substrates channeling from one enzyme to the next one, thus resulting in a high efficient electron transport (Chance and Williams, 1955). New evidence for the existence of stoichiometric assemblies (respiratory supercomplexes) in the respiratory chain of yeast and mammalian mitochondria were published in 2000, thus supporting this model (Schägger and Pfeiffer, 2000; Cruciat et al., 2000). Since that, respiratory supercomplexes of different compositions have been described in bacteria (Stroh et al., 2004), in higher plants (Eubel et al., 2003; Eubel et al., 2004; Krause et al., 2004) and in mitochondria from yeast (Schägger and Pfeiffer, 2000; Cruciat et al., 2000) and from mammals (Schägger and Pfeiffer, 2000; Schägger et al., 2001; Schägger et al., 2004). The main techniques used to support the existence of respiratory supercomplexes are the co-migration of RC complexes on blue native electrophoresis (BN-PAGE) and their co-purification by sucrose gradient centrifugation. In these studies, respiratory supercomplexes of various stoichiometry were identified, such as: assembly of monomeric complex I (I_1) with dimeric complex III (III_2);

assembly of monomeric complex I (I_1), dimeric complex III (III_2) and multiple copies of complex IV (IV_{1-4}); or assembly of dimeric complex III with multiple copies of complex IV (IV_{1-2}).

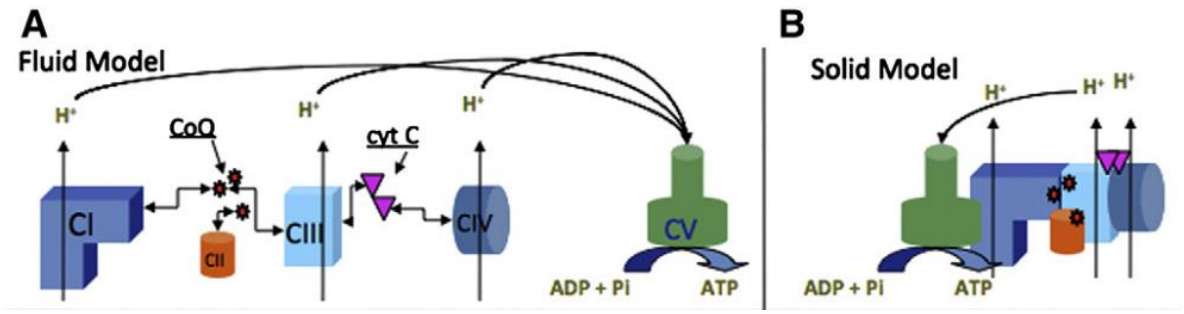

Figure 5. Schematic representation of the different models proposed to explain the arrangement of the respiratory chain. A) Random collision model and B) Solid model (Acin-Perez and Enriquez, 2014).

The first functional evidence of supramolecular organization in bovine heart mitochondria was provided by Bianchi et al., using flux control analysis (Bianchi et al., 2004). This analysis allows evaluating the extent of the control that an enzyme exerts on a metabolic pathway. The result of this kinetic study was that both complexes I and III are highly rate-controlling over NADH oxidation, suggesting the existence of functionally relevant association between the two complexes, whereas complex IV appears randomly distributed. Moreover, the authors showed that Complex II is fully rate-limiting for succinate oxidation, indicating the absence of substrate channeling toward Complexes III and IV. Consequently, this study suggests the co-existence of both RC complex arrangements (random collision and solid-state models) in bovine heart mitochondria.

Recent evidence suggests that supramolecular organization of the respiratory chain is in dynamic equilibrium between respiratory supercomplexes and individual RC complexes, depending on mitochondrial function (so-called the plasticity model) (Acin-Perez et al., 2008; Acin-Perez and Enriquez, 2014). In this model, the supramolecular organization of RC complexes is envisaged to change in response to stimuli, in order to adapt the cell to different physiological conditions (Piccoli et al., 2006; Quarato et al., 2011; Ramirez-Aguilar et al., 2011;

Lapuente-Brun et al., 2013). However, the physiological significance and the plasticity of such an organization are still under discussion.

2. Cardiac Energy Metabolism

Under normoxic conditions, long-chain fatty acids are the major substrates for the heart: about 60 – 90 % of the total acetylCoA produced derives from β-oxidation, while the other 10 – 40 % comes from the oxidation of pyruvate mainly derived from glycolysis (Neely et al., 1974; Gertz et al., 1988; Wisneski et al., 1985; Opie, 2003). Almost all cellular ATP production (95%) is generated by oxidative phosphorylation in the mitochondria, with the remaining coming from glycolysis in the cytosol. The major use of ATP (i.e. ATP hydrolysis) is to sustain heart contraction; the remaining 30 – 40% of ATP produced is used for calcium uptake via the sarcoplasmic reticulum Ca^{2+}-ATPase (SERCA) and for the maintenance of ion homeostasis via the sarcolemmal ion pumps (Gibbs, 1978; Suga, 1990). The rate of ATP hydrolysis in the heart is high (0.5 mol · g wet wt^{-1} · s^{-1} at rest condition), although its cellular content is relatively low (5 mol/g wet wt). As a result, there is a complete turnover of the myocardial ATP pool approximately every 10 s under normal conditions (Ingwall, 2002; Opie, 2003). Thereby, the rate of oxidative phosphorylation has to be precisely controlled by the cellular energy demands.

2.1. Frank-Starling law and Metabolic homeostasis

The heart maintains normal blood circulation under a wide range of workloads, a function governed by the Frank-Starling law (Opie, 2003; Frank, 1885; Starling and Visscher,

1927). This law states that cardiac work increases in response to an increase in the volume of blood filling the heart (the end diastolic ventricular volume). However, this law has wider implications as it addresses the principles of cardiac mechano-energetic coupling (Opie, 2003). The study of Starling and Visscher in 1926 was the first experimental investigation of the connection between cardiac work and energy consumption (measured as the rate of oxygen consumption) (Starling and Visscher, 1927; Evans and Matsuoka, 1915). As both variables increased linearly with the increase in left ventricular end-diastolic volume, the conclusion was that "any increase in the work demanded of the heart is met by a corresponding increase in the oxygen consumption and in the amount of chemical changes taking place" (Starling and Visscher, 1927).

Another key characteristic of heart energetics is that a linear increase in oxygen consumption with cardiac work is observed in the absence of measurable changes in the cellular content of high-energy compounds (e.g. ATP and PCr), which is known as metabolic stability or metabolic homeostasis (Neely et al., 1972; Williamson et al., 1976; Balaban et al., 1986; Wan et al., 1993). This phenomenon was firstly described by Neely *et al.*, and Williamson *et al.*, which measured myocardial high-energy compound levels spectrophotometrically or fluorimetrically using a working isolated rat heart model at different workloads (Neely et al., 1972; Williamson et al., 1976). These results were later confirmed using nuclear magnetic resonance spectroscopy (^{31}P-NMR) for smaller interval of workload changes by Balaban *et al.*, (Balaban et al., 1986).

2.2. Excitation-contraction coupling in cardiac muscle fibers

Cardiac muscle, like all striated muscles, is composed of myofibrils containing contractile units named sarcomeres. Each sarcomere consists of alternating thick and thin protein filaments composed of myosin and actin, respectively. The thin filaments are anchored

in the Z-line (on the outer edges of the sarcomere), where they are cross-linked by α-actinin, whereas the thick filaments are anchored at the center of the sarcomere, region called the M-line. The titins proteins link the thick filaments to the Z-lines, providing additional organization to the overall structure. The structural role of these proteins is to regulate the sarcomere length and to prevent overextension of the muscle. During contraction, the actin filaments slide along the myosin filaments, causing the shortening of the sarcomere from both sides without affecting the length of the thick and thin filaments.

The cardiac muscle contraction begins when a myosin head is extended in order to attach to a binding site on actin filaments forming a cross-bridge. An action called the power-stroke is triggered, allowing the myosin to pull the actin filaments towards the M-line, thereby shortening the sarcomere. ADP and inorganic phosphate are released during the power stroke. Myosin remains attached to actin until a new molecule of ATP binds, freeing the myosin to either go through another cycle of binding, followed by more contraction or remain unattached to allow the muscle to relax. The thin filaments are associated with regulatory proteins called troponin and tropomyosin, which controls the exposition of the myosin binding site on actin. Cardiac muscle contraction is controlled by the calcium phase of the action potential of calcium (calcium-induced calcium release mechanism) and the length of sarcomeres (length-dependent activation mechanism).

Calcium-induced calcium release (CICR) mechanism

In the heart, the autorhythmic cells in the intrinsic conduction system generate action potentials that spread through all the cardiac contractile cells, triggering a coordinated heart contraction. Action potentials generated by the autorhythmic cells create waves of depolarization that spread to contractile cells via gap junctions. The depolarization of cardiomyocytes triggers a plateau phase of the action potential, during which calcium ions

(Ca^{2+}) enter into the cell through dihydropyridine receptor (DHPR) located on the sarcolemma. The amount of calcium entering the cell depends on the duration of this plateau phase, but it is not enough to directly activate contraction. This small calcium current triggers a subsequent massive release of calcium that is stored in the sarcoplasmic reticulum (SR) via ryanodine receptors (RyR) (For a review see Bers, 2002; Endoh, 2006). Calcium released ($[Ca^{2+}] = 1 – 3 \cdot 10^{-6}$ M) from local intracellular stores by CICR mechanisms binds to troponin C causing a conformational change in the troponin-tropomyosin complex, thus leading to the exposure of cross-bridge binding site on actin filaments and the activation of contraction (For a review see Goldman, 1987; Rayment et al., 1993; Cooke, 1997; Gordon et al., 2001; Gordon et al., 2000).

At the end of the plateau phase, calcium entry into the cell slows down and the major intracellular calcium content is pumped back to the SR by SERCA. The remaining calcium is transported out of the cell by the sodium-calcium-exchange and the plasma membrane Ca^{2+}-ATPase. The reduced intracellular calcium level (10^{-7} M) induces a conformational change in the troponin-tropomyosin complex leading to the block of the myosin binding sites on actin. At the end of the cycle, an ATP molecule binds to the myosin head, displacing the ADP, and the initial sarcomere length is restored (Bers, 2002; Lipp et al., 1996). A simplified scheme of these events is given in fig.6.

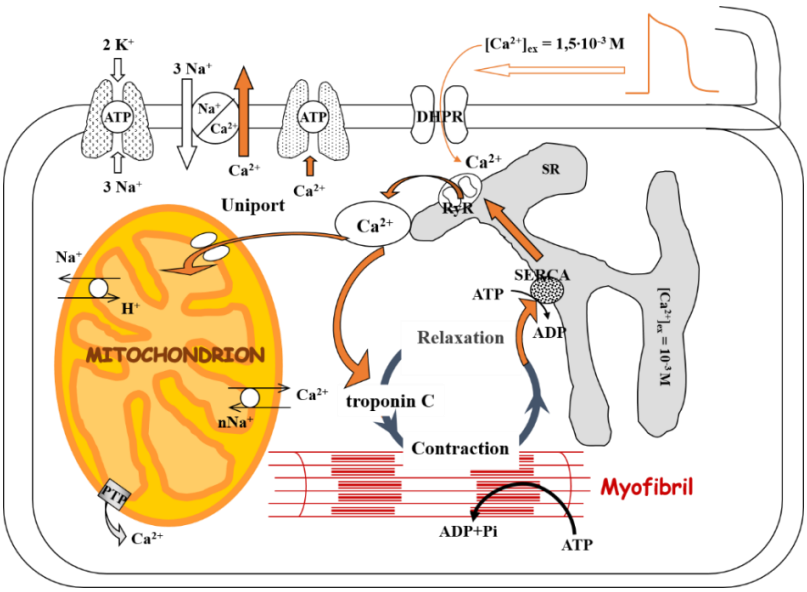

Figure 6. Schematic representation of excitation-contraction coupling in cardiac cells. SR, sarcoplasmic reticulum; SERCA, sarco/endoplasmic reticulum Ca2+-ATPase; RyR, ryanodine receptor; DHPR, dihydropyridine receptor; PTP, permeability transition pore (Saks et al., 2007).

Length-dependent activation mechanism

The mechanism of length-dependent activation is a property of all striated muscles and consists on the modulation of the sensitivity of myofilaments to Ca^{2+} by sarcomere length (Hibberd and Jewell, 1982; Kentish et al., 1986). The decrease in the distance between actin and myosin filaments when the length of the sarcomeres increases results in: increased probability of cross-bridge formation, positive co-operativity of cross-bridge binding to actin and an increase in the affinity of the troponin-tropomyosin complex for calcium (Fig. 7) (Robinson et al., 2002; Gordon et al., 2001; Katz, 2002; Fukuda et al., 2001; Landesberg, 1996; Rayment et al., 1993; Cooke, 1997). In the intact heart, increases in ventricular volume, the ventricular counterpart to muscle length, lead to an increase in ventricular output. Myofilament length-dependent activation thus provides for the cellular basis of the Frank–Starling law of the heart.

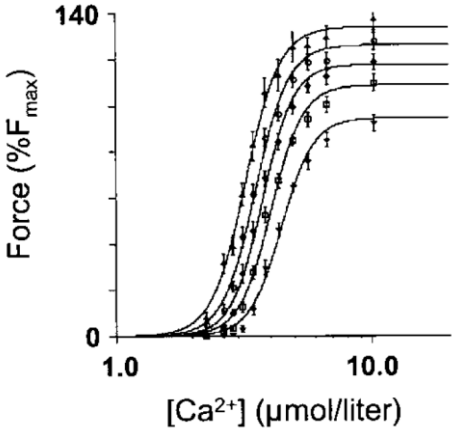

Figure 7. Average Ca^{2+}-force relationships in skinned rat cardiac trabeculae at five sarcomere lengths (SL: 1.85, 1.95, 2.05, 2.15, and 2.25 µm). Force measurements were made at each SL during steady-state activation at varying [Ca^{2+}]. Force is normalized to maximum force measured at SL 2.05 µm. Increases in SL induced a significant increase in maximum Ca^{2+}-saturated force and Ca^{2+} sensitivity (Fukuda et al., 2006).

2.3.Compartmentalized energy transfer via phosphoryl transfer networks

The length-dependent activation mechanism explains how the steady-state rates of ATP consumption can change by an order of magnitude without any changes in calcium signals. However, a question still remains unsolved: how can the ATP production rate increase 15 to 20 folds to match the rates of ATP consumption within increased workloads at the same time that it stays metabolic stable?

Cell structure and metabolic compartmentalization

The first phenomenon to be taken into account to answer this question is that the intracellular medium of cardiac cells presents several obstacles for free diffusion (so-called Brownian motion) of metabolites: protein-protein interactions, physical barriers (membranes, cytoskeletal protein network etc.), ATP/ADP-dependent metabolic processes or molecular crowding among others. In cardiac cells, proteins represent about 20 to 30 % of total cellular volume and physical barriers occupy more than 20 % of total cellular volume, thus reducing the volume available for Brownian motion of metabolites (so-called molecular crowding) (Fulton, 1982; Srere, 2000).

Because of molecular crowding and heterogeneous diffusion, the principal mechanisms of organization of cell metabolism are metabolic compartmentation, metabolic channeling and functional coupling (Saks et al., 2007b). By definition, compartment means "subcellular region of biochemical reactions kinetically isolated from the rest of cellular processes" (Saks et al., 1994; Friedrich, 1985). Metabolic channeling is the direct transfer of an intermediate between two enzymes (or a transporter and an enzyme) without any free diffusion in aqueous phase. The combination of both mechanisms (metabolic channeling and compartmentation) results in functional coupling, which allows the accumulation of reaction intermediates or products in a confined area. The compartmentation of metabolites or enzymes within cardiac cells can lead to the loss of randomness in diffusion, shifting towards a more coordinated and vectorial diffusion (Agutter, 1995; Srivastava, 1986).

The first observations highlighting the existence of metabolic compartmentation were done by Gudbjarnason and Neely in 1970, when they studied the metabolism of the ischemic heart (Gudbjarnason et al., 1970; Neely et al., 1973). In these studies, they always observed very rapid decreases in contractile force associated with a decrease in PCr content induced by the absence of oxygen supply. The complete interruption of contraction was observed after

decreasing PCr about 80 %, although 80 – 90 % of the cellular ATP content was still intact. The explanation of these results is that ATP is compartmentalized within cardiac cells and that only 10% of the total ATP content is used during contraction due to its localization (i.e. close to ATP-consuming processes). Other experimental observations supporting this theory are: 1) cellular ATP content could diminish by 70 % (amount present in the cytoplasm) without impairing contraction (Neely and Grotyohann, 1984; Kupriyanov et al., 1987; Kupriyanov et al., 1991); 2) inactivation of the creatine kinase or replacement of creatine with less active analogues significantly decreases the maximal cardiac performance (Gerken and Schlette, 1968; Kapelko, 1988). Finally, studies based on controlled permeabilization confirmed the existence of adenine nucleotide compartments within cardiac cells. The total nucleotide content per subcellular compartment was 74% in the cytoplasm, 20% in the mitochondria and 6% in other cellular structures (Geisbuhler, 1984).

In conclusion, the experiments described above showed that adenine nucleotides are compartmentalized within the cardiac cells creating different functional pools of ATP interconnected by a very precise energy-sensing mechanism. This mechanism seems to mostly respond to changes in PCr content. Posterior investigations led to the discovery and description of phosphoryl transfer networks and the feedback regulation mechanism.

Phosphoryl transfer and signaling networks in regulation of cellular energy homeostasis

In cardiac cells, the intracellular energy transfer is facilitated via networks consisting of phosphoryl group-transferring enzymes such as creatine kinase, adenylate kinase and glycolytic phosphoryl transfer enzymes. Nuclear magnetic resonance spectroscopy measurements revealed that there is a tight correlation between high-energy phosphoryl fluxes through creatine kinase, adenylate kinase and glycolytic phosphoryl transfer tightly correlate with the cardiac work under different workload conditions (Fig. 8) (Pucar et al., 2004). This result evidences the

importance of phosphoryl transfer reactions as main pathways to transport high-energy phosphoryl between the mitochondria (ATP production site) and cellular ATPases at the ATP-consuming sites (mainly at myofibrils, sarcolemma and sarcoplasmic reticulum).

In the experiments of Langendorff-perfused hearts reported in figure 8, the intracellular high-energy phosphoryl transfer flux through PCr-CK pathway increased linearly with cardiac workload (represented by the rate-pressure product, RPP) and achieved a value close to 300 $nmol \cdot min^{-1} \cdot (mg\ protein)^{-1}$ when the cardiac work was about 30,000 $mmHg \cdot min^{-1}$ (Pucar et al., 2004). Therefore, the PCr-CK pathway is considered the major intracellular high-energy phosphoryl transfer flux in hearts under normoxic condition. Indeed, the adenylate kinase and glycolytic systems carry out the remaining 10 - 15 % of intracellular high-energy phosphoryl transfer. Nevertheless, we should take into account that the quantification analysis of flux distribution between different phosphoryl transfer networks is based on the assumption of parallel phosphoryl transfer pathways (no communication between different pathways). In the cellular environment, these pathways are closely co-localized and interconnected allowing high-energy phosphoryl to flow from one system to another (Wallimann et al., 1992; Janssen et al., 2000; Dzeja and Terzic 2003; Dzeja et al., 2004).

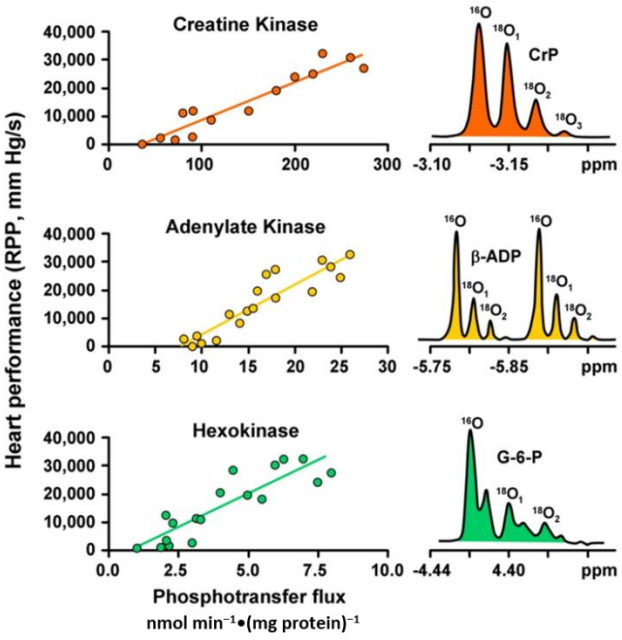

Figure 8. Phosphoryl trasnfer networks mediate coupling between heart function activity and ATP generation. Processing of high-energy phosphoryls through creatine kinase, adenylate kinase and glycolytic (hexokinase) systems correlates linearly with heart functional activity (represented by the rate-pressure product, RPP) (Pucar et al., 2004).

The PCr-CK pathway is schematically represented in figure 9. Creatine kinase is present in the cells as 4 isoenzymes localized in different subcellular compartments: cytosol and mitochondria. The cytosolic CK enzymes consist of two subunits: B (brain type) or M (muscle type), which can be associated in three different ways giving the isoenzymes: MM-CK, BB-CK and MB-CK. The mitochondrial CK (MtCK) occurs in an octameric form contacting the mitochondria inner and outer membrane. MtCK catalyzes the direct transphosphorylation of mitochondrial ATP and cytosolic creatine into ADP and PCr. The ADP produced returns back to the mitochondrial matrix space to stimulate oxidative phosphorylation, giving rise to mitochondrial recycling of a specific pool of ATP and ADP. PCr is the primary high-energy phosphoryl compound that leaves mitochondria to be used by creatine kinase for ATP regeneration *in situ* in the different CK locations within the cell. The close proximity of non-mitochondrial enzyme (MM-CK) with ATPases has the advantage of preventing: the inhibition of the ATPase by ADP and H^+, since they are both substrates of the CK reaction, and the energy dissipation caused by ATP diffusion.

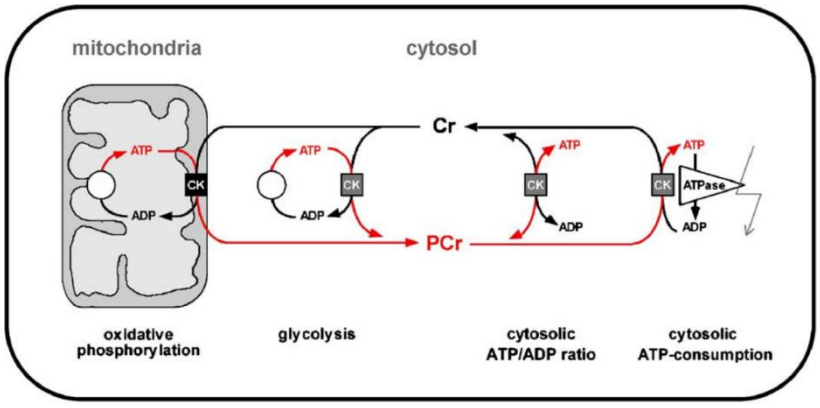

Figure 9. Representative scheme of the PCr-CK pathway. Isoenzymes of CK are localized in different compartments of the cell in soluble form or associated to ATP -delivering or -consuming processes. A large cytosolic PCr pool is built up by CK using Cr and ATP to keep high cytosolic and local ATP/ADP ratios (Schlattner et al., 2006).

2.4. Modular organization of cardiac energy metabolism

Cardiac energy metabolism is organized in structural and functional units called "Intracellular Energetic Units" (ICEU) comprised of a mitochondrion (or several adjacent mitochondria) interacting with surrounding myofibrils, sarcoplasmic reticulum, cytoskeleton

and cytoplasmic enzymes (Saks et al., 2001). ICEU structure (Fig. 10) represents a new type of supramolecular organization that operates at far from equilibrium conditions. They were defined by De la Fuente as cellular metabolic dissipative structures, representing functional enzymatic associations that form a catalytic entity as a whole and carry out their activities in a relatively independent manner (de la Fuente et al., 2008; de la Fuente, 2010). The structural organization of ICEUs results in local compartmentalization of adenine nucleotides in ATP - producing and -consuming sites, which were connected by discrete dynamic energetic circuits called phosphoryl transfer networks (Saks et al., 1998a; Schlattner and Wallimann, 2004; Saks et al., 2004; Saks et al., 2006; Saks et al., 2007b; Dzeja and Terzic, 2003). The efficiency of energy transfer within an ICEU via phosphoryl transfer networks depends on two main factors: 1) the functional coupling of MtCK to ATP Synthase via ANT and 2) the functional compartmentalization of adenine nucleotides in mitochondria (which is controlled by MOM permeability).

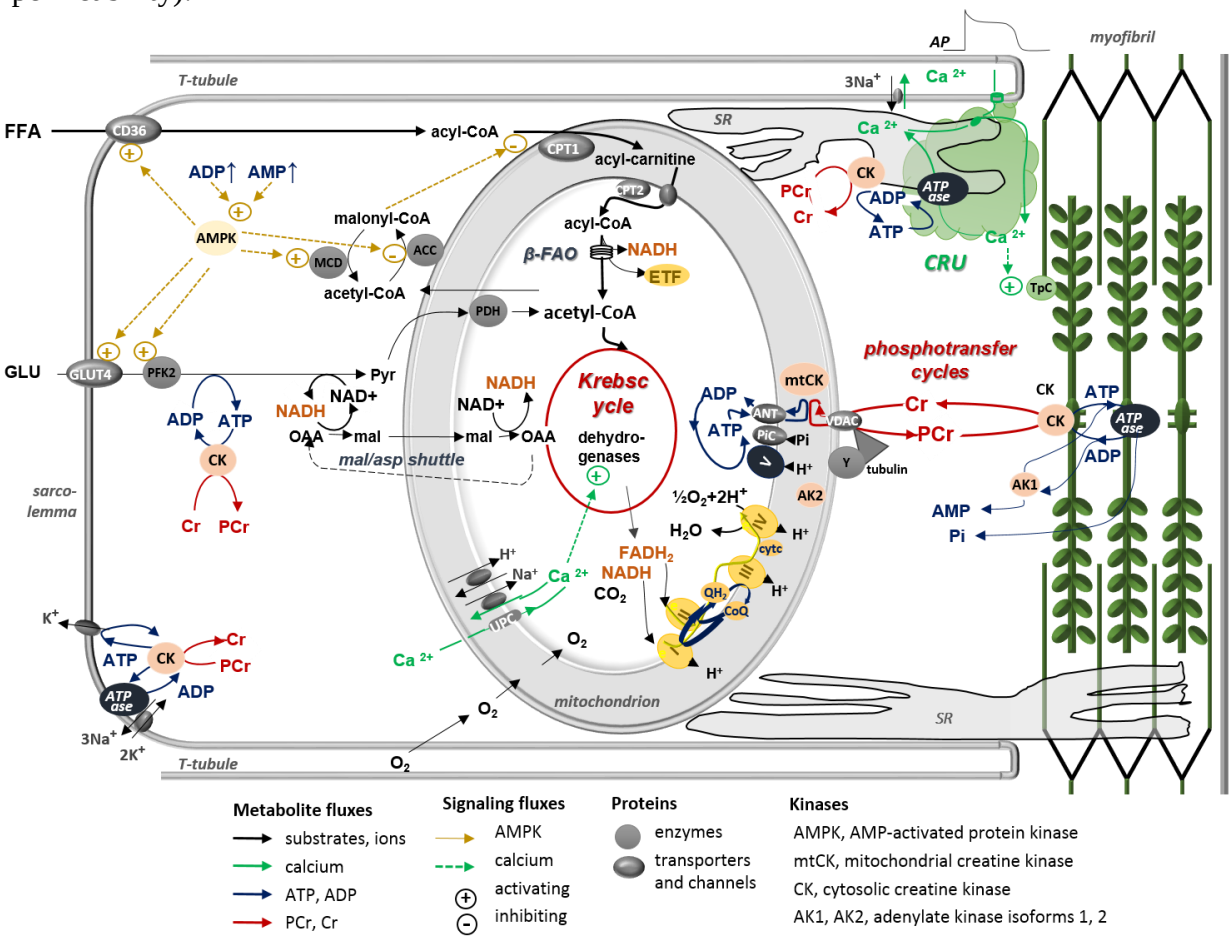

Figure 10. Scheme of the Intracellular Energetic Units in adult cardiomyocytes. The key system in energy transfer from mitochondria to cytoplasm is Mitochondrial Interactosome (MI). MI is a supercomplex, consisting of ATP synthase, adenine nucleotides translocase (ANT), phosphate carrier (PIC), mitochondrial creatine kinase (MtCK), voltage-dependent anion channel (VDAC) with attached cytoskeletal proteins (in particular βII-tubulin). MI controls the tight coupling between ATP/ADP intramitochondria turnover and phosphocreatine (PCr) production. PCr exported from mitochondria is used to locally regenerate ATP by CK localized in the proximity of ATPases (actomyosin ATPase, sarcoplasmic reticulum SERCA and ion pumps ATPases). The rephosphorylation of ADP increases the Cr/PCr ratio which is transferred towards MtCK via CK/PCr system. The shaded area in the upper right corner shows the Calcium Release Unit (CRU). During excitation–contraction coupling, calcium is released from sarcoplasmic reticulum (SR) via calcium-induced calcium release mechanism. The calcium release either activates contraction cycle by binding to troponin C or activates the Krebs cycle dehydrogenases by increasing [Ca^{2+}] in the mitochondrial matrix (Saks et al., 2013).

Mitochondrial Interactosome

In the mitochondrial matrix side, adenine nucleotide translocase forms a supercomplex with ATP Synthase and phosphate carrier (PIC) named ATP Synthasome. This supercomplex is attached to octameric MtCK by electrostatic forces involving three C-terminal lysine residues of MtCK and a negatively charged cardiolipin associated with ANT (Schlattner et al., 2004). The transmembrane supercomplex formed by ATPSynthasome, RC complexes, MtCK, VDAC and cytoskeletal proteins regulating ADP/ATP flux through VDAC was named Mitochondrial Interactosome (MI) (Timohhina et al., 2009; Saks et al., 2012). MI is a key structure in the regulation of high-energy phosphoryl transfer fluxes and metabolic signaling inside the ICEUs since it strongly increases the efficiency of functional coupling of MtCK to ATP Synthasome via ANT (Guzun et al., 2009; Andrienko et al., 2003). In particular, the role of this functional and structural supercomplex is to increase the efficiency of mitochondrial ATP synthesis and cytosolic ATP hydrolysis through the generation of two loops; thus allowing the prevention of energy dissipation by ATP transport (consumption of ATP by competing reactions) and the metabolic signal communication at cellular distances (feedback regulation) (Fig. 9) (Wallimann et al., 1992; Dzeja and Terzic 2003; Tepp et al., 2011; Guzun et al., 2012; Tepp et al., 2010; Saks et al., 2010; Guzun et al., 2011a). One of the loops is the intramitochondrial ATP/ADP flow between ATPsynthase and MtCK. The functional coupling of MtCK to ATP Synthasome allows the direct channeling of ATP produced by ATP Synthase towards the active sites of

MtCK which catalyzes the phosphoryl transfer from ATP to creatine (Wallimann et al., 1992; Schlattner and Wallimann, 2004; Saks et al., 2007a; Vendelin et al., 2004). ADP produced in this reaction can either return back to the mitochondrial matrix via ANT (thus activating oxidative phosphorylation) or leave mitochondria via VDAC (Jacobus and Lehninger, 1973). The flux distribution between these two pathways depends on VDAC permeability for adenine nucleotides and the functional coupling of MtCK to ATP Synthasome. The other loop is the one formed by Cr – PCr between isoforms of creatine kinase localized in different compartments of the cell. PCr produced by MtCK reaction using mitochondrial ATP is exported from mitochondria as the main high-energy phosphoryl compound toward cytosolic CK to locally regenerate ATP. Therefore, PCr restores the local ATP/ADP ratio of the ATPases due to the close vicinity of cytosolic CK enzymes.

Cytoskeleton role on MOM permeability for ADP

The measurements of the apparent Michaelis constant for ADP (app. Km for ADP) in permeabilized cardiomyocytes (mitochondria *in situ*) revealed that this value (about 250-350 µM) is one order of magnitude higher than when it was measured in isolated heart mitochondria (about 10 - 20 µM). The app. Km for ADP is the ADP concentration at which the reaction rate is half of maximal respiration rate, thus reflecting the permeability of MOM to adenine nucleotides. Therefore, this experimental observation suggested that respiration regulation of mitochondria *in situ* could be influenced by the complex structural organization of the cell and by specific interactions of cytoskeletal proteins with mitochondria. Studies removing the possible cytoskeleton-mitochondria interactions using a trypsin treatment showed a drastic decrease in the app. Km for ADP in permeabilized cardiomyocytes after this treatment (from 200-300 µM to 80-40 µM) whereas the app Km for ADP in isolated mitochondria was unaltered (Appaix et al., 2003). These experimental observations proved that cytoskeleton organization

is important for adenine nucleotide diffusion, as well as for respiration regulation because the interaction of cytoskeletal proteins with mitochondria regulates MOM permeability to adenine nucleotides in cardiac cells *in vivo*.

Different cytoskeletal proteins were suggested to participate in the regulation of ATP/ADP flux through MOM by controlling the open and closed state of VDAC, the major porin of the MOM. According to Colombini's model of VDAC, there is a unique open state at 0 mV and two sets of closed states at high potentials (negative or positive). The main features of the closed states are the decreased conductance (about 50 – 60 %), the diminished pore size, and the inverted selectivity (Colombini, 1980; Song et al., 1998; Zimmerberg and Parsegian 1986; Benz et al., 1990). The combination of these modifications envisage the reduction of the negatively charged ATP flux through closed state VDAC. This assumption was confirmed by direct measurements of ATP fluxes through VDAC reconstituted into planar membrane (Rostovtseva and Colombini 1996; Rostovtseva and Colombini, 1997). Consequently, closure of VDAC channels would greatly reduce the diffusion of adenine nucleotides between the intermembrane space and the cytosol. Thus, VDAC could regulate ATP/ADP fluxes through MOM by switching between open and closed states.

One of the cytoskeletal proteins proposed to interact with VDAC either directly or via microtubule-associated protein 2 (MAP2) or plectin is desmin (Leterrier et al., 1994; Reipert et al., 1999). The important physiological role of desmin has been demonstrated in desmin-deficient mice, which display decreased app. Km for ADP, decreased maximal respiration rate and impaired functional coupling of MtCK and ATP Synthasome. Another cytoskeletal protein proposed to interact with VDAC is tubulin since it was shown that αβ heterodimeric tubulin interacts with VDAC and thus controls the ADP/ATP flux through VDAC (Rostovtseva et al., 2008; Monge et al., 2008). The addition of αβ heterodimeric tubulin at nanomolar concentrations (non-polymerized tubulin) causes highly voltage-sensitive reversible closure of

VDAC reconstituted into planar lipid membranes (Rostovtseva et al., 2008). Experiments with isolated mitochondria strongly confirmed the role of αβ heterodimeric tubulin on respiration regulation since the addition of tubulin at non-polymerized concentration (1 – 10 μM) to isolated heart mitochondria increased in one order of magnitude the apparent Km for ADP value (Monge et al., 2008). Our recent immunochemical studies of the distribution of β tubulin isoforms in cardiomyocytes linked this phenomenon to the presence of mitochondria-specific isoform of β tubulin II (Gonzalez-Granillo et al., 2012; Guzun et al., 2011b). Therefore, interaction of αβ heterodimeric tubulin with VDAC in isolated heart mitochondria was described to reduce MOM permeability for adenine nucleotides *in vitro*.

The overall effect of this structural–functional organization of cardiac cells is to increase the compartmentalization of adenine nucleotides in different subcellular compartments and to increase the efficiency of energy transfer via phosphoryl transfer networks. In particular, cytoskeleton-mitochondria interactions play a crucial role on mitochondrial metabolism regulation since they restrict adenine nucleotides diffusion through MOM and enhance the functional coupling of MtCK to ATP Synthasome, (Saks et al., 2008; Saks et al., 2006; Saks et al., 2010; Saks et al., 2007b; Guzun and Saks, 2010; Guzun et al., 2009; Guzun et al., 2011a; Guzun et al., 2011b; Guzun et al., 2015)(Fig. 10).

2.5.Metabolic feedback regulation in cardiac cells

The metabolic feedback regulation mechanism, described using mathematical models, was initially proposed by Aliev and Saks (Aliev and Saks, 1997; Saks et al., 1996; Vendelin et al., 2000; Saks et al., 2000). Mathematical modeling shows that ADP released from cross-bridges is rapidly re-phosphorylated by myofibrillar MM-CK (reaction in non-equilibrium state), producing small but opposite changes in Cr and PCr concentrations. The changes in Cr, PCr and total adenine nucleotides described in these mathematical models are within the range

of the experimental errors, thus giving an overall impression of metabolic stability. However, the cyclic changes of PCr and Cr concentrations during the cardiac cycle described previously were recorded by several authors (Fig. 11B) (Wikman-Coffelt et al., 1983; Honda et al., 2002; Spindler et al., 2001).

The cyclic changes of ADP concentration in ATP-consuming sites immediately displace the cystolic CK reaction towards local ATP regeneration. The amplitude of displacement of CK from equilibrium and the cyclic changes of ADP concentration proportionally increase with workload (Fig. 11A). These cyclic changes are channeled to mitochondria by the intracellular phosphoryl transfer PCr-CK pathway in order to stimulate respiration. However, restricted diffusion of adenine nucleotides through MOM (controlled by cytoskeleton-mitochondria interactions) is required to observe a linear response of mitochondrial respiration to the cyclic changes of ADP. In isolated mitochondria, the regulation of respiration is impossible due to the high apparent affinity of oxidative phosphorylation for ADP (app. Km ADP = 10 – 20 μM). Even in resting conditions, the intracellular ADP concentration (about 40 μM) stimulates respiration close to maximal rates. In contrast, in permeabilized fibers, the apparent Km for ADP is about 250 – 350 μM (ADP diffusion is restricted at the level of MOM) and the respiration rate becomes almost linearly dependent on local ADP concentrations at physiological range ([ADP] = 40 – 400 μM) (Fig. 11C). Under these conditions, cyclic changes in local ADP concentrations within the myofibrillar core become an effective regulatory signal. Moreover, the activation of the functional coupling of MtCK to ATP Synthasome by creatine induces ADP/ATP recycling which will amplify the effect of cytosolic ADP. Consequently, the apparent Km for ADP in the presence of creatine decreases about 5 folds (app. Km for ADP about 50 – 100 μM) (Fig. 11C).

The physiological mechanism of respiration regulation described above has resolved the question raised by Neely's and Williamson's observation (Neely et al., 1972; Williamson et al.,

1976) about which is the mechanism of respiration regulation *in vivo* that could explain the metabolic aspects of the Frank-Starling law.

Figure 11. Mathematical modeling of the respiration regulation in cardiac cells in vivo under physiological conditions

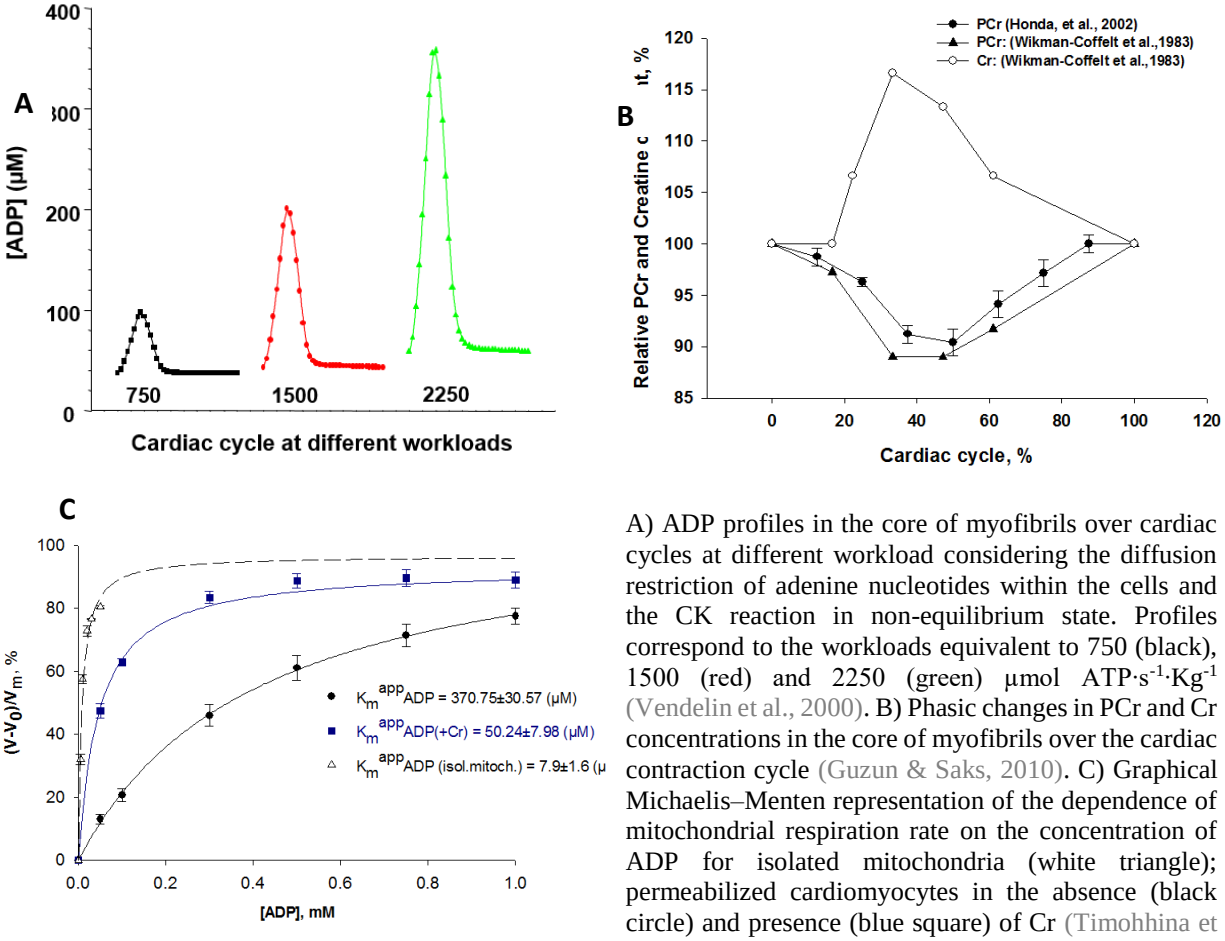

A) ADP profiles in the core of myofibrils over cardiac cycles at different workload considering the diffusion restriction of adenine nucleotides within the cells and the CK reaction in non-equilibrium state. Profiles correspond to the workloads equivalent to 750 (black), 1500 (red) and 2250 (green) μmol $ATP \cdot s^{-1} \cdot Kg^{-1}$ (Vendelin et al., 2000). B) Phasic changes in PCr and Cr concentrations in the core of myofibrils over the cardiac contraction cycle (Guzun & Saks, 2010). C) Graphical Michaelis–Menten representation of the dependence of mitochondrial respiration rate on the concentration of ADP for isolated mitochondria (white triangle); permeabilized cardiomyocytes in the absence (black circle) and presence (blue square) of Cr (Timohhina et al., 2009).

3. Cardiac Energy Metabolism after Ischemia-Reperfusion

Myocardial acute ischemia and reperfusion (IR) decreases mitochondrial OxPhos capacity impairs the compartmentalized intracellular high-energy phosphoryl transfer flux via PCr-CK pathway, thus leading to defects in cardiac performance. Post-ischemic reperfused hearts present a depressed left ventricular developed pressure (LVDevP) and an increased left ventricular end-diastolic pressure (LVEDP). These alterations in LV function depend on the ischemia duration and are associated with reduced mitochondrial function (Makazan et al 2007) and decreased high-energy phosphate compounds (PCr and ATP) content (Dhalla et al 1972; Dhalla et al 1973).

3.1.Mitochondrial function after IR injury

Mitochondrial dysfunction after IR injury has been related to defects in the respiratory complexes I, III, IV and V, and in Krebs cycle enzymes which lead to decreased rates of substrates oxidation (Rouslin 1983; Paradies et al., 2004; Hardy et al., 1991; Lucas and Szweda 1999; Rouslin and Millard 1981; Lesnefsky et al., 1997; Lesnefsky et al., 2001a; Rouslin and Millard 1980; Chouchani et al., 2014). Moreover, complex I (CI) has been identified as a target for oxidative damage in IR injury (Paradies et al., 2004; Hardy et al., 1991; Rouslin and Millard

1981; Rouslin and Millard 1980). Damage to mitochondrial function enhances the production of reactive oxygen species (ROS). In particular, the decreased flux of electron through the respiratory chain increases the reduction of proximal sites in the RC complexes, enhancing the electron leak, and decreases the substrates oxidation, leading to the accumulation of NADH in the mitochondrial matrix. In both cases, these alterations result in an increase in ROS production (Kwong and Sohal 1998; Liu et al., 2002; Paradies et al., 2004). Other mechanism of ROS production is by direct damage to complex I, by interruption of the electron flux due to a defect in the respiratory chain or by reverse electron transfer from complex II to complex I due to the accumulation of succinate during ischemia (Turrens et al., 1991; Lenaz et al., 1999; Lenaz et al., 2000; Chouchani et al., 2014). Ceramide accumulation has been demonstrated in various *in vivo* models of IR and it has been implicated as an important mediator of apoptosis in the injured tissue (Novgorodov and Gudz, 2009). This lipid molecule formed in the endo- and sarco-plasmatic reticulum (Ardail et al., 2003) inhibits complex III activity, thus increasing the production of ROS and predisposing the mitochondria to apoptosis (Gudz et al., 1997; Esposti and McLennan, 1998; Richter and Ghafourifar, 1999).

Enzyme activities of the RC complexes are present in excess relative to oxidative phosphorylation, so decreases in RC enzyme activities of 30–50% are needed to lower the rate of oxidative phosphorylation (Groen et al., 1982; Gellerich et al., 1983a; Borutaite et al., 1995). Recent studies suggest that the decline in mitochondrial OxPhos capacity observed in different disease could be related to a decline in respiratory supercomplex organization (Rosca et al 2008; Rosca et al 2011; Mejia et al 2014). In a canine failing heart model, the decrease of mitochondrial OxPhos capacity was observed in the presence of normal activity for individual RC complexes. In this case, the impairment of mitochondrial function was associated to a decline in supercomplex forms containing complex IV due to post-translational modification of subunits of this complex (Rosca et al 2008; Rosca et al 2011).

3.2.Mitochondrial morphology after IR injury

Mitochondrial cardiolipin content decreased in both *in vitro* (Edoute et al., 1983; Paradies et al., 1999) and *in vivo* (Kayiyama et al., 1999; Vasdev et al., 1980) experimental models of myocardial ischemia. Ischemic damage to cardiolipin is selective because the contents of other mitochondrial phospholipids remain unaltered during ischemia in the isolated rabbit heart (Lesnefsky et al., 2001b). The mitochondrial inner membrane is enriched in cardiolipin, a phospholipid unique to mitochondria (Hoch, 1992) that was shown to be required for stabilizing specific associations between respiratory complexes (Pfeiffer et al., 2003; Zhang et al., 2002; Zhang et al., 2005), as well as, for the functional coupling of MtCK to ATP Synthase via ANT (Schlattner et al., 2004).

The decrease in cardiolipin content occurs in the setting of preserved integrity of the inner membrane measured both by functional and morphologic criteria (Toleikis et al., 1979). However, the viscosity of the inner membrane is increased (Paradies et al., 1999; Ueta et al., 1990), possibly as a consequence of cardiolipin depletion (Paradies et al., 1999). Loss of membrane fluidity decreases the activity of inner membrane transport systems and potentially of RC complexes (Paradies et al., 1993). In addition, the defect in cardiolipin remodeling in patients with Barth Syndrome has been associated with supramolecular organization destabilization (attenuated supercomplex assembly), which was proposed as the mechanism underlying the mitochondrial dysfunction observed in this disease (McKenzie et al., 2006; Gonzalvez et al., 2013). The alteration of cardiolipin species is also observed during the development of the chronic heart failure (CHF) and is associated with the decrease in mitochondrial supercomplex formation and in complex I activity within these supercomplexes (Mejia et al 2014).

Mitochondrial injury defined as matrix depletion, membrane disruption and scrolling is positively correlated with indexes of heart failure severity like left ventricle (LV) end-diastolic pressure and ejection fraction (Sabbah et al., 1992). The Optic Atrophy type 1 (OPA1) has been shown to control the structure of mitochondrial inner membrane and thereby, to regulate mitochondrial resistance to apoptosis induced by reshaping of cristae and cytochrome c release (Scorrano et al., 2002; Frezza et al., 2006; Varanita et al., 2015) and to control physical and functional organization of the RC complexes into respiratory supercomplexes (Cogliati et al., 2013; Civiletto et al., 2015). The expression of this protein was showed to be dropped in human and rodent failing hearts (Chen et al., 2009; Chen et al., 2012), which evidences its potential implication in the mitochondrial dysfunction observed in cardiomyopathies.

3.3. Feedback regulation mechanism after IR injury

Cardiac energy metabolism after IR injury is characterized by a decrease in the apparent affinity of OxPhos for ADP (app. Km for ADP) and in the control of respiration by creatine. The decrease in app. Km for ADP of hearts subjected to ischemia-reperfusion was hypothesized to be related to IR-induced alterations of cellular architecture and loss of intracellular adenine nucleotide compartmentalization (Belmadani et al., 2002; Capetanaki, 2002; Appaix et al., 2003; Andrienko et al., 2003). In addition, the decrease in the control of respiration by creatine, evaluated by the ratio of app. Km for ADP with and without creatine, is related to the reduced functional coupling of MtCK to ATP Synthase. These IR-induced alterations lead to the control of respiration by cytosolic ADP concentration and the attenuation of the intracellular phosphoryl flux transfer via PCr-CK pathways (Pucar et al., 2001). The impairment of this phosphoryl flux transfer pathway causes the accumulation of ADP and H^+ in the cytoplasm due to the reduced capacity of MM-CK to rephosphorylate ADP produced by ATPases, thus leading to an inhibition in ATPases activity. As a result, the mitochondrial function is no longer

regulated by intracellular ATP-demands (i.e. feedback mechanism), resulting in cardiac dysfunction and a decline in the Frank-Starling relationship (For a review see Seppet et al., 2005 and Boudina et al., 2002).

The degree of impairment of phosphoryl flux transfer and the reduction of PCr/ATP ratio has been shown to be an excellent prognostic indicator in CHF patients (Neubauer 2007). The PCr/ATP ratio is considered an index of the energetic state of the heart, which reflects both the mitochondrial ATP production and the efficacy of energy transfer by CK system. The decrease in this ratio is due to the diminishment of PCr content about 50 – 70 % in the early stages of the CHF, although myocardial ATP level is almost preserved until advanced stages of the disease (Weiss et al., 2005; Nascimben et al., 1996). In the case of cardiac IR, the decreased communication between mitochondrial ATP production and ATP-consuming reactions is related to a dimishment of intracellular PCr content (Gudbjarnason et al., 1970; Neely et al., 1973) or a decrease in CK activity and in the MtCK octamer/dimer ratio (Soboll et al., 1999; Sousa et al., 1999). In accordance with these studies, the perfusion of isolated rat hearts with the creatine kinase inhibitor iodoacetamide, prior to hypoxia period, reduces the mitochondrial capacity to regenerate PCr leading to cardiac dysfunction (Hamman et al., 1995). Moreover, mice with genetic ablation of guanidinoacetate methyltransferase (GAMT) (i.e. enzyme that catalyses creatine formation) or M-CK and MtCK are more susceptible to IR injury (Spindler et al., 2004; ten Hove et al., 2005). The results of these publications evidence that an intact CK system is essential for the communication of mitochondrial ATP with ATP-consuming reactions and for the recovery of cardiac function after myocardial IR.

4. Skeletal Muscle Energy Metabolism

Skeletal muscles can be differentiated by their muscle fiber type content in slow twitch oxidative and fast twitch glycolytic skeletal muscles. Muscle fibers can be classified into three main types: ‘slow twitch oxidative fiber’ (type I), ‘fast twitch oxidative’ (type IIA) and ‘fast twitch glycolytic’ fibers (type IIB, IIX). This classification is based on their myosin isoforms content (i.e. defines the myofibrillar ATPase activity and contraction speed), metabolic enzyme pattern and mitochondrial content (Schiaffino, 1996). Slow twitch oxidative muscles display three- to five-folds lower ATPase activity than fast glycolytic muscles since these muscles sustain low intensity workloads for long periods of time. In contrast, fast twitch glycolytic muscles displaying high ATPase activity support high intensity workloads for short periods of time (Delp and Duan, 1996; Kuznetsov et al., 1996).

4.1. Excitation-contraction coupling in skeletal muscles

Skeletal muscles are considered striated muscles since they present a common contractile unit named sarcomere and a similar mechanism of contraction based on the conversion of free energy from ATP hydrolysis (i.e. ATPase reaction) into mechanical energy for contractile function. The striking differences between cardiac muscle and skeletal muscle contraction are the mechanism for contraction activation and for calcium release.

In skeletal muscle fibers, the contraction is stimulated by an action potential driven from a single motor neuron arising in the brain or spinal cord. The action potential travels across the entire sarcolemma and is rapidly conducted into the interior of the muscle fiber by structures called Transverse tubules or T-tubules. The T-tubules are regularly spaced invagination of the sarcolemma that branch extensively throughout the muscle fiber. T-tubules make contact with the SR, where intracellular calcium ions are stored, through a complex of proteins which controls the calcium release from SR. These complexes present a L-type voltage-dependent calcium channels (dihydropyridine receptors, DHPRs) in the T-tubule membrane and a calcium-release channel (ryanodine receptors, RyR type 1) in the adjacent sarcoplasmic reticulum. The voltage sensor changes its conformation in response to the depolarization of the action potential, thus triggering the opening of ryanodine receptors. This rapid influx of calcium into cytoplasm triggers the contraction of the skeletal muscle fibers.

4.2. Skeletal muscle energy metabolism

The implication of mitochondria for ATP production varies between muscle types depending on the contractile pattern. Slow twitch oxidative muscles present high capacity for oxidative phosphorylation (mitochondrial content is about 5 – 10 % respect to total cellular volume), whereas the mitochondrial content in fast glycolytic muscles is about 1% (Delp and Duan, 1996; Kuznetsov et al., 1996). The variation on the amount of mitochondria was considered for a long time the main difference of energy metabolism across fiber types. However, this notion has progressively changed by the observation of fiber type-specific differences in the respiratory regulation and the mechanism coupling mitochondrial ATP production to ATP consumption at different subcellular compartments. These properties were largely uncovered following the development of saponin-permeabilized fibers, which allowed

the study of mitochondria in a relatively preserved cytoarchitectural environment (Kay et al., 1997a; Saks et al., 2010; Saks et al., 1998b).

One of the most striking differences between skeletal muscle-types is that the app. Km for ADP of permeabilized slow twitch oxidative muscle fibers is in the range of 250 – 350 µM, while the app. Km for ADP of permeabilized fast twitch glycolytic muscle fibers is about 10-folds lower (about 10 - 30 µM). The difference in apparent sensitivity of OxPhos for ADP was not explained by a difference in mitochondrial respiratory capacity across muscles types, because isolated mitochondria have been shown to display no fiber type difference for maximal ADP-stimulated respiration. Indeed, isolated mitochondria from different muscle types present similar activities of individual RC complexes and similar maximal activity of components of the oxidative phosphorylation machinery (Armstrong et al., 1984; Glancy and Balaban, 2011). Hypo-osmotic shock decreases the app. Km for ADP of slow twitch oxidative fibers up to values close to that observed in isolated mitochondria and in mitochondria from fast twitch glycolytic muscles (Kuznetsov et al., 1996). Therefore, it was suggested that the high app. Km for ADP observed in permeabilized fibers of slow twitch oxidative muscles is explained by the restricted diffusion of adenine nucleotides through MOM in this muscle type.

Another remarkable feature of skeletal muscles is that they do not present metabolic stability within increased workloads (Hochachka and McClelland, 1997; Kushmerick et al., 1992). During exercise, the increase in oxygen consumption is associated with decreased PCr and increased Pi cellular contents. However, the pattern of these metabolites changes was qualitatively and quantitatively different depending on the skeletal muscle phenotype (Kushmerick et al., 1992). In fast twitch glycolytic muscles, the extent of the chemical changes (PCr and Pi) depended on the stimulation rates and their recovery to initial values (before stimulation) followed first-order kinetics. In contrast, the time courses of PCr and Pi changes, during recovery in the slow twitch oxidative muscles, were faster and they could not be

described by a first-order process. This study suggests that mitochondrial respiration in fast twitch glycolytic muscles is controlled by cytosolic ADP concentration, while in slow twitch oxidative muscles the mitochondrial function is controlled by the feedback mechanism since the recovery kinetics of PCr and Pi were not first order (Kushmerick et al., 1992). These results are consistent with previous studies suggesting different role of CK system depending on the muscle-type contractile pattern (Ventura-Clapier et al., 1998; Newsholme et al., 1978; Brecker and Winters 1988; Kupriyanov et al., 1984). Fast twitch glycolytic muscles display a burst of intense activity at the expense of high-energy compounds reserves, which can exhibit a tenfold change in ATP consumption within few seconds. In this muscle-type, the activity of glycolytic enzymes and cytosolic CK activities as well as the cellular ATP and PCr content are high in order to maintain the high-energy compounds reserves (Ishida et al., 1994; Ventura-Clapier et al., 1998). In contrast, slow twitch oxidative muscles, displaying prolonged or cyclic activity of low intensity, present low CK activity and cellular ATP and PCr content, which indicates that this muscle type relies on simultaneous energy production by mitochondria and energy transfer, rather than on high-energy compounds reserves. In this muscle-type, the function of CK is the intracellular phosphoryl transfer from mitochondria towards ATPases. Therefore, the changes of workload in this muscle-type are reflected by the oxygen consumption and the response time of mitochondria is of the order of a few seconds (Van Beek and Westerhof, 1991; Kushmerick et al., 1992).

5. Objectives of the study

Cellular architecture plays an important role in the energetic homeostasis of highly differentiated cells, among other reasons, because the organization of the cytoskeleton was suggested to be a key factor in the regulation of energy transfer. Among other functions, cytoskeleton is responsible for positioning mitochondria in close vicinity to energy consuming systems (such as myofibrils, sarcoplasmic reticulum or sarcolemmal ions pumps) and for controlling MOM permeability to adenine nucleotides (Capetanaki, 2002; Appaix et al., 2003; Andrienko et al., 2003; Rostovtseva et al., 2008; Monge et al., 2008). Numerous studies have evidenced that cell architecture is different across striated muscles of different phenotypes and is remodeled in pathological conditions such as cardiac ischemia-reperfusion (Ogata and Yamasaki, 1997; Hein et al., 2000; Belmadani et al., 2002; Di Somma et al., 2004; Devillard et al., 2008). In both cases, the difference on cytoskeleton organization was associated to variations of mitochondrial metabolism regulation indicated by apparent sensitivity of OxPhos to ADP, creatine control of respiration and communication between mitochondria and intracellular energy needs (Kushmerick et al., 1992; Seppet et al., 2005; Pucar et al., 2001; Boudina et al., 2002). The alteration of cardiac energy metabolism after ischemia-reperfusion was also associated to a decrease in the mitochondrial OxPhos capacity, which was recently observed in the absence of the decrease in the individual RC complex activity. This

phenomenon was suggested to be explained by a decline in respiratory supercomplex (RCS) organization (Rosca et al., 2008; Rosca et al., 2011).

The working hypothesis of this study is that the changes in structural and functional organization of energy metabolism, including cytoskeleton-mitochondria interactions and respiratory supercomplex (RSC) organization, result in alteration of metabolic compartmentation, respiration regulation and intracellular phosphoryl flux transfer. In the present work, our aim was to study the regulation of mitochondrial activity by β tubulin II interaction with MOM and by RSC organization, under physiological conditions as well as in ischemia-reperfusion in striated muscles. For this purpose, different types of striated muscles (cardiac and skeletal) were used for studying the link between β tubulin II and MOM permeability to adenine nucleotides. In addition, the role of β tubulin II, RSC organization and mitochondrial morphology was studied in the pathophysiological context of cardiac ischemia-reperfusion. The results of this work are compiled in three articles entitled:

1) **Role of mitochondria-cytoskeleton interactions in respiration regulation and mitochondrial organization in striated muscles** (accepted in *Biochimica et Biophysica Acta – Bioenergetics*; February 2014; 1837(2):232-45. doi: 10.1016/j.bbabio.2013.10.011)

2) **The impact of cardiac ischemia/reperfusion on the mitochondria-cytoskeleton interactions** (under revision in *Biochimica et Biophysica Acta - Molecular Basis of Disease*; Manuscript number: BBADIS-15-333)

3) **Respiratory supercomplex organization: an adaptive mechanism in cardiac ischemia-reperfusion?** (article in preparation)

6. Results

6.1. Role of mitochondria-cytoskeleton interactions in respiration regulation and mitochondrial organization in striated muscles

Minna Varikmaa[1,2*], Rafaela Bagur[1,3*], Tuuli Kaambre[4], Alexei Grichine[5], Natalja Timohhina[4], Kersti Tepp[4], Igor Shevchuk[4], Vladimir Chekulayev[4], Madis Metsis[2], François Boucher[3], Valdur Saks[1,4], Andrey V. Kuznetsov[6] and Rita Guzun[1,7]

Accepted in Biochimica et Biophysica Acta – Bioenergetics; 2014 Feb;1837(2):232-45. doi: 10.1016/j.bbabio.2013.10.011.

* ***These authors contributed equally to this work***

[1] INSERM U1055 Laboratory of Fundamental and Applied Bioenergetics, Joseph Fourier University, Grenoble, France

[2] Tallinn University of Technology, Faculty of Science, Centre for Biology of Integrated Systems

[3] Experimental, Theoretical and Applied Cardio-Respiratory Physiology, Laboratory TIMC-IMAG, Joseph Fourier University, Grenoble, France

[4] Laboratory of Bioenergetics, National Institute of Chemical Physics and Biophysics, Tallinn, Estonia

[5] Life science imaging – *in vitro* platform, IAB CRI U823 Inserm, Joseph Fourier University, Grenoble, France

[6] Cardiac Surgery Laboratory, Department of Heart Surgery, Innsbruck Medical University, Innsbruck, A-6020, Austria

[7] Department of Rehabilitation and Physiology, University Hospital Grenoble, France

Running title: Mitochondria-cytoskeleton interactions in striated muscles

Keywords: skeletal muscles, energy fluxes, respiration, metabolic control analysis, intracellular energy units

Conflict of interest: None of the co-authors of this article have any conflict of interest.

Abstract

The aim of this work was to study the regulation of respiration and energy fluxes in permeabilized oxidative and glycolytic skeletal muscle fibers, focusing also on the role of cytoskeletal protein tubulin βII isotype in mitochondrial metabolism and organization. By analyzing accessibility of mitochondrial ADP, using respirometry and pyruvate kinase – phosphoenolpyruvate trapping system for ADP, we show that the apparent affinity of respiration for ADP can be directly linked to the permeability of the mitochondrial outer membrane (MOM). Previous studies have shown that MOM permeability in cardiomyocytes can be regulated by VDAC interaction with cytoskeletal protein, βII tubulin. We found that in oxidative soleus skeletal muscle the high apparent Km for ADP is associated with low MOM permeability and high expression of non-polymerized βII tubulin. Very low expression of non-polymerized form of βII tubulin in glycolytic muscles is associated with high MOM permeability for adenine nucleotides (low apparent K_m for ADP).

Introduction

Striated muscles such as cardiac and skeletal muscles have a common contractile unit named sarcomere and similar mechanism of contraction based on the conversion of free energy of ATP hydrolysis in ATPase reaction into mechanical energy for contraction. In cardiac cells, structural and functional organization of metabolism allowing connection of ATP-consuming sites such as sarcomere, sarcoplasmic reticulum and subsarcolemmal ion pumps with ATP-synthesizing systems was named Intracellular Energetic Units (ICEUs) (Saks et al., 2012; Saks et al., 2007b; Saks et al., 2001). In mitochondria the energy transfer is carried out by Mitochondrial Interactosome (MI) supercomplex (Saks et al., 2012; Timohhina et al., 2009). This complex is situated at the contact sites of the outer and inner mitochondrial membranes (MIM) and is composed of ATP Synthasome (including ATP synthase, coupled to the RC complexes, adenine nucleotide translocase (ANT) and Inorganic Phosphate Carrier, mitochondrial creatine kinase (MtCK) and Voltage Dependent Anion Channel (VDAC), interacting with cytoskeletal protein βII tubulin and possibly with some other cytoskeletal proteins (Saks et al., 2012; Timohhina et al., 2009; Saks et al., 2010; Pedersen et al., 2007). The restriction of adenine-nucleotides diffusion at the level of MOM creates a basis for the compartmentalization of energy transfer within ICEUs (Wallimann et al., 1992; Kay et al., 2000). The intracellular energy flux within ICEUs is supported by phosphocreatine / creatine kinase (PCr/CK) pathway and the transfer of phosphoryl groups mainly occurs via the system of various specifically localized isoenzymes of CK and other phosphoryl-transferring kinases (Saks et al., 2007a; Wallimann et al., 1992; Kay et al., 2000; Saks et al., 2006).

These mechanisms have been shown mostly for cardiac cells, but the information regarding the regulation of respiration and control of energy fluxes in various skeletal muscles is still limited. According to the myofibrillar ATPase activity, enzyme pattern and mitochondrial content, muscle fibers can be divided into three main groups: ‘slow twitch

oxidative fiber' (type I), 'fast twitch oxidative' (type IIA) and 'fast twitch glycolytic' fibers (type IIB, IIX) (Schiaffino et al., 1996). Slow twitch oxidative muscles such as *m. soleus* (consisting of about 84 % type I and 7 % type IIA fibers) display relatively low ATPase activity and large capacity for oxidative phosphorylation with high mitochondrial content (still significantly lower than in the heart) (Delp and Duan, 1996). They are able to sustain low intensity workloads for long periods of time. Fast glycolytic muscles, i.e white portion of rats *m. gastrocnemius* (GW) (consisting of about 92 % type IIB fibers) display three- to fivefold higher ATPase activity than oxidative muscles and are able to support high intensity workloads for short periods of time (Delp and Duan, 1996, Kuznetsov et al., 1996). As a general rule, skeletal muscles consist of mixture of oxidative and glycolytic muscle fibers. For example, red portion of gastrocnemius muscle (GR) is formed of 51 % type I and 35 % type IIA fibers (Delp and Duan, 1996). Relative to the cell volume mitochondria occupy about 35 % in cardiac myocytes, about 6 – 10 % in oxidative and only 1 % in glycolytc skeletal muscle cells (Barth et al., 1992; Ogata and Yamasaki, 1997; Picard et al., 2012). It has been shown that isolated mitochondria from oxidative and glycolytic muscles display similar characteristics. For instance, there are similar maximal rates of ADP-stimulated respiration per mg of mitochondrial protein and similar activities of isolated RC complexes (Armstrong et al., 1984; Glancy and Balavan. 2011). Proteomic analysis of isolated mitochondria has revealed only few differences of protein contents between them (Glancy and Balavan. 2011). However, several experimental studies using cell permeabilization have indicated distinct patterns of mitochondrial regulation in oxidative and glycolytic muscle fibers. Major differences were found in the apparent affinity of oxidative phosphorylation for ADP. In particular, the apparent K_m for ADP in the heart and *m. soleus* has been shown to be an order of magnitude higher than that of glycolytc muscles (Kuznetsov et al., 1996; Kay et al., 1997a; Saks et al., 1995; Saks et al., 1998b). Several recent studies suggested that it can be associated with different permeability of MOM for ADP

regulated by the binding of heterodimeric αβ tubulin to VDAC (Saks et al., 2012; Rostovtseva et al., 2008; Monge et al., 2008; Rostovtseva and Bezrukov, 2008; Rostovtseva et al., 2010; Rostovtseva et al., 2012). Our recent immunochemical studies of the distribution of β tubulin isoforms in cardiomyocytes linked this phenomenon to the presence of mitochondria-specific isoform of βII tubulin (Gonzalez-Granillo et al., 2012; Guzun-Karu et al., 2011).

In the present work, we studied: i) the relationship between the apparent K_m for ADP and MOM permeability in skeletal muscle fibers by estimating respirometrically accessibility of mitochondrial ADP in the presence of excess of PK-PEP trapping system for external ADP, ii) flux control that different MI complexes exert on the total energy flux in oxidative and glycolytic permeabilized skeletal muscle fibers and iii) the dependence of MOM permeability on βII tubulin distribution, considering polymerization-depolymerisation equilibrium of tubulin and mitochondrial arrangement. We hypothesized that the differences in mitochondrial affinity for ADP between oxidative and glycolytic muscles might be explained by different distribution pattern and/or by different free protein content of βII tubulin which may participate in feedback regulation of mitochondrial metabolism.

Material and methods

Laboratory animals and chemicals

Male Wistar rats weighing 150-200g were used in the experiments. The animals were housed at constant temperature (22ºC) in environmental facilities with a 12:12h light-dark cycle. Animal procedures were approved by "*Comité d'éthique pour l'expérimentation animale"* of Grenoble (33_LBFA-VS-01) and National Committee for Ethics in Animal Experimentation (Estonian Ministry of Agriculture)..

Preparation of permeabilized fibers

Rats were anaesthetized with sodium pentobarbital (40-50 $mg \cdot kg^{-1}$) intraperitoneal injection, decapitated and, the muscles of interest was placed into a plastic Petri dish containing ice-cold isolation solution A of the following composition: 10 mM Ca-EGTA buffer (2.77 mM of CaK_2EGTA + 7.23 mM K_2EGTA) free concentration of calcium 0.1 µM, 20 mM imidazole, 20 mM taurine, 49 mM K-MES, 3 mM K_2HPO_4, 9.5 mM $MgCl_2$, 5.7 mM ATP, 15 mM PCr, pH 7.1. Muscle-fibers bundles were separated from each other using extra-sharp antimagnetic forceps under a microscope of a cold light source. To study the regulation of mitochondrial respiration of muscle, fibers were permeabilized by saponin treatment (50 µg/mL) keeping the mitochondrial membranes intact (Saks et al., 1998b; Kuznetsov et al., 2008). The permeabilization procedure was followed by triple wash in ice-cold Mitomed solution containing 0.5 mM EGTA, 3 mM MgCl2, 60 mM K-lactobionate, 3mM KH2PO4, 20 mM taurine, 20mM HEPES, 110 mM sucrose, 0.5 mM dithiothreitol, 2 $mg \cdot mL^{-1}$ fatty acid free BSA, pH 7.1. The aim is to wash out saponin and other metabolites, especially traces of ADP or ATP, and proteases released for damaged lysosomes due to the saponin effect. To protect fibers of the proteolytic effect of lysosomal enzymes during experiments Mitomed is supplemented with 2 $mg \cdot mL^{-1}$ BSA and leupeptin 1µM (Kuznetsov et al., 2012). Studied muscles: soleus; red portion of gastrocnemius muscle (GR), white portion of gastrocnemius muscle (GW), extensor digitorum longus (EDL), left ventricle muscle (LV).

Heart mitochondria were isolated as described previously in (Guzun et al., 2009) using trypsin.

Measurements of oxygen consumption

The rates of oxygen uptake were determined with a high-resolution respirometer (oxygraph-2 K, OROBOROS Instruments, Austria) in Mitomed solution supplemented with 5 mM glutamate and 2 mM malate. These measurements were carried out at 25ºC and taken the

solubility of oxygen as 240 nmol·ml^{-1} (Gnaiger, 2001). The respiration rates of permeabilized cardiomyocytes were expressed in nmol of oxygen consumed per minute per nmol of cytochrome aa3. The content of mitochondrial cytochrome aa3 was measured spectrophotometrically according to the method described previously (Timohhina et al., 2009). Measurements of cytochnrome aa3 content in skeletal muscles were limited by the necessity to increase the amount of the samples because of their lower mitochondrial content. As a result, decreased optical density compromised the quality of cytochnrome aa3 measurements in spectrophotometry. The respiration rates of permeabilized muscle fibers were expressed in nmolO_2·min^{-1}·mg^{-1} dry weight fibers. Wet fibers were dried at 100°C for 24 h. Respiration rates were not compared between different muscles, but inside each muscle fiber-type between ADP- and Cr-stimulated respirations.

One of the most reliable quality tests of the intactness of membrane structures for permeabilized fibers is the cytochrome *c* test used to check the integrity of MOM (Kuznetsov et al., 2008). Measurement of cytochrome c release from mitochondria in permeabilized cells can be studied qualitatively by Western blot and quantitatively by spectrophotometry. Western Blot analysis is highly specific for cytoschrome c, but it's time-consuming and requires separate labelling of isolated mitochondrial and cytosolic fractions. Isolation of mitochondria embedded into muscle fibers cytoskeleton gives two fractions: light or damaged mitochondria with increased MOM permeability and cytochrome c release and intact mitochondria. Time is also very important factor because the aim of the cytochrome c release study is to select permeabilized fibers with intact mitochondria for the measurements of oxygen consumption. Permeabilized fibers or cells were used for respirometry studies during first three hours after permeabilisation. Appaix et al., (2000) developing method of spectrophotometric measurement of cytochrome c in permeabilized cells showed that their results were equal to those of oxygraphic determination of cytochrome c-dependent respiration of permeabilized

cardiomyocytes (Appaix et al., 2000). This experiment is carried out in KCl-solution (125 mM KCl, 20 mM HEPES, 5 mM KH2PO4, 3 mM Mg acetate, 0.4 mM EGTA, 0.3 mM DTT) supplemented with respiratory substrates (glutamate and malate) and 2 mM of ADP to get the maximal rate of respiration. Cytochrome *c* is a highly soluble hemoprotein of the respiratory chain that transfers electrons and is loosely associated with the outer side of the inner mitochondrial membrane. If MOM is disrupted, cytochrome c leaves mitochondria decreasing maximal respiration rate and consequently, in this situation its addition in presence of ADP will increase respiration rate. Fig. 1A shows high maximal rates of ADP-stimulated respiration and high respiration control ratio (RCR) which is estimated by the ratio between maximal ADP-stimulated and basal respiration rates (V_{maxADP} / V_0), and indicats preserved flux through the electron transport chain after saponin permeabilisation. Subsequently, the addition of carboxyatractyloside (CAT) gives us information about the integrity of mitochondrial inner membrane (MIM). CAT inhibits in irreversible way ANT interrupting ATP/ADP exchange between mitochondrial matrix and intermembrane space. Therefore, if MIM is intact, addition of CAT decreases oxygen consumption rate back to initial level. In our experiments only fibers with intact mitochondria and with a high maximal rate of respiration were used for experiments. All experiments were performed in the presence of proteases inhibitor in order to avoid the influence of lysosomal proteolysis on kinetic parameters described by Perry et al., (Kuznetsov et al., 2012; Perry et al., 2011).

Determination of flux control coefficients

Metabolic Control Analysis (MCA) allows quantitative determination of the degree of control that a given enzyme exerts on metabolic flux (Groen et al., 1982; Fell, 1992). To understand mechanisms by which a given enzyme exerts high or low control on metabolic pathway, its flux control coefficient (FCC) is evaluated. The flux control coefficient is the

degree of control that the rate (v) of a given enzyme i exerts on flux J. Groen in 1982 derived a method to determine experimentally the FCC using titration curves with specific enzyme inhibitors. As the amount of inhibitor tends to zero the response of the flux to the inhibitor can be expressed in MCA terms (Groen et al., 1982). The flux control coefficient of enzyme i on flux J is given by the symbol $C_{V_i}^J$ and defined according to the equation (Fell, 1992):

$$C_{V_i}^J = \left(\frac{dJ}{dv_i}\right) \Big/ \left(\frac{J}{v_i}\right) = \frac{d\ln J}{d\ln v_i}$$

in which (dJ/dv_i) describes the variation in flux (J) when an infinitesimal change takes place in the enzyme i concentration or activity. In practice, the infinitesimal changes in v_i are undetectable, and hence measurable noninfinitesimal changes are undertaken. If a small change in v_i promotes a significant variation in J, then this enzyme exerts a high flux control. In contrast, if a rather small or negligible change in the flux is observed when v_i is greatly varied then the enzyme does not exert a significant flux control. For the case of irreversible specific inhibitor, an estimation of FCC value is given by Groen et al., (1982) and Moreno-Sanches et al., (2008) as (Groen et al., 1982; Moreno-Sanchez et al., 2008):

$$C_{V_i}^J = \left(\frac{\Delta J}{\Delta I}\right) * \left(\frac{I_{max}}{J_0}\right)$$

where ($\Delta J/\Delta I$) is initial slope of the stepwise inhibition of oxygen respiration graph, I_{max} is the inhibitor concentration giving complete inhibition, and J_0 is the initial steady-state flux value. The flux control coefficients in permeabilized skeletal fibers were determined by using graphical method described by Fell (Fell, 1992).

The inhibitors used in our work and considered as pseudo-irreversible and non-competitive in these conditions were: carboxyatractyloside (CAT) for ATP/ADP transporter, oligomycin for ATP Synthase, rotenone for complex I, antimycin-A (ANM) for complex III, sodium cyanide (NaCN) for complex IV and 1-Fluoro-2,4-dinitrobenzene (DNFB) for MtCK. The respiration rates were measured in the presence of glutamate, malate and succinate. High

quality fibers preparations with respiratory control ratio (RCR = V_{maxADP} / V_0) and acceptor control ratio (ACR = $V_{max(ATP+Cr)}$ / V_0) higher than five were used (Table 2).

Western blot analysis

Free and polymerized tubulin were assessed using Microtubule/Tubulin In Vivo Assay Kit (Cytoskeleton). Tissue powder was suspended in 37^{0}C microtubule stabilization buffer (5 mM MgCl2, 1 mM EGTA, 0.1 mM ATP, 100 mM PIPES, 30% glycerol, 0.1% Nonidet-P40, 0.1% Triton X-100, 0.1% Tween-20, 0.1% β-mercaptoethanol, 0.001% antifoam, 0.1% BME, pH 7.4, Complete Protease Inhibitor Coctail (Roche)), homogenized using 25G syringe and centrifuged at 37^{0}C for 5 minutes at 2000*g. Supernatants were centrifuged at 100000*g for 30 min at 37^{0}C to yield supernatant containing free tubulin and pellet containing polymerized tubulin. The pellet was resuspended in Brinkley buffer (80 mM PIPES, 1 mM $MgCl_2$, 1 mM EGTA) containing 4M urea, incubated on ice for 45 min and centrifuged at 12000 g for 10 minutes to remove any unsoluble material. The protein concentration was determined using the Pierce BCA Protein Kit. For assessment of MtCK expression, only soluble protein extract was used. Protein samples were resuspended in 1x SDS sample buffer containing 10% β-ME, heated at 95 °C for 5 min and 50 µg of protein was loaded onto 12 % polyacrylamide gels. Electrophoresis was performed on the Mini Protean II from BioRad on in the Tris-tricine buffer solution. Blotting of the unstained gels was performed on the Trans-Blot SD Semi-Dry Transfer Cell (BioRad) using PVDFmembranes (Millipore). The blotting buffer contained 48 mM Tris, 39 mM glycine, 0.1% SDS and 20% methanol. Equal protein transfer was verified by staining membrane with Ponceau solution (0.1% Ponceau S in 5% acetic acid). The membranes were blocked for 1 h in 3% BSA PBS or 0.5% skimmed milk, 0.05% Tween-20 PBS solution and treated with 1:250 rabbit polyclonal anti-MtCK (Abcam), 1:250 mouse monoclonal anti-βII tubulin (Abcam) and 1:500 rabbit polyclonal anti-β-tubulin (Abcam) antibodies 2 h at room

temperature. Immunoblots were detected by 1:45000 anti-mouse or 1:1000 antirabbit secondary antibodies conjugated to peroxidase (IgG HRP; Abcam). Detection was conducted using chemiluminescence kit (SuperSignal West Dura Extended Duration substrate).

Immunolabelling of muscle fibers

Labelling of cytoskeletal and mitochondrial proteins was performed on intact rat skeletal or heart left ventricular muscle fibers in suspension. Fibers were fixed in 4% paraformaldehyde in PBS at 37ºC for 15min. For immunolabelling of mitochondrial proteins (VDAC, MtCK) heat-mediated antigen retrieval was performed by incubating fibers in Antigen Retrieval Buffer (10 mM Tris, 5 % urea, pH 9.5) at 95ºC for 3 min. After washing with PBS fibers were permeabilized with 1 % Triton X-100 at room temperature for 30 min., washed again with PBS, and blocked in PBS solution containing 2% BSA (bovine serum albumin) for 60 min at 25ºC. Subsequently fibers were incubated overnight with primary cytoskeletal and mitochondrial antibodies. Monoclonal mouse anti-tubulin βII(β2) antibody (Abcam, ab28036) at 1:250, mouse anti-α-actinin antibody (Abcam,) at 1:250, and polyclonal rabbit VDAC antibody serum (kindly provided Dr. Catherine Brenner, Universite Paris-Sud, Paris, France) at 1:1000 were used. Next day samples were rinsed 3 times for 3 min in 2 % BSA solution, and stained for 2 h at room temperature with secondary antibody DyLight 488 goat anti-rabbit IgG (Abcam, ab96899) at 1:250 and Dylight 549 goat anti-mouse IgG (Abcam, ab96880) at 1:250. After washing three times with 2 % BSA PBS solution and once with bidistilled water, fibers were mounted in ProLong® Gold Antifade Reagent with DAPI (LifeTechnologies), deposited on glass coverslips and observed by confocal microscope.

Confocal microscopy and 3D modeling

The fluorescence images were acquired by Zeiss LSM 510 confocal microscope (Carl Zeiss) equipped with a Plan-Apofluar 63x/1.30 glycerol objective. Laser excitation 488 nm was used for DyLight 488with emission detected through a 505- to 530 band-pass filter, DyLight549 was excited at 561 nm and detected through 575- to 615 nm band-pass filter. Pinhole was adjusted to the optical slice thickness 0.27 μm for both channels. Processing of all confocal data sets were done with LSM Image Browser software performing rotation, cropping, linear contrast adjustment, channel balancing and addition of scale bar. Images presented were copy–pasted from LSM Image Browser to Photoshop CS4 without further modifications. Confocal images were collected at least 0.5 μm below the sarcolemma. Reconstruction of a 3D-model was done with Imaris software (Bitplane) using 6-7 image stacks acquired with z-step 0.27 μm. Confocal images were collected at least 0.5 μm below the sarcolemma.

Results

Inter-relationship between the apparent affinity of mitochondrial respiration for ADP and MOM permeability

The apparent affinity of mitochondrial respiration for ADP was estimated by measuring ADP concentration reaching half-maximal rate of respiration (i.e. apparent affinity Michaelis constant, K_m). The apparent K_m for ADP in oxidative soleus muscle fibers was high (~ 300 μM, Table 1, Fig. 1B) and comparable with that of cardiomyocytes. Conversely, the apparent K_m for ADP in glycolytic GW and EDL muscle fibers was very low (~ 4 - 7 μM, Table 1, Fig. 1B) and comparable with that of isolated mitochondria. Red portion of *m. gastrocnemius* was characterized by intermediate K_mADP (about 150 μM) due to its mixed composition of slow- and fast-twitch muscle fibres. It was assumed that different apparent affinity of respiration to ADP could be explained by the restriction of ADP diffusion at the level of MOM.

The permeability of MOM was studied respirometrically measuring changes of respiration rate induced by the leakage of ADP from mitochondria. Fig. 1A summarizes main experimental conditions necessary for studying the relationship between the affinity of mitochondria respiration for ADP and MOM permeability. One of the main conditions is the equal maximal rate of creatine- ($V_{max(ATP+Cr)}$) and ADP-stimulated respiration (V_{maxADP}) measured in the presence of a saturating concentration of ADP. This similarity means that all ADP produced in MtCK reaction is returned back to matrix to stimulate respiration. As shown in Fig. 1A and Table 1 the maximal rates of ADP- and creatine-stimulated respiration are similar for each studied fiber-type. Fig. 2A shows the experimental protocol for studying ADP-fluxes through MOM in permeabilized cells. The addition of exogenous ATP stimulates mitochondrial respiration due to the production of endogenous ADP in ATPase reactions. Respiration rate stabilizes because of the establishment of the steady state between ADP production (in myofibrillar and sarcolemmal ATPase reactions) and oxidative phosphorylation. The subsequent addition of creatine in the presence of exogenous ATP enhances respiration rates due to the additional source of endogenous ADP generated by the MtCK reaction in intermembrane space. In this case, the respiration rate is activated and stabilized due to the recycling of ADP in mitochondria between MtCK, ANT and the mitochondrial matrix. In all cases stabilized respiration rate means steady state. In the absence of PK-PEP system, ADP issued from ATP hydrolysis in ATPase reactions and from MtCK reaction is available for mitochondrial matrix. The PK-PEP system can decrease respiration rate by phosphorylating ADP into ATP. In experiments with permeabilized cardiomyocytes and oxidative soleus muscle fibers creatine (Cr) was added concomitantly with ATP (Fig. 2B, C). In experiments with permeabilized glycolytic GR, GW and EDL muscle fibers creatine was added after the stabilization of respiration rates in the presence of exogenous ATP (Fig. 2D-F). Separate addition of creatine allowed us to highlight its role in the control of respiration in GR, GW and

EDL muscles characterized by low MtCK expression (Western blot analysis from Fig. 1C). The addition of PK-PEP to permeabilized cardiomyocytes and soleus muscle fibers did not inhibit significantly the maximal rate of creatine-stimulated respiration (Fig. 2B and C). In contrast, in permeabilized GR, GW and EDL muscle fibers, the addition of PK-PEP system decreased creatine-stimulated respiration by about 50% (Fig. 2D-F).

Fig. 3 shows the relationship between PK-PEP inhibition of creatine-stimulated respiration, which is used to bring to evidence the MOM permeability and the apparent K_m for ADP in different permeabilized muscle fibers and cardiomyocytes in comparison with isolated heart mitochondria. To compare the inhibition effect of PK-PEP in muscle fibers with different amount of mitochondria and proteins, we expressed it as a percentage of the maximal Cr-stimulated respiration rate (Fig. 3A). Very low inhibition of Cr-stimulated respiration by PK-PEP system in permeabilized cardiomyocytes and oxidative soleus muscle fibers (about 2-5%, Fig. 3A) is related to high apparent Km for ADP (Fig. 3B). In contrast, the low app. K_m for ADP in GW and EDL muscles is associated with high ADP-trapping effect of PK-PEP system (Fig. 3A and B). The red portion of gastrocnemius muscle, due to its mixed composition of fiber-types, has an intermediate apparent KmADP between that of oxidative and glycolytic fiber-types and a high PK-PEP inhibition.

Study of energy fluxes in permeabilized skeletal muscle fibers using Metabolic Control Analysis

The quantitative study of the control that the RC complexes (I, III, IV), ANT and ATP synthase exert on the energy flux in oxidative soleus and glycolytic GW permeabilized muscle fibers was performed using Metabolic Control Analysis under conditions of ADP-stimulated respiration. Additionally, the role of MtCK in the control of energy flux in soleus permeabilized muscle fibers was studied using experimental setting described in Fig. 2A (i.e. Cr-stimulated respiration). We could not apply the same protocol to GW muscle fibers because of the

inhibitory effect of PK-PEP on creatine-stimulated respiration. After the addition of PK-PEP system, the resultinglower level of creatine- in comparison with ADP- stimulated respiration did not allow us to compare the flux control coefficients of the same complexes measured under both conditions.

Fig. 4A and B show two respirometry traces and Fig. 4C summarizes statistics of the oligomycin stepwise inhibition of ADP- (Fig. 4A) and Cr-stimulated respiration (Fig. 4B) in permeabilized soleus muscle fibers. The inhibition of the initial (J_0) flux in the presence of activated MtCK, which was faster and induced with lower amounts of oligomycin, indicates to the higher control that ATP synthase exerts on the flux when respiration is controlled by Cr in comparison with direct control by ADP (Fig 4A-C, Table 2). Similarly higher FCC in the presence of activated MtCK in comparison with ADP-stimulated respiration was found for ANT (Fig. 4E, Table 2). High Flux Control Coefficients of respiratory complexes (I, III, IV) indicate their relevance in the control of the metabolic flux (Fig. 4, Table 2). Table 2 additionally shows Flux Control Coefficients of all studied complexes for permeabilized soleus and GW muscle fibers. Concentrations of rotenone, antimycin and oligomycin necessary to achieve the maximal rates of inhibition of ADP-stimulated respiration were in good agreement with previously published data (Table 2) (Kuznetsov et al., 1996; Wisniewski et al., 1995; Kuznetsov et al., 1997; Kunz et al., 2000; Fritzen et al., 2007). Flux Control Coefficients of ATP synthase and ANT estimated for soleus muscle fibers were also consistent with previously reported results. Conversely, Flux Control Coefficient of complex IV (NaCN titration) estimated for *m. soleus* fibers was higher than reported in literature (Tashiro and Komiya, 1989). This difference can be explained by higher initial flux (J_0) due to the utilization of respiratory substrates for complexes I and II. The strong dependence of control coefficients on the flux was previously described by Kunz et al., (Kunz et al., 2000). The sum of Flux Control Coefficients in both muscle-types and under ADP- and Cr-stimulated respiration largely

exceeding unity suggests organization of the RC complexes I, II, IV, ATP synthase and ANT into supercomplex (Table 2).

The expression and distribution of βII tubulin in striated muscle fibers

According to several recent reports the MOM permeability for adenine nucleotides is governed by the interaction of VDAC with heterodimeric tubulin (Rostovtseva et al., 2008; Monge et al., 2008; Rostovtseva and Bezrukov, 2008; Rostovtseva et al., 2010; Rostovtseva et al., 2012; Gonzalez-Granillo et al., 2012; Guzun et al., 2011b). The expression of free and polymerized βII tubulin was assessed by Western Blot analysis. The content of free βII tubulin was highest in oxidative heart and soleus muscles, whereas in mixed-type GR and glycolytic EDL and GW muscles its levels are markedly lower (Fig. 5A). To assess the content of polymerized βII tubulin, extraction of cold-insoluble tubulin in up to 2 mM $CaCl_2$ or 4M urea containing resuspension buffer was tested. In both cases, no polymerized βII tubulin was detected in skeletal muscles and only minor levels were observed in heart muscle (Fig. 5A). Similar observation was reported earlier for nerve axons, where large amounts of tubulin were left unextracted with high concentration of urea, Ca^{2+}, colchicine, and nocodazole (Tashiro and Komiya, 1989). Of note, βII tubulin isoform accounts for over 50% of total β-tubulin present in nerve axons (Banerjee et al., 1988). Since quantitative estimation of polymerized to free βII tubulin ratio of was not possible due to its scarcity in glycolytic muscles, we analyzed additionally the content of total β tubulin. Both forms of free and polymerized β tubulin were higher in heart and oxidative soleus muscles than in GR, EDL and GW (Fig. 5A). The densitometric analysis showed that polymer to dimer ratio of total β tubulin is allmost equal across muscle fiber types with estimated values as follows:heart 0.06±0.015; soleus 0.074±0.03; GR 0.043±0.007; EDL 0.066±0.01 and GW 0.034±0.005 (Fig. 5B).

Intracellular localization of βII tubulin relative to mitochondria was studied using co-immunolabelling of fixed muscle fibers with antibodies for βII tubulin and for mitochondrial protein VDAC, and assessed their localization by confocal microscopy. The presence of βII tubulin was detected in all studied muscle fiber types, including EDL and GW. In heart and soleus muscle fibers βII tubulin apperead as thick segregated bundles alined closly to mitochondria between Z-lines as shown in Fig. 6A-C, D-F and further highlighted in higher magnification image of heart fibers in Fig.G-I. In gastrocnemius and EDL muscle fibers (image shown only for GW muscle fibers) βII tubulin is seen as thin continuous filaments situated at Z-lines and similarly to heart and soleus covered by mitochondria (Fig. 8A-C, E-G, D, H, I).

Co-immunolabelling of β-tubulin and α-actinin showed that in oxidative muscles β-tubulin is concentrated entirely at the area between Z-lines, similarly to βII isoform, while in GW and EDL (image shown only for GW) two subpopulations of β-tubulins are present (Fig.9). One at the level of Z-lines, similarly to βII tubulin, and second at the level of A-band, as in oxidative muscles.

All together these results lead us to believe that differences in MOM permeability for ADP stem from the variances in expression levels of βII tubulin relative to mitochondria.

Discussion

The apparent K_m for ADP in permeabilized cardiomyocytes and oxidative soleus muscle fibers is an order of magnitude higher than in glycolytic GW and EDL muscles (Table 1, Fig. 1B) (Kuznetsov et al., 1996; Appaix et al., 2003). We hypothesized that the differences in mitochondrial affinity for ADP between oxidative and glycolytic muscles might be explained by different distribution pattern and/or by different free protein content of βII tubulin.

Inter-relationship between the apparent affinity of mitochondrial respiration for ADP and MOM permeability

The dependence of the apparent affinity of respiration for ADP on the MOM permeability was previously hypothesized based on kinetic analysis of respiration control by ADP (Kuznetsov et al., 1996). We studied ADP fluxes through MOM in permeabilized fibers using PK-PEP system which competes with oxidative phosphorylation for ADP produced in mitochondrial intermembrane space by activated MtCK reaction (Gellerich et al., 1983b). In glycolytic gastrocnemius and EDL muscles, characterized by low apparent K_mADP the addition of PK-PEP system decreased Cr-stimulated respiration by about 50 % of $V_{max(ATP+Cr)}$ (Fig. 3B). Effect observed in glycolytic muscles can be due to neither saponin permeabilization nor low MtCK expression. MOM intactness was confirmed by the absence of stimulatory effect of exogenous cytochrome c on the maximal ADP-stimulated respiration rate. Using electron microscopy it was shown that 100 µg/mL of saponin used to permeabilized cells for 30 min did not alter MOM connections with cytoskeleton (Lin et al., 1990). However, taking into account that by removing cholesterol from lysosomal membranes, saponin hypothetically could increase cytoskeleton proteolysis, all experiments were lead in the presence of protease inhibitors (Kuznetsov et al., 2012; Perry et al., 2011). Low MtCK expression in glycolytic muscles is another factor capable of influencing Cr-stimulated respiration. However, it was shown that the low expression of MtCK in *m. gastrocnemius* is related to the low volume that mitochondria occupy in this muscle fibers (Qin et al., 1999). Fig. 1A shows that the maximal rate of Cr-stimulated respiration was identical for each muscle fiber-type with the maximal rate of ADP-stimulated respiration. This means that activated MtCK efficiently stimulates respiration in the absence of trapping system for ADP.

Fig. 3B shows that isolated heart mitochondria with low apparent Km for ADP (i.e. high apparent affinity of respiration for ADP) display high PK-PEP inhibition. In spite of saponine

permeabilisation, cardiomyocytes have high apparent Km for ADP (i.e. low apparent affinity of respiration to ADP) and also low PK-PEP inhibition. In permeabilized cardiomyocytes and oxidative soleus muscle fibers the addition of PK-PEP inhibited Cr-stimulated respiration by only 2-5 % of $V_{max(ATP+Cr)}$ (Fig. 3B). Very low inhibition of Cr-stimulated respiration in the presence of trapping system for ADP can be explained by restricted diffusion of adenine nucleotides at the level of MOM. These results confirm the hypothesis linking the apparent K_m for ADP and MOM permeability.

Study of energy fluxes in permeabilized skeletal muscle fibers using Metabolic Control Analysis

Restricted diffusion of adenine nucleotides at the level of MOM in permeabilized cardiomyocytes increases mitochondrial compartmentation and control of respiration by creatine (Saks et al., 2012; Saks et al., 2007b; Timohhina et al., 2009; Wallimann et al., 1992; Kuznetsov et al., 1996; Saks et al., 1995; Guzun et al., 2009; Tepp et al., 2010). The role of MOM permeability in the distribution of mitochondrial energy flux in skeletal muscle fibers was studied using the method of Metabolic Control Analysis (Groen et al., 1982; Fell, 1992; Moreno-Sanchez et al., 2008; Wisniewski et al., 1995; Kuznetsov et al., 1997; Kunz et al., 2000; Fritzen et al., 2007). The Metabolic Control Analysis allows the estimation of the Flux Control Coefficients that each metabolic pathway component exerts on the metabolic flux (Groen et al., 1982; Fell, 1992; Moreno-Sanchez et al., 2008).

In oxidative soleus muscle fibers flux control coefficients of ATP synthase and ANT were higher under Cr- than ADP-stimulated respiration (Table 2). The increase of Flux Control Coefficients under Cr-stimulated respiration was described previously for permeabilized cardiomyocytes and explained by the ADP-recycling in MtCK reaction (Tepp et al., 2010). In this case respiration was supported by small amounts of ADP continuously regenerated by MtCK within the intermembrane space which can be favored by two factors: MtCK-ANT

functional coupling allowing direct ADP transfer to ATP synthase and adenine nucleotides micro-compartmentation due to their restricted diffusion through MOM. Due to high MOM permeability, initial flux of Cr-stimulated respiration of permeabilized GW muscle fibers measured after the addition of PK-PEP was lower than that of ADP-stimulated respiration making impossible comparison of Flux Control Coefficients between both conditions for this muscle-type.

In the case of a linear metabolic pathway, the sum of FCCs does not exceed a unit (Lenaz and Genova 2010; Lenaz et al., 2010). In our experiments the sum of Flux Control Coefficients of respiratory complexes (I, III and IV), ANT and ATP synthase estimated under conditions of ADP-stimulated respiration was higher than 1 in both permeabilized soleus and GW muscle fibers (Table 2). According to Lenaz et al., the sum of FCC exceeding unity can be explained by the spatial organization of respiratory complexes as supramolecular associations rather than randomly dispersed complexes in mitochondrial inner membrane (Lenaz and Genova 2010; Lenaz et al., 2010). According to the 3D molecular reconstruction of complexes I, III and IV, the ubiquinone and cytochrome c binding sites are facing each other favoring direct electron channeling (Vonck and Schäfer, 2009; Schäfer et al., 2007). Additional association of ATP synthase, ANT and phosphate carrier to the respiratory chain supercomplex was proposed by many authors (Schäfer et al., 2007; Schägger and Pfeiffer, 2001; Schägger et al., 2004) and used to explain the regulation of mitochondrial energy fluxes in cardiomyocytes (Saks et al., 2012; Timohhina et al., 2009). One of the main properties of supramolecular assemblies is assumed to be the direct electron channeling between complexes resulting in the increase of oxidative phosphorylation efficiency, prevention of the excessive oxygen radical formation and stabilization of individual complexes by supramolecular assembly (Schäfer et al., 2007; Schägger et al., 2004; Genova et al., 2008). The supercomplex formation with direct electron flow between protein-bound CoQ instead of the lateral diffusion of CoQ is highly dependent

on the properties and composition of membrane (Hackenbrock et al., 1986). In spite of saponine permeabilization, there is no risk of supercomplex formation due to the alteration of MIM fluidity. Saponin removes cholesterol from membranes due to its hydrophobic steroid core. The main constituent lipid of MIM is cardiolipin which cannot be removed by saponin. Otherwise inhibition of ADP-stimulated respiration up to V_0 by atractylosyde was used to confirm the integrity of mitochondrial inner membrane.

Role of cytoskeletal proteins in regulation of respiration in skeletal muscle fibers

In spite of broadly similar structure and embedment of mitochondria into cytoskeleton in oxidative and glycolytic striated muscle fibers, the apparent affinity of mitochondrial respiration for ADP is different (Fig. 1B, Table 1). This difference, as we have shown above, depends on MOM permeability. Based on our previous results showing tubulin-dependent increase of the apparent Km for ADP in isolated heart mitochondria (Rostovtseva et al., 2008; Monge et al., 2008; Rostovtseva and Bezrukov, 2008; Rostovtseva et al., 2010; Rostovtseva et al., 2012), we hypothesized that MOM permeability in skeletal muscles could also be regulated by βII tubulin.

Bernier-Valentin was the first to show in 1982 that heterodimeric tubulin binds to VDAC decreasing MOM permeability to ADP in isolated heart mitochondria (Bernier-Valentin and Rousset, 1982). Further evidence for direct tubulin-mitochondria interaction came from co-immunopreciptation experiments with different non-cancerous and cancerous cell lines evidencing complexation between tubulin and VDAC (Carre et al., 2002). Finally, the influence of free tubulin on mitochondrial metabolism was showed in experiments with depolymerization of tubulin in cancerous hepatoma cells which increased mitochondrial membrane potential (Maldonado et al., 2010).

In our experiments, the expression of the total β tubulin accounting for non-polymerized and polymerized forms is in line with the results observed earlier, being higher in oxidative and lower in glycolytic muscles (Guerrero et al., 2010). The expression of non-polymerized βII tubulin is high in heart and oxidative soleus muscle, low in the red portion of *m. gastrocnemius* and very low in the white portion of gastrocnemius and in EDL muscles (Fig. 5A, B). We hypothesized that free non-polymerized βII tubulin may participate in the regulation of MOM permeability in oxidative muscle fibers, while polymerized form of βII tubulin could be involved in mitochondrial organization. Evidence for the preferential expression of βII tubulin in tissues with oxidative phenotype has been reported already before. In addition to its abundance in heart and oxidative skeletal muscles, high expression of βII tubulin was found in brain and testis (Leandro-Garcia et al., 2010; Nakamura et al., 2003; Narishige et al., 1999). High expression of βII tubulin in sinaptosomes was associated with high apparent Km for ADP (about 110 µM in sinaptosomes and about 10 µM in isolated brain mitochondria) (Monge et al., 2008). Moreover the addition of heterodimeric tubulin increased the apparent Km for ADP of isolated brain mitochondria as previously described in the case of isolated heart mitochondria (Monge et al., 2008).

Assessment of intracellular distribution of βII tubulin using immunofluorescent labeling revealed its presence in all studied muscles, including GW and EDL characterized by a very low level of the free βII tubulin expression (Fig. 6-8). In all studied muscles the distribution of βII tubulin followed that of mitochondria. In soleus muscle fibers βII tubulin and VDAC immunofluorescent labelings were seen between Z-lines (Fig. 7), while in GW muscle fibers they were seen at the level of Z-lines (Fig. 8). The close proximity of βII tubulin to mitochondria in oxidative and glycolytic skeletal muscles regardless of their affinity to ADP (K_mADP) suggests that the intracellular distribution of this protein is not the main factor regulating the

MOM permeability. The regulation of MOM permeability could be dependent on the expression of the dimeric fraction of βII tubulin.

How different muscle types achieve compartment specific targeting of mitochondria is to our knowledge largely uncovered. However it is well known that higher eukaryotes use predominantly microtubule (MT) tracks to distribute mitochondria. To realize location specific mitochondrial organization, a subset of MTs are exploited that distinguish by their isoform composition, dynamic stability and post-translational modifications (MacAskill and Kittler, 2010). Therefore we hypothesized that βII tubulin subcellular arrangement could be associated with muscle type specific localization of mitochondria. To test this hypothesis, we compared localization of overall β-tubulin relative to α-actinin in soleus and in GW muscle fibers (Fig. 9A). We found that in soleus muscle fibers β-tubulin is concentrated in the area between Z-lines similarly to that of βII tubulin (Fig. 7F). Whereas in GW muscle fibers the two subpopulations of β-tubulins can be seen, one at the level of Z-lines, similarly to that of βII tubulin and second at the level of A-band (Fig. 9D). Thus, despite the presence of significant part of β-tubulin at the level of A-band in GW muscle fibers, mitochondria reside at the level of Z-lines (aligned along βII tubulin). These results support the idea that mitochondria position is defined by subset of microtubules that correlate in both muscle fiber types with organization of βII tubulin.

In live cells restriction of the adenine nucleotides diffusion through MOM is overcome by free diffusion of PCr which carries intracellular energy flux via the system of compartmentalized CK iso-enzymes (Saks et al., 2012; Saks et al., 2010; Wallimann et al., 1992; Schlattner et al., 2006). Conversely, purified and reconstituted into planar phospholipid membrane VDAC in its closed state is impermeable for ATP, ADP and PCr (Rostovtseva et al., 2012). Similar results were shown for isolated mitochondria from hematopoietic pro-B cell lines (Vander Heiden et al., 2000). The selective permeability of VDAC depends on many

factors, among which are the cell-specific pattern of VDAC iso-forms; VDAC interaction with different proteins (tubulin, HKII, MAP2, plectin, desmin ...) regulated by distinct signalling cascades (growth factor or energy cascades); cell-specific pattern of intracellular proteins capable to interact with VDAC and their functional state (polymerization state or post-translational modifications, PTMs); biophysical properties of the channel itself, molecules going through the channel and MOM phospholipids (Rostovtseva et al., 2012). All these aspects are component parts of the structural and functional organisation of cellular energy metabolism oriented to support specific intracellular energy demanding processes such as the sarcomere contraction in highly differentiated cardiomyocytes or biosynthesis in actively growing and dividing cancer cells.

Differences in MOM permeability for ADP across muscle fiber types could stem from distinct expression patterns of VDAC isoforms. Striated muscles express three isoforms of VDAC (DePinto et al., 2010). According to Anflous-Pharayra et al., VDAC2 is mainly expressed in heart of wild-type murins and its delition is embryologically lethal (Anflous et al., 2001; Anflous-Pharayra et al., 2011). The decrease of the apparent affinity for ADP in permeabilized cardiac muscle fibers of VDAC1$^{-/-}$ mice and VDAC3$^{-/-}$ mice indicates the possible role of VDAC2 in the restriction of adenine nucleotides diffusion (Anflous et al., 2001;Anflous-Pharayra et al., 2011,Anflous-Pharayra et al., 2007). Interaction of microtubule-associated protein (MAP2) with VDAC2 (Linden et al., 1989) reinforce our belief that βII tubulin bind to VDAC2 regulating its permeability for phosphometabolites.

Glycolytic gastrocnemius muscle (mixture of red and white portions) of wild-type murins over-expresses VDAC1 (Anflous et al., 2001) and VDAC3 (Anflous-Pharayra et al., 2011) isoforms. VDAC1 and VDAC3 are permeable to ATP/ADP and this could be linked to the control by HKII (Anflous-Pharayra et al., 2007; Maldonado et al., 2012). VDAC1/3 null

cells do not contain HKII bind to VDAC (Chiara et al., 2008). More studies are necessary to address the mechanism of regulation of the VDAC selective permeability.

Based on these results, we can link MOM permeability regulation with non-polymerized βII tubulin. Nevertheless it cannot be excluded that other β-tubulin or α-tubulin isoforms could also bind to VDAC and influence its conductance. At present the distribution of α-tubulins in muscle cells is totally uncovered and it is also unclear whether tubulin post-translational modifications could influence the interaction of tubulin with VDAC. The elucidation of these modification patterns in different skeletal muscles, could give an important contribution to unravel the complex interplay between microtubular network, metabolism, mitochondria dynamics and muscle contraction.

Acknowledgments

This work was supported by by Agence Nationale de la Recherche (SYBECAR project, nr RA0000C407), by INSERM, France, by research grant SF0180114Bs08 from Estonian Ministry of Education and by the Austrian Science Fund (FWF): [P 22080-B20]. The authors would like to acknowledge support from BioHealth Computing Erasmus Mundus programme for Rafaela Bagur.

Tables and Figures

Table 1. Respiratory parameters of permeabilized skeletal muscle fibers.

	V_0	V_{max} (ADP)	V_{max} (ATP+Cr)	K_mADP	K_mADP (+Cr)	PK-PEP inhibition
	$nmolO_2 \cdot min^{-1} \cdot mg^{-1}$ dry weight fibers			µM		%
Soleus	1.55±0.09	10.6±0.4	9.8±0.1	294.2±15.9	66.6±4,7	2.2±0.5
Gastrocnemius Red	2.10±0.08	9.1±0.4	9.0±0.3	122.0±16.0	49.5±2.8	52.8±5.2
Gastrocnemius White	0.70±0.01	3.8±0.1	5.3±0.27	4.5±1.8	3.6±0.3	48.6±0.2
Extensor Digitorum Longus	1.10±0.05	9.1± 0.5	9.4±0.2	7.4±1.7	5.2±0.6	49.0±3.0

Respiration of permeabilized skeletal muscle fibers was measured in the presence of 5 mM glutamate and 2 mM malate in Mitomed solution at 25°C. (Values are means ± SEM)

Table 2. Metabolic Control Analysis of permeabilized skeletal muscle fibers respiration

	Inhibitor	Sample	ADP-stimulated respiration				Creatine-stimulated respiration			
			FCC	I_{max}, µM	J_0,nmolO_2·min^{-1}·mg^{-1} dw fibers	RCR	FCC	I_{max}, µM	J_0,nmolO_2·min^{-1}·mg^{-1} dw fibers	RCR
ATP/ADP carrier	Carboxy-atractyloside	Soleus m.	0.61±0.04	0.11±0.01	14.1±1.9	6.6±0.8	0.86±0.05	0.12±0.09	14.76±2.80	6.3±0.9
		GW m.	0.90±0.05	0.030±0.002	7.56±0.30	3.90±0.05				
		Cardiomyocytes *	0.20±0.05	0.6			0.92±0.05	0.6		
ATP synthase	Oligomycin	Soleus	0.44±0.03	0.11±0.01	16.17±0.90	7.7±1.1	0.61±0.07	0.12±0.07	18.42±4.10	8.7±2.5
		GW m.	0.67±0.02	0.024±0.001	9.53±0.90	5.64±0.61				
		Cardiomyocytes *	0.065±0.01				0.38±0.05			
NADH-CoQ oxidoreductase, Complex I	Rotenone	Soleus m.	0.69±0.05	0.036±0.001	14.6±1.1	5.3±0.1	0.71±0.02	0.026±0.001	16.8±0.6	7.2±0.4
		GW m.	0.54±0.06	0.028±0.001	12.83±1.83	8.67±1.61				
		Cardiomyocytes *	0.20±0.04	0.1			0.64±0.03	0.1		
CoQ cytochrome-c oxidoreductase, Complex III	Antimycin A	Soleus m.	0.47±0.01	0.025±0.002	15.4±0.2	6.5±0.05	0.61±0.01	0.033±0.003	15.4±0.3	7.3±0.4
		GW m.	0.82±0.01	0.0200±0.0004	10.92±0.23	6.81±0.23				
		Cardiomyocytes *	0.41±0.08				0.40±0.01	0.2		
Cytochrome c oxidase, Complex IV	NaCN	Soleus m.	0.73±0.03	20.0±2.5	15.6±1.2	6.6±0.7	0.94±0.01	13.74±2.9	14.6±0.6	5.7±0.6
		GW m.	0.84±0.01	8.05±0.45	10.44±0.22	6.34±0.13				
		Cardiomyocytes *	0.39±0.09	75			0.49±0.08	75		
Mitochondrial creatine kinase	DNFB	Soleus m.					0.76±0.01	0.09±0.01		
		Cardiomyocytes *					0.95±0.02	40		
Sum		Soleus m.	3.05±0.06				4.49±0.03			
		GW m.	3.77±0.02							
		Cardiomyocytes *	1.33±0.31				3.84±0.29			

Respiration of permeabilized skeletal muscle fibers was measured in the presence of 5 mM glutamate and 2 mM malate and 10 mM succinate in Mitomed solution at 25°C. The ADP-stimulated respiration means that the respiration is stimulated by exogenous ADP (2 mM). The creatine stimulated respiration means that the respiration is stimulated by endogenous ADP produced in MtCK reaction within mitochondrial intermembrane space. MtCK reaction is activated by the addition of 20 mM creatine in the presence of 2 mM ATP. Extramitochondrial ADP is trapped up by system consisting of 20 IU/mL pyruvate kinase (PK) and 5 mM phosphoenolpyruvate (PEP). * - data for cardiomyocytes was taken from Tepp et al., 2011 for comparison [Tepp2010]. I_{max} - inhibitor concentration giving complete inhibition, J_{0-} initial flux or maximal respiration rate in the absence of inhibitor, GW.m – gastrocnemius white muscle. The estimation of the Flux Control Coefficient (FCC) was done with $n \geq 3$. (Values are means ± SEM).

Figure 1

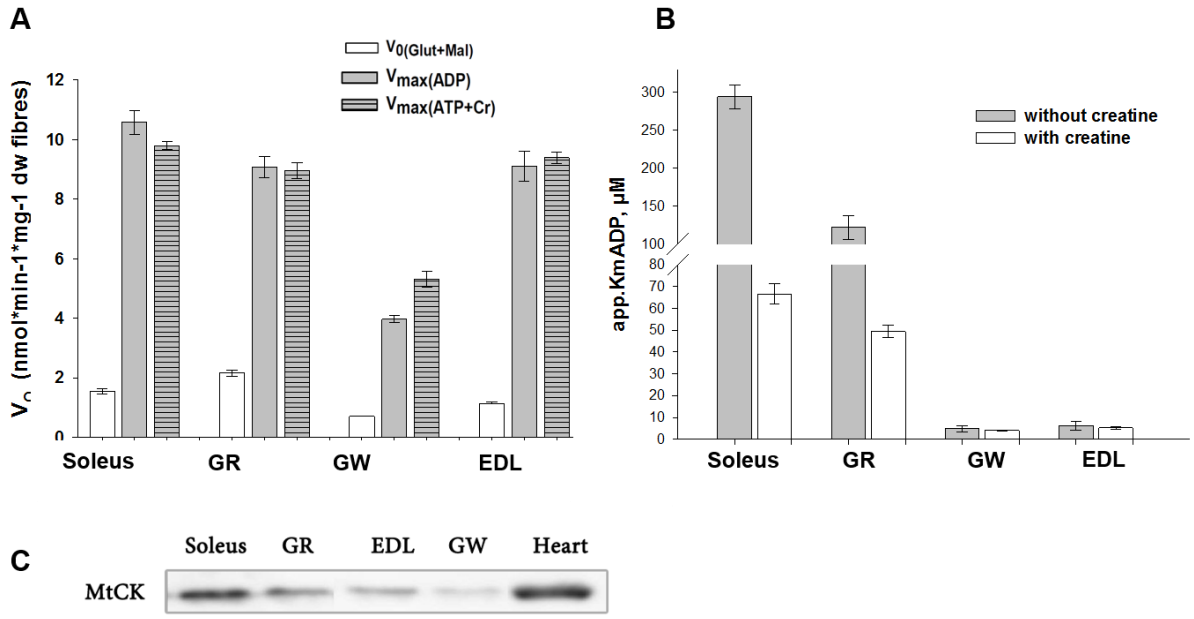

Respiration rates and regulation of mitochondrial function in permeabilized skeletal muscle fibers. A) Basal (V_0) and maximal respiration rates stimulated by ADP (V_{max}ADP) or by creatine in the presence of ATP (V_{max}(ATP+Cr)). In the presence of ATP and creatine mitochondrial respiration can be stimulated by ADP generated from the hydrolysis of ATP in ATPase reactions and by ADP re-cycled in the activated MtCK reaction coupled with ANT. B) The apparent K_m for ADP of Soleus; EDL, extensor digitorum longus; GR, gastrocnemius red; GW, gastrocnemius white and LV, left ventricle is estimated in the absence and in the presence of 30 mM creatine. C) Western blot analysis of mitochondrial creatine kinase (MtCK) in heart and skeletal muscles reveals the expression of protein in all samples studied. Equal loading (25 µg) of protein was confirmed by membrane Ponceau staining. The data are representative of at least three independent experiments.

Figure 2

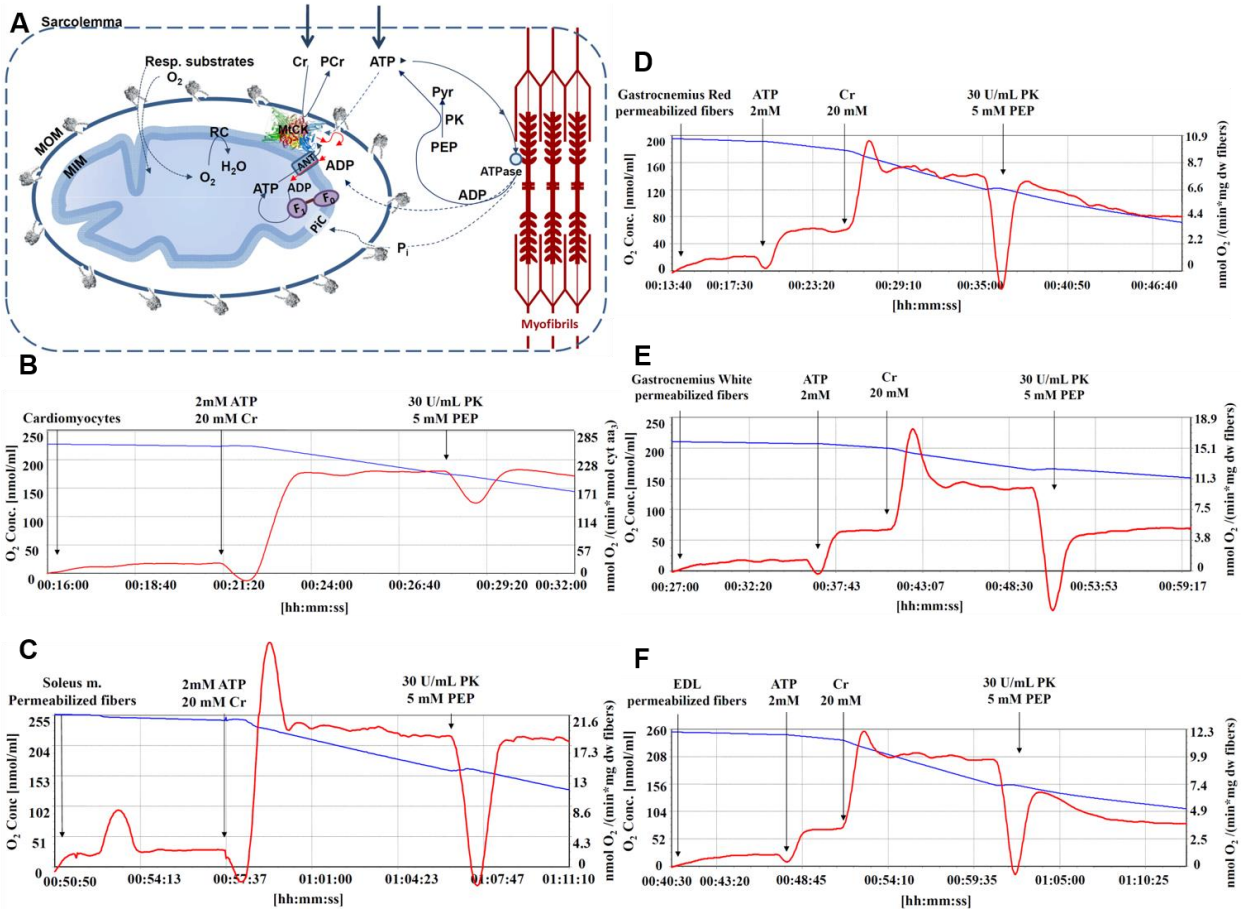

Measurement of ADP fluxes from mitochondria *in situ*, in permeabilized muscle cells. A) Scheme showing mitochondrion in permeabilized cell. MOM - mitochondrial outer membrane. Exogenous ATP is hydrolyzed by cellular ATPases into extra-mitochondrial ADP and inorganic phosphate (Pi). Mitochondrial (MtCK) in the presence of creatine and ATP locally produces endogenous intra-mitochondrial ADP. The system is supplemented with phosphoenolpyruvate (PEP) and pyruvate kinase (PK) which remove extramitochondrial ADP produced by intracellular ATP consuming reactions and continuously regenerate extramitochondrial ATP. Endogenous intramitochondrial ADP is re-imported into the matrix for re-phosphorylation *via* adenine nucleotide translocase (ANT) due to its functional coupling with MtCK. B) Respiration trace of permeabilized cardiomyocytes recorded using high resolution respirometer. C-F). Measurements

of ADP fluxes from mitochondria *in situ* in permeabilized soleus (C), gastrocnemius red, GR (D), gastrocnemius white, GW (E) and extensor digitorum longus, EDL (F) muscle fibers. The left scale and the blue trace indicate the oxygen concentration ($nmolO_2\ ml^{-1}$). The right scale and the red trace show the rate of oxygen uptake expressed in $nmolO_2\ min^{-1}\ nmol^{-1}cytochrome^{-1}\ aa_3$ for cardiomyocytes (B) and in $nmolO_2min^{-1}\ mg^{-1}$dry weight fibers for skeletal muscle fibers (C-F). Trapping PK-PEP system did not change the respiration rates of cardiomyocytes (B) and soleus muscle fibers (C) indicating that intramitochondrial ADP is not available for PK-PEP system. In contrast, this system effectively inhibits the respiration rates of GR, GW and EDL permeabilized muscle fibers (D-F).

Figure 3

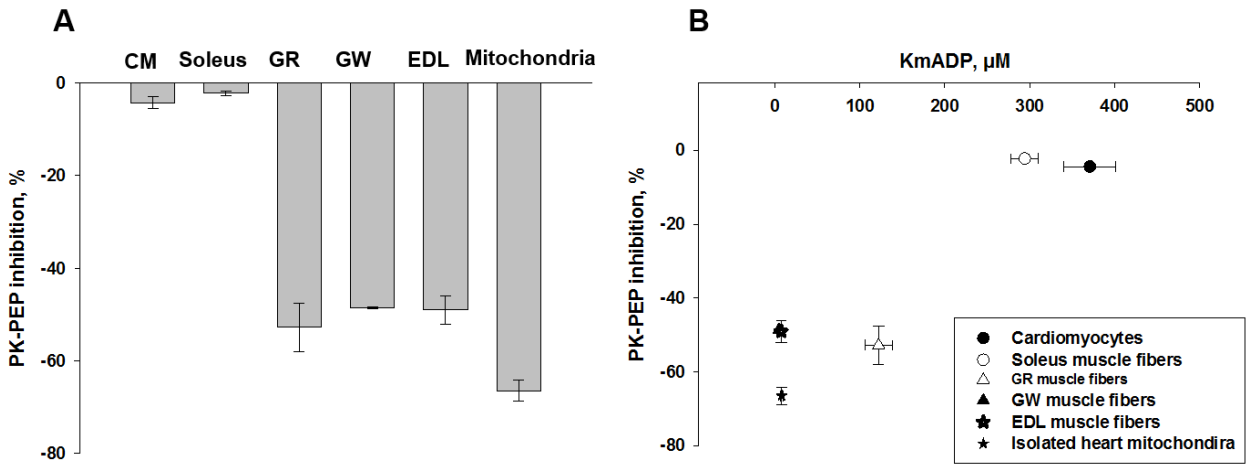

Distribution of energy fluxes through the mitochondrial outer membrane studied using PK-PEP trapping system for ADP. A) The inhibition of creatine-activated respiration by the PK-PEP observed in different skeletal muscles. B) Diagram representing relationship between the inhibition of creatine-activated respiration and the apparent K_m for ADP. Low apparent affinity of oxidative phosphorylation for ADP (i.e. high app. K_mADP) is directly linked to low MOM permeability for ADP (i.e. low PK-PEP inhibition of the creatine-stimulated respiration) and *vice versa*.

Figure 4

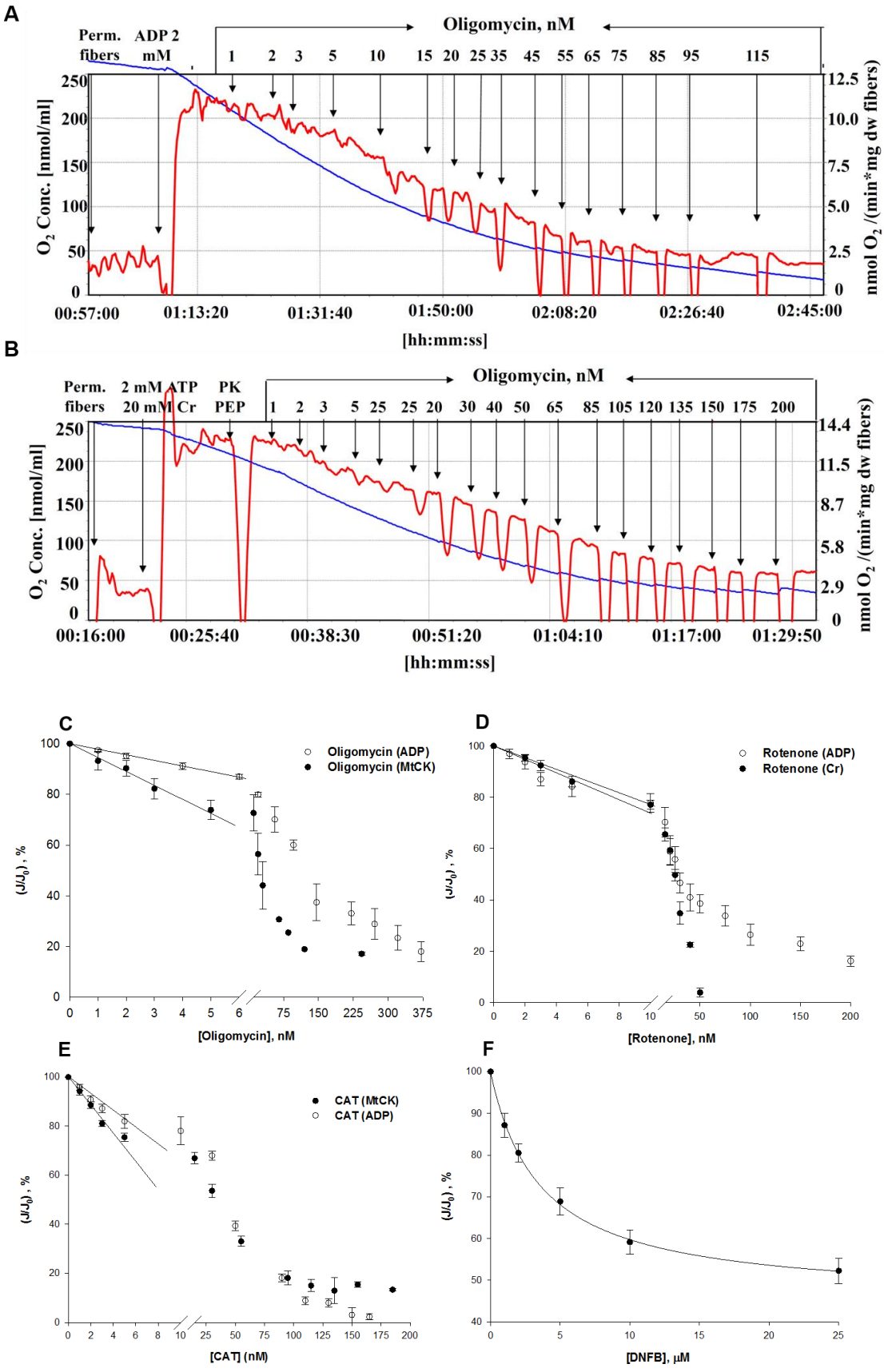
A
Perm. fibers
ADP 2 mM
Oligomycin, nM
1 2 3 5 10 15 20 25 35 45 55 65 75 85 95 115
O2 Conc. [nmol/ml]
nmol O2 /(min*mg dw fibers)
00:57:00 01:13:20 01:31:40 01:50:00 02:08:20 02:26:40 02:45:00
[hh:mm:ss]
B
Perm. fibers
2 mM ATP
20 mM Cr
PK
PEP
Oligomycin, nM
1 2 3 5 25 25 20 30 40 50 65 85 105 120 135 150 175 200
O2 Conc. [nmol/ml]
nmol O2 /(min*mg dw fibers)
00:16:00 00:25:40 00:38:30 00:51:20 01:04:10 01:17:00 01:29:50
[hh:mm:ss]
C
Oligomycin (ADP)
Oligomycin (MtCK)
(J/J0), %
[Oligomycin], nM
D
Rotenone (ADP)
Rotenone (Cr)
(J/J0), %
[Rotenone], nM
E
CAT (MtCK)
CAT (ADP)
(J/J0), %
[CAT] (nM)
F
(J/J0), %
[DNFB], µM

Metabolic flux control analysis of permeabilized soleus muscle fibers. Rates of oxygen consumption of permeabilized soleus muscle fibers recorded under conditions of: A) respiration stimulated by the addition of ADP and B) and by the addition of 20 mM of creatine in the presence of 2 mM ATP. The values of maximal respiration rates and initial fluxes (J_0) are comparable under both conditions. The PK-PEP system was added to remove the effect of exogenous ADP on the respiration. Respiration of permeabilized soleus fibers was progressively inhibited by stepwise addition of oligomyocin. C) Inhibition titration curves for oligomycin, D) rotenone, E) carboxyatractyloside (CAT) and F) 1-Fluoro-2,4-dinitrobenzene (DNFB) are shown under conditions of respiration stimulated by both ADP and creatine.

Figure 5

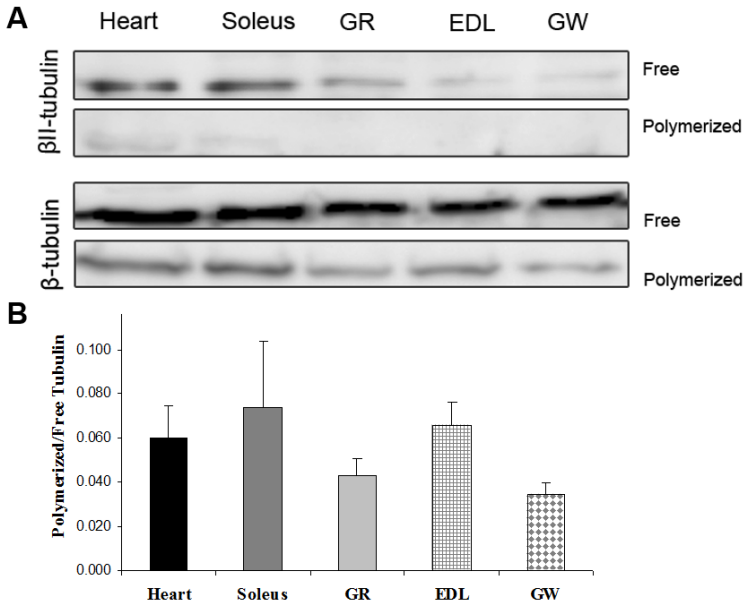

Western blot analysis of free and polymerized βII tubulin and total β tubulin in rat heart and skeletal muscles. (A) Upper panel shows immunoblot of free and polymerized βII tubulin and total β tubulin in soluble and insoluble muscle extracts prepared under microtubule stabilizing conditions. (B) Lower panel shows densitometric quantification of the total β-tubulin in the soluble and insoluble fractions. Equal proportion of free and polymerized samples were loaded onto the lanes and an equal amount (35 µg) of protein for each muscle sample. The data shown are representative of 3-4 independent experiments. Statistical comparison were done by one-way ANOVA and results represent means ± SEM. $P < 0.05$.

Figure 6

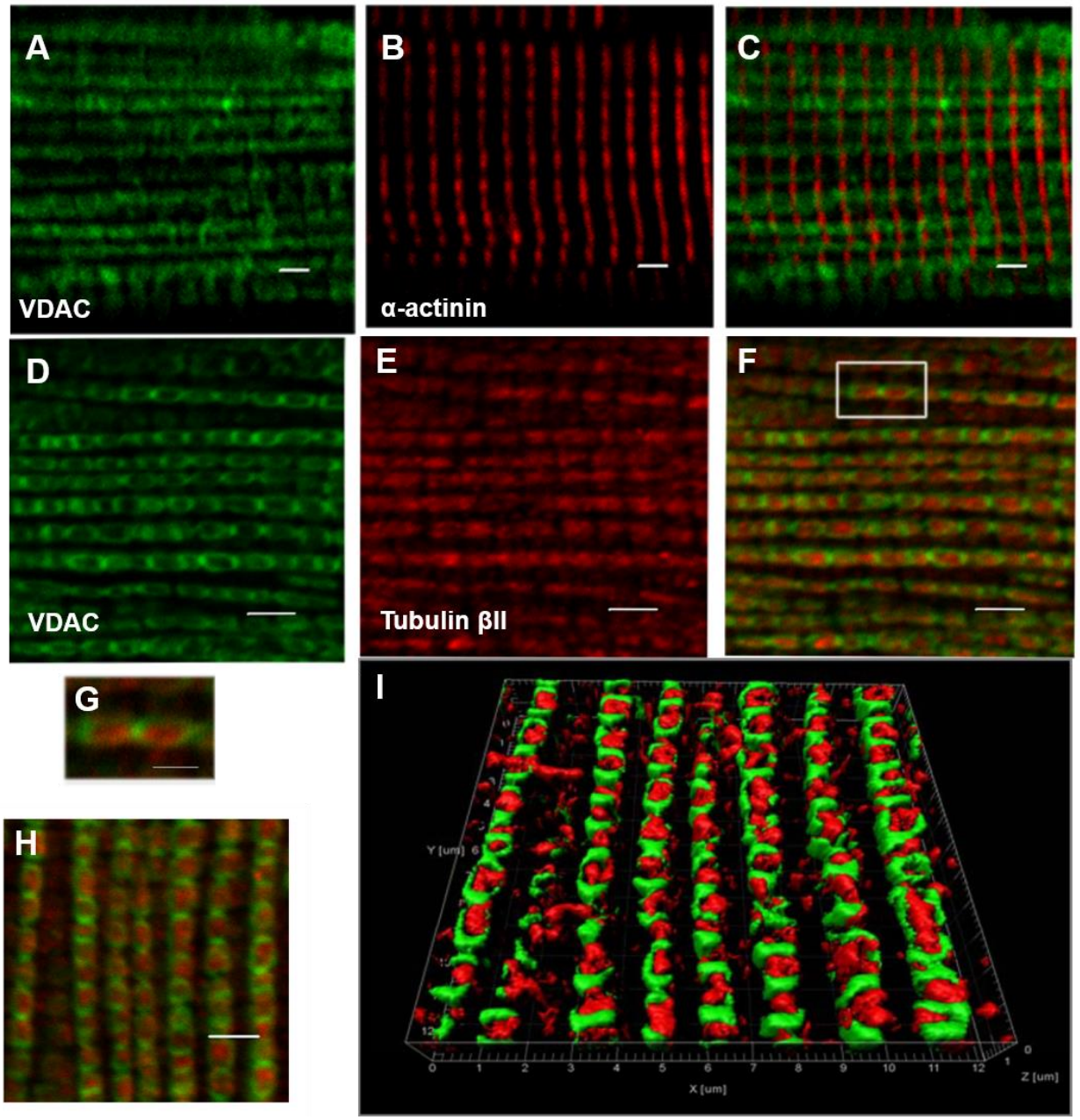

Confocal microscopy images of mitochondria and βII tubulin arrangement in adult cardiac muscle fibers. Optical slices of fibers co-immunabelled for VDAC (A) and α-actinin (B), and for VDAC (D) and βII tubulin (E) are optained at least 0.5 µm beneath sarcolemma and specimens are all oriented so that the long axis of the fiber is directed longitudinally. Images show that both

mitochondria and βII tubulin are arranged regularly between Z-lines. Scale bar 2 µm. I) Three-dimensional reconstruction of confocal image represented in Fig. 5H). Heart fibers immunolabelled for VDAC and βII tubulin were scanned at 0.27-µm intervals along the z-axis (maximum 10 planes, depending on the signal intensity) and 3D surface model was reconstructed by Imaris software (Bitplane). Scale bar, 2 µm. Image is oriented so that the long axis of the fiber is directed along y-axes.

Figure 7

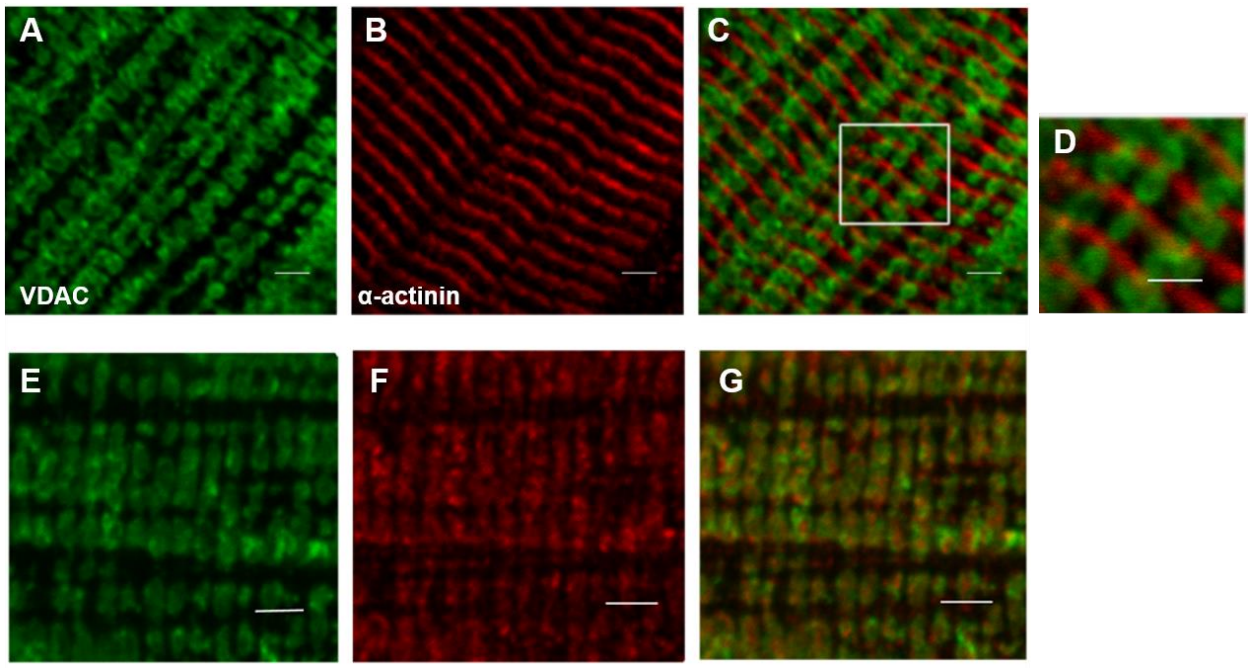

Confocal images of mitochondria and βII tubulin arrangement in fixed soleus muscle fibers. Optical slice of soleus fiber co-immunabelled for VDAC (A) and α-actinin (B), and for VDAC (E) and βII tubulin (F). Images show that mitochondria and tubulin βII structures are arranged regularly between Z-lines. Higher magnification image highlights mitochondria (indicated by arrows) extending across the A-band. Optical sections presented here are obtained at least 0.5 µm beneath sarcolemma and specimens are oriented so that the long axis of the fiber is directed diagonally in upper-panel image longitudinally in the bottom-panel image.(Inset) Higher magnification image highlights mitochondria stalks (indicated by arrows) extending across the A-band. Scale bar 2 µM.

Figure 8

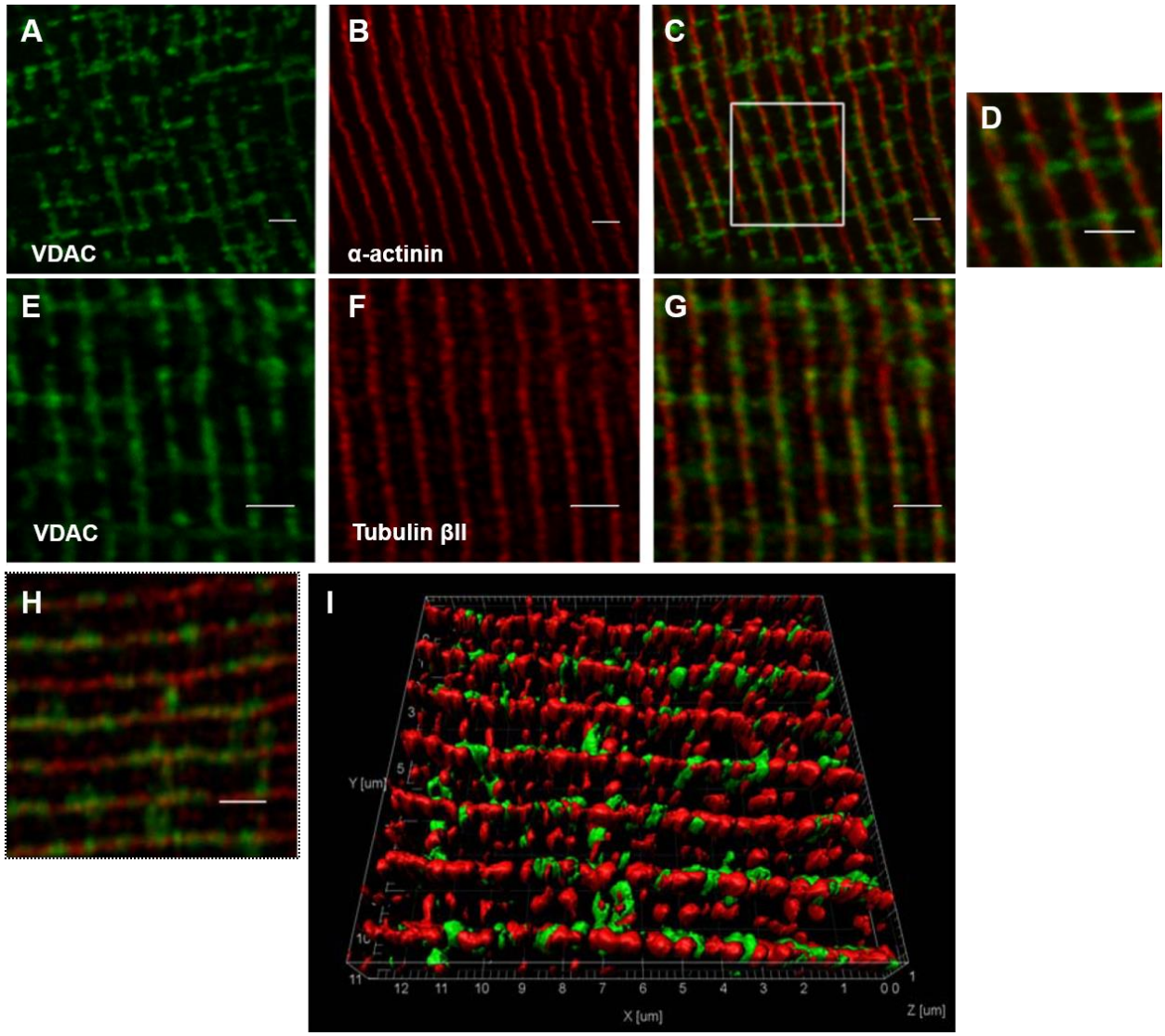

Confocal images of mitochondrial and βII tubulin arrangement in fixed gastrocnemius white muscle fibers. Optical slices of GW fiber co-immunolabelled for VDAC (A) and α-actinin (B), and for VDAC (E) and βII tubulin (F) are optained at least 0.5 µm beneath sarcolemma and specimens are all oriented so that the long axis of the fiber is directed longitudinally. Scale bar, 2 µm. Images show that mitochondria and βII tubulin are arranged close to Z-lines. Mitochondria highlighted in Inset rarely extend across the A-band level. I) Three-dimensional reconstruction of confocal image

represented in Fig. 7H. Fibers immunolabelled for VDAC and βII tubulin were scanned at 0.27 µm intervals along z-axis (maximum 10 planes, depending on the signal intensity) and 3D surface model was reconstructed by Imaris software (Bitplane). Scale bar, 2 µm. Image is oriented so that the long axis of the fiber is directed along y-axes and show continuous filaments of βII tubulin running along x-axis of image.

Figure 9

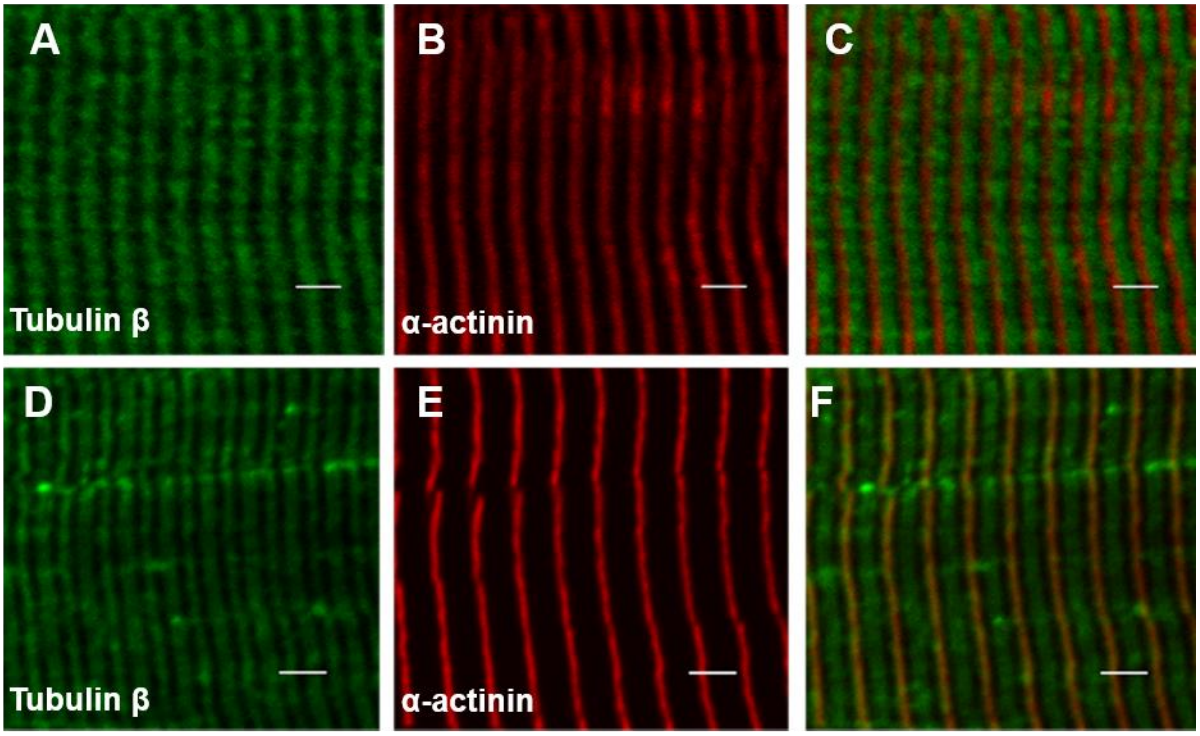

Comparison of overall β-tubulin distribution relative to Z-lines in oxidative soleus and glycolytic GW skeletal muscle fibers. Optical slices of soleus (A-C) and GW (D-F) muscle fibers co-immunabelled for VDAC (A, D) and α-actinin (B, E). In heart muscle fibers, transversely aligned β-tubulin stretches are located between Z-lines. In glycolytic GW muscle fibers, β-tubulin is present both between and along Z-lines. Scale bar 2 µm.

6.2. The impact of cardiac ischemia/reperfusion on the mitochondria-cytoskeleton interactions

Rafaela Bagur [1,2], Stéphane Tanguy[2], Sarah Foriel[1], Alexei Grichine[3], Caroline Sanchez[2], Karin Pernet-Gallay[4,5], Tuuli Kaambre[6], Andrey V. Kuznetsov[7], Yves Usson[2], François Boucher[2], Rita Guzun[1,8]

Under revision in Biochimica et Biophysica Acta - Molecular Basis of Disease; Manuscript number: BBADIS-15-333

[1] University Grenoble Alpes, Laboratory of Fundamental and Applied Bioenergetics, INSERM U1055, Grenoble, France

[2] University Grenoble Alpes, TIMC-IMAG, CNRS, UMR5525, Grenoble, France

[3] University Grenoble Alpes, Life science imaging – *in vitro* platform, IAB, INSERM CRI U823, Grenoble, France

[4] INSERM, U836, F-38000 Grenoble, France

[5] University Grenoble Alpes, GIN, F-38000 Grenoble, France

[6] National Institute of Chemical Physics and Biophysics, Laboratory of Bioenergetics, Tallinn, Estonia

[7] Innsbruck Medical University Cardiac Surgery Research Laboratory, Innsbruck, A-6020, Austria

[8] Hospital of the University Grenoble Alpes, Department Thorax (EFCR), France

Keywords: heart, ischemia/reperfusion, mitochondria, tubulin, respiration

Conflict of interest. None of the co-authors of this article have any conflict of interest

Abstract

Cardiac ischemia-reperfusion (IR) injury compromises mitochondrial oxidative phosphorylation (OxPhos) and compartmentalized intracellular energy transfer via the phosphocreatine/creatine kinase (CK) network. The restriction of ATP/ADP diffusion at the level of the mitochondrial outer membrane (MOM) is an essential element of compartmentalized energy transfer. In adult cardiomyocytes, the MOM permeability to ADP is regulated by the interaction of voltage-dependent anion channel with cytoskeletal proteins, particularly with β tubulin II. The IR-injury alters the expression and the intracellular arrangement of cytoskeletal proteins. The objective of the present study was to investigate the impact of IR on the interaction of mitochondria with β tubulin II and its effect on the regulation of mitochondrial respiration. Perfused rat hearts were subjected to total ischemia (for 20 min (I_{20}) and 45 min (I_{45})) or to ischemia followed by 30 min of reperfusion ($I_{20}R$ and $I_{45}R$ groups). High resolution respirometry and fluorescent confocal microscopy were used to study respiration, β tubulin II and mitochondrial arrangements in cardiac fibers. The results of these experiments evidence a heterogeneous response of mitochondria to IR-induced damage. Moreover, the intracellular rearrangement of β tubulin II, which in the control group colocalized with mitochondria, was associated with increased apparent affinity of OxPhos for ADP and decreased functional coupling of OxPhos with mitochondrial CK. The results of this study allow us to highlight changes of mitochondrial interactions with cytoskeleton as one of the possible mechanisms underlying cardiac IR injury.

Introduction

Oxygen deprivation related to the cardiac ischemia disrupts OxPhos, ATP synthesis and ATP-utilizing cellular processes. Post-ischemic reperfusion restores oxygen supply, but alters continually mitochondrial function due to increased production of the reactive oxygen species and calcium overload. In adult cardiomyocytes, mitochondrial ATP synthesis is tightly connected with ATP hydrolysis in energy utilizing systems (mostly myofibrils) through compartmentalized energy transfer (Saks et al., 1998a; Saks et al., 2012). Restricted diffusion of adenine nucleotides at the level of MOM enhances mitochondrial compartmentalization, functional coupling of OxPhos with mitochondrial CK (MtCK) and intracellular energy transfer by phosphocreatine (PCr) through the PCr/CK network. Compartmentalized energy transfer is also required for feedback regulation of mitochondrial ATP synthesis by cellular energy needs (Dzeja and Terzic, 2003; Dzeja et al., 2011; Saks et al., 2014; Schlattner et al., 2006; Wallimann et al., 1992). Due to restricted diffusion of ADP at the level of MOM, feedback regulation is supported by the Cr/PCr ratio, Pi and only small amounts of ADP.

MOM permeability to adenine nucleotides is regulated in adult cardiomyocytes by the interaction of voltage-dependent anion channel (VDAC) with cytoskeletal proteins (Saks et al., 2014). The apparent affinity of OxPhos for ADP, which is represented by the app. Km for ADP, is very low in permeabilized cardiomyocytes and increases drastically in isolated heart mitochondria due to the disruption of mitochondrial interactions with cytoskeleton (Saks et al., 1998b; Kuznetsov et al., 2008; Anmann et al., 2006). Among other cytoskeletal proteins, the role of tubulin in the regulation of voltage-dependent anion channels (VDAC) was extensively studied since 2002 (Carré et al., 2002; Rostotseva et al., 2008; Rostotseva et al., 2012). It has been demonstrated that heterodimeric αβ tubulin induces reversible closure of purified VDAC

restricting its permeability to ATP (Rostovtseva et al., 2008; Noskov et al., 2013). The addition of αβ tubulin to isolated heart mitochondria (at concentrations far below the critical value for polymerization) induced an increase in app. Km for ADP indicating restricted ADP diffusion (Rostovtseva et al., 2008; Monge et al., 2008). We have found that, in adult rat cardiomyocytes, β tubulin II is co-distributed with mitochondria (Guzun et al., 2011b). In contrast, cancerous cells of cardiac phenotype (non-beating HL1 cells) do not express β tubulin II and are characterized by high apparent affinity of OxPhos to ADP (Guzun et al., 2011b; Gonzalez-Granillo et al., 2012; Saks et al., 2012).

Ischemic cardiomyopathy is associated with altered expression and intracellular rearrangement of cytoskeletal proteins (Pucar et al., 2001; Ventura-Clapier et al., 2004; Devillard et al., 2006; Devillard et al., 2008; Vandroux et al., 2004; Decker et al., 2002). The objective of the present study was to investigate how IR impacts the interaction of mitochondria with cytoskeletal proteins β tubulin II, and how induced modifications influence the regulation of mitochondrial respiration. In order to achieve this objective, we have studied the effect of total ischemia (20 min and 45 min) and reperfusion on the left ventricular function, mitochondrial metabolism, morphology and intracellular distribution of β tubulin II.

Materials and methods

This study was approved by the local research ethics committee (Comité Régional d'Ethique, no: 380814) in accordance with the regulations of the French Ministry of Agriculture and it complied with the requirements of the Guide for the Care and Use of Laboratory Animals published by the US National Institutes of Health (NIH Publications No. 85-23, revised 1996). Eighty male Wistar rats (4 months old; Charles River Laboratories, France) were used in this study. All reagents were purchased from Sigma-Aldrich except Na_2-ATP, Na_2-ADP and pyruvate kinase (PK) which were purchased from MP biomedicals, and leupeptine, fatty acid free Bovine Serum Albumin (BSA) and phosphoenol pyruvate (PEP) which were purchased from Roche.

Perfusion of isolated rat hearts

Male Wistar rats received an intraperitoneal injection of 60 mg/kg sodium pentobarbital as anesthesia, and an intravenous injection of 500 U per kg body weight sodium heparin to prevent blood coagulation. Isolated hearts were placed on a Langendorff perfusion apparatus and perfused via the aorta under a constant pressure of 100 cm H_2O (9.807 kPa) with a Krebs-Henseleit Buffer (KHB, containing 118.5 mM NaCl, 25.0 mM $NaHCO_3$, 4.8 mM KCl, 1.2 mM $MgSO_4$, 1.2 mM KH_2PO_4, 1.36 mM $CaCl_2$:$2H_2O$, 11 mM glucose at 37°C) equilibrated with a gas mixture of 95% O_2 / 5% CO_2 (pH 7.4). A fluid-filled non-compliant balloon connected to a pressure transducer (P23ID, Statham, USA) was inserted into the left ventricle (LV) and it was inflated to impose a LV end-diastolic pressure (LVEDP) of 5±1 mmHg (1 mmHg = 0.133 kPa) (Curtis et al., 1986). Heart rate was imposed by electrical atrial pacing at 300 beats/min (Boucher et al., 1998).

Study design

All hearts were subjected to 15 minutes of normoxic perfusion, i.e. stabilization period, followed by total zero flow normothermic ischemia (I) for 20 or 45 minutes. At the end of ischemia, some hearts from each time-condition were removed from the system, I_{20} group (n = 21) and I_{45} group (n = 8), and the others were subjected to post-ischemic normoxic reperfusion (R) for 30 minutes, $I_{20}R$ (n = 20) and $I_{45}R$ (n = 16). Parameters of the left ventricle (LV) cardiac function estimated at the end of stabilization period were used as "control" for each group. All other data of hearts subjected to ischemia and post-ischemic reperfusion were compared with that of non-perfused adult rat hearts (n = 15).

The $I_{45}R$ protocol was chosen as a reference state for highly IR-damaged hearts and, in order to test our hypothesis under conditions closer to the real pathological state, we used the $I_{20}R$ protocol. The reason why we chose the $I_{45}R$ protocol as a reference for damaged hearts is because the mitochondrial ATP turnover and intracellular energy flux distribution in hearts were described precisely by Dzeja's group from Mayo clinic, Rochester (Pucar et al., 2001).

Left ventricle cardiac function

Left ventricular function was monitored throughout perfusion using Chart 5 (ADInstument, Bella Vista, Australia). LV contractility was assessed by LV systolic, end-diastolic, and developed (LVDevP) pressures, and by the positive and negative first derivatives of LVDevP (+dP/dt and –dP/dt, respectively). Coronary flow rate was measured by timed collection of coronary effluent over 30 s periods, every 5 minutes.

Preparation of permeabilized cardiac fibers

Left ventricular fibers from isolated hearts were prepared according to the protocol described by Kuznetsov et al., (Kuznetsov et al., 2008). Permeabilized fibers were kept into ice-cold Mitomed solution (0.5 mM EGTA, 3.0 mM $MgCl_2$, 60 mM K-lactobionate, 3.0 mM KH_2PO_4, 20 mM taurine, 20 mM HEPES, 110 mM sucrose, 0.5 mM dithiothreitol, 2 mg·mL-1 BSA at pH 7.1) for about three hours of experiments. Solution was supplemented with 1 µM leupeptine to protect cytoskeletal proteins from lysosomal proteolysis (Kuznetsov et al., 2012).

Respirometry studies

Oxygen consumption rates were measured in Mitomed solution at 25ºC and taken the solubility of oxygen as 240 nmol·ml-1 (Gnaiger, 2001) using a high-resolution respirometer (oxygraph-2 K, OROBOROS Instruments, Austria). The rate of oxygen consumption of permeabilized fibers was expressed in nmolO_2·min-1·mg-1 dry weight fibers. To normalize the respiration rate by the dry weight fibers, the wet fibers were dried at 100°C for 48 h.

Oxygen consumption rates of permeabilized fibers were measured in the presence of respiratory substrates for complex I (CI, 5 mM glutamate and 2 mM malate) or complex II (CII, 10 mM succinate and 3 µM rotenone). Maximal respiration rate (Vm(ADP)) was measured in the presence of saturating concentrations of ADP (2 mM). Respiratory control ratio (RCR) was estimated as the ratio between Vm(ADP) and basal respiration rates measured in the presence of respiratory substrates. Addition of cytochrome c (8 µM) was used to check the integrity of MOM and atractyloside (30 µM) to check the integrity of inner membrane.

The regulation of mitochondrial OxPhos was studied by stimulating the respiration of permeabilized cardiac fibres by ADP at increasing concentrations (from 0.025 to 2 mM). The apparent Michaelis constant for ADP (app. KmADP) reflects the concentration in ADP yielding

half-maximal rate of respiration. Its value is calculated from the double-reciprocal plot of $1/VO_2$ as a function of 1/[ADP]. The addition of 20 mM creatine into the reaction medium allowed us to estimate the regulation of mitochondrial respiration by endogenous ADP produced in activated MtCK reaction. Functional coupling of MtCK with OxPhos was assessed by the ratio between the apparent Km for ADP estimated in the absence and in the presence of creatine (20 mM).

Inhibition of Cr-stimulated respiration induced by pyruvate kinase (PK) and phospoenolpyruvate (PEP) was used to estimate ADP leak throughout MOM. Creatine in the presence of ATP stimulates respiration of permeabilized cardiomyocytes due to the production of ADP in activated MtCK reaction. The trapping system for ADP, consisted of PK and PEP, phosphorylates extramitochondrial ADP to ATP. If the ADP diffusion throughout MOM is restricted, the addition of PK-PEP system cannot inhibit respiration rate. In contrast, increased ADP diffusion from mitochondria is characterized by PK-PEP inhibition of Cr-stimulated respiration (Guzun et al., 2009).

Measurement of enzymatic activities

Creatine kinase and complex I activities were measured spectrophotometrically (Specord 210 spectrophotometer (Analytik Jena AG, Germany)) as described in Schlattner et al., 2000 and Spinazzi et al., 2012 in LV samples (Schlattner et al., 2000; Spinazzi et al., 2012). Muscle samples were homogenized using a potter tissue grinders in sucrose buffer (250 mM) and centrifuged at 600 g (10 min, 4 °C). Complex I activity was normalized by mitochondrial cytochrome aa3 content, measured as described previously (Monge et al., 2008) with slight modifications to avoid the interference of myoglobin or blood contamination to the oxidation-reduction difference spectrum (Balaban et al., 1996).

Immunocytochemistry

Left ventricular fibers from isolated hearts were fixed in 4% paraformaldehyde supplemented with 0.5 % glutaraldehyde and permeabilized in 1% Triton X-100. After blocking, fibers were incubated with primary antibodies, followed by incubation of secondary antibodies. Mitochondria were visualized by autofluorescence or polyclonal rabbit anti-TOMM20 antibody (Abcam ab78547); β tubulin II was labeled using monoclonal mouse anti-β-tubulin II antibody, raised against the epitope -CEEEEGEDEA at the C-terminus (Abcam, ab28036); and α-actinin was labeled using anti-alpha actinin antibody (Abcam, ab82247). All slides were analyzed using Zeiss LSM 70 AxioObserver confocal microscope (Carl Zeiss) equipped with a Plan-Apochromat 63x/1.40 Oil DIC M27 objective.

Colocalization of β tubulin II with MOM labelled by TOMM20 antibody (protein of mitochondrial outer membrane), was analyzed using the FluoCorr software developed by Dr Yves Usson. This software evaluates the overlay between channel 1 (CH1, red signal) and channel 2 (CH2, green signal) regarding the total fluorescent signal; and the percentage of signal from channel 1 or 2 that is comprised in the overlay (Overlay CH1 and 2, respectively). All parameters were measured with a restricted threshold (high intensity fluorescent signal) in order to avoid the interference of background signal in our analysis.

Electron Microscopy

LV tissue cut in cubes of 1 mm^3 were fixed with 0.1 M Cacodylate buffer pH 7.2 containing 2% paraformaldehyde and 2% glutaraldehyde for 2 hours at room temperature and then washed twice in 0.1 M Cacodylate buffer. The samples were subsequently post-fixed with 1% osmium tetraoxide in 0.1 M Cacodylate buffer for 1 h at 4 °C and then stained with 0.5% uranyl acetate in

water pH 4.0 overnight at 4 °C. Next day, samples were dehydrated by incubation in a graded series of ethanol solutions (30%, 60%, 90% and three times in 100%) prior to be infiltrated with an ethanol/resin mixture (1:1) for 1 hour at room temperature. Once the tissue was embedded in Epon and polymerized for 2 days at 60 °C, ultrathin sections were prepared with a diamond knife on an UC6 Leica ultramicrotome and collected on Formvar-coated 200 μm mesh copper grids. Sections were post-stained with 5% uranyl acetate in water and 0.4% lead citrate in water before being examined under a transmission electron microscope (1200EX JEOL, Japan) at 80 kV. Images were acquired with a digital camera (Veleta, Olympus, Tokyo, Japan) and analyzed with iTEM Software (Olimpus, Tokyo, Japan).

Statistical analysis

Values are presented as mean ± SEM. Statistical comparison of data from the same group was performed by t-test, for parametric variables, and Mann-Whitney test, for non-parametric variables. Statistical comparison of data from different groups was performed by One Way Anova with Holm-Sidak method as post-hoc, for parametric variables, and Kruskal-Wallis test with Dunn's method as post-hoc, for non-parametric variables. Correlation analysis was done using the Pearson's test for parametric variables. In all cases, a value of $P < 0.05$ was considered a significant difference.

Results

To uncover the role of β tubulin II in the regulation of MOM permeability to adenine nucleotides, we studied induced by IR injury changes in the regulation of mitochondrial respiration by ADP and creatine, leak of endogenous ADP from mitochondria and intracellular distribution of β tubulin II.

Left ventricular function of isolated perfused hearts

Left ventricular systolic and diastolic functions of isolated perfused hearts were evaluated at the end of stabilization and post-ischemic reperfusion periods (Table 1). No difference in LV function was observed between groups at the end of stabilization period. All parameters used to describe the LV function were significantly lower in post-ischemic reperfusion period compared to those in stabilization period. Alteration of LV function was evidenced by the decrease in the positive first derivative of LVDevP, +dP/d*t*, by about 36.9 % and 68.2 % in the $I_{20}R$ and the $I_{45}R$ groups, respectively. Diastolic function of LV was characterized by the decrease in –dP/dt, by about 41.5 % and 70.2 % and the remarkable increase in LVEDP by 6 and 12 fold in the $I_{20}R$ and the $I_{45}R$ groups, respectively. The decrease in coronary flow was about 28 % and 38.2 % in $I_{20}R$ and $I_{45}R$, respectively. The rate of recovery of LV function in the post-ischemic reperfusion period was lower in hearts subjected to 45 minutes of ischemia compared to those subjected to 20 minutes of ischemia. Large variability of LV diastolic function was observed in the $I_{20}R$ group (Fig. 1F). The IR-induced alteration of LV function observed in our study was comparable to previously published data (Boucher et al., 1998; Pucar et al., 2001).

The regulation of respiration of permeabilized fibers

Results of respirometry studies are summarized in Table 2. Basal respiration rates of permeabilized cardiac fibers from hearts subjected to IR injury were comparable to that of control group. High respiratory control ratio in the control group indicated tight coupling of OxPhos and good oxygen penetration in the core of permeabilized fibers. In spite of being in contact with ice-cold solutions during fibers' preparation and storage, fibers from hearts subjected to ischemia alone (I_{20} and I_{45} groups) did not present reperfusion-like damaged OxPhos capacity. The Vm(ADP) values in ischemic hearts were similar to that of the control group. In contrast, Vm(ADP) decreased after post-ischemic reperfusion (RCR of about 5 and 3 for $I_{20}R$ and $I_{45}R$, respectively), indicating decreased OxPhos capacity. The addition of the exogenous cytochrome c did not stimulate significantly Vm(ADP) in the $I_{20}R$ group, indicating the integrity of MOM. In the $I_{45}R$ group exogenous cytochrome c stimulated slightly maximal respiration rate. Atractyloside inhibited respiration rates up to the basal level, indicating the integrity of the inner mitochondrial membrane (Table 2). Similar values of Vm(ADP) measured in the presence of complex I substrates with that measured in the presence of complex II substrates indicated the absence of the CI inhibition in the $I_{20}R$ and $I_{45}R$ groups. This statement was confirmed by the unaltered enzymatic activity of CI in all studied groups (Table 2).

Kinetic analysis of respiration regulation by ADP revealed high values of app. Km for ADP in control and ischemic hearts, while hearts from the $I_{20}R$ and $I_{45}R$ groups revealed significantly lower values of app. Km for ADP (Table 2, Fig. 1A - D). In spite of the high average value of app. Km ADP obtained in I_{20} group (Table 2), the double reciprocal plot of the dependence of respiration rates on ADP concentration showed two app. Km ADP for the same fiber samples: high app. Km for ADP (356.18 ± 32.78 µM), comparable to that of the control group, and low app.

Km for ADP (79.00 ± 7.59 µM) (Fig. 1E). The proportion of mitochondria populations with low and high app. Km for ADP, calculated using a previously published approach (Saks et al., 1998b), was about 44 % and 56 %, respectively. This result evidences the existence of two populations of mitochondria within fiber samples of the I_{20} group. After reperfusion, these two mitochondrial populations were not evidenced since the previous analysis revealed just one app. Km ADP and one Vm(ADP) value within fiber samples of the $I_{20}R$ group (Fig. 1E). Nevertheless, distinct values of app. Km for ADP were obtained for different hearts from the $I_{20}R$ group (Fig. 1F).

Functional coupling of MtCK with OxPhos was evaluated by the ratio between the app. KmADP measured in the absence and the presence of creatine. The diminishment of this ratio in the $I_{20}R$ and $I_{45}R$ groups (Fig. 2A) evidenced the switch in the control of respiration from ADP produced in MtCK reaction towards exogenous ADP. Total CK activity and the expression of sarcomeric MtCK were similar between groups (Fig. 2B).

Changes in app. Km for ADP were explained in the past by changes in MOM permeability to ADP (Saks et al., 1998b; Saks et al., 2012; Kuznetsov et al., 2008). In order to link app. Km for ADP with the restriction of ADP diffusion at the level of MOM in our study, we evaluated ADP leak from mitochondria under conditions of its production by activated MtCK and adding the PK-PEP system trapping for ADP. According to literature, the addition of PK-PEP system cannot inhibit significantly maximal creatine-stimulated respiration rates when mitochondria are studied *in situ* in permeabilized cardiomyocytes. This effect was explained by the restriction of ADP diffusion at the level of MOM (Guzun et al., 2009; Timohhina et al., 2009). In contrast, PK-PEP system inhibits Vm(ATP+Cr) of isolated heart mitochondria by about 50 % due to high leak of ADP through MOM (Jacobus and Saks 1982). In our study, the addition of the PK-PEP system to permeabilized cardiac fibers from the control group did not inhibit significantly Vm(ATP+Cr). In

contrast, the addition of the PK-PEP system to permeabilized fibers from the $I_{20}R$ and $I_{45}R$ groups inhibited Vm(ATP+Cr) by 47.55 ± 8.10 % and 37.07± 4.84 % respectively, thus implying a leak of endogenous ADP from mitochondrial intermembrane space. It is important to mention that before the addition of the PK-PEP system, the maximal Cr-stimulated respirations rates were equal to maximal ADP-stimulated respiration rates indicating that all ADP produced in activated MtCK reaction was transferred into the matrix for re-phosphorylation (Table 2). Two different patterns were observed in permeabilized muscle fibers of the I_{20} group. A part of samples displayed low PK-PEP inhibition of Vm(ATP+Cr) (16.44 ± 2.25 %, Fig. 3A) while another part of samples displayed high PK-PEP inhibition (47.27 ± 3.97 %, Fig. 3B).

The IR-induced changes in intracellular distribution of β tubulin II

In control hearts, mitochondria are located between sarcomeric Z-lines (Figs. 4I – K) and colocalized with β tubulin II (Figs. 4A – D). Figures 4A-D show colocalization of β tubulin II with well-organized intermyofibrillar mitochondria (regions framed in yellow boxes) and clustered perinuclear mitochondria (regions framed in white boxes). In hearts from the $I_{45}R$ group, β tubulin II was partially displaced from intermyofibrillar mitochondria positions (Figs. 4E-H) towards the regions of sarcomeric Z-lines, where it colocalized with α-actinin (Figs. 4L-N). The β tubulin II was completely displaced from perinuclear regions, which are characterized by the presence of clusters of mitochondria and the absence of sarcomeric structures (Figs. 4E – G, regions framed in white boxes). While in the previous cases the β tubulin II distribution was homogeneous, 20 minutes of ischemia and reperfusion resulted in a heterogeneous pattern, both within a heart and across different hearts. In some fibers, β tubulin II colocalized with mitochondria (Figs. 5A – C), reminiscent of control hearts and, in others, it was displaced from mitochondria (Figs. 5D – F), as in $I_{45}R$ hearts.

The colocalization analysis evidenced a significant decrease in the overlay between β tubulin II and TOMM20 (protein used to label MOM surface) signals. The overlay after IR injury was about 5.3 ± 0.48 and 3.85 ± 0.46, for the $I_{20}R$ and $I_{45}R$ groups, respectively, while control hearts had an overlay of 17.53 ± 0.73 % (Fig. 5G). The graphical representation of the β tubulin II signal overlay percentage versus the TOMM20 signal overlay percentage shows re-distribution of fluorescence in cardiac fibers (Fig. 5H). In particular, for control hearts the β tubulin II signal matched the TOMM20 signal. However, after 45 minutes of ischemia and reperfusion the β tubulin II signal was displaced, resulting in colocalization restricted to smaller regions of MOM surface. In the case of $I_{20}R$ group, the distribution of fluorescence signal from β tubulin II is heterogeneous, exhibiting both patterns of distribution.

Electron Micrograph of LV muscle tissue

In the control group, mitochondria were precisely positioned between the Z-lines, at the level of the A-band, and firmly attached to the myofibrils (Fig. 6A). The mitochondria presented dense and tight cristae resulting in a dark appearance. After 45 minutes of ischemia and reperfusion, remarkable changes in mitochondria morphology were observed (Fig. 6B). Mitochondria were homogenously detached from the myofibrils, and the presence of clusters and swollen mitochondria increased. Another important change was at the cristae level: cristae density was lower and the space between consecutive cristae (intercristae space) was higher, resulting in a more white appearance.

In the case of $I_{20}R$ group, samples presented at least three types of mitochondria: mitochondria with dense and tight cristae as in control group; mitochondria with large intercristae space as in $I_{45}R$ group; and mitochondria with an intermediate pattern. The heterogeneity in the $I_{20}R$ group could take place in two different ways: within the cell (mitochondria in the same cell

are affected heterogeneously, Fig. 6D) or at the cellular level (mitochondria in the same cell are affected homogenously and there is heterogeneity between cells, Fig. 6C).

Discussion

This study allowed us to evaluate the impact of cardiac IR injury on mitochondria interactions with cytoskeletal protein β tubulin II and its effect on the regulation of mitochondrial respiration. In adult cardiomyocytes this interaction restricts diffusion of adenine nucleotides at the level of MOM favoring mitochondrial compartmentalization and intracellular energy phosphoryl transfer though the PCr/CK network. The disruption of mitochondria interactions with cytoskeleton will result in decreased intracellular compartmentalized energy transfer.

The IR-induced structural changes of the intracellular energetic units

Two patterns of β tubulin II intracellular arrangement were found in cardiac fibers from the $I_{20}R$ group: colocalized with mitochondria (Figs. 5A – C), as it was seen in the control group, and displaced from mitochondria (Figs. 5D – F). The IR-induced alterations of the intracellular β tubulin II arrangement are dependent on the reperfusion but also on the duration of ischemia. According to the literature 15 minutes of ischemia did not affect the normal pattern of β tubulin intracellular distribution in cardiac cells (Sato et al., 1993; Iwai et al., 1990), while 20 minutes of ischemia induced non-homogeneous lesions of the microtubular structure (Sato et al., 1993). The microtubular structure was further disrupted substantially by the post-ischemic reperfusion (Sato et al., 1993; Iwai et al., 1990). Interestingly, the IR-induced β tubulin alterations in cardiac cells were reversible when the action of the stress factor stopped before the increase in the sarcolemmal permeability (Sato et al., 1993; Vandroux et al., 2004).

Binding capacities of tubulin and VDAC can be also modified by the IR-dependent posttranslational modifications (Fassett et al., 2013; Janke and Bulinski, 2011; Cassimeris et al., 2012; Belmadani et al., 2002; Sato et al., 1997; Rostovtseva et al., 2012; Sheldon et al., 2011). The increase in expression and post-translational modifications of the C-terminus of αβ tubulin I and II were found in chronic cardiac hypertrophy (Tsutsui et al., 1994; Chinnakkannu et al., 2010; Koide et al., 2000; Nederlof et al., 2014; Belmadani et al., 2004). Applying mathematical modeling Noskov et al., found that the presence of the unstructured C-terminal tail of tubulin inside VDAC lumen decreases its conduction by 40 % and renders ATP transport through VDAC virtually impossible (Noskov et al., 2013). The disruption of mitochondria interactions with cytoskeleton by trypsin proteolysis drastically increases app. affinity of OxPhos for ADP. Thus, isolated heart mitochondria, which are devoid of β tubulin II, display lower app. Km for ADP than mitochondria in situ in permeabilized cardiomyocytes (Guzun et al., 2011b). Cancerous cells of cardiac phenotype (non-beating HL1 cells), which are also devoid of β tubulin II, have very low app. Km for ADP comparable with that of isolated mitochondria (Guzun et al., 2011b; Gonzalez-Granillo et al., 2012; Saks et al., 2012).

The displacement of β tubulin II from mitochondria observed in the $I_{45}R$ group is consistent with the recently published observation by Yancey et al., for volume overload heart injury (Yancey et al., 2015) and could be also linked to protein degradation (Figs. 4E – H). Moreover, 30 minutes of ischemia followed by reperfusion decreased expression of VDAC2 (Kim et al., 2006) which was described to regulate MOM permeability to ATP/ADP (Anflous-Pharayra et al., 2007; Anflous-Pharayra et al., 2011).

Relationship between structural and functional changes induced by IR-injury

Observed structural changes were associated with increased MOM permeability to ADP. The addition of the trapping system for ADP (PK-PEP) to permeabilized cardiac fibers from the $I_{20}R$ and $I_{45}R$ groups inhibited significantly the maximal Cr-stimulated respiration rate (i.e. respiration stimulated by endogenous ADP produced in the activated MtCK reaction). These changes were already present after ischemia. Two types of responses were obtained by adding the PK-PEP system to permeabilized fibers from the I_{20} group: high inhibition of maximal rates of Cr-stimulated respiration and low inhibition, comparable to that of the control group and evidencing restricted ADP diffusion at the level of MOM (Fig. 2).

Decreased mitochondrial compartmentalization of ADP in hearts subjected to IR injury was associated with decreased app. Km for ADP (Table 2). Although the mean value of app. Km for ADP in the $I_{20}R$ group was lower than in the control group, significant variations were observed between hearts (Table 1, Fig. 1B). A heterogeneous pattern of app. Km for ADP was already present after 20 minutes of ischemia and it was associated with unaltered OxPhos capacity (Fig. 1A, Table 2). Kinetic analysis of ADP-stimulated respiration revealed two populations of mitochondria: with high app. Km for ADP, comparable to that of the control group, and low app. Km for ADP (Fig. 1B). Decreased ratio between app. Km for ADP measured in the absence and in the presence of creatine indicates the decrease of the functional coupling of OxPhos with MtCK and decreased intracellular energy transfer through the PCr/CK nettwork (Figs. 3A). The decrease of app. Km for ADP and the regulation of respiration by creatine are common hallmarks of cardiac IR injury (Kay et al., 1997b; Boudina et al., 2002; Ventura-Clapier et al., 2004). Pucar et al., (2001) showed that 45 min of ischemia followed by reperfusion induced a decrease in the energy phosphoryl flux through the CK reaction by four times (Pucar et al., 2001). The app. Km for ADP

obtained for hearts from the control group and hearts subjected to IR injury correlated inversely with LVEDP (Fig. 1B).

A different response to stress of mitochondria was evidenced previously in experiments with IR injury at cold temperature (Kuznetsov et al., 2004) and was explained by the electrical discontinuity of individual mitochondria, which prevents the collapse of the entire cell energy metabolism (Beraud et al., 2009). The EM study of muscle samples from the $I_{20}R$ group revealed mitochondria with dense cristae, as it is characteristic for the control group, randomly dispersed between mitochondria with decreased cristae space and increased interspace between cristae (Fig. 6C, D). Also, cardiomyocytes with dense mitochondria were located next to cells with altered mitochondria. This phenomenon could be also related to the regional ischemia which appears during the restoration of the normal global flow due to the physiological heterogeneity of the terminal vascular beds in the LV (Pries and Secomb, 2009; Marshall et al., 2003).

Results of this study allowed us to highlight changes of mitochondrial interactions with cytoskeleton as one of the possible mechanisms underlying cardiac IR injury. More studies at the molecular level are necessary to describe in details this mechanism. Recently, Dr R. D. Vale's group developed the recombinant α- and β- tubulins, including β tubulin II C-terminal tail and its post-translational modifications (Sirajuddin et al., 2014). The use of the recombinant proteins will help to understand the mechanism of interaction with different isotypes of VDAC. The role of α tubulin in the regulation of VDAC permeability in cardiomyocytes is still unknown and should be uncover. Another approach to address this question could be to study β tubulin II and α tubulin intracellular distribution *in vivo* using stochastic optical reconstruction microscopy (STORM). To do this, further development of specific antibodies and fluoroproteins for the *in vivo* studies is needed.

Acknowledgments

This work was supported by Agence Nationale de la Recherche (SYBECAR project, nr RA0000C407), by INSERM, France and by institutional research funding IUT (IUT23-1) of the Estonian Ministry of Education and Research. We are grateful to Cindy Telier and Regis Montmayeul for technique assistance

Tables and Figures

Table 1

	$I_{20}R$ group (n= 11)	$I_{45}R$ group (n= 7)
Stabilization period		
Coronary flow, mL·min^{-1}	11.72 ± 0.96	12.16 ± 0.52
LVEDP, mmHg	5.34 ± 0.63	5.09 ± 0.47
LVDevP, mmHg	107.44 ± 7.86	103.0 ± 6.20
(+) dP/dt, mmHg·sec^{-1}	3460.07 ± 258.35	3286.54 ± 211.43
(-) dP/dt, mmHg·sec^{-1}	2451.35 ± 163.49	2454.57 ± 164.67
Reperfusion after ischemia		
Coronary flow, mL·min^{-1}	8.44 ± 0.90*	7.51 ± 1.16*†
LVEDP, mmHg	32.59 ± 5.77*	61.71 ± 5.78*†
LVDevP, mmHg	65.24 ± 6.20*	33.70 ±7.74*†
(+) dP/dt, mmHg·sec^{-1}	2181.44 ± 211.95*	1043.89 ± 253.86*†
(-) dP/dt, mmHg·sec^{-1}	1434.67 ± 143.99*	732.28 ± 168.61*†

Functional parameters of isolated perfused hearts measured at the end of the stabilization period and the end of post-ischemic reperfusion following either 20 min or 45 min of ischemia ($I_{20}R$ and $I_{45}R$ groups, respectively). LVEDP, left ventricular end diastolic pressure; LVDevP, left ventricular developed pressure; +dP/dt, maximal positive first derivative of left ventricular pressure; -dP/dt, maxmal negative first derivative of left ventricular pressure. * - Intragroup statistical differences (reperfusion versus stabilization period), † - Intergroups statistical differences, *,† $P < 0.01$. (Values are mean ± SEM).

Table 2

Respiration rates ($nmolO_2 \cdot min^{-1} \cdot mg^{-1}$ dwf)					
	control	I_{20}	I_{45}	$I_{20}R$	$I_{45}R$
V0, CI	6.63 ± 0.4	6.01 ± 0.6	6.57 ± 0.5	5.12 ± 1.3	6.34 ± 0.3
Vm(ADP), CI	46.21 ± 4.3	40.80 ± 4.1	43.65 ± 5.6	24.67 ± 2.3*	20.42 ± 1.8*
Vm(ADP+Cytc), CI	48.56 ± 4.5	47.8 ± 5.1	46.61 ± 4.2	28.69 ± 2.6*	27.39 ± 3.7*
Vm(ADP+Cytc), CII	48.62 ± 9.54			33.35 ± 2.1	28.10 ± 0.9
Vm(Cr+ATP)	46.33 ± 5.69			36.61± 3.6	24.45 ± 1.94*
Kinetic analysis (µM)					
app. Km for ADP	320.24 ± 23.2	311.83 ± 37.5	292.33 ± 27.6	230.83 ± 22.9*	180.76 ± 20.2*
app. Km for ADP(+Cr)	80.67 ± 24.9	125.13 ± 6.9	107.07 ± 33.9	74.01 ± 6.18	107.85 ± 12.9
CI activity, $IU/nmol_{cytaa3}$	0.15 ± 0.02	0.13 ± 0.02	0.20 ± 0.01	0.16 ± 0.02	0.15 ± 0.01

Respiration rates and ADP kinetic parameters of permeabilized muscle fibers from control hearts, hearts subjected to 20 or 45 min of global zero flow ischemia (I_{20} and I_{45} groups, respectively), and hearts subjected to 30 min of post-ischemic reperfusion ($I_{20}R$ and $I_{45}R$ groups, respectively). Respiration rates were measured in the presence of respiratory substrates for complex I (CI, 5mM glutamate and 2mM malate) or complex II (CII, 10 mM succinate plus 3 µM rotenone to inhibit CI). V0, basal rate of respiration (state 2 of respiration according to Chance (Chance and Williams 1956)); Vm, maximal rate of respiration stimulated by saturating amounts of ADP (2 mM, state 3 of respiration according to Chance); Vm(+Cytc), maximal ADP-stimulated respiration rates measured in the presence of exogenous 8µM Cytochrome c; app. Km ADP, apparent Michaelis-Menten constant for ADP; app. Km ADP(+Cr), apparent Michaelis-Menten constant for ADP measured in the presence of 20 mM creatine; CI activity, activity of the Electron Transport Chain complex I measured spectrophotometrically in whole tissue homogenates. Statistical significance (all studied groups versus control) is marked by: * $P < 0.05$; (Values are mean ± SEM).

Figure 1

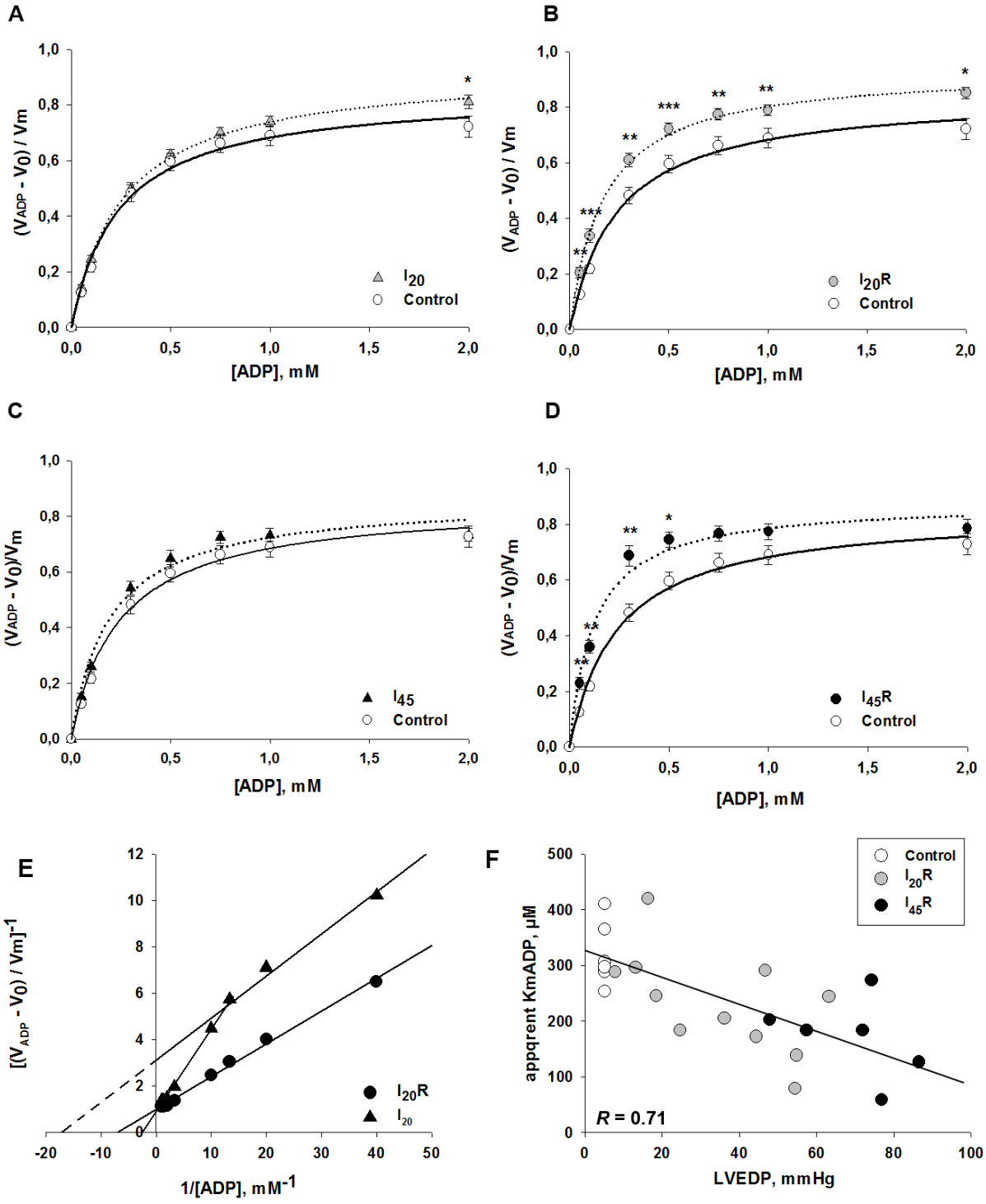

Kinetic analysis of respiration regulation of permeabilized left ventricular (LV) fibers by ADP. A, C) The apparent Michaelis constant for ADP (app. Km ADP) of LV fibers from hearts subjected

to 20 min (I_{20}, gray triangles) and 45 min (I_{45}, black triangles) of ischemia) were similar to that of control group (open circles). B, D) The app. Km ADP of LV fibers from hearts subjected to the post-ischemic reperfusion (gray circles for $I_{20}R$ and black circles for $I_{45}R$) were significantly lower than in control group. E) Double reciprocal plot of the dependence of respiration rates of permeabilized fibers on ADP concentration shows two app. Km ADP and two Vm values for the same fiber samples in I_{20} group (solid triangles), and one app. Km ADP and one Vm values for the same fiber samples in $I_{20}R$ group (solid circles). F) Negative correlation of the app. Km ADP with the left ventricular end-diastolic pressure (LVEDP) in the plot formed by control hearts and hearts subjected to post-ischemic reperfusion (Pearson's correlation coefficient, R, -0.708, $p < 0.001$). V_{ADP}, ADP-stimulated respiration rate; V0, basal respiration rate. Experiments were performed in the presence of respiratory substrates for complex I (5 mM Glutamate and 2 mM Malate). $^{*}P < 0.05$, $^{**}P < 0.01$, $^{***}P < 0.001$.

Figure 2

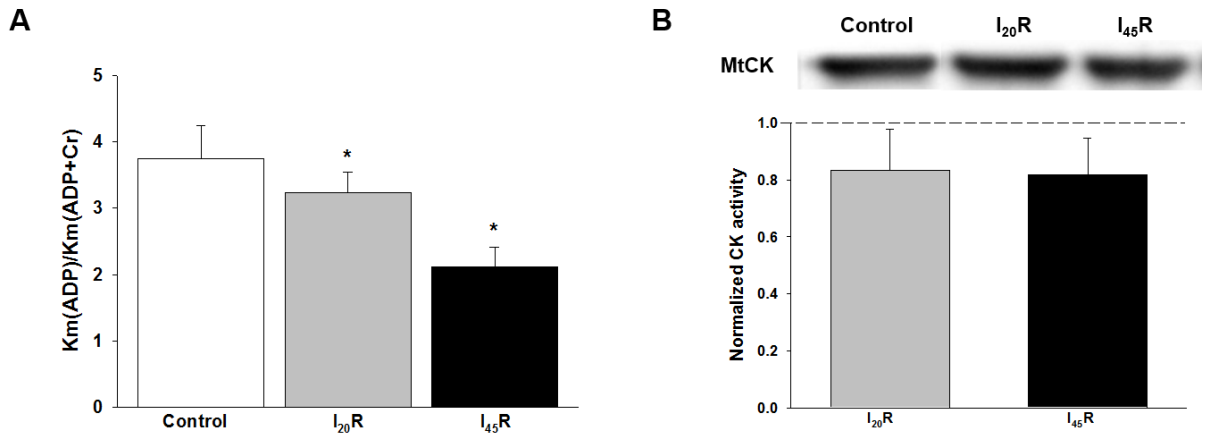

Kinetic analysis of the regulation of respiration of permeabilized left ventricular fibers by creatine. A) Catalytic efficiency of OxPhos to Cr estimated at the ratio $[(Vm/Km)_{Cr}]/[(Vm/Km)_{ADP}]$ indicates decreased creatine control of respiration in $I_{20}R$ and $I_{45}R$ groups. B) Western blot shows comparable with control group expression of MtCK in $I_{20}R$ and $I_{45}R$ groups. Total creatine kinase activity measured spectrophotometrically in whole tissue homogenates of post-ischemic reperfused hearts was not significantly different from that of the control group.

Figure 3

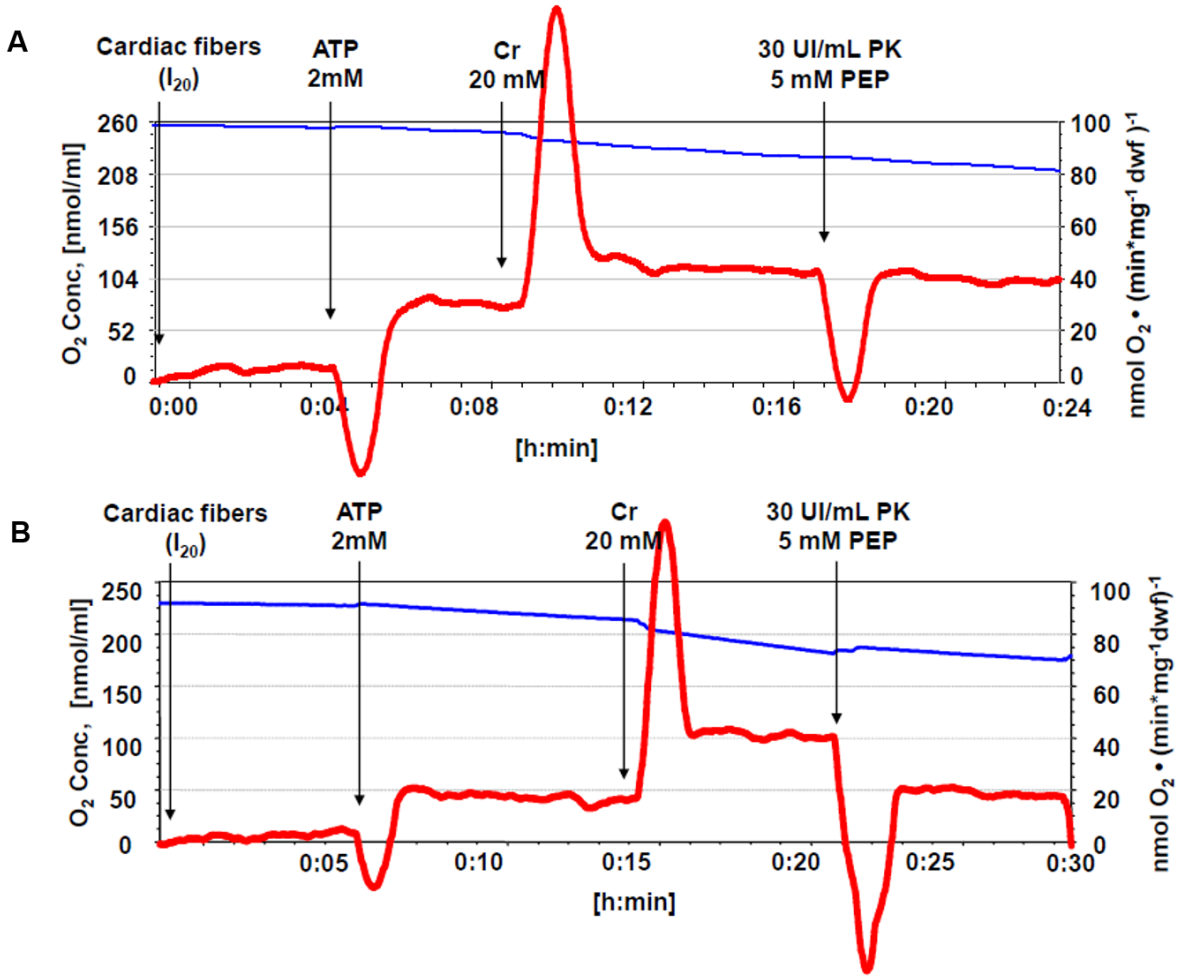

Representative respiration traces of permeabilized LV fibers from hearts subjected to 20 min ischemia (I_{20}) recorded using a two-channel high resolution respirometer (Oroboros oxygraph 2k, Innsbruck, Austria). The left scale and the blue trace indicate the oxygen concentration ($nmolO_2 \cdot ml^{-1}$) in the experimental milieu. The right scale and the red trace show the rate of oxygen uptake expressed in $nmolO_2 \cdot min^{-1} \cdot mg^{-1}$dry weight fibers. This experiment was designed to measure ADP fluxes from mitochondria. The respiration rate is stimulated by ADP produced by intracellular ATP consuming reactions from exogenous ATP (2 mM). The addition of creatine (20 mM) enhances respiration rates due to the production of endogenous ADP by MtCK within inter-

membrane space. Phosphenolpyruvate (PEP) and pyruvate kinase (PK) are used to remove extramitochondrial ADP. Figures show two different behaviors observed in I_{20} group: low (A, 16.44 ± 2.25 %) and high (B, 47.27 ± 3.97 %) PK-PEP inhibition of maximal creatine-stimulated respiration rates.

Figure 4

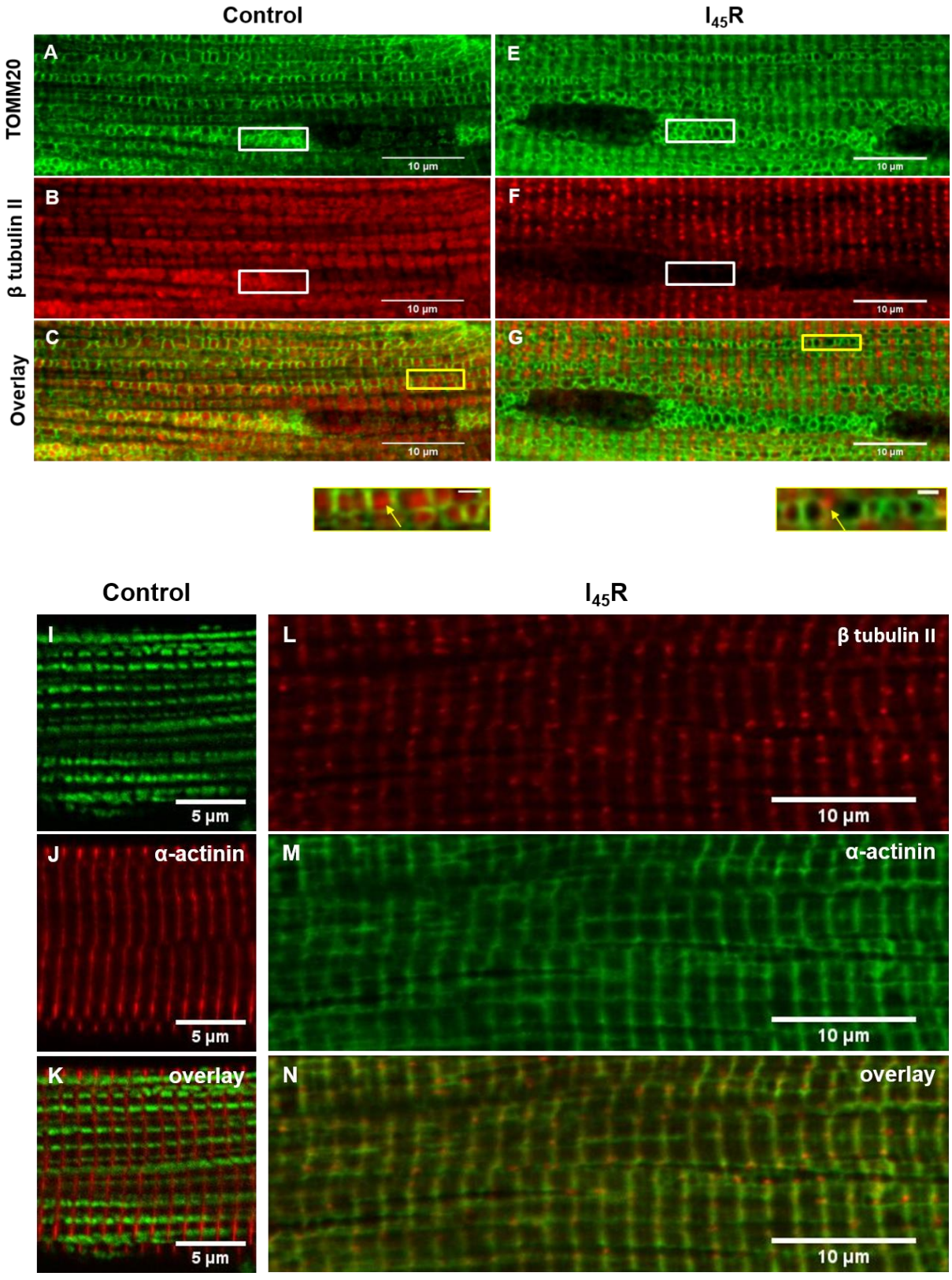
Control
I45R
TOMM20
β tubulin II
Overlay
A
B
C
E
F
G
10 µm
I
J
K
L
M
N
α-actinin
overlay
5 µm
10 µm

Confocal images showing immunocytochemistry based analysis of ischemia-reperfusion effect on β tubulin II distribution within fixed left ventricular heart fibers. Mitochondria were labeled in all cases using anti-TOMM20 antibody (mitochondrial outer membrane protein) except for image I where MitoTracker green was used. Sarcomeric Z-lines were labeled using anti-α-actinin antibody. A – D) Distribution of mitochondria (A, green color) and β tubulin II (B, red color) in fixed fibers from control hearts. Colocalization of β tubulin II with intermyofibrillar mitochondria was evidenced by the overlay (C) of confocal images A and B and the zoom (D) in the region of interest (ROI) delimited by a yellow box in image C. The ROI delimited by a white box in image A and B shows the co-localization of perinuclear mitochondria with β tubulin II. I - K) Distribution of mitochondria (I, green color) regarding α-actinin localization (J, red color) in fibers from control group. Merge (K) of confocal images I and J shows mitochondrial position between Z-lines. E – H) Distribution of mitochondria (E, green color) and β tubulin II (F, red color) in fixed fibers from hearts subjected to reperfusion after 45 minutes ischemia. Partial displacement of β tubulin II from intermyofibrillar mitochondria was evidenced by the overlay (H) of confocal images E and F and the zoom (H) of the ROI delimited by a yellow box in image G. The ROI delimited by a white box in images F and E shows the complete displacement of β tubulin II from perinuclear mitochondria. L – N) Intracellular distribution of β tubulin II (L, red color) regarding sarcomeric Z-lines labeled by anti-α-actinin antibody (M, green color) in fixed fibers from hearts subjected to reperfusion after 45 minutes of ischemia. N) Merge of confocal images L and M showing the colocalization of β tubulin II and α-actinin.

Figure 5

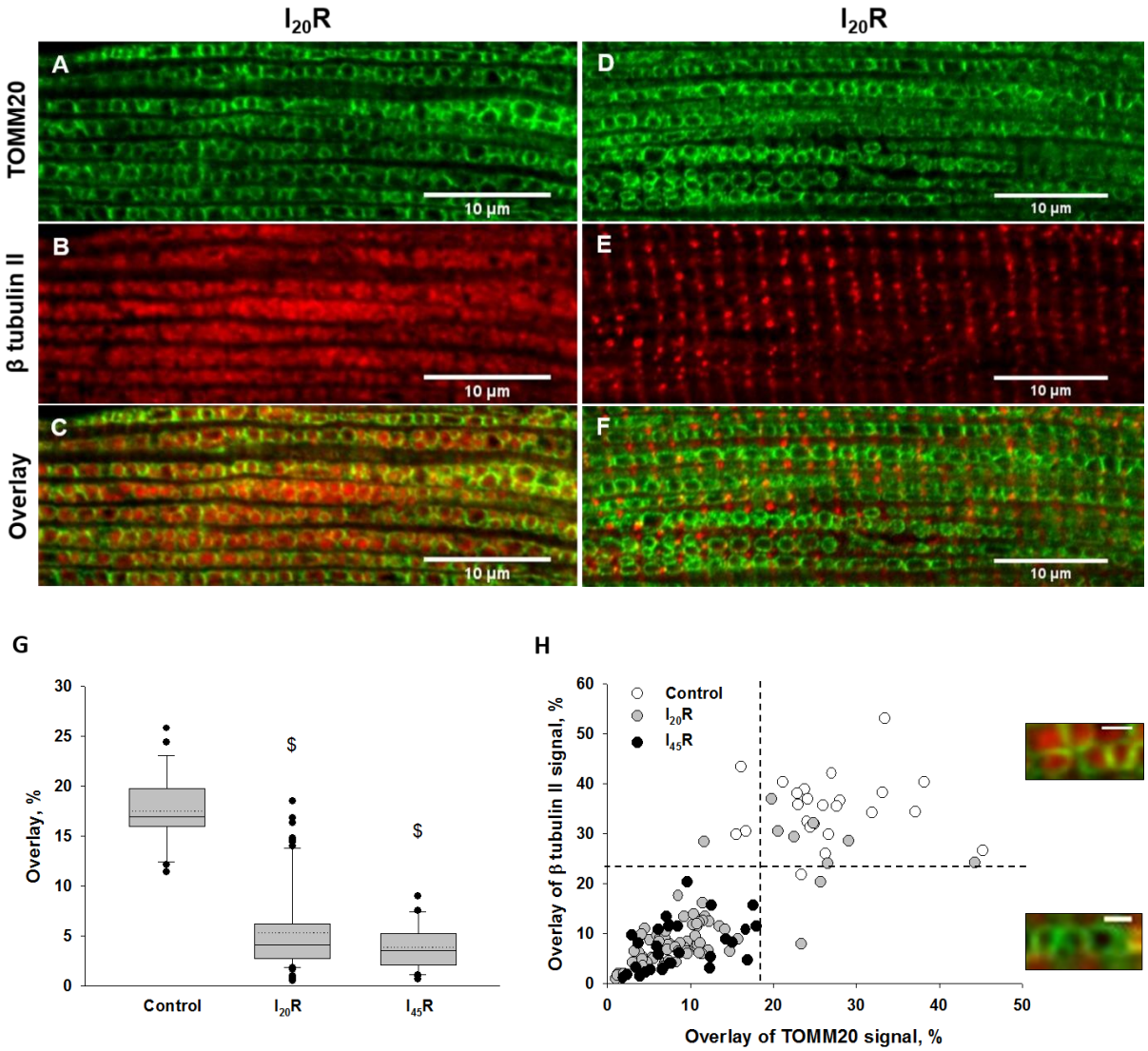

Immunocytochemistry of β tubulin II distribution within fixed fibers from hearts subjected to reperfusion after 20 minutes ischemia. Two different patterns of β tubulin II distribution (B and E, red color) regarding mitochondria labeled with anti-TOMM20 antibody (A and D, green color) were found. C) Merge of confocal images A and B shows co-localization of β tubulin II with mitochondria as it was seen in control group. F) Merge of confocal images D and E shows displacement of β tubulin II from intermyofibrillar mitochondria as in $I_{45}R$ group. G) Quantitative analysis of overlay between red fluorescence (channel 1, CH1) corresponding to β tubulin II

labeling and green fluorescence (channel 2, CH2) corresponding to TOMM20 labeling (i.e. mitochondrial outer membrane) of hearts from control, $I_{20}R$ and $I_{45}R$ groups. Analysis was done using FluoCorr imageJ plugging. H) Representation of the overlay CH1 versus the overlay CH2. The colocalization analysis evidenced a significant decrease in the overlay between β tubulin II and mitochondrial outer membrane surface and the re-distribution of overlaid fluorescence signal after ischemia-reperfusion.

Figure 6

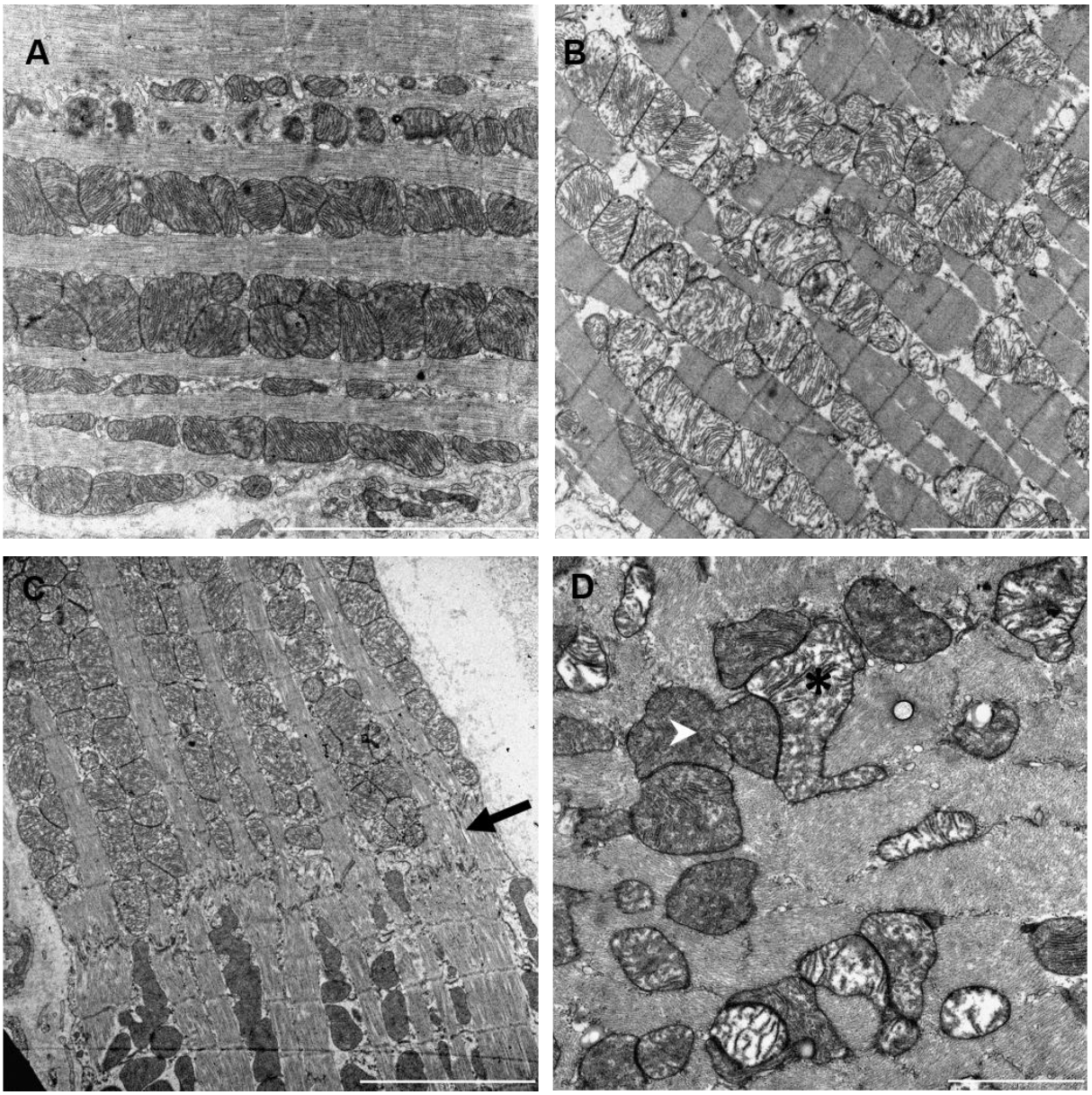

Transmition electron micrograph of the structural changes in left ventricular tissue of hearts subjected to ischemia-reperfusion injury. A) Heart from the control group. Scale bar 5 µm. B) Heart subjected to 45 min ischemia followed by 30 min reperfusion. Scale bar 5 µm. C – D) Heart subjected to 20 min ischemia followed by 30 min reperfusion. C) Heterogeneity of mitochondrial morphology could be observed between two adjacent cells. The arrow in this figure points the

junction between two cells. Scale bar 5 µm. D) Heterogeneity of mitochondrial morphology could also be observed in the same cell (cross-section of cardiomyocyte showing mitochondria with dense cristae (labelled by “arrowhead”) and mitochondria with remodelled cristae (labelled by “asterisk”). Scale bar 2 µm.

6.3. Respiratory supercomplex organization: an adaptive mechanism in cardiac ischemia-reperfusion?

Article in preparation

Abstract

Cardiac ischemia-reperfusion (IR) impairs energy metabolism, more specifically, it alters the regulation of mitochondrial function by intracellular energy needs and decreases mitochondrial oxidative phosphorylation (OxPhos) capacity. Recent evidence suggests that mitochondrial OxPhos capacity may be controlled by respiratory supercomplex (RSC) organization, which depends on mitochondrial morphology. The mitochondrial inner membrane protein OPA1 (Optic Atrophy type 1) was suggested to control cristae structure and thereby, RSC organization and apoptosis resistance. The aim of this study was to investigate the role that RSC organization plays in cardiac energy metabolism, as well as OPA1 cleavage and mitochondrial morphology in acute myocardial ischemia and reperfusion. Isolated langendorff-perfused rat hearts were subjected to 20 min or 45 min of total ischemia followed by reperfusion ($I_{20}R$ and $I_{45}R$ groups). RSC organization in the $I_{20}R$ group was heterogeneous across hearts, with the content of respiratory supercomplexes containing complex I being unaffected in some hearts whereas increased in others. The heterogeneity in RSC assembly observed in this group reflected the recovery of left ventricular function and mitochondrial OxPhos capacity, which reached almost normal values in some hearts and were dramatically altered in others. In contrast, all hearts from the $I_{45}R$ group exhibited severe left ventricular dysfunction and reduced mitochondrial OxPhos capacity, as well as a complete absence of RSC reorganization. Impaired mitochondrial function was associated with OPA1 cleavage, cristae remodeling and cytochrome c release. These results suggest that the RSC

reorganization observed in the $I_{20}R$ group could be an adaptive mechanism to overcome the IR-induced alterations of mitochondrial function.

Introduction

Cardiac ischemia-reperfusion (IR) impairs energy metabolism, more specifically, it alters the coupling of mitochondrial function to intracellular energy needs and decreases mitochondrial oxidative phosphorylation (OxPhos) capacity. Under physiological conditions, the cross talk between mitochondria and cellular energy-consuming systems depends on the specific structure of adult cardiomyocytes and the mitochondrial OxPhos capacity may be controlled by the arrangement of the RC complexes, which depends on mitochondrial morphology.

In adult cardiomyocytes, intermyofibrillar mitochondria are localized at the A-band level within the sarcomere limits, in close proximity to the T-tubular system and the sarcoplasmic reticulum (Fawcett and McNutt, 1969; Ogata and Yamasaki, 1997; Hayashi et al., 2009). This specific structure is the basis of "Intracellular Energetic Units" –basic pattern of organization of cardiac energy metabolism–, which permits the connection between ATP-synthesis sites and ATP-hydrolysis sites through intracellular phosphoryl transfer networks (Saks et al., 1998a; Saks et al., 2012; Vendelin et al., 2004; Abraham et al., 2002; Selivanov et al., 2004). The major high-energy phosphoryl transfer in normal hearts is the creatine kinase (CK) system, which represents the 80 – 88 % of total energy transferred within the cell (Pucar et al., 2001). At the mitochondrial level, the restricted diffusion of adenine nucleotides through mitochondrial outer membrane (MOM) enhances the functional coupling between mitochondrial creatine kinase (MtCK) and OxPhos, thus allowing intracellular energy transfer via CK system. The compartmentalization of energy transfer permits the feedback regulation of mitochondrial function by cellular energy needs in adult

cardiomyocytes under physiological conditions (Dzeja and Terzic, 2003; Dzeja et al., 2011; Saks et al., 2014; Schlattner et al., 2006; Wallimann et al., 1992).

Accumulating evidence in the literature suggests that the RC complexes are found in a balanced distribution between free respiratory complexes and RSC assemblies (so-called the plasticity model) (Acin-Perez et al., 2008; Acin-Perez and Enriquez, 2014). In heart mitochondria, the presence of supercomplexes of various stoichiometry was identified by blue native electrophoresis (BNGE), flux control analysis, electron microscopy or cryo-electron tomography among others techniques (Schägger and Pfeiffer, 2000; Schäfer et al., 2006; Bianchi et al., 2004; Althoff et al., 2011; Dudkina et al., 2011). RC complexes may be arranged like: complex III attached to complex I in the absence or presence of complex IV (I+III or I+III+IV); or complex III attached to complex IV (III+IV). The RC complexes organization was suggested to depend on mitochondrial morphology, which is controlled by a protein located in mitochondria inner membrane named Optic Atrophy type 1 (OPA1) (Cogliati et al., 2013; Civiletto et al., 2015; Scorrano et al., 2002; Frezza et al., 2006; Varanita et al., 2015).

Recent studies suggest that the deficiency of respiratory supercomplexes could be the mechanism underlying the mitochondrial dysfunction observed in several diseases (McKenzie et al., 2006; Huang et al., 2015; Gonzalvez et al., 2013; Frenzel et al., 2010; Gomez et al., 2012; Rosca et al., 2008; Rosca et al., 2011; Mejia et al., 2014). In the present work, we hypothesize that respiratory supercomplex (RSC) organization might be implicated in the IR-induced alterations of cardiac energy metabolism. To investigate this hypothesis, we have focused on the IR-induced effects on mitochondrial metabolism, RSC assembly and mitochondrial morphology of hearts subjected to 20 or 45 minutes of total ischemia followed by reperfusion.

Material and methods

This study was approved by the local research ethics committee (Comité Régional d'Ethique, no: 380814) in accordance with the regulations of the French Ministry of Agriculture and it complied with the requirements of the Guide for the Care and Use of Laboratory Animals published by the US National Institutes of Health (NIH Publications No. 85-23, revised 1996). All reagents were purchased from Sigma-Aldrich except: Na_2-ATP, Na_2-ADP and pyruvate kinase (PK) purchased from MP biomedicals; and leupeptine, fatty acid free Bovine Serum Albumin (BSA) and phosphoenol pyruvate (PEP) purchased from Roche.

Perfusion of isolated rat hearts

Isolated hearts from male Wistar rats (3 – 4 months aged) were placed on a Langendorff perfusion apparatus and perfused via the aorta under a constant pressure of 100 cm H_2O (9.807 kPa). The hearts were perfused using Krebs-Henseleit Buffer (KHB), containing 118.5 mM NaCl, 25.0 mM $NaHCO_3$, 4.8 mM KCl, 1.2 mM $MgSO_4$, 1.2 mM KH_2PO_4, 1.36 mM $CaCl_2$:$2H_2O$, 11 mM glucose at 37°C), and equilibrated with a gas mixture of 95% O_2 / 5% CO_2 (pH 7.4). In order to record the left ventricular (LV) function along the perfusion, a fluid-filled non-compliant balloon connected to a pressure transducer (P23ID, Statham, USA) was inserted into the left ventricle and was inflated to impose a LV end-diastolic pressure (LVEDP) of 5±1 mmHg (1 mmHg = 0.133 kPa) (Curtis et al., 1986). The sinoatrial node was removed to stop spontaneous heart beating and external electrical atrial pacing was imposed at a heart rate of 300 beats/min (Boucher et al., 1998).

Left ventricular cardiac function

LV function was assessed by the LV systolic (LVSP) and diastolic (LVDP) pressures and the difference between them, named LV developed pressure (LVDevP). Another variable measured was the positive and negative first derivative of LV pressure (+dP/dt and –dP/dt), that represents the kinetics of contraction and relaxation, respectively. These variables were calculated at the end of the stabilization and post-ischemic reperfusion periods using Chart 5 (ADInstument, Bella Vista, Australia). Moreover, we evaluated the coronary perfusion by measuring coronary flow rate. This variable is obtained by timed collection of coronary effluent over 30 s periods, every 5 minutes throughout perfusion.

Study design

All hearts were normoxically perfused for 15 minutes (i.e. stabilization period), and then subjected to 20 or 45 minutes of total zero flow normothermic ischemia followed by 30 minutes of reperfusion ($I_{20}R$ and $I_{45}R$, respectively). Variables of LV function estimated at the end of post-ischemic reperfusion were compared to those at the end of stabilization period for each group. All other data of hearts subjected to post-ischemic reperfusion were compared with that of non-perfused adult rat hearts.

Respirometry studies of permeabilized cardiac fibers

Permeabilized LV fibers from isolated hearts were prepared according to the protocol described by Kuznetsov et al., (Kuznetsov et al., 2008) and kept into ice-cold Mitomed solution of the following composition: 0.5 mM EGTA, 3.0 mM $MgCl_2$, 60 mM K-lactobionate, 3.0 mM KH_2PO_4, 20 mM taurine, 20 mM HEPES, 110 mM sucrose, 0.5 mM dithiothreitol, 2 mg·mL-1 BSA at pH 7.1. All solutions were supplemented with 1 µM leupeptine to protect cytoskeletal

proteins from lysosomal proteolysis (Kuznetsov et al., 2012). Oxygen consumption rates were measured in Mitomed solution at 25ºC using a high-resolution respirometer (oxygraph-2 K, OROBOROS Instruments, Austria). The solubility of oxygen was taken as 240 nmol·ml-1 (Gnaiger 2001) and oxygen consumption was expressed in nmolO_2·min-1·mg-1 dry weight fibers. Permeabilized fiber dry weight was assessed after 48 h at 100°C.

a) Respiration rates and ADP kinetics parameters

Basal respiration rates (V0) of permeabilized LV fibers were measured in the presence of respiratory substrates for: complex I (CI, 5 mM glutamate and 2 mM malate), complex II (CII, 10 mM succinate and 3 µM rotenone) or both complexes (CI+II, 5 mM glutamate, 2 mM malate and 10 mM succinate). Addition of saturating concentration of ADP (2 mM) in the presence of respiratory substrates, results in the maximal respiration rate (Vm(ADP)). The respiratory control ratio (RCR) is the ratio between Vm(ADP) and V0 and indicates the coupling of OxPhos. Integrity of mitochondrial outer membrane (MOM) was evaluated by addition of cytochrome c (8 µM). The effect of cytochrome c addition on the maximal respiration rate (Vm) was calculated as the ratio between the difference of maximal respiration before and after addition of cytochrome c and the maximal respiration in the presence of cytochrome c [(Vm(+Cytc) – Vm) / Vm(+Cytc)].

Regulation of respiration by ADP in permeabilized LV fibers was assessed by stimulating respiration by increasing concentrations of ADP (from 0.05 to 2 mM) in the absence and the presence of creatine (20 mM). The addition of creatine (Cr) allows us to estimate the regulation of respiration by endogenous ADP produced in activated MtCK reaction. The apparent Michaelis constant for ADP (app. KmADP) is the ADP concentration at which the reaction rate is half of maximal respiration rate, thus reflecting the permeability of MOM for adenine nucleotides. This

parameter was calculated from double reciprocal plots of the dependence of respiration rate on ADP concentration. Functional coupling between MtCK and OxPhos via ANT was assessed by the ratio between the apparent Km for ADP estimated in the absence and in the presence of creatine (app.KmADP(-Cr)/ app.KmADP(+Cr)).

b) Determination of flux control coefficient (FCC)

The flux control coefficient (FCC) is the degree of control that the rate (*v*) of a given enzyme *i* exerts on flux *J*. FCC can be determined experimentally by titration curves using specific enzyme inhibitors. For the case of irreversible specific inhibitor, an estimation of FCC value for a given enzyme *i* on the flux *J* is defined according to the following equation (Fell, 1992):

$$C_{v_i}^{J} = \frac{\Delta J}{\Delta I} \cdot \frac{I_{max}}{J_0}$$

where (ΔJ/ΔI) is initial slope of the stepwise inhibition of oxygen respiration graph, I_{max} is the inhibitor concentration giving complete inhibition, and J_0 is the initial steady-state flux value. Because of this kind of mathematical analysis, the FCC shown in this report could not be in the form of mean values with standard errors. However, it can be emphasize that the FCC values of permeabilized LV fibers from the control group were similar to previously published data (Bianchi et al., 2004; Tepp et al., 2010). In the present work, the FCC of complex IV (CIV) was determined by cyanide titration of ADP-stimulated respiration of permeabilized LV fibers from all studied groups. The FCC of CIV was measured in the presence of respiratory substrates for CI or both complexes (CI+II).

Measurement of complex I activity

LV samples were homogenized in sucrose buffer (250 mM) using a Potter tissue grinder and centrifuged at 600 g (10 min, 4 °C). Complex I activity was measured spectrophotometrically (Specord 210 spectrophotometer (Analytik Jena AG, Germany)) as described in Spinazzi et al., 2012. The activity was normalized by mitochondrial cytochrome aa3 content, which was measured as described previously (Monge et al., 2008) with slight modifications to avoid the interference of myoglobin or blood contamination to the oxidation-reduction difference spectrum (Balaban et al., 1996).

Determination of CK activity and isoenzyme distribution

Creatine Kinase (CK) is present in the cells as 4 isoenzymes localized in different subcompartments: cytosol and mitochondria. The cytosolic CK enzymes consist of two subunits: B (brain type) or M (muscle type), which can be associated in three different ways giving the isoenzymes: CK-MM, CK-BB and CK-MB. On the other hand, the mitochondrial CK (MtCK) can be found in dimeric or octameric forms, being the former an inactivated form. CK isoenzymes in homogenized LV samples (concentration equal to 3 mg prot/mL) were separated by native cellulose polyacetate electrophoresis (CPAE) run at 150V for 1h 30min (Wyss et al., 1990). Subsequently, the CK bands were visualized by a color reaction coupled to the CK enzyme activity (Walimmann et al., 1985). The reaction mixture was supplemented with 100 μM P1P5-di(adenosine-5′)-pentaphosphate to inhibit interfering adenylate kinase activity. Finally, the relative contributions of individual isoenzymes to total CK activity was determined by quantifying their expression using ImageQuant LAS 4000 (GE Healthcare Life Sciences). Total CK activity of samples from different groups was measured spectrophotometrically (Specord 210

spectrophotometer (Analytik Jena AG, Germany)) as described in Schlattner et al., 2000, in order to normalize the relative contributions of individual CK isoenzymes between different groups.

Electron Microscopy

LV tissue from different samples was fixed with 0.1 M Cacodylate buffer pH 7.2 supplemented with 2% paraformaldehyde and 2% glutaraldehyde for 2 hours at room temperature and then washed twice in 0.1 M Cacodylate buffer. Samples were subsequently post-fixed with 1% osmium tetraoxide in 0.1 M Cacodylate buffer for 1 h at 4 °C and then stained with 0.5% uranyl acetate in water pH 4.0 overnight at 4 °C. Next day, samples were dehydrated by incubation in a graded series of ethanol solutions (30%, 60%, 90% and three times in 100%) prior to be infiltrated with an ethanol/resin mixture (1:1) for 1 hour at room temperature. Once the tissue was embedded in Epon and polymerized for 2 days at 60 °C, ultrathin sections were prepared with a diamond knife on an UC6 Leica ultramicrotome and collected on Formvar-coated 200 μm mesh copper grids. Sections were post-stained with 5% uranyl acetate in water and 0.4% lead citrate in water before being examined under a transmission electron microscope (1200EX JEOL, Japan) at 80 kV. Images were acquired with a digital camera (Veleta, Olympus, Tokyo, Japan) and analyzed with iTEM Software (Olympus, Tokyo, Japan).

Western blotting

LV samples were homogenized in a buffer containing: 50% glycerol, 5% DMSO, 10 mM Na2HPO4, 0.5 mM EGTA, 0.5 mM MgSO4 at pH 6.95 and supplemented with protease inhibitor cocktail (Sigma P8340). Eight percent SDS-PAGE gel was loaded with different samples at the same concentration and run at 120 V. Proteins in SDS-PAGE gel were transferred to a

nitrocellulose membrane during 1h 20min at 120 V. Samples were probed with the primary antibody anti-OPA1 (BD 612607) and anti-MtCK (generously provided by Dr. Malgorzata Tokarska-Schlattner) followed by incubation with their respective horseradish peroxidase secondary antibody. Antibody reactivity was visualized using an enhanced chemiluminescent immunodetection system (GE Healthcare Life Sciences) and quantified using ImageQuant LAS 4000 (GE Healthcare Life Sciences). All data were expressed relative to the MtCK band.

Blue-native polyacrylamide gel electrophoresis (BN-PAGE) analysis

Mitochondria were isolated from LV samples as described previously (Fernandez-Vizarra et al., 2002) and permeabilized with digitonin at a concentration of 10 mg per mg of mitochondrial protein. Each assay was loaded by 50 - 75 µg of digitonin-treated isolated mitochondria for each sample. BN-PAGE was performed as described by Wittig et al., (Wittig et al., 2006). The blots were probed with an anti-core1 antibody to reveal complex III (CIII) and an anti-FpSDH antibody to reveal complex II (CII). The CIII signal was normalized by CII expression in the same sample. RSC organization is indicated by the ratio of CIII dedicated to NADH (SC-containing CIII attached to CI) versus CIII dedicated to FAD (CIII free or attached to complex IV, CIV). In-gel activity measurement is a method that allows semiquantitative assessments of the activity of individual respiratory enzymes within each respiratory supercomplex separated by BN-PAGE. CI- and CIV-specific in-gel activity consist in incubating the BN-PAGE during 1h to 3h into either 0.1M Tris-HCl pH 7.5; 1mg/ml NBT; 0.14mM NADH to reveal CI activity or 50 mM phosphate buffer; 0.5 mg/ml DAB; 1mg/ml cytochrome c to reveal CIV activity.

Statistical analysis

Values are presented as mean ± SEM. Statistical comparison of data from the same group was performed by t-test, for parametric variables, and Mann-Whitney test, for non-parametric variables. Statistical comparison of data from different groups was performed by One Way Anova with Holm-Sidak method as post-hoc, for parametric variables, and Kruskal-Wallis test with Dunn's method as post-hoc, for non-parametric variables. In all cases, a value of $P < 0.05$ was considered a significant difference, which was pointed with an asterisk (*****) for the comparison regarding the control group and with a cross (†) for the comparison between the post-ischemic reperfused groups.

Results

Left ventricular function of isolated perfused hearts

Ischemia-reperfusion induced a significant decrease in LV developed pressure associated with the increase in LVEDP (6 and 12 times in the $I_{20}R$ and $I_{45}R$ groups, respectively) (Table 1). The kinetics of contraction (+dP/dt) and relaxation (-dP/dt) were reduced about 40 % in the $I_{20}R$ group and about 70 % in the $I_{45}R$ group (Table 1). LV function alterations were accompanied by the decrease of the coronary flow after post-ischemic reperfusion. This decrease was more pronounced in $I_{45}R$ than in the $I_{20}R$ group (about 45 % and 30 %, respectively), thus indicating a higher perfusion constriction in the former group (Table 1). Overall, this data evidences an IR-induced alteration of diastolic function, which depends on the ischemia duration. All LV functional variables were more affected in the $I_{45}R$ than in the $I_{20}R$ group (Table 1). Moreover, LV functional variables of the $I_{20}R$ group comprised values between normal and those of the $I_{45}R$ group (phenomenon represented in Fig. 1A). The IR-induced alterations of LV function in our study are similar to previously published data (Boucher et al., 1998; Pucar et al., 2001).

Respirometry studies

a) Maximal respiration rates of permeabilized cardiac fibers

Maximal respiration rates (Vm(ADP)) of permeabilized LV fibers measured in the presence of substrates for CI significantly decreased after ischemia-reperfusion (Table 2). This decrease was associated with a significant reduction of respiratory control ratio (RCR), since basal respiration rates (V0) were similar between control and post-ischemic reperfused groups (Table 2). This data evidences IR-induced damage on the OxPhos capacity. Maximal respiration rates between post-ischemic reperfused groups were significantly different, this parameter being more reduced in $I_{45}R$ than in the $I_{20}R$ group (Table 2). Consequently, RCR values decreased about 60 % in the $I_{45}R$ group and 25 % in the $I_{20}R$ group with respect to the control group. These results indicate that the IR-induced damage on OxPhos capacity depends on the duration of ischemia. Figure 1B shows that RCR values of the $I_{20}R$ group are comprised between those of the control and $I_{45}R$ groups, thus revealing heterogeneity in the IR-induced decrease of OxPhos capacity across hearts of this group. In contrast, $I_{45}R$ hearts presents homogenously reduced OxPhos capacity compared to controls. These results are in accordance with IR-induced alteration on LV function of post-ischemic reperfused hearts.

MOM integrity was assessed by the addition of exogenous cytochrome c, which did not increase maximal respiration rates of the control and $I_{20}R$ groups (Table 2). In contrast, maximal respiration rates of the $I_{45}R$ group were increased by about 26 % by addition of cytochrome c. Despite the stimulatory effect of cytochrome c in this group, maximal respiration rates in the presence of this protein remained significantly lower than those in the control group (Table 2). Therefore, these results evidence the integrity of MOM in the $I_{20}R$ group, whereas the $I_{45}R$ group

presents mitochondria with damaged MOM that allows the release of cytochrome c. However, it seems that this alteration of MOM integrity cannot be sufficient to explain the reduced OxPhos capacity in the $I_{45}R$ group.

Maximal respiration rates stimulated by complex II substrates in the post-ischemic groups were similar to those stimulated by complex I substrates (Table 2). This indicates the absence of CI inhibition in the $I_{20}R$ and $I_{45}R$ groups, which was confirmed by the unaltered enzymatic activity of CI in these groups measured spectrophotometrically (Table 2). Maximal respiration rates stimulated by substrates for both complexes (VmADP(CI+II)) were significantly reduced in the $I_{45}R$ group (Table 2). This decrease was associated with a significant reduction of RCR and a stimulatory effect of cytochrome c, although maximal respiration rates in the presence of cytochrome c were still significantly lower compared to control (Table 2). In contrast, the $I_{20}R$ group presented maximal respiration rates measured in the presence of substrates for CI and CII similar to those of control group (Table 2). The apparent contradiction of this result with the absence of CI inhibition described previously could be due to the low number of samples (n = 3) for VmADP (CI+II) and the heterogeneous results of this group. These samples (n = 3) presented high RCR values in the presence of substrates for CI, similar to those of the control group (RCR equal to 7.41 ± 0.70). In order to have a more representative value for VmADP (CI+II) of the $I_{20}R$ group, we shall increase the group size.

b) Regulation of respiration of permeabilized cardiac fibers

High apparent Km for ADP of permeabilized cardiac fibers from control group reflects the restricted diffusion of adenine nucleotides through MOM (Fig. 1C). The addition of 20 mM creatine decreased the app. Km for ADP due to the Cr-induced activation of MtCK reaction (Fig. 1C). In this group, the respiration is controlled by ADP produced in MtCK reaction and localized

at the intermembrane space. This is possible as long as MOM permeability for ADP is restricted and there is a functional coupling between MtCK and OxPhos via ANT. This functional coupling is evaluated by the ratio between the app. Km for ADP measured in the absence and presence of creatine [KmADP(-Cr) / KmADP(+Cr)]. This ratio is equal to 3.74 ± 0.70 in the control group.

Kinetic analysis of respiration regulation by ADP showed a significant decrease in app. Km for ADP after ischemia-reperfusion (Fig. 1C). The addition of creatine decreased app. Km for ADP up to a similar value in all groups. However, the ratio between the app. Km for ADP, with and without creatine, diminished in post-ischemic reperfused groups (3.25 ± 0.71 and 2.28 ± 0.27 in the $I_{20}R$ and $I_{45}R$ respectively). This ratio was significantly lower in the $I_{45}R$ group compared to that of the control group ($P < 0.05$). The study of CK isoenzyme distribution by CPEA revealed that MtCK activity in post-ischemic reperfused groups was similar to controls (Fig. 1D). Moreover, the ratio between MtCK dimeric and octameric forms was not affected by ischemia-reperfusion. In contrast, the total CK activity decreased about 20 % in post-ischemic reperfused groups which is explained by the decreased activity of cytosolic CK isoenzymes (BBCK, BMCK and MMCK) in these groups (Fig. 1D). These results are consistent with maximal respiration rates stimulated by ADP produced by MtCK reaction (Vm(ATP+Cr)) in post-ischemic reperfused hearts (36.61 ± 3.57 and 24.45 ± 1.94 in the $I_{20}R$ and $I_{45}R$ groups, respectively). These rates were comparable to those of maximal respiration stimulated by ADP for the same group. Altogether, these data evidence the IR-induced increase in MOM permeability for adenine nucleotides, which affects the functional coupling between MtCK and OxPhos. Therefore, ischemia-reperfusion induces a switch in the control of respiration from ADP produced in MtCK reaction towards cytosolic ADP.

c) Flux Control Coefficient of CIV

Oxygen consumption rates of oligomycin-treated permeabilized fibers measured in the presence of 0.5 mM TMPD and 1 mM ascorbate were similar between post-ischemic reperfused and control hearts (Table 2). This data suggests unaltered activity of CIV after ischemia-reperfusion, since oxygen consumption (under these conditions) can be attributed to the isolated CIV. Cyanide titrations of ADP-stimulated respiration of permeabilized LV fibers from all groups was carried out in order to check possible IR-induced alterations of the control of electron flux by CIV. Figure 2 shows the averages of a series of titration curves measured in the presence of substrates for complex I (Fig. 2A) or for both complexes (CI+II) (Fig. 2B). The cyanide titration curves in the presence of substrates for complex I were similar amongst all studied groups. Therefore, the flux control coefficients of CIV (FCC(CIV)), when respiration was stimulated by electrons provided via NADH oxidation, were similar between post-ischemic reperfused groups (0.38 for both $I_{20}R$ and $I_{45}R$) and control group (0.37) (Table 2). The FCC(CIV) values of LV permeabilized fibers from control group were comparable to previously published data for heart mitochondria and cardiomyocytes (Bianchi et al., 2004; Tepp et al., 2010). In contrast, the cyanide titration curve measured in the presence of substrates for CI and CII was less steep in the $I_{45}R$ group than in the $I_{20}R$ or control groups. Thus, the FCC(CIV) in this group (0.34) was lower than in the control group (0.49), whereas the FCC(CIV) of the $I_{20}R$ group (0.48) was comparable to that of the control group (Table 2). Overall, these results indicated that although the control that CIV exerted on the electron flux provided by NADH oxidation was comparable in all studied groups, the control exerted by CIV on the electron flux provided by NADH and $FADH_2$ oxidation is reduced in the $I_{45}R$ group, while it is unaffected in the $I_{20}R$ group, as compared to control.

Mitochondrial Morphology studied by Electron Microscopy (EM)

a) Mitochondrial organization in post-ischemic reperfused hearts

In adult cardiomyocytes under physiological conditions (control group), intermyofibrillar mitochondria are organized in a crystal-like pattern (between the Z-lines at the level of the A-band (Fig. 3A)) and in close proximity to the sarcomeric reticulum, T-tubular system and the myofibril (Fawcett and McNutt 1969; Ogata and Yamasaki, 1997; Hayashi et al., 2009). This specific structure was found to be optimal for the intracellular energy transfer via phosphoryl transfer networks (mainly CK system under physiological conditions) (Saks et al., 1998a; Saks et al., 2012; Vendelin et al., 2004; Abraham et al., 2002; Selivanov et al., 2004; Pucar et al., 2004). The LV tissue from the $I_{45}R$ group presented disorganized intermyofibrillar mitochondria with increased space between mitochondria and myofibrils, as well as juxtaposed mitochondria (Fig. 3B). Moreover, the surface area occupied by mitochondria increased in this group by about 24 %, although the mitochondrial density decreased by about 10% (Table 3). On the contrary, the $I_{20}R$ group presented regions with mitochondria still arranged in a crystal-like pattern (Fig. 3C), and others with alterations of mitochondrial organization reminiscent to the $I_{45}R$ group (Fig. 3D). Mitochondrial density in this group was similar to control, even if the surface area occupied by mitochondria (Mitochondrial area / Total area) increased by about 20% (Table 3). This data evidences that the regular intermyofibrillar mitochondrial organization was altered in post-ischemic reperfused hearts, depending on the severity of the IR-induced injury. In particular, our results showed that the $I_{20}R$ group displays heterogeneous alterations of mitochondrial organization across hearts. These morphological results observed in these groups are in accordance with the previously described LV function and OxPhos capacity.

b) Mitochondrial inner membrane structure in post-ischemic reperfused hearts

At the level of cristae structure, in the control group most mitochondria presented tightly packed cristae (mitochondria Class I from Fig. 4A), characterized by low distance between juxtaposed cristae (i.e. intercristae space) and high cristae density (Fig. 4 D, E; Table 3). In this group there are about 25% of mitochondria with cristae remodeled (Class II) and less than 5% mitochondria with disorganized cristae (Class III) (Fig. 4A). The proportion of class-type mitochondria in the $I_{20}R$ group was similar to control, whereas the $I_{45}R$ group presented significantly decreased class I mitochondria in favor of mitochondria of class II and III (Fig. 4A). All cristae measurements were performed from mitochondria of class I and II from each condition (Fig. 4 D, E; Table 3). The result of this analysis indicates that the $I_{45}R$ group presented mitochondria with a decrease of about 40 % in cristae density (Fig. 4E) and an increase of about 35 % in intercristae space (Fig. 4C – D). These morphological alterations may be explained by the significant increase in mitochondrial area, as well as, by cristae degradation, since the number of cristae per mitochondrion in this group decreased significantly (Table 3). In contrast, the $I_{20}R$ group presented mitochondria with the cristae structure either similar to control or similar to the $I_{45}R$ group due to the heterogeneity observed in this group (Figure 3 C – D). In average, the morphological alterations observed in this group are characterized by a 13% decrease in cristae density and a 10 % increase in intercristae space (Fig. 4 D, E; Table 3). These modifications were observed from mitochondria with normal cristae size and number of cristae per mitochondrion (Table 3). Thereby, this suggests that the cristae structure alterations observed in the $I_{20}R$ group should be explained by the significant increase in mitochondrial area due to swelling (Table 3).

Determination of OPA1 processing

The MIM protein Optic Atrophy 1 (OPA1) was shown to control mitochondrial morphology and resistance to apoptosis. In cardiac tissue, there are two OPA1 splice variants (denoted as band *a* and *b*), each of which seems to be subsequently processed to form several isoforms with distinct molecular sizes. OPA1 splice variants can be either processed by the mitochondrial proteases OMA1 or Yme1L, depending on the cleavage site (S1 and S2, respectively). Therefore, OPA1 splice variant denoted as band *a* can be processed by Yme1L to generate the OPA1 isoform denoted band *d* or by OMA1 to generate the OPA1 isoform denoted band *c*, whereas the OPA1 splice variant denoted band *b* can only be processed by OMA1 to generate the OPA1 isoform denoted band *e*. In the case of the OPA1 isoforms denoted band *c*, it can be further processed by Yme1L to generate the OPA1 isoform denoted band *d*.

In this work, we studied OPA1 expression and cleavage in all studied groups using western blot. The expression of OPA1 was normalized by MtCK, since this mitochondrial intermembrane protein was shown to be unaltered by ischemia-reperfusion. The total expression of OPA1 in post-ischemic reperfused hearts was similar to that in control hearts (Fig. 5 B). However, the contribution of each OPA1 isoform to the total expression was different between studied groups (Fig. 5 A, C). Our results showed that in the $I_{45}R$ group OPA1 splice variants were drastically cleaved, resulting in the absence of OPA1 long forms (band *a* and *b*) in favor of OPA1 short forms (mainly band *c* and *e*). In contrast, the $I_{20}R$ group presented only a slight increase in short forms of OPA1, mainly band *c* and *e* (Fig. 5 A, C). Therefore, western blotting studies evidence that the IR-induced OPA1 cleavage depends on the ischemia duration and that these cleavages are induced by the activation of the stress protease OMA1.

Supramolecular complex assembly and their in-gel activity

Respiratory Supercomplex (RSC) organization was studied in post-ischemic reperfused and control hearts using blue-native gel electrophoresis (BNGE) (Fig. 6). Respiratory complexes can be organized in respirasome [SC containing complexes I, III, and IV (I+III+IV)], other supercomplexes ($(I+III)_{1-2}$ or III+IV), and individual populations. The distribution of complex III in its different pools (CIII attached or disassociated with complex I) indicates which substrates are favorable to be oxidized. The former pool (I+III+IV; I+III; $(I+III)_2$) enhances NADH oxidation to feed electrons to the respiratory chain via CI, whereas the latter pool (free CIII and III+IV) promotes $FADH_2$ oxidation to feed electrons to the respiratory chain via CIII. The distribution of complex III in its different pools pointed to RSC reorganization only for the $I_{20}R$ group. The ratio of complex III dedicated to NADH versus Complex III dedicated to FAD (III NADH / III FAD) increased in this group compared to that in the control group. (Fig. 6 A, C). These results evidence that the flux of electrons feeding the respiratory chain is higher through CI than directly through CIII compared to control. This IR-induced reorganization of RSC assembly was heterogeneous across hearts from the $I_{20}R$ group, since the ratio of III NADH / III FAD in this group comprised values between those of control and twice control's values (Fig. 6C). In contrast, in the $I_{45}R$ group the ratio of III NADH / III FAD was similar to that in the control group, thus pointing out the absence of RSC reorganization in this group (Fig. 6 B, C). These results were confirmed by complex I and complex IV in-gel activity measurements (Fig. 7). This method allows semiquantitative assessment of the activity of individual respiratory enzymes (in this case, Complex I and IV) within each respiratory supercomplex separated by BN-PAGE. In-gel activity measurements revealed that the activities of RSC-containing CIII attached to CI increased in the $I_{20}R$ group, while in the $I_{45}R$ group they were similar to control (Fig. 7A, C and Fig. 7B, D respectively).

Discussion

In the present work, we have studied the effect of IR-induced injury on supramolecular organization of RC complexes and its implications on cardiac energy metabolism. In addition, we have addressed the emerging hypothesis that proteins controlling mitochondrial morphology, such as OPA1, play an important role in cardiac energy metabolism since they may control resistance to apoptosis.

IR-induced effects on cardiac function, mitochondrial metabolism and structural organization

Our results evidence the IR-induced reduction of mitochondrial OxPhos capacity and impairment of mitochondrial metabolism regulation, which was characterized by the increase in MOM permeability for adenine nucleotides (low app. Km ADP) and the decrease in creatine control on respiration due to the reduced functional coupling of MtCK to ATP Synthase (low ratio between app. Km for ADP without and with creatine) (Fig. 1C). These alterations were associated with cardiac left ventricular dysfunction, which is indicated among others by the increase in LV end-diastolic pressure (i.e. LV function variable considered an index of heart failure severity) (Table 1). The severity of the IR-induced alterations of mitochondrial function and regulation as well as LV function are shown in our work to be dependent on ischemia duration. Whereas 45 minutes of ischemia followed by reperfusion ($I_{45}R$ group) causes homogenously severe damage, hearts subjected to 20 minutes of ischemia followed by reperfusion ($I_{20}R$ group) are heterogeneously affected across hearts (Fig. 1A, B). The mitochondrial function and regulation is heterogeneous in this group, which is indicated by the RCR and app. Km for ADP displaying values between those of control hearts and those of the $I_{45}R$ group (Fig 1B; app. Km for ADP in

the I20R group is comprised between 419.81 - 79.09 µM). In this group, LV functional variables also present values comprised between those of control hearts and those of the $I_{45}R$ group (phenomenon represented in Fig. 1A). These alterations are related to the structural modifications after IR injury revealed by our electron microscopy analysis. In the $I_{20}R$ group, we observe regions with intermyofibrillar mitochondria still organized in a crystal-like pattern (Fig. 3C), like in control hearts (Fig. 3A), and others with intermyofibrillar mitochondria disorganized, reminiscent of that observed in the $I_{45}R$ group (Fig. 3D and B for the $I_{20}R$ and $I_{45}R$ groups, respectively). The main features of mitochondrial disorganization induced by IR injury are the increase of clusters and the increment of the distance between mitochondria and myofibrils, as well as between juxtaposed mitochondria (Fig. 3B).

According to published data, the IR-induced decrease in app. Km for ADP and functional coupling of MtCK to ATP Synthase results in the decrease in intracellular phosphoryl flux transfer between mitochondria and energy-consuming reactions (De Sousa et al., 1999; Pucar et al., 2001; Boudina et al., 2002). In particular, Pucar et al. showed that the energy phosphoryl fluxes through creatine kinase dropped over 4 times in an experimental model similar to our $I_{45}R$ group (Pucar et al., 2001). The impaired feedback regulation of mitochondrial function leads to a decline in the Frank-Starling relationship and ADP accumulation within ICEU, thus inducing the inhibition of ATPase activity and the calcium uptake by sarcoplasmic reticulum (for a review see Seppet et al., 2005). Previous studies have linked the decline in phosphoryl flux transfer via creatine kinase to the IR-induced decrease in the MtCK activity, expression or ratio between octameric and dimeric forms (Sobollet al., 1999; Wendt et al., 2003). In both models, myocardial acute ischemia *ex vivo* (Langendorff perfusion) and chronic ischemia *in vivo* (left anterior descending artery infarction), impairment of cardiac function and mitochondrial metabolism were associated with a significant

decrease in MtCK activity and octamer/dimer. These findings, together with recent data showing that MtCK is a prime target of peroxynitrite induced damage, suggest that oxygen radicals generated during ischemia and reperfusion could be an important factor for the decreased octamer stability.

However, in our model, MtCK expression and activity are unaltered since the maximal rates of respiration stimulated by addition of exogenous ADP or addition of ATP and creatine to activate MtCK reaction (endogenous ADP) are comparable. Moreover, the CPEA analysis of the activity and content of the different CK isoenzymes reveals that IR didn't affect the MtCK activity or octamer/dimer ratio and that the decrease in total CK activity observed in post-ischemic reperfused hearts is due to the decrease in cytosolic CK activities (Fig. 1D). Therefore, these results suggest that the impaired feedback regulation of mitochondrial function observed in our model is not explained by a defect in MtCK function. Nevertheless, the increase in adenine nucleotide diffusion through MOM indicated by the decreased app. Km for ADP may affect the intracellular phosphoryl flux transfer via phosphotransfer networks since the functional coupling of MtCK to ATP Synthase is enhanced by the compartmentalization of adenine nucleotides.

Another important factor to meet the intracellular energy demands is the mitochondrial OxPhos capacity, which depends on the organization of the RC complexes. Recent studies have suggested that mitochondrial OxPhos capacity could be reduced by a decline in respiratory supercomplex organization rather than inhibition of individual respiratory complexes (McKenzie et al., 2006; Huang et al., 2015; Gonzalvez et al., 2013; Frenzel et al., 2010; Gomez et al., 2012; Rosca et al., 2008; Rosca et al., 2011; Mejia et al., 2014). The decrease in OxPhos capacity would lead to the reduction of electron flux through respiratory chain and thereby, lower the proton gradient generation and ATP synthesis. The decrease in ATP production causes the decrease in

intracellular phosphoryl flux transfer and cardiac dysfunction due to the deficit of energy (Seppet et al., 2005).

Effects of IR on respiratory complex organization and consequences on mitochondrial function

RC complex organization is modified by 20 minutes of ischemia followed by reperfusion, whereas longer ischemia did not alter their organization ($I_{45}R$ group) (Fig. 6). In the $I_{20}R$ group, we observe an increase in respiratory supercomplexes containing complex I compared to control. This phenomenon is made obvious by the increase in the ratio between complex III dedicated to NADH (i.e. respiratory supercomplexes containing CIII attached to I) and Complex III dedicated to FAD (free complex III or III+IV) (Fig. 6C). The RSC organization is heterogeneous across hearts of the $I_{20}R$ group since the ratio of III NADH / III FAD in this group comprises values between those of control hearts and twice their value. Therefore, some hearts from this group have RSC organization similar to controls and others present increased content of respiratory supercomplexes containing CI (Fig. 6 C). The RSC organization in post-ischemic reperfused groups is associated with mitochondrial OxPhos capacity and maximal respiration rates, which decreased drastically when the RSC organization is unaltered like in the $I_{45}R$ group (Fig.1B).

In addition, we showed that the hearts from the $I_{20}R$ group displaying normal OxPhos capacity present normal flux control coefficients of complex IV (FCC(CIV)) when respiration is stimulated by substrates of CI or both complexes (CI+II) (Fig. 1A, B and Table 2). In contrast, in the $I_{45}R$ group the control that complex IV exerts on electron flux (low FCC(CIV)) is reduced when respiration was stimulated by substrates of both complexes, although FCC(CIV) in this group is similar when respiration is stimulated by substrates of CI (Fig.1A, B and Table 2). The reduced FCC(CIV) in the $I_{45}R$ group is not related to a decrease in complex IV activity, since the

oxygen consumption rate in the presence of TMPD and ascorbate (substrates for complex IV) is comparable in all groups (Table 2). Previous studies using a canine failing heart model have shown that impaired OxPhos capacity in the presence of normal individual complex activities is explained by the instability of respiratory supercomplexes containing complex IV (Rosca et al., 2008; Rosca et al., 2011). On the contrary, our CIV in-gel activity measurement revealed that the activity of respiratory supercomplexes containing complex IV does not decrease after IR injury in our experimental model (Fig. 7D). This result is also confirmed by the ratio of III NADH / III FAD which is similar or higher than that of control hearts (Fig. 6 C).

The results of the present work suggest that the RSC reorganization observed after reversible IR-induced damage ($I_{20}R$ group) could be an adaptive mechanism to overcome the IR-induced alterations of mitochondrial function. This assumption is based on the literature which shows that the increase in the respiratory supercomplex I+III+IV content results in the increase in individual respiratory complex stabilization (Schägger et al., in 2004; Acin-Perez et al., 2004; Stroh et al., 2004; Diaz et al., 2006; Li et al., 2007; Vempati et al., 2009) and the increase in efficient electrons transfer to complex IV by metabolic channeling (Bianchi et al., 2003; Bianchi et al., 2004, Schäfer et al., 2007; Acin-Perez et al., 2008). This assumption is in accordance with the plasticity model which envisages a dynamic equilibrium between supercomplexes and randomly diffusing individual complexes depending on mitochondrial function (Acin-Perez et al., 2008; Acin-Perez and Enriquez, 2014). A fundamental prediction of this model is that the structural organization of the respiratory chain is variable, allowing the cell to adapt to different substrates sources and varying physiological conditions (D'aurelio et al., 2006; Piccoli et al., 2006; Quarato et al., 2011; Ramirez-Aguilar et al., 2011; Lapuente-Brun et al., 2013).

According to the literature, the increase in any respiratory supercomplex containing CIII attached to CI (not only the respiratory supercomplex I+III+IV) could be associated to the prevention of reactive oxygen species (ROS) production (Lenaz and Genova 2007; Quarato et al., 2011; Diaz et al., 2012; Ghelli et al., 2013; Maranzana et al., 2013). In isolated mitochondria there are three ways to drive ROS production: through NADH accumulation in the mitochondrial matrix, through reverse electron transport and, during normal mitochondrial oxidative phosphorylation, due to electron leaks. Chouchani *et al.,* have shown that the selective accumulation of the Krebs cycle intermediate succinate is a universal metabolic feature of ischemia and is responsible for mitochondrial ROS production during reperfusion by reverse electron transport at mitochondrial complex I (Chouchani et al., 2014). Therefore, we speculate that the increase in respiratory supercomplexes containing complex III attached to complex I (CIII dedicated to NADH) may protect the cell from further damage induced by ROS generation. This speculation is based on the idea that reverse electron transport will be prevented in supercomplex containig CIII attached to CI since the association between complex III and I would limit the access of ubiquinone binding site of complex I for electron transfer. This idea is in accordance with the previous speculation that the different susceptibility of different types of cells and tissues to ROS damage depends on, among other reasons, the extent and tightness of supercomplex organization of respiratory chain complexes (Lenaz and Genova 2007). In this review, the authors have speculated that complex I possess two different quinone-binding sites for direct and for reverse electron transfer, and thereby, two different routes exist for forward and reverse electron transfer within the complex. These two site were proposed to become alternatively accessible depending on the membrane potential, which was recently showed to control the supramolecular organization of the respiratory chain complexes within the MIM (Piccoli et al., 2006; Quarato et al., 2011). Moreover, the disruption of the

association of complexes I and III was shown to increase ROS production by complex I itself (Maranzana et al., 2013). The assembly of complex I into respiratory supercomplex results in the stabilization of this complex (Schägger et al., 2004; Acin-Perez et al., 2004; Stroh et al., 2004) and in a conformational change of its structure that limits the exposure of its redox centers to oxygen (Radermacher et al., 2006).

Effects of IR on OPA1 cleavage and consequences on mitochondrial morphology and resistance to apoptosis

Our studies did not reveal cytochrome c release in hearts from the $I_{20}R$ group, as indicated by the absence of stimulatory effect by exogenous cytochrome c on maximal respiration (Table 2). This observation was accompanied by unaltered amount of OPA1 long forms (Fig. 5) and moderate alterations of mitochondrial cristae morphology in this group (Fig. 4). The impairment of mitochondrial function in the $I_{45}R$ group was associated with a drastic IR-induced OPA1 cleavage, leading to a significant decrease in OPA1 long forms compared to those in the $I_{20}R$ or control groups (Table 2; Fig. 5). In particular, the cleavage of OPA1 was mainly at the S1 cleavage site, thus resulting in the decrease in the long forms *a* and *b* in favor of the short forms *c* and *e*, respectively (Fig.5). Previous studies have shown that the processing of OPA1 at this cleavage site is regulated by OMA1 (overlapping activity with m-AAA protease). This MIM protease is activated among others by the decrease in mitochondrial ATP levels or the dissipation of membrane potential (Anand et al., 2014; Ehses et al., 2009; Zhang et al., 2013; Baricault et al., 2007). Moreover, the stress-induced OPA1 processing by OMA1 has been shown to increase the sensitivity of cells to apoptotic stimuli and to induce cristae remodeling. These alterations were associated with the loss of OPA1 long forms, which were suggested to be responsible for most of

OPA1 function (Anand et al., 2014). Our results are in agreement with this study, since the absence of OPA1 long forms in the $I_{45}R$ group is associated with cytochrome c release (indicated by the stimulatory effect of exogenous cytochrome c on maximal respiration) and the increased proportion of mitochondria with cristae disorganized (Class III) or remodeled (Class II) (Table 2; Fig. 4A).

According to the literature, OPA1 is known to regulate mitochondrial inner membrane structure and thereby, to control apoptosis associated with the reshaping of mitochondrial cristae and cytochrome c release (Scorrano et al., 2002; Frezza et al., 2006). Overexpression of OPA1 has been shown to protect mice from denervation-induced muscular atrophy, ischemic heart and brain damage, as well as hepatocellular apoptosis (Varanita et al., 2015). This phenomenon suggests that OPA1-dependent mitochondrial cristae stabilization increases mitochondrial respiratory efficiency and blunts mitochondrial dysfunction, cytochrome c release, and ROS production. In contrast, loss of OPA1 (Cipolat et al., 2006) or the selective loss of OPA1 long forms alone (Merkwirth et al., 2008) increases the apoptotic sensitivity of mitochondria. Anand *et al.*, have showed that the presence of long forms of OPA1 is essential for preserving cristae morphology and for the cellular apoptosis resistance (Anand et al., 2014). Moreover, the loss of OMA1 was showed to protect cells against apoptosis (Quirós et al., 2012; Stiburek et al., 2012) since the stress-induced OPA1 cleavage by OMA1 converts OPA1 completely into short isoforms. In particular, mice with OMA1 deficiency were prevented of acute kidney injury as indicated by better renal function, less mitochondrial fragmentation, and decreased apoptosis (Xiao et al., 2014).

Conclusions

The results of this study, to the best of our knowledge, show for the first time that *ex-vivo* myocardial IR triggers the increase of RSCs containing CI, which is suggested to be an adaptive mechanism to overcome the IR-induced alterations of mitochondrial function. Moreover, our results reveal that *ex-vivo* myocardial IR leads to OPA1 cleavage, which depends on ischemia duration and mitochondrial function. The cleavage of OPA1 and thereby, the loss of OPA1 long forms content, is associated to reshaping of cristae structure and release of cytochrome c. The results of the present work reveal a potential adaptive mechanism to overcome mitochondrial dysfunction after cardiac IR injury.

Limitations of the study and perspectives

In the present work, the different response of mitochondria to stress, which was observed in the $I_{20}R$ group, hinders the observation of the link between RSC organization and mitochondria OxPhos capacity. The IR-induced heterogeneous response at the mitochondrial level was previously described in other IR experimental model (Kuznetsov et al., 2004) and confirmed by EM studies (Article 2). This phenomenon was explained by the electrical discontinuity of individual mitochondria, which prevents the collapse of the entire cell energy metabolism (Beraud et al., 2009). Thereby, specific *in vivo* techniques should be developed in order to be able to measure mitochondrial function and to visualize RSC organization in the same mitochondrion. Another possibility to face this challenge would be to study the IR-induced damage on mitochondrial function in an animal model deficient of supramolecular organization of the respiratory chain (C57BL/6J) compared to the same animal model presenting RSC organization (C57BL/6J overexpressing SCAFI). A recent study has demonstrated that the presence of

supercomplex assembly factor I (SCAFI) is related to the interaction between complexes III and IV. Animal models SCAFI deficient, such as C57BL/6J, are characterized by the absence of interaction between complexes III and IV, whereas overexpression of SCAFI induces the formation of RSCs containing CIV (Lapuente et al., 2013).

Our work has also suggested that the IR-induced cleavage of OPA1 could be controlled by OMA1 which is activated by mitochondrial impairment. Recent studies have shown that overexpression of OPA1 protects mice from ischemic heart damage (Varanita et al., 2015) and ameliorates the mitochondrial respiration in mouse models presenting a defect in the respiratory chain (Civiletto et al., 2015). However, the implication of OMA1-induced OPA1 cleavage on mitochondrial metabolism and RSC organization has not yet been addressed. In order to further investigate this question, the effect of *ex-vivo* myocardial IR on mitochondrial metabolism, morphology and RSC organization should be studied in a mouse model deficient in OMA1.

Acknowledgments

This work was supported by Agence Nationale de la Recherche (SYBECAR project, nr RA0000C407), by INSERM, France and by institutional research funding IUT (IUT23-1) of the Estonian Ministry of Education and Research. We are grateful to Cindy Telier and Regis Montmayeul for technique assistance.

Tables and Figures

Table 1

	$I_{20}R$ group	$I_{45}R$ group
Stabilization period		
Coronary flow, mL·min^{-1}	11.59 ± 0.61	12.01 ± 0.35
LVEDP, mmHg	5.41 ± 0.38	6.17 ± 0.41
LVDevP, mmHg	113.15 ± 5.30	103.0 ± 6.20
(+) dP/dt, mmHg·sec^{-1}	3480.83 ± 159.84	3425.43 ± 122.52
(-) dP/dt, mmHg·sec^{-1}	2476.81 ± 100.00	2487.27 ± 85.86
Post-ischemic Reperfusion		
Coronary flow, mL·min^{-1}	8.12 ± 0.53 *	6.54 ± 0.71 *†
LVEDP, mmHg	31.41 ± 4.13*	72.45 ± 4.32 *†
LVDevP, mmHg	69.75 ± 4.16 *	33.70 ±7.74 *†
(+) dP/dt, mmHg·sec^{-1}	2219.38 ± 136.54 *	846.50 ± 145.97 *†
(-) dP/dt, mmHg·sec^{-1}	1539.55 ± 96.27 *	622.00 ± 97.25 *†

Left ventricular (LV) functional variables and coronary flow in isolated perfused hearts measured at the end of the stabilization period and at the end of the post-ischemic reperfusion ($I_{20}R$: n = 20; $I_{45}R$: n = 15). LVEDP, left ventricular end diastolic pressure; LVDevP, left ventricular developed pressure; (+) dP/dt, maximal positive first derivative of left ventricular pressure; (-) dP/dt, maximal negative first derivative of left ventricular pressure. * - Intragroup statistical differences (reperfusion versus stabilization period), † - Intergroup statistical differences, *,† $P < 0.05$ Values are mean ± SEM.

Table 2

	Control	$I_{20}R$	$I_{45}R$
Respiration rates ($nmolO_2 \cdot min^{-1} \cdot mg^{-1} dwf$)			
V0, CI	6.03 ± 0.39	5.24 ± 0.15	5.92 ± 0.29
Vm (ADP), CI	42.94 ± 3.10	28.42 ± 1.97 *	17.69 ± 1.78 *†
RCR, CI	7.20 ± 0.44	5.47 ± 0.40 *	2.96 ± 0.20 *†
Vm (ADP + Cyt c), CI	45.68 ± 3.40	31.04 ± 2.14 *	23.90 ± 2.87 *
Vm (ADP + Cyt c), CII	48.62 ± 9.54	33.35 ± 2.11	27.36 ± 1.09 *
V0, CI+II	11.91 ± 0.72	12.09 ± 0.24	12.10 ± 0.33
Vm (ADP), CI+II	43.27 ± 2.87	46.63 ± 1.88	21.92 ± 3.47 *†
RCR, CI+CII	3.65 ± 0.29	3.69 ± 0.09	1.80 ± 0.23 *†
Vm (ADP + Cytc), CI+II	44.45 ± 3.46	47.57 ± 1.60	32.51 ± 5.57 *†
Vm (TMPD + Asc + Cyt c)	145.99 ± 30.81	106.48 ± 31.08	108.87 ± 14.92
FCC (CIV), CI	0.37	0.38	0.38
FCC (CIV), CI+II	0.49	0.48	0.34
Complex I activity, IU/nmolcytaa3	0.15 ± 0.02	0.16 ± 0.02	0.15 ± 0.01

Respiration rates of permeabilized cardiac fibers from control (n = 2 – 8) and post-ischemic reperfused hearts ($I_{20}R$: n = 2 – 17; $I_{45}R$: n = 2 – 7). Respiration rates were measured in the presence of respiratory substrates for complex I (CI, 5 mM glutamate and 2 mM malate), complex II (CII, 10 mM succinate plus 3 µM rotenone to inhibit CI) or both substrates (5 mM glutamate, 2 mM malate and 10 mM succinate). V0, basal respiration rate (state 2 of respiration according to Chance (Chance and Williams 1956)); Vm (ADP), maximal respiration rate stimulated by 2 mM of ADP (state 3 of respiration according to Chance); RCR, respiratory control ratio measured as the ratio between Vm and V0; Vm(ADP + Cytc), maximal ADP-stimulated respiration rates measured in the presence of exogenous 8µM Cytochrome c; Vm(TMPD + Asc + Cytc), maximal oxygen consumption rate stimulated by CIV substrates (0.5 mM TMPD and 1 mM ascorbate) in the presence of the respiratory chain inhibitors (10 µM Antimycin and 3 µM Rotenone); FCC (CIV),

flux control coefficient of complex IV (CIV) measured in the presence of substrates for complex I (CI) or both complexes (CI+II); CI activity, activity of complex I measured spectrophotometrically in LV tissue homogenates. * - Statistical differences compared to control group, † - Statistical differences between post-ischemic reperfused groups, *, † $P < 0.05$. Values are mean ± SEM except in the case of FCC (CIV) since these values are indexes due to the kind of mathematical analysis used to estimate this parameter.

Table 3

	Control	$I_{20}R$	$I_{45}R$
Mitochondrial organization			
Mitochondrial density, mito./µm^2	0.36 ± 0.01	0.38 ± 0.01	0.32 ± 0.01*†
Mitochondrial area / Total area, %	34.43 ± 0.76	41.76 ± 0.96 *	42.79 ± 1.15 *
Mitochondrial morphology			
Individual mitochondrial area, nm^2			
Cristae size, nm	21.8 ± 0.2	22.4 ± 0.3	23.0 ± 0.3*
Cristae number, n°cristae/mito.	23.4 ± 0.8	23.7 ± 0.8	21.0 ± 0.6†

Morphological parameters of mitochondria from post-ischemic reperfused hearts and control hearts indicating IR-induced alteration on mitochondrial organization and morphology. Parameters assessing mitochondrial organization are the average of the measurement of 20 images per heart (n = 3). Parameters assessing mitochondrial morphology were measured from mitochondria of class I or II, whereas mitochondria of class III were not considered for this analysis (mitochondria classification from fig. 4A). Mitochondrial morphology parameters are the average of the measurement of more than 100 mitochondria per heart (n = 3). * - Statistical differences compared to control group, † - Statistical differences between post-ischemic reperfused groups, *,† $P < 0.05$. Values are mean ± SEM.

Figure 1

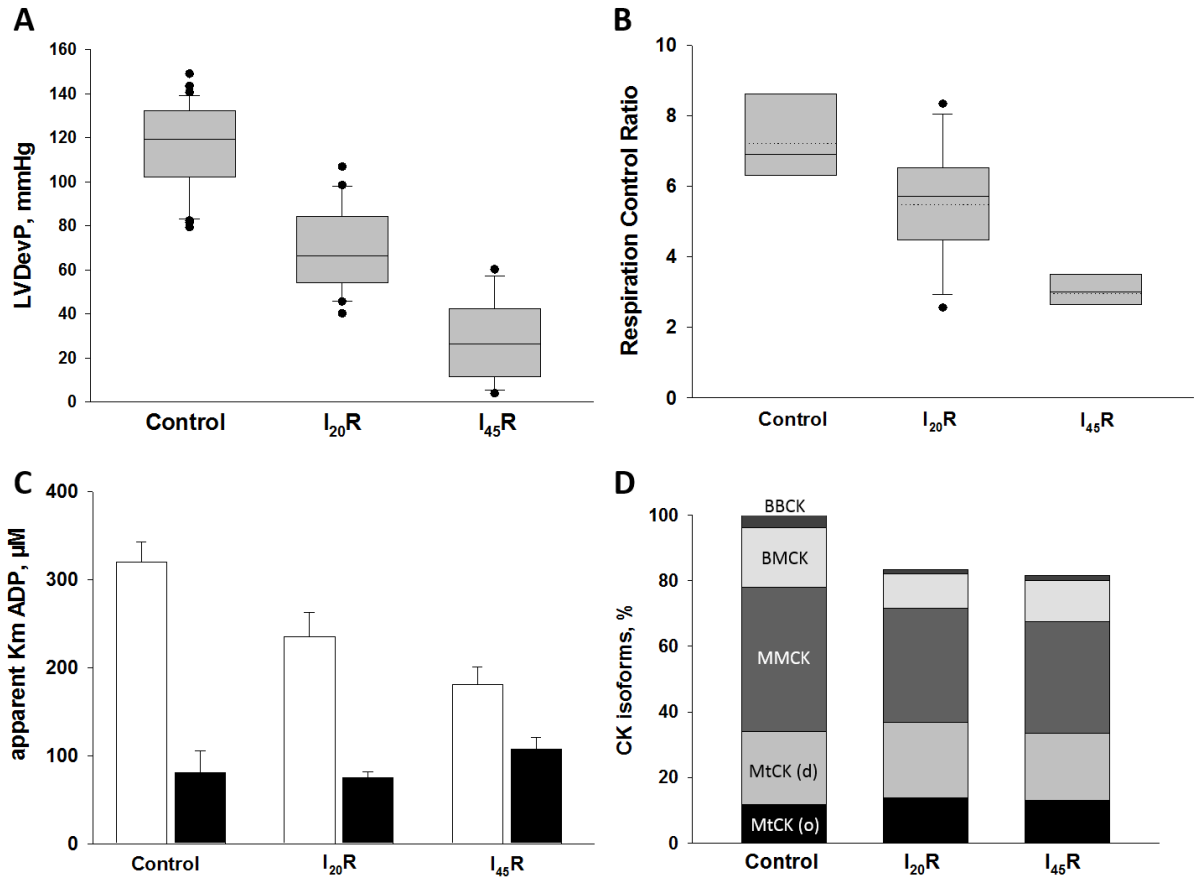

Respirometry analysis, left ventricular function and CK isoenzymes activities of post-ischemic reperfused hearts compared to control hearts. A – B) Represent the heterogeneity observed across hearts of the I20R group in LV function (indicated by LVEDP) and mitochondrial oxidative phosphorylation (OxPhos) capacity (evaluated by respiration control ratio). C) The apparent K_m for ADP of permeabilized cardiac fibers from all studied groups was measured in the absence (white bars) and in the presence (black bars) of creatine (Cr). The ratio between app. Km for ADP (-Cr) and Km for ADP (+Cr) indicates the functional coupling between MtCK and OxPhos via ANT. D) The graph represents the contribution of each CK isoenzymes in the total CK activity of each group. The total CK activity of the post-ischemic reperfused groups was normalized by that

in control group. * - Statistical differences compared to control group, † - Statistical differences between post-ischemic reperfused groups, *, † $P < 0.05$. Values are mean ± SEM.

Figure 2

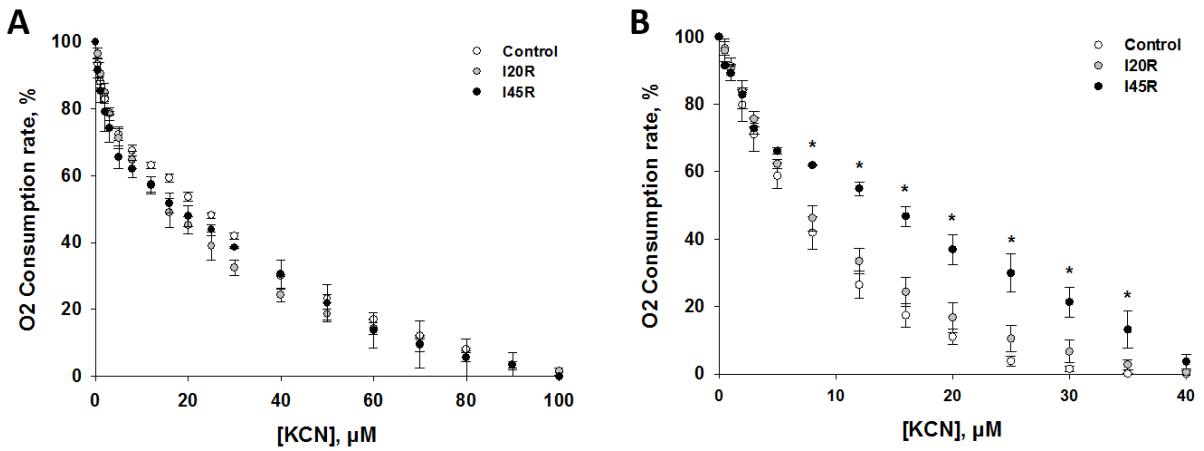

Flux control coefficient of complex IV in control (white), $I_{20}R$ (grey) or $I_{45}R$ (black) groups. Respiration of permeabilized cardiac fibers was progressively inhibited by stepwise addition of potassium cyanide. The averages of a series of titration curves measured in the presence of substrates for A) complex I (5mM glutamate and 2mM malate) and B) both substrates (5mM glutamate, 2mM malate and 10 mM succinate). * - Statistical differences compared to control group, * $P < 0.05$. Values are mean ± SEM.

Figure 3

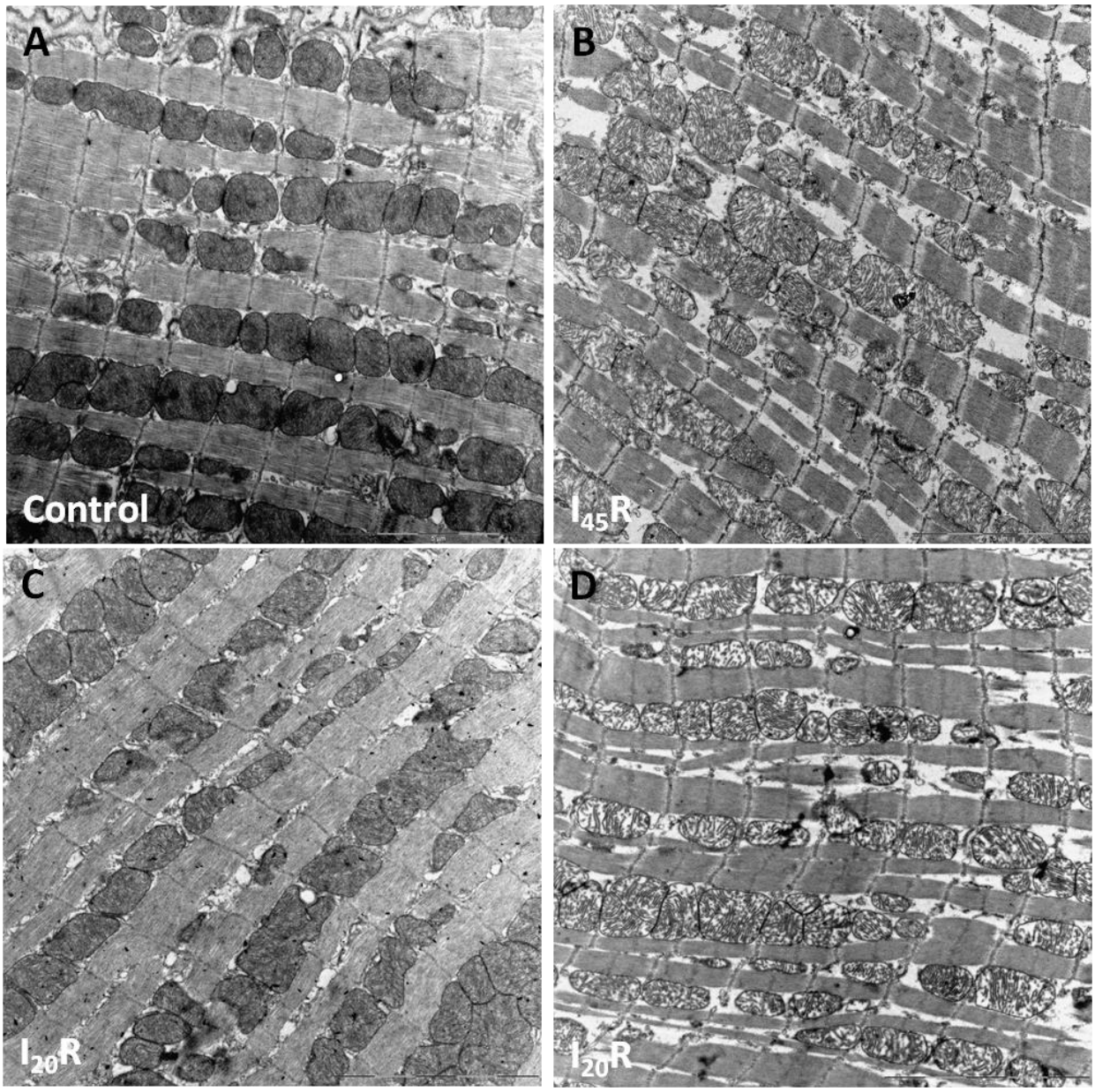

Transmition electron micrograph of the structural changes in left ventricular tissue of hearts subjected to ischemia-reperfusion injury. A) Control group. Scale bar 5 µm. B) I45R (hearts subjected to 45 min ischemia followed by 30 min reperfusion). Scale bar 5 µm. C – D) I20R (hearts subjected to 20 min ischemia followed by 30 min reperfusion). Mitochondrial organization and

morphology is heterogeneous in this group, some regions being reminiscent to control (C) and others to $I_{45}R$ group (D).

Figure 4

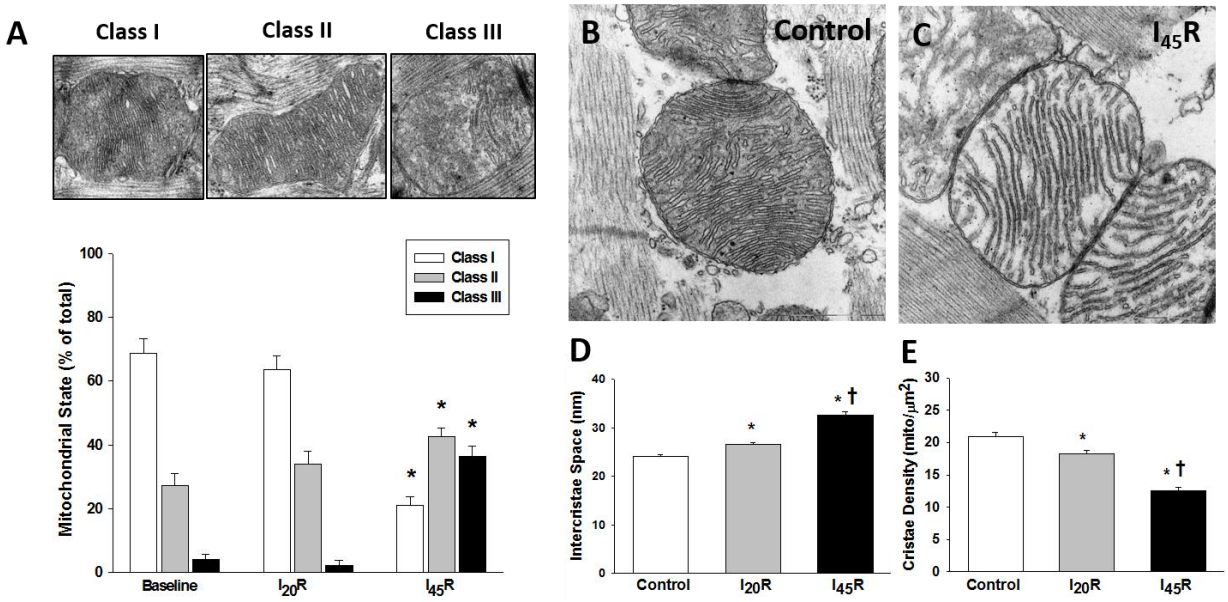

Morphometric analysis of mitochondria from post-ischemic reperfused hearts compared to control. A) Distribution of the proportion of different class-type mitochondria in all studied groups. Mitochondria were assigned to morphological classes I to III depending on cristae state (I- cristae intact; II- cristae remodeled; III- cristae disorganized). B) Representative electron micrograph of mitochondria from control group. Scale bar 1 µm. C) Representative electron micrograph of mitochondria from the $I_{45}R$ group. Scale bar 1 µm. D) Morphometric quantification of the distance between juxtaposed cristae (i.e. intercristae space) from mitochondria of different groups. E) Morphometric quantification of the cristae density from mitochondria of different groups. * - Statistical differences compared to control group, † - Statistical differences between post-ischemic reperfused groups, *,† $P < 0.05$. Values are mean ± SEM.

Figure 5

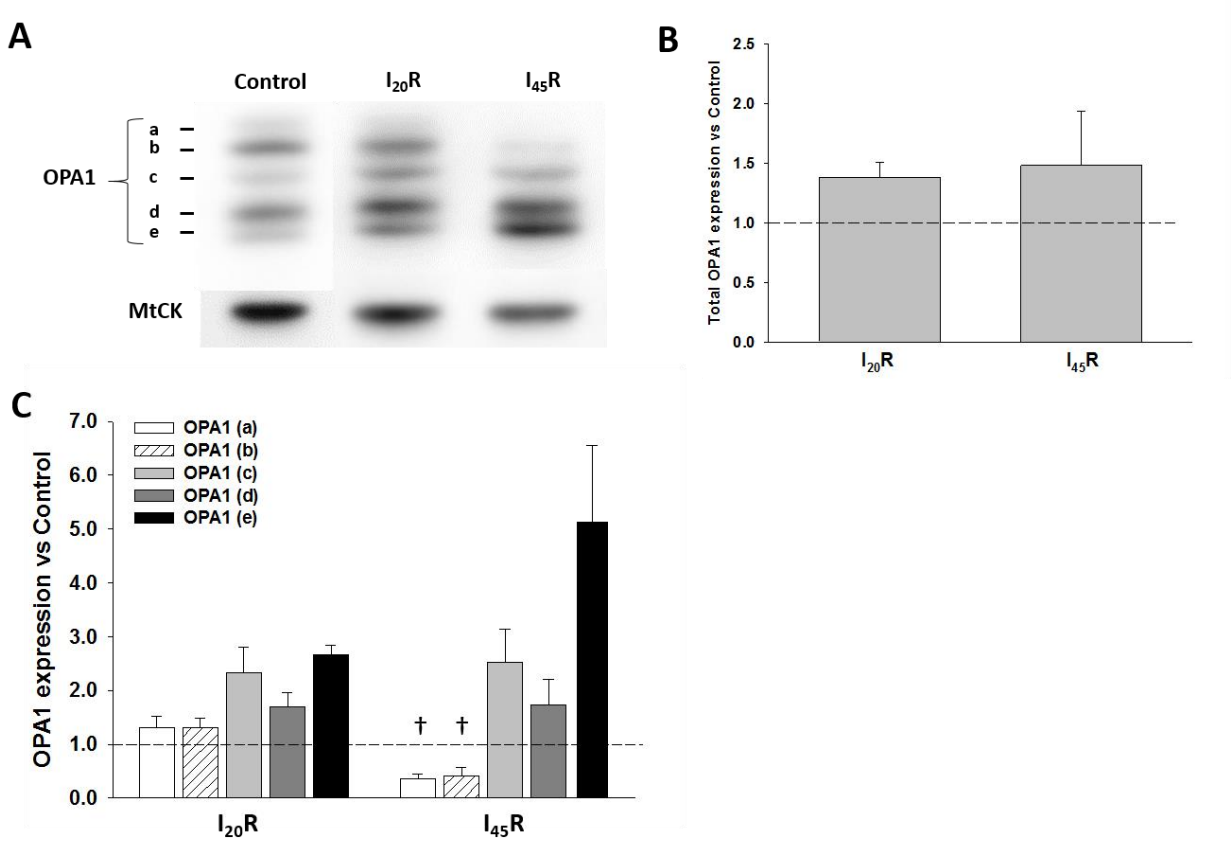

Western blot analyses of the OPA1 expression and cleavage of splice variants in left ventricular homogenates from control and post-ischemic reperfused groups. A) OPA1 is present in 5 splice variants which appear on western blot as two doublets and a single band between the doublets (molecular weight spanning from 75 to 100 kDa). These bands are denoted as *a* and *b* for the long forms and *c*, *d* and *e* for the short forms. B) Quantification of each of the OPA1 splice variant expression in post-ischemic reperfused groups compared to those in control group. † - Statistical differences between post-ischemic reperfused groups, † $P < 0.05$. Values are mean ± SEM.

Figure 6

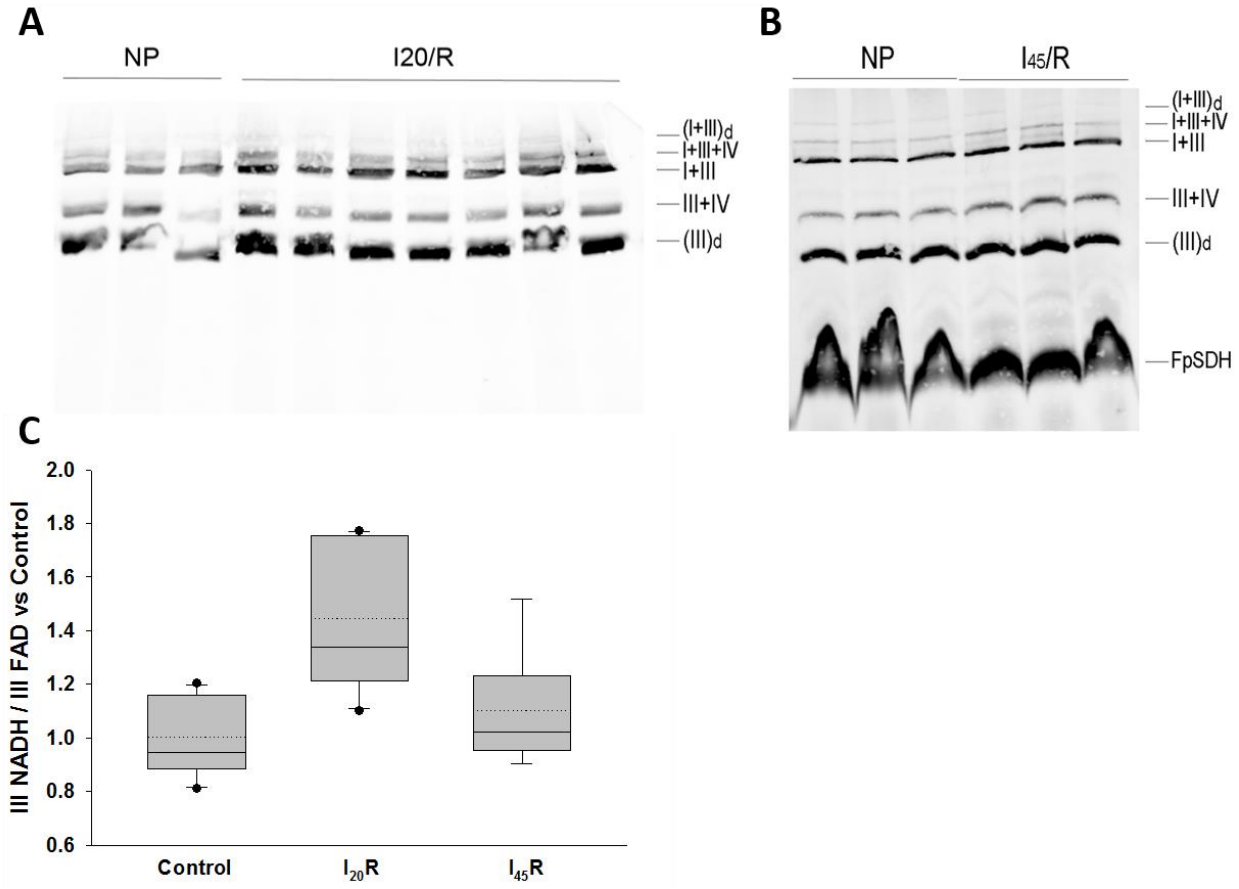

Respiratory Supercomplex (RSC) organization determined using blue-native gel electrophoresis (BNGE) of LV homogenates from post-ischemic reperfused and control hearts. A – B) Western blot analysis of RSC-containing complex III (CIII) using BN-PAGE of digitonin-treated isolated mitochondria from LV tissue of hearts from the $I_{20}R$ group (A) or the $I_{45}R$ group (B) compared to control. The blot was probed with an anti-core1 antibody and anti-FpSDH antibody (complex II expression was used to normalize CIII signal). C) Ratio of RSC-containing CIII attached to complex I (complex III dedicated to NADH) versus CIII free or attached to CIV (complex III dedicated to FAD) in post-ischemic reperfused groups compared to that in control group. * - Statistical differences compared to control group, † - Statistical differences between post-ischemic reperfused groups, *,† $P < 0.05$. Values are mean ± SEM.

Figure 7

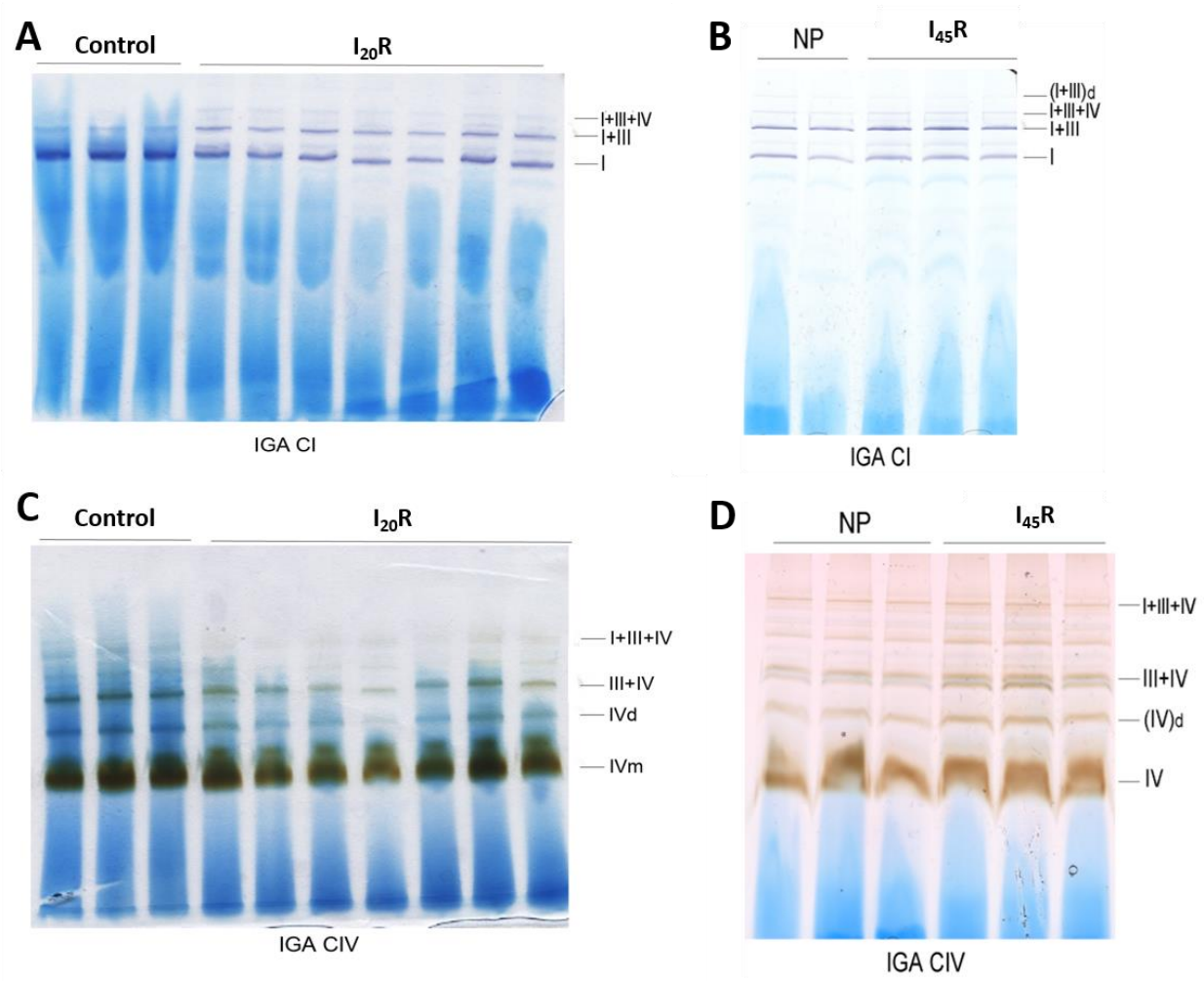

CI- and CIV-specific BNGE in-gel activity estimate in a qualitatively form the activities of RSC-containing CI and CIV, respectively. A, C) CI-specific BNGE in-gel activity of isolated mitochondria from LV tissue of hearts from the $I_{20}R$ (A) and $I_{45}R$ (C) groups compared to control. B, D) CIV-specific BNGE in-gel activity of isolated mitochondria from LV tissue of hearts from the $I_{20}R$ (B) and $I_{45}R$ (D) groups compared to control.

7. Discussion

The focus of these studies is the role of cytoskeleton-mitochondria interaction and the RC complex organization in the mitochondrial metabolism regulation. To ascertain this question, we used two experimental models: striated muscles of different phenotypes, under physiological conditions, and cardiac muscle after an *ex vivo* sequence of myocardial ischemia-reperfusion.

On the one hand, we studied the regulation of respiration and energy fluxes in permeabilized muscle fibers of striated muscles of different phenotypes under physiological conditions (Article 1). This study revealed that the difference of app. Km for ADP across striated muscle-types is related to fiber type-specific MOM permeability to adenine nucleotides. The β tubulin II distribution across striated muscles of different phenotype was in close proximity to mitochondrial position. However, the content of non-polymerized β tubulin II appeared to be tissue-specific, with a higher content for muscles with oxidative phenotype (high app. Km for ADP and low MOM permeability) than for skeletal muscle of glycolytic phenotype (low app. Km for ADP and high MOM permeability). Therefore, although the β tubulin II localization was close to mitochondria

in fast twitch glycolytic muscle fibers, the non-polymerized β tubulin II content in this muscle-type was almost absent.

The difference of functional and structural organization of energy metabolism observed between striated muscles of oxidative or glycolytic phenotype was confirmed by metabolic control analysis. The flux control coefficients of ATP Synthase and ANT are higher under Cr- than ADP-stimulated respiration in striated muscles of oxidative phenotype, thus evidencing the creatine control of respiration in these muscles. Restricted diffusion of adenine nucleotides at the level of MOM enhances energy compartmentation and the control of respiration by creatine. The functional coupling of MtCK to ATP Synthase via ANT allows the communication between the oxidative phosphorylation and the cellular energy-demands via the phosphoryl transfer networks (Tepp et al., 2010; Seppet et al., 2006; Saks et al., 2008; Saks et al., 2006; Saks et al., 2010; Guzun et al., 2009; Guzun et al., 2011a). In contrast, the regulation of respiration in striated muscles of glycolytic phenotype is mediated by cytosolic ADP since these muscles present high MOM permeability for ADP and no-functional coupling of MtCK to ATP Synthase (indicated by the absence of creatine effect on the apparent sensitivity of OxPhos for ADP). Therefore, this data evidence the implication of intracellular β tubulin II distribution and non-polymerized content on the control of energy fluxes and the regulation of respiration in striated muscles of oxidative phenotype.

On the other hand, we studied the respiration regulation and cardiac LV function of hearts subjected to ischemia-reperfusion, which revealed that app. Km for ADP is inversely correlated to LVEDP (Article 2). The LV function variable increases in post-ischemic reperfused hearts with respect to control hearts and is considered a severity index of IR-induced damage. Cardiac energy

metabolism in post-ischemic reperfused hearts is characterized by a decrease in app. Km for ADP, which depends on the ischemia duration and the severity of the IR-induced damage, evaluated by LVEDP. The decrease of app. Km for ADP in post-ischemic reperfused hearts is associated with the increase of free ATP/ADP fluxes through MOM. This result is in accordance with the observed link between app. Km for ADP and MOM permeability to adenine nucleotides across striated muscles under physiological conitions (Article 1).

Moreover, the study of β tubulin II distribution in cardiac muscle in physiological and pathophysiological conditions (IR injury) suggested that the IR-induced alterations of this cytoskeletal protein could be related to the app. Km for ADP. Normal adult cardiomyocytes characterized by high app. Km for ADP and low MOM permeability to adenine nucleotides present β tubulin II co-localizing with MOM surface. After ischemia-reperfusion, app. Km for ADP significantly decreases and MOM permeability for ADP increases. Under these conditions, β tubulin II is displaced from mitochondria positioning towards Z-lines, decreasing the possibility of interaction with VDAC. Previous *in vitro* studies have shown that adenine nucleotide diffusion through VDAC (more abundant porin of the MOM) is controlled by mitochondria-cytoskeleton interactions, specially the binding of heterodimeric αβ tubulin to VDAC (Rostosteva et al., 2008; Monge et al., 2008; Rostovtseva 2010). Interaction of VDAC with αβ-tubulin has been shown to be influenced by post-translational modifications of interacting proteins, phospholipid composition of MOM, and pH (Teijido et al., 2014; Rostovtseva and Bezrukov 2012; Sheldon et al., 2011). Therefore, the binding capacities of tubulin and VDAC could be compromised after IR due to the reduction of non-polymerized tubulin content or an increase of post-translational modifications as it was previously shown in other pathophysiological models (Fassett et al., 2013;

Sato et al., 1993; Sato et al., 1997; Belmadani et al., 2002; Janke and Bulinski 2011; Cassimeris et al., 2012).

The functional and structural organization of the cardiac energy metabolism is altered by IR injury. In particular, IR-induced alterations of cellular architecture, such as the displacement of β tubulin II, affect cytoskeleton-mitochondria interactions, causing the decrease in app. Km for ADP due to the increase in MOM permeability to adenine nucleotides. The increase in adenine nucleotides free diffusion through MOM (loss of adenine nucleotide compartmentalization) affects the functional coupling of MtCK to ATP Synthase and thereby, decreases the control of respiration by creatine. According to published data, the IR-induced decrease in app. Km for ADP and functional coupling of MtCK to ATP Synthase results in the decrease in intracellular phosphoryl flux transfer between mitochondria and energy-consuming reactions (De Sousa et al., 1999; Pucar et al., 2001; Boudina et al., 2002). The impaired feedback regulation of mitochondrial function leads to a decline in the Frank-Starling relationship and ADP accumulation within ICEU, thus inducing the inhibition of the ATPase activity and the calcium uptake by sarcoplasmic reticulum (Seppet et al., 2005).

A key element in the feedback regulation mechanism of adult normal cardiac cells is the MtCK reaction, which is strongly shifted away from thermodynamic equilibrium towards PCr production. This phenomenon is possible due to the compartmentalization of adenine nucleotides, which depends on MOM permeability, and the metabolic channeling of ATP from ANT to MtCK (Jacobus and Saks 1982; Saks et al., 1985; Kuznetsov et al., 1989). Another important factor to meet intracellular energy needs in the hearts is the mitochondrial OxPhos capacity, which decreases after IR injury. Recent studies have suggested that mitochondrial OxPhos capacity could be reduced by a decline in respiratory supercomplex organization rather than inhibition of

individual respiratory complexes (McKenzie et al., 2006; Huang et al., 2015; Gonzalvez et al., 2013; Frenzel et al., 2010; Gomez et al., 2012; Rosca et al., 2008; Rosca et al., 2011; Mejia et al., 2014). The decrease in OxPhos capacity would lead to the reduction of electron flux through respiratory chain and thereby, lowers the proton gradient generation and ATP synthesis. The decrease in ATP production causes the decrease in intracellular phosphoryl flux transfer, cardiac dysfunction and ROS production, which will induce further damage on energy metabolism (Pucar et al., 2001; Seppet et al., 2005; Elimban et al., 2014).

RSC organization in our experimental IR model changes depending on the duration of ischemia (Article 3). Hearts subjected to irreversible IR-induced damage, indicated by the release of cytochrome c, present unaltered RSC organization. In contrast, hearts subjected to reversible IR-induced damage ($I_{20}R$ group, no cytochrome c release observed) present the increase in respiratory supercomplex containing CI. These alterations are associated with the IR-induced alterations of mitochondrial morphology, which were shown to control the physical and functional organization of the RC complexes into respiratory supercomplexes (Cogliati et al., 2013; Civiletto et al., 2015). According to the literature, OPA1 is the only protein known to control mitochondrial inner membrane structure so far. In our IR experimental model, hearts subjected to reversible IR-induced damage on mitochondria activity present unaltered OPA1 long forms content and moderate cristae structure alterations (Article 3). On the contrary, the irreversible IR-induced damage on mitochondrial activity ($I_{45}R$ group) is related to the drastic cleavage of OPA1 long forms, the increase in mitochondria with remodeled or disorganized cristae structure and cytochrome c release. Therefore, these results suggest that the IR-induced RSC organization could be an adaptive mechanism to overcome the damage of mitochondrial function when the IR-induced

damage is reversible. In the case of irreversible IR-induced damage, the cleavage of OPA1 induces a reshape of cristae structure leading to cytochrome c release and apoptosis.

According to the literature, respiratory supercomplex containing CI stabilizes individual respiratory complexes, increases electron transfer efficiency and thereby, reduces ROS production by electron leak (Schägger et al., in 2004; Acin-Perez et al., 2004; D'aurelio et al., 2006; Bianchi et al., 2003; Bianchi et al., 2004; Ghelli et al., 2013; Maranzana et al., 2013). Moreover, we suggest that the IR-induced RSC reorganization might protect the cell from further stress-induced damage since the RSC reorganization may protect the cell from reverse electron transfer (i.e. electron transfer from complex II to complex I) (Chouchani et al., 2014). We suppose that the increase in respiratory supercomplexes containing complex I may protect the cell from reverse electron transfer and ROS production from complex I since the intermediates are embedded in the RSC assembly (metabolic channeling increases) and electrons are driven by NADH oxidation (independent of complex II activity). In addition, the described implication of OPA1cleavage, and in particular the content of OPA1 long forms, in apoptosis resistance after cardiac IR injury is supported by recent studies revealing that OPA1 long forms are responsible for mitochondrial cristae structure and resistance to apoptosis (Anand et al., 2014). On the one hand, studies have shown that the loss of OMA1 protects cells against apoptosis (Quirós et al., 2012; Stiburek et al., 2012) since the stress-induced OPA1 cleavage by OMA1 converts OPA1 completely into short isoforms. In particular, mice with OMA1 deficiency were resistant to *in vivo* acute kidney injury as indicated by better renal function, less mitochondrial fragmentation, and decreased apoptosis (Xiao et al., 2014). On the other hand, the overexpression of OPA1 in two mouse models presenting a defect in the respiratory chain has ameliorated their phenotype (Civiletto et al., 2015). Overall, these studies suggest that OPA1-dependent mitochondrial cristae stabilization increases

mitochondrial respiratory efficiency and blunts mitochondrial dysfunction, cytochrome c release, and ROS production.

8.Conclusion

Our study confirms that the difference in apparent sensitivity of OxPhos for ADP is linked to the MOM permeability to adenine nucleotides, which is controlled by the interactions between cytoskeletal proteins, such as β tubulin II, and mitochondria. Moreover, we highlight that the modifications of mitochondrial interactions with cytoskeleton may be one of the possible mechanisms underlying IR-induced alterations of cardiac energy metabolism. In addition, we show for the first time that cardiac IR leads to the increase of RSCs containing CI, which could be an adaptive mechanism to overcome the IR-induced damage on mitochondrial function. The alteration of the RSC organization depends on ischemia duration as well as mitochondrial morphology and cytochrome c release, which are controlled by OPA1 cleavage. The results of the present work shed some light on the mechanisms underlying IR-induced alterations of cardiac energy metabolism and reveal a potential adaptive mechanism to overcome mitochondrial dysfunction under this pathophysiological condition.

9.Perspectives

The results of the present work allowed us to highlight changes of mitochondrial interactions with cytoskeleton as one of the possible mechanisms underlying IR-induced alterations of cardiac energy metabolism. However, more molecular studies using the recently developed recombinant α- and β- tubulins by Dr R. D. Vale's group (Sirajuddin et al., 2014) are required to describe in detail the mechanism of interaction of tubulins with different VDAC isotypes. The use of the recombinant proteins will allow us to confirm the β tubulin II involvement in the regulation of VDAC permeability in cardiomyocytes and to uncover the possible role of both α tubulin and post-translational modifications of tubulin in this process. Another approach to address this question could be to study β tubulin II and α tubulin intracellular distribution *in vivo* using stochastic optical reconstruction microscopy (STORM). To do this, further development of specific antibodies and fluoroproteins for the *in vivo* studies is needed.

Moreover, our work reveals that RSC rearrangement after cardiac IR could be a potential adaptive mechanism to overcome mitochondrial dysfunction under this pathophysiological condition. A recent study has demonstrated that the presence of supercomplex assembly factor I

(SCAFI) is related to the interaction between complexes III and IV. Animal models SCAFI deficient, such as C57BL/6J, are characterized by the absence of interaction between complexes III and IV, whereas overexpression of SCAFI induces the formation of RSCs containing CIV (Lapuente et al., 2013). The study of cardiac IR effects on mitochondrial OxPhos capacity, ROS production and apoptosis resistance of an animal model with or without RSC organization could reveal the physiological advantage of presenting RSC organization for mitochondrial function under stress situation like cardiac IR.

Another important observation of our study is that the cleavage of OPA1 after cardiac IR is controlled by mitochondrial impairment which activates OMA1 protease. The selective loss of OPA1 long forms alone were shown to increase the sensitivity of mitochondria to apoptosis (Merkwirth et al., 2008) because their presence was shown to be essential for preserving cristae morphology and for the cellular apoptosis resistance (Anand et al., 2014). Moreover, the loss of OMA1 was shown to protect cells against apoptosis (Quirós et al., 2012; Stiburek et al., 2012) and mice with OMA1 deficiency were prevented of acute kidney injury as indicated by better renal function, less mitochondrial fragmentation, and decreased apoptosis (Xiao et al., 2014). This phenomenon is explained by the unaltered content of OPA1 long forms when OMA1 is deficient because this protease is the responsible of the cleavage of OPA1 completely into short isoforms. Nevertheless, the implication of OMA1-induced OPA1 cleavage on mitochondrial metabolism and RSC organization has not yet been addressed. In order to further investigate this question, the effect of *ex-vivo* myocardial IR on mitochondrial metabolism, morphology and RSC organization should be studied in a mouse model deficient in OMA1.

10. Bibliography

Abraham, M.R., Selivanov, V.A., Hodgson, D.M., Pucar, D., Zingman, L.V., Wieringa, B., Dzeja, P.P., Alekseev, A.E., and Terzic, A. (2002). Coupling of cell energetics with membrane metabolic sensing. Integrative signaling through creatine kinase phosphotransfer disrupted by M-CK gene knock-out. J. Biol. Chem. *277*, 24427–24434.

Acin-Perez, R., Bayona-Bafaluy, M.P., Fernández-Silva, P., Moreno-Loshuertos, R., Pérez-Martos, A., Bruno, C., Moraes, C.T., and Enríquez, J.A. (2004). Respiratory complex III is required to maintain complex I in mammalian mitochondria. Mol. Cell *13*, 805–815.

Acín-Pérez, R., Fernández-Silva, P., Peleato, M.L., Pérez-Martos, A., and Enriquez, J.A. (2008). Respiratory active mitochondrial supercomplexes. Mol. Cell *32*, 529–539.

Acin-Perez, R., and Enriquez, J.A. (2014). The function of the respiratory supercomplexes: the plasticity model. Biochim. Biophys. Acta *1837*, 444–450.

Agutter, P.S., Malone, P.C., and Wheatley, D.N. (1995). Intracellular transport mechanisms: a critique of diffusion theory. J. Theor. Biol. *176*, 261–272.

Aliev, M.K., and Saks, V.A. (1997). Compartmentalized energy transfer in cardiomyocytes: use of mathematical modeling for analysis of in vivo regulation of respiration. Biophys. J. *73*, 428–445.

Althoff, T., Mills, D.J., Popot, J.-L., and Kühlbrandt, W. (2011). Arrangement of electron transport chain components in bovine mitochondrial supercomplex I1III2IV1. EMBO J. *30*, 4652–4664.

Anand, R., Wai, T., Baker, M.J., Kladt, N., Schauss, A.C., Rugarli, E., and Langer, T. (2014). The i-AAA protease YME1L and OMA1 cleave OPA1 to balance mitochondrial fusion and fission. J. Cell Biol. *204*, 919–929.

Andrienko, T., Kuznetsov, A.V., Kaambre, T., Usson, Y., Orosco, A., Appaix, F., Tiivel, T., Sikk, P., Vendelin, M., Margreiter, R., et al. (2003). Metabolic consequences of functional complexes of mitochondria, myofibrils and sarcoplasmic reticulum in muscle cells. J. Exp. Biol. *206*, 2059–2072.

Anflous, K., Armstrong, D.D., and Craigen, W.J. (2001). Altered mitochondrial sensitivity for ADP and maintenance of creatine-stimulated respiration in oxidative striated muscles from VDAC1-deficient mice. J. Biol. Chem. *276*, 1954–1960.

Anflous-Pharayra, K., Cai, Z.-J., and Craigen, W.J. (2007). VDAC1 serves as a mitochondrial binding site for hexokinase in oxidative muscles. Biochim. Biophys. Acta *1767*, 136–142.

Anflous-Pharayra, K., Lee, N., Armstrong, D.L., and Craigen, W.J. (2011). VDAC3 has differing mitochondrial functions in two types of striated muscles. Biochim. Biophys. Acta *1807*, 150–156.

Anmann, T., Guzun, R., Beraud, N., Pelloux, S., Kuznetsov, A.V., Kogerman, L., Kaambre, T., Sikk, P., Paju, K., Peet, N., et al. (2006). Different kinetics of the regulation of respiration in permeabilized cardiomyocytes and in HL-1 cardiac cells. Importance of cell structure/organization for respiration regulation. Biochim. Biophys. Acta *1757*, 1597–1606.

Appaix, F., Minatchy, M., Riva-Lavieille, C., Olivares, J., Antonsson, B., and Saks, V.A. (2000). Rapid spectrophotometric method for quantitation of cytochrome c release from isolated mitochondria or permeabilized cells revisited. Biochim. Biophys. Acta *1457*, 175–181.

Appaix, F., Kuznetsov, A.V., Usson, Y., Kay, L., Andrienko, T., Olivares, J., Kaambre, T., Sikk, P., Margreiter, R., and Saks, V. (2003). Possible role of cytoskeleton in intracellular arrangement and regulation of mitochondria. Exp. Physiol. *88*, 175–190.

Ardail, D., Popa, I., Bodennec, J., Louisot, P., Schmitt, D., and Portoukalian, J. (2003). The mitochondria-associated endoplasmic-reticulum subcompartment (MAM fraction) of rat liver contains highly active sphingolipid-specific glycosyltransferases. Biochem. J. *371*, 1013–1019.

Armstrong, R.B., and Phelps, R.O. (1984). Muscle fiber type composition of the rat hindlimb. Am. J. Anat. *171*, 259–272.

Balaban, R.S., Kantor, H.L., Katz, L.A., and Briggs, R.W. (1986). Relation between work and phosphate metabolite in the in vivo paced mammalian heart. Science *232*, 1121–1123.

Balaban, R.S., Mootha, V.K., and Arai, A. (1996). Spectroscopic determination of cytochrome c oxidase content in tissues containing myoglobin or hemoglobin. Anal. Biochem. *237*, 274–278.

Banerjee, A., Roach, M.C., Wall, K.A., Lopata, M.A., Cleveland, D.W., and Ludueña, R.F. (1988). A monoclonal antibody against the type II isotype of beta-tubulin. Preparation of isotypically altered tubulin. J. Biol. Chem. *263*, 3029–3034.

Baricault, L., Ségui, B., Guégand, L., Olichon, A., Valette, A., Larminat, F., and Lenaers, G. (2007). OPA1 cleavage depends on decreased mitochondrial ATP level and bivalent metals. Exp. Cell Res. *313*, 3800–3808.

Barth, E., Stämmler, G., Speiser, B., and Schaper, J. (1992). Ultrastructural quantitation of mitochondria and myofilaments in cardiac muscle from 10 different animal species including man. J. Mol. Cell. Cardiol. *24*, 669–681.

Van Beek, J.H., and Westerhof, N. (1991). Response time of cardiac mitochondrial oxygen consumption to heart rate steps. Am. J. Physiol. *260*, H613–H625.

Belmadani, S., Poüs, C., Ventura-Clapier, R., Fischmeister, R., and Méry, P.-F. (2002). Post-translational modifications of cardiac tubulin during chronic heart failure in the rat. Mol. Cell. Biochem. *237*, 39–46.

Belmadani, S., Poüs, C., Fischmeister, R., and Méry, P.-F. (2004). Post-translational modifications of tubulin and microtubule stability in adult rat ventricular myocytes and immortalized HL-1 cardiomyocytes. Mol. Cell. Biochem. *258*, 35–48.

Benz, R., Kottke, M., and Brdiczka, D. (1990). The cationically selective state of the mitochondrial outer membrane pore: a study with intact mitochondria and reconstituted mitochondrial porin. Biochim. Biophys. Acta *1022*, 311–318.

Beraud, N., Pelloux, S., Usson, Y., Kuznetsov, A.V., Ronot, X., Tourneur, Y., and Saks, V. (2009). Mitochondrial dynamics in heart cells: very low amplitude high frequency fluctuations in adult cardiomyocytes and flow motion in non beating Hl-1 cells. J. Bioenerg. Biomembr. *41*, 195–214.

Bernier-Valentin, F., and Rousset, B. (1982). Interaction of tubulin with rat liver mitochondria. J. Biol. Chem. *257*, 7092–7099.

Bernier-Valentin, F., Aunis, D., and Rousset, B. (1983). Evidence for tubulin-binding sites on cellular membranes: plasma membranes, mitochondrial membranes, and secretory granule membranes. J. Cell Biol. *97*, 209–216.

Bers, D.M. (2002). Cardiac excitation-contraction coupling. Nature *415*, 198–205.

Bianchi, C., Fato, R., Genova, M.L., Parenti Castelli, G., and Lenaz, G. (2003). Structural and functional organization of Complex I in the mitochondrial respiratory chain. Biofactors *18*, 3–9.

Bianchi, C., Genova, M.L., Parenti Castelli, G., and Lenaz, G. (2004). The mitochondrial respiratory chain is partially organized in a supercomplex assembly: kinetic evidence using flux control analysis. J. Biol. Chem. *279*, 36562–36569.

Borutaite, V., Mildaziene, V., Brown, G.C., and Brand, M.D. (1995). Control and kinetic analysis of ischemia-damaged heart mitochondria: which parts of the oxidative phosphorylation system are affected by ischemia? Biochim. Biophys. Acta *1272*, 154–158.

Boucher, F., Tanguy, S., Besse, S., Tresallet, N., Favier, A., and de Leiris, J. (1998). Age-dependent changes in myocardial susceptibility to zero flow ischemia and reperfusion in isolated perfused rat hearts: relation to antioxidant status. Mech. Ageing Dev. *103*, 301–316.

Boudina, S., Laclau, M.N., Tariosse, L., Daret, D., Gouverneur, G., Bonoron-Adèle, S., Saks,

V.A., and Dos Santos, P. (2002). Alteration of mitochondrial function in a model of chronic ischemia in vivo in rat heart. Am. J. Physiol. Heart Circ. Physiol. *282*, H821–H831.

Boyer, P.D. (1993). The binding change mechanism for ATP synthase--some probabilities and possibilities. Biochim. Biophys. Acta *1140*, 215–250.

Breckler, J.L., and Winters, R.B. (1988). Myosin ATPase activity during avian cardiac and skeletal muscle development. Mech. Ageing Dev. *46*, 47–58.

Capetanaki, Y. (2002). Desmin cytoskeleton: a potential regulator of muscle mitochondrial behavior and function. Trends Cardiovasc. Med. *12*, 339–348.

Carré, M., André, N., Carles, G., Borghi, H., Brichese, L., Briand, C., and Braguer, D. (2002). Tubulin is an inherent component of mitochondrial membranes that interacts with the voltage-dependent anion channel. J. Biol. Chem. *277*, 33664–33669.

Casini, S., Tan, H.L., Demirayak, I., Remme, C.A., Amin, A.S., Scicluna, B.P., Chatyan, H., Ruijter, J.M., Bezzina, C.R., van Ginneken, A.C.G., et al. (2010). Tubulin polymerization modifies cardiac sodium channel expression and gating. Cardiovasc. Res. *85*, 691–700.

Cassimeris, L., Silva, V.C., Miller, E., Ton, Q., Molnar, C., and Fong, J. (2012). Fueled by microtubules: does tubulin dimer/polymer partitioning regulate intracellular metabolism? Cytoskeleton (Hoboken) *69*, 133–143.

Chance, B., and Williams, G.R. (1955). Respiratory enzymes in oxidative phosphorylation. III. The steady state. J. Biol. Chem. *217*, 409–427.

Chance, B., and Williams, G.R. (1956). The respiratory chain and oxidative phosphorylation. Adv Enzymol Relat Subj Biochem *17*, 65–134.

Chen, L., Gong, Q., Stice, J.P., and Knowlton, A.A. (2009). Mitochondrial OPA1, apoptosis, and heart failure. Cardiovasc Res *84*, 91–99.

Chen, L., Liu, T., Tran, A., Lu, X., Tomilov, A.A., Davies, V., Cortopassi, G., Chiamvimonvat, N., Bers, D.M., Votruba, M., et al. (2012). OPA1 Mutation and Late-Onset Cardiomyopathy: Mitochondrial Dysfunction and mtDNA Instability. J Am Heart Assoc *1*, e003012.

Cheng, G., Kasiganesan, H., Baicu, C.F., Wallenborn, J.G., Kuppuswamy, D., and Cooper, G. (2012). Cytoskeletal role in protection of the failing heart by β-adrenergic blockade. Am. J. Physiol. Heart Circ. Physiol. *302*, H675–H687.

Chiara, F., Castellaro, D., Marin, O., Petronilli, V., Brusilow, W.S., Juhaszova, M., Sollott, S.J., Forte, M., Bernardi, P., and Rasola, A. (2008). Hexokinase II detachment from mitochondria triggers apoptosis through the permeability transition pore independent of voltage-dependent anion channels. PLoS ONE *3*, e1852.

Chinnakkannu, P., Samanna, V., Cheng, G., Ablonczy, Z., Baicu, C.F., Bethard, J.R., Menick, D.R., Kuppuswamy, D., and Cooper, G. (2010). Site-specific microtubule-associated protein 4

dephosphorylation causes microtubule network densification in pressure overload cardiac hypertrophy. J. Biol. Chem. *285*, 21837–21848.

Chouchani, E.T., Pell, V.R., Gaude, E., Aksentijević, D., Sundier, S.Y., Robb, E.L., Logan, A., Nadtochiy, S.M., Ord, E.N.J., Smith, A.C., et al. (2014). Ischaemic accumulation of succinate controls reperfusion injury through mitochondrial ROS. Nature *515*, 431–435.

Cipolat, S., Rudka, T., Hartmann, D., Costa, V., Serneels, L., Craessaerts, K., Metzger, K., Frezza, C., Annaert, W., D'Adamio, L., et al. (2006). Mitochondrial rhomboid PARL regulates cytochrome c release during apoptosis via OPA1-dependent cristae remodeling. Cell *126*, 163–175.

Civiletto, G., Varanita, T., Cerutti, R., Gorletta, T., Barbaro, S., Marchet, S., Lamperti, C., Viscomi, C., Scorrano, L., and Zeviani, M. (2015). Opa1 overexpression ameliorates the phenotype of two mitochondrial disease mouse models. Cell Metab. *21*, 845–854.

Cogliati, S., Frezza, C., Soriano, M.E., Varanita, T., Quintana-Cabrera, R., Corrado, M., Cipolat, S., Costa, V., Casarin, A., Gomes, L.C., et al. (2013). Mitochondrial cristae shape determines respiratory chain supercomplexes assembly and respiratory efficiency. Cell *155*, 160–171.

Colombini, M. (1980). Structure and mode of action of a voltage dependent anion-selective channel (VDAC) located in the outer mitochondrial membrane. Ann. N. Y. Acad. Sci. *341*, 552–563.

Cooke, R. (1997). Actomyosin interaction in striated muscle. Physiol. Rev. *77*, 671–697.

Cruciat, C.M., Brunner, S., Baumann, F., Neupert, W., and Stuart, R.A. (2000). The cytochrome bc1 and cytochrome c oxidase complexes associate to form a single supracomplex in yeast mitochondria. J. Biol. Chem. *275*, 18093–18098.

Curtis, M.J., Macleod, B.A., Tabrizchi, R., and Walker, M.J. (1986). An improved perfusion apparatus for small animal hearts. J Pharmacol Methods *15*, 87–94.

D'Aurelio, M., Gajewski, C.D., Lenaz, G., and Manfredi, G. (2006). Respiratory chain supercomplexes set the threshold for respiration defects in human mtDNA mutant cybrids. Hum. Mol. Genet. *15*, 2157–2169.

Decker, R.S., Decker, M.L., Nakamura, S., Zhao, Y.-S., Hedjbeli, S., Harris, K.R., and Klocke, F.J. (2002). HSC73-tubulin complex formation during low-flow ischemia in the canine myocardium. Am. J. Physiol. Heart Circ. Physiol. *283*, H1322–H1333.

Degli Esposti, M., and McLennan, H. (1998). Mitochondria and cells produce reactive oxygen species in virtual anaerobiosis: relevance to ceramide-induced apoptosis. FEBS Letters *430*, 338–342.

Delp, M.D., and Duan, C. (1996). Composition and size of type I, IIA, IID/X, and IIB fibers and citrate synthase activity of rat muscle. J. Appl. Physiol. *80*, 261–270.

Devillard, L., Vandroux, D., Tissier, C., Brochot, A., Voisin, S., Rochette, L., and Athias, P. (2006). Tubulin ligands suggest a microtubule-NADPH oxidase relationship in postischemic cardiomyocytes. Eur. J. Pharmacol. *548*, 64–73.

Devillard, L., Vandroux, D., Tissier, C., Dumont, L., Borgeot, J., Rochette, L., and Athias, P. (2008). Involvement of microtubules in the tolerance of cardiomyocytes to cold ischemia-reperfusion. Mol. Cell. Biochem. *307*, 149–157.

Dhalla, N.S., Yates, J.C., Walz, D.A., McDonald, V.A., and Olson, R.E. (1972). Correlation between changes in the endogenous energy stores and myocardial function due to hypoxia in the isolated perfused rat heart. Can. J. Physiol. Pharmacol. *50*, 333–345.

Dhalla, N.S., Matoushek, R.F., Sun, C.N., and Olson, R.E. (1973). Metabolic, ultrastructural, and mechanical changes in the isolated rat heart perfused with aerobic medium in the absence or presence of glucose. Can. J. Physiol. Pharmacol. *51*, 590–603.

Diaz, F., Fukui, H., Garcia, S., and Moraes, C.T. (2006). Cytochrome c oxidase is required for the assembly/stability of respiratory complex I in mouse fibroblasts. Mol. Cell. Biol. *26*, 4872–4881.

Diaz, F., Enríquez, J.A., and Moraes, C.T. (2012). Cells lacking Rieske iron-sulfur protein have a reactive oxygen species-associated decrease in respiratory complexes I and IV. Mol. Cell. Biol. *32*, 415–429.

Dudkina, N.V., Kudryashev, M., Stahlberg, H., and Boekema, E.J. (2011). Interaction of complexes I, III, and IV within the bovine respirasome by single particle cryoelectron tomography. Proc. Natl. Acad. Sci. U.S.A. *108*, 15196–15200.

Duncan, T.M., Bulygin, V.V., Zhou, Y., Hutcheon, M.L., and Cross, R.L. (1995). Rotation of subunits during catalysis by Escherichia coli F1-ATPase. Proceedings of the National Academy of Sciences *92*, 10964–10968.

Dzeja, P.P., and Terzic, A. (2003). Phosphotransfer networks and cellular energetics. J. Exp. Biol. *206*, 2039–2047.

Dzeja, P.P., Terzic, A., and Wieringa, B. (2004). Phosphotransfer dynamics in skeletal muscle from creatine kinase gene-deleted mice. Mol. Cell. Biochem. *256-257*, 13–27.

Dzeja, P.P., Hoyer, K., Tian, R., Zhang, S., Nemutlu, E., Spindler, M., and Ingwall, J.S. (2011). Rearrangement of energetic and substrate utilization networks compensate for chronic myocardial creatine kinase deficiency. J. Physiol. (Lond.) *589*, 5193–5211.

Edoute, Y., Merwe, E. van der, Sanan, D., Kotzé, J.C., Steinmann, C., and Lochner, A. (1983). Normothermic ischemic cardiac arrest of the isolated working rat heart. Effects of time and reperfusion on myocardial ultrastructure, mitochondrial oxidative function, and mechanical recovery. Circulation Research *53*, 663–678.

Ehses, S., Raschke, I., Mancuso, G., Bernacchia, A., Geimer, S., Tondera, D., Martinou, J.-C., Westermann, B., Rugarli, E.I., and Langer, T. (2009). Regulation of OPA1 processing and

mitochondrial fusion by m-AAA protease isoenzymes and OMA1. J. Cell Biol. *187*, 1023–1036.

Elimban, V., Tappia, P.S., and Dhalla, N.S. (2014). Defects in Mitochondrial Oxidative Phosphorylation in Hearts Subjected to Ischemia-Reperfusion Injury. In Cardiac Energy Metabolism in Health and Disease, G.D. Lopaschuk, and N.S. Dhalla, eds. (Springer New York), pp. 183–197.

Endoh, M. (2006). Signal transduction and Ca2+ signaling in intact myocardium. J. Pharmacol. Sci. *100*, 525–537.

Eubel, H., Jänsch, L., and Braun, H.-P. (2003). New insights into the respiratory chain of plant mitochondria. Supercomplexes and a unique composition of complex II. Plant Physiol. *133*, 274–286.

Eubel, H., Heinemeyer, J., Sunderhaus, S., and Braun, H.-P. (2004). Respiratory chain supercomplexes in plant mitochondria. Plant Physiol. Biochem. *42*, 937–942.

Evans, C.L., and Matsuoka, Y. (1915). The effect of various mechanical conditions on the gaseous metabolism and efficiency of the mammalian heart. J. Physiol. (Lond.) *49*, 378–405.

Fassett, J.T., Hu, X., Xu, X., Lu, Z., Zhang, P., Chen, Y., and Bache, R.J. (2013). AMPK attenuates microtubule proliferation in cardiac hypertrophy. Am. J. Physiol. Heart Circ. Physiol. *304*, H749–H758.

Fawcett, D.W., and McNutt, N.S. (1969). The ultrastructure of the cat myocardium. I. Ventricular papillary muscle. J. Cell Biol. *42*, 1–45.

Fell, D.A. (1992). Metabolic control analysis: a survey of its theoretical and experimental development. Biochem. J. *286 (Pt 2)*, 313–330.

Fernández-Vizarra, E., López-Pérez, M.J., and Enriquez, J.A. (2002). Isolation of biogenetically competent mitochondria from mammalian tissues and cultured cells. Methods *26*, 292–297.

Fiore, C., Trézéguet, V., Le Saux, A., Roux, P., Schwimmer, C., Dianoux, A.C., Noel, F., Lauquin, G.J., Brandolin, G., and Vignais, P.V. (1998). The mitochondrial ADP/ATP carrier: structural, physiological and pathological aspects. Biochimie *80*, 137–150.

Frank O. (1885). Zur Dynamik des Herzmuskels. Z Biologie. 32:370–447.

Frenzel, M., Rommelspacher, H., Sugawa, M.D., and Dencher, N.A. (2010). Ageing alters the supramolecular architecture of OxPhos complexes in rat brain cortex. Exp. Gerontol. *45*, 563–572.

Frezza, C., Cipolat, S., Martins de Brito, O., Micaroni, M., Beznoussenko, G.V., Rudka, T., Bartoli, D., Polishuck, R.S., Danial, N.N., De Strooper, B., et al. (2006). OPA1 controls apoptotic cristae remodeling independently from mitochondrial fusion. Cell *126*, 177–189.

Friedrich (1985). Dynamic compartmentation in in soluble multienzyme system. In Organized Multienzyme Systems: Catalytic Properties., (New York–London: Academic Press), pp. 141–176.

Fritzen, A.J., Grunnet, N., and Quistorff, B. (2007). Flux control analysis of mitochondrial oxidative phosphorylation in rat skeletal muscle: pyruvate and palmitoyl-carnitine as substrates give different control patterns. Eur. J. Appl. Physiol. *101*, 679–689.

De la Fuente, I.M. (2010). Quantitative analysis of cellular metabolic dissipative, self-organized structures. Int J Mol Sci *11*, 3540–3599.

Fukuda, N., and Granzier, H.L. (2005). Titin/connectin-based modulation of the Frank-Starling mechanism of the heart. J. Muscle Res. Cell. Motil. *26*, 319–323.

Fukuda, N., Sasaki, D., Ishiwata, S., and Kurihara, S. (2001). Length dependence of tension generation in rat skinned cardiac muscle: role of titin in the Frank-Starling mechanism of the heart. Circulation *104*, 1639–1645.

Fulton, A.B. (1982). How crowded is the cytoplasm? Cell *30*, 345–347.

Geisbuhler, T., Altschuld, R.A., Trewyn, R.W., Ansel, A.Z., Lamka, K., and Brierley, G.P. (1984). Adenine nucleotide metabolism and compartmentalization in isolated adult rat heart cells. Circ. Res. *54*, 536–546.

Gellerich, F.N., Bohnensack, R., and Kunz, W. (1983a). Control of mitochondrial respiration. The contribution of the adenine nucleotide translocator depends on the ATP- and ADP-consuming enzymes. Biochim. Biophys. Acta *722*, 381–391.

Gellerich, F.N., Schlame, M., and Saks, V.A. (1983b). Creatine kinase of heart mitochondria: no changes in its kinetic properties after inhibition of the adenine nucleotide translocator. Biomed. Biochim. Acta *42*, 1335–1337.

Gennis, R.B., Barquera, B., Hacker, B., Van Doren, S.R., Arnaud, S., Crofts, A.R., Davidson, E., Gray, K.A., and Daldal, F. (1993). The bc1 complexes of Rhodobacter sphaeroides and Rhodobacter capsulatus. J. Bioenerg. Biomembr. *25*, 195–209.

Genova, M.L., Baracca, A., Biondi, A., Casalena, G., Faccioli, M., Falasca, A.I., Formiggini, G., Sgarbi, G., Solaini, G., and Lenaz, G. (2008). Is supercomplex organization of the respiratory chain required for optimal electron transfer activity? Biochim. Biophys. Acta *1777*, 740–746.

Gercken, G., and Schlette, U. (1968). Metabolite status of the heart in acute insufficiency due to 1-fluoro-2,4-dinitrobenzene. Experientia *24*, 17–19.

Gertz, E.W., Wisneski, J.A., Stanley, W.C., and Neese, R.A. (1988). Myocardial substrate utilization during exercise in humans. Dual carbon-labeled carbohydrate isotope experiments. J. Clin. Invest. *82*, 2017–2025.

Ghelli, A., Tropeano, C.V., Calvaruso, M.A., Marchesini, A., Iommarini, L., Porcelli, A.M., Zanna, C., De Nardo, V., Martinuzzi, A., Wibrand, F., et al. (2013). The cytochrome b p.278Y>C mutation causative of a multisystem disorder enhances superoxide production and alters supramolecular interactions of respiratory chain complexes. Hum. Mol. Genet. *22*, 2141–2151.

Gibbs, C.L. (1978). Cardiac energetics. Physiol. Rev. *58*, 174–254.

Glancy, B., and Balaban, R.S. (2011). Protein composition and function of red and white skeletal muscle mitochondria. Am J Physiol Cell Physiol *300*, C1280–C1290.

Gnaiger, E. (2001). Oxygen Solubility in Experimental Media (Innsbruck, Austria: OROBOROS Bioenergetics Newsletter MiPNet 6.3).

Goldman, Y.E. (1987). Kinetics of the actomyosin ATPase in muscle fibers. Annu. Rev. Physiol. *49*, 637–654.

Gómez, L.A., and Hagen, T.M. (2012). Age-related decline in mitochondrial bioenergetics: does supercomplex destabilization determine lower oxidative capacity and higher superoxide production? Semin. Cell Dev. Biol. *23*, 758–767.

Gonzalez-Granillo, M., Grichine, A., Guzun, R., Usson, Y., Tepp, K., Chekulayev, V., Shevchuk, I., Karu-Varikmaa, M., Kuznetsov, A.V., Grimm, M., et al. (2012). Studies of the role of tubulin beta II isotype in regulation of mitochondrial respiration in intracellular energetic units in cardiac cells. J. Mol. Cell. Cardiol. *52*, 437–447.

Gonzalvez, F., D'Aurelio, M., Boutant, M., Moustapha, A., Puech, J.-P., Landes, T., Arnauné-Pelloquin, L., Vial, G., Taleux, N., Slomianny, C., et al. (2013). Barth syndrome: cellular compensation of mitochondrial dysfunction and apoptosis inhibition due to changes in cardiolipin remodeling linked to tafazzin (TAZ) gene mutation. Biochim. Biophys. Acta *1832*, 1194–1206.

Gordon, A.M., Homsher, E., and Regnier, M. (2000). Regulation of contraction in striated muscle. Physiol. Rev. *80*, 853–924.

Gordon, A.M., Regnier, M., and Homsher, E. (2001). Skeletal and cardiac muscle contractile activation: tropomyosin "rocks and rolls." News Physiol. Sci. *16*, 49–55.

Groen, A.K., Wanders, R.J., Westerhoff, H.V., van der Meer, R., and Tager, J.M. (1982). Quantification of the contribution of various steps to the control of mitochondrial respiration. J. Biol. Chem. *257*, 2754–2757.

Gudbjarnason, S., Mathes, P., and Ravens, K.G. (1970). Functional compartmentation of ATP and creatine phosphate in heart muscle. J. Mol. Cell. Cardiol. *1*, 325–339.

Gudz, T.I., Tserng, K.Y., and Hoppel, C.L. (1997). Direct inhibition of mitochondrial respiratory chain complex III by cell-permeable ceramide. J. Biol. Chem. *272*, 24154–24158.

Guerrero, K., Monge, C., Brückner, A., Puurand, U., Kadaja, L., Käämbre, T., Seppet, E., and Saks, V. (2010). Study of possible interactions of tubulin, microtubular network, and STOP protein with mitochondria in muscle cells. Mol. Cell. Biochem. *337*, 239–249.

Guzun, R., and Saks, V. (2010). Application of the principles of systems biology and Wiener's cybernetics for analysis of regulation of energy fluxes in muscle cells in vivo. Int J Mol Sci *11*, 982–1019.

Guzun, R., Timohhina, N., Tepp, K., Monge, C., Kaambre, T., Sikk, P., Kuznetsov, A.V., Pison, C., and Saks, V. (2009). Regulation of respiration controlled by mitochondrial creatine kinase in permeabilized cardiac cells in situ. Importance of system level properties. Biochim. Biophys. Acta *1787*, 1089–1105.

Guzun, R., Timohhina, N., Tepp, K., Gonzalez-Granillo, M., Shevchuk, I., Chekulayev, V., Kuznetsov, A.V., Kaambre, T., and Saks, V.A. (2011a). Systems bioenergetics of creatine kinase networks: physiological roles of creatine and phosphocreatine in regulation of cardiac cell function. Amino Acids *40*, 1333–1348.

Guzun, R., Karu-Varikmaa, M., Gonzalez-Granillo, M., Kuznetsov, A.V., Michel, L., Cottet-Rousselle, C., Saaremäe, M., Kaambre, T., Metsis, M., Grimm, M., et al. (2011b). Mitochondria-cytoskeleton interaction: distribution of β-tubulins in cardiomyocytes and HL-1 cells. Biochim. Biophys. Acta *1807*, 458–469.

Guzun, R., Gonzalez-Granillo, M., Karu-Varikmaa, M., Grichine, A., Usson, Y., Kaambre, T., Guerrero-Roesch, K., Kuznetsov, A., Schlattner, U., and Saks, V. (2012). Regulation of respiration in muscle cells in vivo by VDAC through interaction with the cytoskeleton and MtCK within Mitochondrial Interactosome. Biochim. Biophys. Acta *1818*, 1545–1554.

Guzun, R., Kaambre, T., Bagur, R., Grichine, A., Usson, Y., Varikmaa, M., Anmann, T., Tepp, K., Timohhina, N., Shevchuk, I., et al. (2015). Modular organization of cardiac energy metabolism: energy conversion, transfer and feedback regulation. Acta Physiol (Oxf) *213*, 84–106.

Hackenbrock, C.R., Chazotte, B., and Gupte, S.S. (1986). The random collision model and a critical assessment of diffusion and collision in mitochondrial electron transport. J Bioenerg Biomembr *18*, 331–368.

Hamman, B.L., Bittl, J.A., Jacobus, W.E., Allen, P.D., Spencer, R.S., Tian, R., and Ingwall, J.S. (1995). Inhibition of the creatine kinase reaction decreases the contractile reserve of isolated rat hearts. Am. J. Physiol. *269*, H1030–H1036.

Hardy, L., Clark, J.B., Darley-Usmar, V.M., Smith, D.R., and Stone, D. (1991). Reoxygenation-dependent decrease in mitochondrial NADH:CoQ reductase (Complex I) activity in the hypoxic/reoxygenated rat heart. Biochem J *274*, 133–137.

Hargreaves, A.J., and Avila, J. (1985). Localization and characterization of tubulin-like proteins associated with brain mitochondria: the presence of a membrane-specific isoform. J. Neurochem. *45*, 490–496.

Hayashi, T., Martone, M.E., Yu, Z., Thor, A., Doi, M., Holst, M.J., Ellisman, M.H., and Hoshijima, M. (2009). Three-dimensional electron microscopy reveals new details of membrane systems for Ca2+ signaling in the heart. J. Cell. Sci. *122*, 1005–1013.

Hein, S., Kostin, S., Heling, A., Maeno, Y., and Schaper, J. (2000). The role of the cytoskeleton in heart failure. Cardiovasc. Res. *45*, 273–278.

Hibberd, M.G., and Jewell, B.R. (1982). Calcium- and length-dependent force production in rat

ventricular muscle. J. Physiol. (Lond.) *329*, 527–540.

Hoch, F.L. (1992). Cardiolipins and biomembrane function. Biochim. Biophys. Acta *1113*, 71–133.

Hochachka, P.W., and McClelland, G.B. (1997). Cellular metabolic homeostasis during large-scale change in ATP turnover rates in muscles. J. Exp. Biol. *200*, 381–386.

Honda, H., Tanaka, K., Akita, N., and Haneda, T. (2002). Cyclical changes in high-energy phosphates during the cardiac cycle by pacing-Gated 31P nuclear magnetic resonance. Circ. J. *66*, 80–86.

Ten Hove, M., Lygate, C.A., Fischer, A., Schneider, J.E., Sang, A.E., Hulbert, K., Sebag-Montefiore, L., Watkins, H., Clarke, K., Isbrandt, D., et al. (2005). Reduced inotropic reserve and increased susceptibility to cardiac ischemia/reperfusion injury in phosphocreatine-deficient guanidinoacetate-N-methyltransferase-knockout mice. Circulation *111*, 2477–2485.

Huang, Y., Powers, C., Madala, S.K., Greis, K.D., Haffey, W.D., Towbin, J.A., Purevjav, E., Javadov, S., Strauss, A.W., and Khuchua, Z. (2015). Cardiac metabolic pathways affected in the mouse model of barth syndrome. PLoS ONE *10*, e0128561.

Ingwall, J.S. (2002). ATP and the Heart (Boston: Springer).

Ishida, Y., Riesinger, I., Wallimann, T., and Paul, R.J. (1994). Compartmentation of ATP synthesis and utilization in smooth muscle: roles of aerobic glycolysis and creatine kinase. Mol. Cell. Biochem. *133-134*, 39–50.

Iwai, K., Hori, M., Kitabatake, A., Kurihara, H., Uchida, K., Inoue, M., and Kamada, T. (1990). Disruption of microtubules as an early sign of irreversible ischemic injury. Immunohistochemical study of in situ canine hearts. Circ. Res. *67*, 694–706.

Jacobus, W.E., and Lehninger, A.L. (1973). Creatine kinase of rat heart mitochondria. Coupling of creatine phosphorylation to electron transport. J. Biol. Chem. *248*, 4803–4810.

Jacobus, W.E., and Saks, V.A. (1982). Creatine kinase of heart mitochondria: changes in its kinetic properties induced by coupling to oxidative phosphorylation. Arch. Biochem. Biophys. *219*, 167–178.

Janke, C., and Bulinski, J.C. (2011). Post-translational regulation of the microtubule cytoskeleton: mechanisms and functions. Nat. Rev. Mol. Cell Biol. *12*, 773–786.

Janssen, E., Dzeja, P.P., Oerlemans, F., Simonetti, A.W., Heerschap, A., de Haan, A., Rush, P.S., Terjung, R.R., Wieringa, B., and Terzic, A. (2000). Adenylate kinase 1 gene deletion disrupts muscle energetic economy despite metabolic rearrangement. EMBO J. *19*, 6371–6381.

Kajiyama, K., Pauly, D.F., Hughes, H., Yoon, S.B., Entman, M.L., and McMillin-Wood, J.B. (1987). Protection by verapamil of mitochondrial glutathione equilibrium and phospholipid changes during reperfusion of ischemic canine myocardium. Circ. Res. *61*, 301–310.

Kapelko, V.I., Kupriyanov, V.V., Novikova, N.A., Lakomkin, V.L., Steinschneider AYa, null, Severina MYu, null, Veksler, V.I., and Saks, V.A. (1988). The cardiac contractile failure induced by chronic creatine and phosphocreatine deficiency. J. Mol. Cell. Cardiol. *20*, 465–479.

Katz, A.M. (2002). Ernest Henry Starling, his predecessors, and the "Law of the Heart." Circulation *106*, 2986–2992.

Kay, L., Li, Z., Mericskay, M., Olivares, J., Tranqui, L., Fontaine, E., Tiivel, T., Sikk, P., Kaambre, T., Samuel, J.L., et al. (1997a). Study of regulation of mitochondrial respiration in vivo. An analysis of influence of ADP diffusion and possible role of cytoskeleton. Biochim. Biophys. Acta *1322*, 41–59.

Kay, L., Rossi, A., and Saks, V. (1997b). Detection of early ischemic damage by analysis of mitochondrial function in skinned fibers. Mol. Cell. Biochem. *174*, 79–85.

Kay, L., Nicolay, K., Wieringa, B., Saks, V., and Wallimann, T. (2000). Direct evidence for the control of mitochondrial respiration by mitochondrial creatine kinase in oxidative muscle cells in situ. J. Biol. Chem. *275*, 6937–6944.

Kentish, J.C., ter Keurs, H.E., Ricciardi, L., Bucx, J.J., and Noble, M.I. (1986). Comparison between the sarcomere length-force relations of intact and skinned trabeculae from rat right ventricle. Influence of calcium concentrations on these relations. Circ. Res. *58*, 755–768.

Kim, N., Lee, Y., Kim, H., Joo, H., Youm, J.B., Park, W.S., Warda, M., Cuong, D.V., and Han, J. (2006). Potential biomarkers for ischemic heart damage identified in mitochondrial proteins by comparative proteomics. Proteomics *6*, 1237–1249.

Klingenberg, M. (1980). The ADP-ATP translocation in mitochondria, a membrane potential controlled transport. J. Membr. Biol. *56*, 97–105.

Koide, M., Hamawaki, M., Narishige, T., Sato, H., Nemoto, S., DeFreyte, G., Zile, M.R., Cooper G, I.V., and Carabello, B.A. (2000). Microtubule depolymerization normalizes in vivo myocardial contractile function in dogs with pressure-overload left ventricular hypertrophy. Circulation *102*, 1045–1052.

Krause, F., Reifschneider, N.H., Vocke, D., Seelert, H., Rexroth, S., and Dencher, N.A. (2004). "Respirasome"-like supercomplexes in green leaf mitochondria of spinach. J. Biol. Chem. *279*, 48369–48375.

Kunz, W.S., Kudin, A., Vielhaber, S., Elger, C.E., Attardi, G., and Villani, G. (2000). Flux control of cytochrome c oxidase in human skeletal muscle. J. Biol. Chem. *275*, 27741–27745.

Kupriyanov, V.V., Ya Steinschneider, A., Ruuge, E.K., Kapel'ko, V.I., Yu Zueva, M., Lakomkin, V.L., Smirnov, V.N., and Saks, V.A. (1984). Regulation of energy flux through the creatine kinase reaction in vitro and in perfused rat heart. 31P-NMR studies. Biochim. Biophys. Acta *805*, 319–331.

Kupriyanov, V.V., Lakomkin, V.L., Kapelko, V.I., Steinschneider AYa, null, Ruuge, E.K., and

Saks, V.A. (1987). Dissociation of adenosine triphosphate levels and contractile function in isovolumic hearts perfused with 2-deoxyglucose. J. Mol. Cell. Cardiol. *19*, 729–740.

Kupriyanov, V.V., Lakomkin, V.L., Korchazhkina, O.V., Steinschneider AYa, null, Kapelko, V.I., and Saks, V.A. (1991). Control of cardiac energy turnover by cytoplasmic phosphates: 31P-NMR study. Am. J. Physiol. *261*, 45–53.

Kushmerick, M.J., Moerland, T.S., and Wiseman, R.W. (1992). Mammalian skeletal muscle fibers distinguished by contents of phosphocreatine, ATP, and Pi. Proc. Natl. Acad. Sci. U.S.A. *89*, 7521–7525.

Kuznetsov, A.V., Khuchua, Z.A., Vassil'eva, E.V., Medved'eva, N.V., and Saks, V.A. (1989). Heart mitochondrial creatine kinase revisited: the outer mitochondrial membrane is not important for coupling of phosphocreatine production to oxidative phosphorylation. Arch. Biochem. Biophys. *268*, 176–190.

Kuznetsov, A.V., Tiivel, T., Sikk, P., Kaambre, T., Kay, L., Daneshrad, Z., Rossi, A., Kadaja, L., Peet, N., Seppet, E., et al. (1996). Striking differences between the kinetics of regulation of respiration by ADP in slow-twitch and fast-twitch muscles in vivo. Eur. J. Biochem. *241*, 909–915.

Kuznetsov, A.V., Winkler, K., Kirches, E., Lins, H., Feistner, H., and Kunz, W.S. (1997). Application of inhibitor titrations for the detection of oxidative phosphorylation defects in saponin-skinned muscle fibers of patients with mitochondrial diseases. Biochim. Biophys. Acta *1360*, 142–150.

Kuznetsov, A.V., Schneeberger, S., Renz, O., Meusburger, H., Saks, V., Usson, Y., and Margreiter, R. (2004). Functional heterogeneity of mitochondria after cardiac cold ischemia and reperfusion revealed by confocal imaging. Transplantation *77*, 754–756.

Kuznetsov, A.V., Veksler, V., Gellerich, F.N., Saks, V., Margreiter, R., and Kunz, W.S. (2008). Analysis of mitochondrial function in situ in permeabilized muscle fibers, tissues and cells. Nat Protoc *3*, 965–976.

Kuznetsov, A.V., Guzun, R., Boucher, F., Bagur, R., Kaambre, T., and Saks, V. (2012). Mysterious Ca(2+)-independent muscular contraction: déjà vu. Biochem. J. *445*, 333–336.

Kwong, L.K., and Sohal, R.S. (1998). Substrate and site specificity of hydrogen peroxide generation in mouse mitochondria. Arch. Biochem. Biophys. *350*, 118–126.

De La Fuente, I.M., Martínez, L., Pérez-Samartín, A.L., Ormaetxea, L., Amezaga, C., and Vera-López, A. (2008). Global self-organization of the cellular metabolic structure. PLoS ONE *3*, e3100.

Landesberg, A. (1996). End-systolic pressure-volume relationship and intracellular control of contraction. Am. J. Physiol. *270*, H338–H349.

Lapuente-Brun, E., Moreno-Loshuertos, R., Acín-Pérez, R., Latorre-Pellicer, A., Colás, C., Balsa,

E., Perales-Clemente, E., Quirós, P.M., Calvo, E., Rodríguez-Hernández, M.A., et al. (2013). Supercomplex assembly determines electron flux in the mitochondrial electron transport chain. Science *340*, 1567–1570.

Leandro-García, L.J., Leskelä, S., Landa, I., Montero-Conde, C., López-Jiménez, E., Letón, R., Cascón, A., Robledo, M., and Rodríguez-Antona, C. (2010). Tumoral and tissue-specific expression of the major human beta-tubulin isotypes. Cytoskeleton (Hoboken) *67*, 214–223.

Lenaz, G., Bovina, C., Formiggini, G., and Parenti Castelli, G. (1999). Mitochondria, oxidative stress, and antioxidant defences. Acta Biochim. Pol. *46*, 1–21.

Lenaz, G., D'Aurelio, M., Merlo Pich, M., Genova, M.L., Ventura, B., Bovina, C., Formiggini, G., and Parenti Castelli, G. (2000). Mitochondrial bioenergetics in aging. Biochim. Biophys. Acta *1459*, 397–404.

Lenaz, G., and Genova, M.L. (2007). Kinetics of integrated electron transfer in the mitochondrial respiratory chain: random collisions vs. solid state electron channeling. Am. J. Physiol., Cell Physiol. *292*, C1221–C1239.

Lenaz, G., and Genova, M.L. (2010). Structure and organization of mitochondrial respiratory complexes: a new understanding of an old subject. Antioxid. Redox Signal. *12*, 961–1008.

Lenaz, G., Baracca, A., Barbero, G., Bergamini, C., Dalmonte, M.E., Del Sole, M., Faccioli, M., Falasca, A., Fato, R., Genova, M.L., et al. (2010). Mitochondrial respiratory chain super-complex I-III in physiology and pathology. Biochim. Biophys. Acta *1797*, 633–640.

Lesnefsky, E.J., Tandler, B., Ye, J., Slabe, T.J., Turkaly, J., and Hoppel, C.L. (1997). Myocardial ischemia decreases oxidative phosphorylation through cytochrome oxidase in subsarcolemmal mitochondria. Am. J. Physiol. *273*, H1544–H1554.

Lesnefsky, E.J., Gudz, T.I., Migita, C.T., Ikeda-Saito, M., Hassan, M.O., Turkaly, P.J., and Hoppel, C.L. (2001a). Ischemic injury to mitochondrial electron transport in the aging heart: damage to the iron-sulfur protein subunit of electron transport complex III. Arch. Biochem. Biophys. *385*, 117–128.

Lesnefsky, E.J., Slabe, T.J., Stoll, M.S., Minkler, P.E., and Hoppel, C.L. (2001b). Myocardial ischemia selectively depletes cardiolipin in rabbit heart subsarcolemmal mitochondria. Am. J. Physiol. Heart Circ. Physiol. *280*, H2770–H2778.

Leterrier, J.F., Rusakov, D.A., Nelson, B.D., and Linden, M. (1994). Interactions between brain mitochondria and cytoskeleton: evidence for specialized outer membrane domains involved in the association of cytoskeleton-associated proteins to mitochondria in situ and in vitro. Microsc. Res. Tech. *27*, 233–261.

Li, Y., D'Aurelio, M., Deng, J.-H., Park, J.-S., Manfredi, G., Hu, P., Lu, J., and Bai, Y. (2007). An assembled complex IV maintains the stability and activity of complex I in mammalian mitochondria. J. Biol. Chem. *282*, 17557–17562.

Lin, A., Krockmalnic, G., and Penman, S. (1990). Imaging cytoskeleton--mitochondrial membrane attachments by embedment-free electron microscopy of saponin-extracted cells. Proc. Natl. Acad. Sci. U.S.A. *87*, 8565–8569.

Lindén, M., Nelson, B.D., Loncar, D., and Leterrier, J.F. (1989). Studies on the interaction between mitochondria and the cytoskeleton. J. Bioenerg. Biomembr. *21*, 507–518.

Lipp, P., and Niggli, E. (1996). Submicroscopic calcium signals as fundamental events of excitation--contraction coupling in guinea-pig cardiac myocytes. J. Physiol. (Lond.) *492 (Pt 1)*, 31–38.

Liu, Y., Fiskum, G., and Schubert, D. (2002). Generation of reactive oxygen species by the mitochondrial electron transport chain. J. Neurochem. *80*, 780–787.

Lodish, H., Berk, A., Zipursky, S.L., Matsudaira, P., Baltimore, D., and Darnell, J. (2000). Molecular Cell Biology (W. H. Freeman).

Lucas, D.T., and Szweda, L.I. (1999). Declines in mitochondrial respiration during cardiac reperfusion: age-dependent inactivation of alpha-ketoglutarate dehydrogenase. Proc. Natl. Acad. Sci. U.S.A. *96*, 6689–6693.

MacAskill, A.F., and Kittler, J.T. (2010). Control of mitochondrial transport and localization in neurons. Trends Cell Biol. *20*, 102–112.

Makazan, Z., Saini, H.K., and Dhalla, N.S. (2007). Role of oxidative stress in alterations of mitochondrial function in ischemic-reperfused hearts. Am. J. Physiol. Heart Circ. Physiol. *292*, H1986–H1994.

Maldonado, E.N., and Lemasters, J.J. (2012). Warburg revisited: regulation of mitochondrial metabolism by voltage-dependent anion channels in cancer cells. J. Pharmacol. Exp. Ther. *342*, 637–641.

Maldonado, E.N., Patnaik, J., Mullins, M.R., and Lemasters, J.J. (2010). Free tubulin modulates mitochondrial membrane potential in cancer cells. Cancer Res. *70*, 10192–10201.

Maranzana, E., Barbero, G., Falasca, A.I., Lenaz, G., and Genova, M.L. (2013). Mitochondrial respiratory supercomplex association limits production of reactive oxygen species from complex I. Antioxid. Redox Signal. *19*, 1469–1480.

Marshall, R.C., Powers-Risius, P., Reutter, B.W., Schustz, A.M., Kuo, C., Huesman, M.K., and Huesman, R.H. (2003). Flow heterogeneity following global no-flow ischemia in isolated rabbit heart. Am. J. Physiol. Heart Circ. Physiol. *284*, H654–H667.

McKenzie, M., Lazarou, M., Thorburn, D.R., and Ryan, M.T. (2006). Mitochondrial respiratory chain supercomplexes are destabilized in Barth Syndrome patients. J. Mol. Biol. *361*, 462–469.

Mejia, E.M., Cole, L.K., and Hatch, G.M. (2014). Cardiolipin metabolism and the role it plays in

heart failure and mitochondrial supercomplex formation. Cardiovasc Hematol Disord Drug Targets *14*, 98–106.

Merkwirth, C., Dargazanli, S., Tatsuta, T., Geimer, S., Löwer, B., Wunderlich, F.T., von Kleist-Retzow, J.-C., Waisman, A., Westermann, B., and Langer, T. (2008). Prohibitins control cell proliferation and apoptosis by regulating OPA1-dependent cristae morphogenesis in mitochondria. Genes Dev. *22*, 476–488.

Mitchell, P. (1961). Coupling of Phosphorylation to Electron and Hydrogen Transfer by a Chemi-Osmotic type of Mechanism. Nature *191*, 144–148.

Mitchell, P. (1976a). Vectorial chemistry and the molecular mechanics of chemiosmotic coupling: power transmission by proticity. Biochem. Soc. Trans. *4*, 399–430.

Mitchell, P. (1976b). Possible molecular mechanisms of the protonmotive function of cytochrome systems. J. Theor. Biol. *62*, 327–367.

Mitchell, P. (1977). Vectorial chemiosmotic processes. Annu. Rev. Biochem. *46*, 996–1005.

Monge, C., Beraud, N., Kuznetsov, A.V., Rostovtseva, T., Sackett, D., Schlattner, U., Vendelin, M., and Saks, V.A. (2008). Regulation of respiration in brain mitochondria and synaptosomes: restrictions of ADP diffusion in situ, roles of tubulin, and mitochondrial creatine kinase. Mol. Cell. Biochem. *318*, 147–165.

Moreno-Sánchez, R., Saavedra, E., Rodríguez-Enríquez, S., and Olín-Sandoval, V. (2008). Metabolic Control Analysis: A Tool for Designing Strategies to Manipulate Metabolic Pathways. J Biomed Biotechnol *2008*.

Nakamura, Y., Yamamoto, M., Oda, E., Yamamoto, A., Kanemura, Y., Hara, M., Suzuki, A., Yamasaki, M., and Okano, H. (2003). Expression of tubulin beta II in neural stem/progenitor cells and radial fibers during human fetal brain development. Lab. Invest. *83*, 479–489.

Narishige, T., Blade, K.L., Ishibashi, Y., Nagai, T., Hamawaki, M., Menick, D.R., Kuppuswamy, D., and Cooper, G. (1999). Cardiac hypertrophic and developmental regulation of the beta-tubulin multigene family. J. Biol. Chem. *274*, 9692–9697.

Nascimben, L., Ingwall, J.S., Pauletto, P., Friedrich, J., Gwathmey, J.K., Saks, V., Pessina, A.C., and Allen, P.D. (1996). Creatine kinase system in failing and nonfailing human myocardium. Circulation *94*, 1894–1901.

Nederlof, R., Eerbeek, O., Hollmann, M.W., Southworth, R., and Zuurbier, C.J. (2014). Targeting hexokinase II to mitochondria to modulate energy metabolism and reduce ischaemia-reperfusion injury in heart. Br. J. Pharmacol. *171*, 2067–2079.

Neely, J.R., and Grotyohann, L.W. (1984). Role of glycolytic products in damage to ischemic myocardium. Dissociation of adenosine triphosphate levels and recovery of function of reperfused ischemic hearts. Circ. Res. *55*, 816–824.

Neely, J.R., and Morgan, H.E. (1974). Relationship between carbohydrate and lipid metabolism and the energy balance of heart muscle. Annu. Rev. Physiol. *36*, 413–459.

Neely, J.R., Denton, R.M., England, P.J., and Randle, P.J. (1972). The effects of increased heart work on the tricarboxylate cycle and its interactions with glycolysis in the perfused rat heart. Biochem. J. *128*, 147–159.

Neely, J.R., Rovetto, M.J., Whitmer, J.T., and Morgan, H.E. (1973). Effects of ischemia on function and metabolism of the isolated working rat heart. Am. J. Physiol. *225*, 651–658.

Neubauer, S. (2007). The failing heart--an engine out of fuel. N. Engl. J. Med. *356*, 1140–1151.

Newsholme, E.A., Beis, I., Leech, A.R., and Zammit, V.A. (1978). The role of creatine kinase and arginine kinase in muscle. Biochem. J. *172*, 533–537.

Noskov, S.Y., Rostovtseva, T.K., and Bezrukov, S.M. (2013). ATP transport through VDAC and the VDAC-tubulin complex probed by equilibrium and nonequilibrium MD simulations. Biochemistry *52*, 9246–9256.

Novgorodov, S.A., and Gudz, T.I. (2009). CERAMIDE AND MITOCHONDRIA IN ISCHEMIA/REPERFUSION. J Cardiovasc Pharmacol *53*, 198–208.

Ogata, T., and Yamasaki, Y. (1997). Ultra-high-resolution scanning electron microscopy of mitochondria and sarcoplasmic reticulum arrangement in human red, white, and intermediate muscle fibers. Anat. Rec. *248*, 214–223.

Opie, L.H. (2003). Heart Physiology: From Cell to Circulation (Philadelphia: Lippincott Williams and Wilkins).

Paradies, G., Ruggiero, F.M., Petrosillo, G., and Quagliariello, E. (1993). Age-dependent decrease in the cytochrome c oxidase activity and changes in phospholipids in rat-heart mitochondria. Arch Gerontol Geriatr *16*, 263–272.

Paradies, G., Petrosillo, G., Pistolese, M., Di Venosa, N., Serena, D., and Ruggiero, F.M. (1999). Lipid peroxidation and alterations to oxidative metabolism in mitochondria isolated from rat heart subjected to ischemia and reperfusion. Free Radic. Biol. Med. *27*, 42–50.

Paradies, G., Petrosillo, G., Pistolese, M., Di Venosa, N., Federici, A., and Ruggiero, F.M. (2004). Decrease in mitochondrial complex I activity in ischemic/reperfused rat heart: involvement of reactive oxygen species and cardiolipin. Circ. Res. *94*, 53–59.

Pedersen, P.L. (2007). Transport ATPases into the year 2008: a brief overview related to types, structures, functions and roles in health and disease. J. Bioenerg. Biomembr. *39*, 349–355.

Perry, C.G.R., Kane, D.A., Lin, C.-T., Kozy, R., Cathey, B.L., Lark, D.S., Kane, C.L., Brophy, P.M., Gavin, T.P., Anderson, E.J., et al. (2011). Inhibiting myosin-ATPase reveals a dynamic range of mitochondrial respiratory control in skeletal muscle. Biochem. J. *437*, 215–222.

Pfeiffer, K., Gohil, V., Stuart, R.A., Hunte, C., Brandt, U., Greenberg, M.L., and Schägger, H. (2003). Cardiolipin stabilizes respiratory chain supercomplexes. J. Biol. Chem. *278*, 52873–52880.

Picard, M., Hepple, R.T., and Burelle, Y. (2012). Mitochondrial functional specialization in glycolytic and oxidative muscle fibers: tailoring the organelle for optimal function. Am. J. Physiol., Cell Physiol. *302*, C629–C641.

Piccoli, C., Scrima, R., Boffoli, D., and Capitanio, N. (2006). Control by cytochrome c oxidase of the cellular oxidative phosphorylation system depends on the mitochondrial energy state. Biochem. J. *396*, 573–583.

De Pinto, V., Guarino, F., Guarnera, A., Messina, A., Reina, S., Tomasello, F.M., Palermo, V., and Mazzoni, C. (2010). Characterization of human VDAC isoforms: a peculiar function for VDAC3? Biochim. Biophys. Acta *1797*, 1268–1275.

Pries, A.R., and Secomb, T.W. (2009). Origins of heterogeneity in tissue perfusion and metabolism. Cardiovasc. Res. *81*, 328–335.

Pucar, D., Dzeja, P.P., Bast, P., Juranic, N., Macura, S., and Terzic, A. (2001). Cellular energetics in the preconditioned state: protective role for phosphotransfer reactions captured by 18O-assisted 31P NMR. J. Biol. Chem. *276*, 44812–44819.

Pucar, D., Dzeja, P.P., Bast, P., Gumina, R.J., Drahl, C., Lim, L., Juranic, N., Macura, S., and Terzic, A. (2004). Mapping hypoxia-induced bioenergetic rearrangements and metabolic signaling by 18O-assisted 31P NMR and 1H NMR spectroscopy. Mol. Cell. Biochem. *256-257*, 281–289.

Qin, W., Khuchua, Z., Boero, J., Payne, R.M., and Strauss, A.W. (1999). Oxidative myocytes of heart and skeletal muscle express abundant sarcomeric mitochondrial creatine kinase. Histochem. J. *31*, 357–365.

Quarato, G., Piccoli, C., Scrima, R., and Capitanio, N. (2011). Variation of flux control coefficient of cytochrome c oxidase and of the other respiratory chain complexes at different values of protonmotive force occurs by a threshold mechanism. Biochimica et Biophysica Acta (BBA) - Bioenergetics *1807*, 1114–1124.

Quirós, P.M., Ramsay, A.J., Sala, D., Fernández-Vizarra, E., Rodríguez, F., Peinado, J.R., Fernández-García, M.S., Vega, J.A., Enríquez, J.A., Zorzano, A., et al. (2012). Loss of mitochondrial protease OMA1 alters processing of the GTPase OPA1 and causes obesity and defective thermogenesis in mice. EMBO J. *31*, 2117–2133.

Radermacher, M., Ruiz, T., Clason, T., Benjamin, S., Brandt, U., and Zickermann, V. (2006). The Three-dimensional Structure of Complex I from Yarrowia lipolytica: A highly dynamic Enzyme. J Struct Biol *154*, 269–279.

Ramírez-Aguilar, S.J., Keuthe, M., Rocha, M., Fedyaev, V.V., Kramp, K., Gupta, K.J., Rasmusson, A.G., Schulze, W.X., and van Dongen, J.T. (2011). The composition of plant mitochondrial supercomplexes changes with oxygen availability. J. Biol. Chem. *286*, 43045–

43053.

Rayment, I., Holden, H.M., Whittaker, M., Yohn, C.B., Lorenz, M., Holmes, K.C., and Milligan, R.A. (1993). Structure of the actin-myosin complex and its implications for muscle contraction. Science *261*, 58–65.

Reipert, S., Steinböck, F., Fischer, I., Bittner, R.E., Zeöld, A., and Wiche, G. (1999). Association of mitochondria with plectin and desmin intermediate filaments in striated muscle. Exp. Cell Res. *252*, 479–491.

Richter, C., and Ghafourifar, P. (1999). Ceramide induces cytochrome c release from isolated mitochondria. Biochem. Soc. Symp. *66*, 27–31.

Robinson, J.M., Wang, Y., Kerrick, W.G.L., Kawai, R., and Cheung, H.C. (2002). Activation of striated muscle: nearest-neighbor regulatory-unit and cross-bridge influence on myofilament kinetics. J. Mol. Biol. *322*, 1065–1088.

Rosca, M., Minkler, P., and Hoppel, C.L. (2011). Cardiac mitochondria in heart failure: normal cardiolipin profile and increased threonine phosphorylation of complex IV. Biochim. Biophys. Acta *1807*, 1373–1382.

Rosca, M.G., Vazquez, E.J., Kerner, J., Parland, W., Chandler, M.P., Stanley, W., Sabbah, H.N., and Hoppel, C.L. (2008). Cardiac mitochondria in heart failure: decrease in respirasomes and oxidative phosphorylation. Cardiovasc. Res. *80*, 30–39.

Rostovtseva, T.K. (2010). Control of Mitochondrial Outer Membrane Permeability: Vdac Regulation by Dimeric Tubulin and Cytosolic Proteins (Hauppauge: Nova Science Publishers, Inc).

Rostovtseva, T., and Colombini, M. (1996). ATP flux is controlled by a voltage-gated channel from the mitochondrial outer membrane. J. Biol. Chem. *271*, 28006–28008.

Rostovtseva, T., and Colombini, M. (1997). VDAC channels mediate and gate the flow of ATP: implications for the regulation of mitochondrial function. Biophys. J. *72*, 1954–1962.

Rostovtseva, T.K., and Bezrukov, S.M. (2008). VDAC regulation: role of cytosolic proteins and mitochondrial lipids. J. Bioenerg. Biomembr. *40*, 163–170.

Rostovtseva, T.K., and Bezrukov, S.M. (2012). VDAC inhibition by tubulin and its physiological implications. Biochim. Biophys. Acta *1818*, 1526–1535.

Rostovtseva, T.K., Sheldon, K.L., Hassanzadeh, E., Monge, C., Saks, V., Bezrukov, S.M., and Sackett, D.L. (2008). Tubulin binding blocks mitochondrial voltage-dependent anion channel and regulates respiration. Proc. Natl. Acad. Sci. U.S.A. *105*, 18746–18751.

Rostovtseva, T.K., Gurnev, P.A., Chen, M.-Y., and Bezrukov, S.M. (2012). Membrane lipid composition regulates tubulin interaction with mitochondrial voltage-dependent anion channel. J. Biol. Chem. *287*, 29589–29598.

Rouslin, W. (1983). Mitochondrial complexes I, II, III, IV, and V in myocardial ischemia and autolysis. Am. J. Physiol. *244*, H743–H748.

Rouslin, W., and Millard, R.W. (1980). Canine myocardial ischemia: Defect in mitochondrial electron transfer complex I. Journal of Molecular and Cellular Cardiology *12*, 639–645.

Rouslin, W., and Millard, R.W. (1981). Mitochondrial inner membrane enzyme defects in porcine myocardial ischemia. Am. J. Physiol. *240*, H308–H313.

Sabbah, H.N., Sharov, V., Riddle, J.M., Kono, T., Lesch, M., and Goldstein, S. (1992). Mitochondrial abnormalities in myocardium of dogs with chronic heart failure. J. Mol. Cell. Cardiol. *24*, 1333–1347.

Saks, V. (2007). Molecular System Bioenergetics: Energy for Life (John Wiley and Sons).

Saks, V., Kuznetsov, A.V., Kupriyanov, V.V., Miceli, M.V., and Jacobus, W.E. (1985). Creatine kinase of rat heart mitochondria. The demonstration of functional coupling to oxidative phosphorylation in an inner membrane-matrix preparation. J. Biol. Chem. *260*, 7757–7764.

Saks, V., Khuchua, Z.A., Vasilyeva, E.V., Belikova OYu, null, and Kuznetsov, A.V. (1994). Metabolic compartmentation and substrate channelling in muscle cells. Role of coupled creatine kinases in in vivo regulation of cellular respiration--a synthesis. Mol. Cell. Biochem. *133-134*, 155–192.

Saks, V., Ventura-Clapier, R., and Aliev, M.K. (1996). Metabolic control and metabolic capacity: two aspects of creatine kinase functioning in the cells. Biochim. Biophys. Acta *1274*, 81–88.

Saks, V., Dos Santos, P., Gellerich, F.N., and Diolez, P. (1998a). Quantitative studies of enzyme-substrate compartmentation, functional coupling and metabolic channelling in muscle cells. Mol. Cell. Biochem. *184*, 291–307.

Saks, V., Veksler, V.I., Kuznetsov, A.V., Kay, L., Sikk, P., Tiivel, T., Tranqui, L., Olivares, J., Winkler, K., Wiedemann, F., et al. (1998b). Permeabilized cell and skinned fiber techniques in studies of mitochondrial function in vivo. Mol. Cell. Biochem. *184*, 81–100.

Saks, V., Kongas, O., Vendelin, M., and Kay, L. (2000). Role of the creatine/phosphocreatine system in the regulation of mitochondrial respiration. Acta Physiol. Scand. *168*, 635–641.

Saks, V., Kaambre, T., Sikk, P., Eimre, M., Orlova, E., Paju, K., Piirsoo, A., Appaix, F., Kay, L., Regitz-Zagrosek, V., et al. (2001). Intracellular energetic units in red muscle cells. Biochem. J. *356*, 643–657.

Saks, V., Kuznetsov, A.V., Vendelin, M., Guerrero, K., Kay, L., and Seppet, E.K. (2004). Functional coupling as a basic mechanism of feedback regulation of cardiac energy metabolism. Mol. Cell. Biochem. *256-257*, 185–199.

Saks, V., Dzeja, P., Schlattner, U., Vendelin, M., Terzic, A., and Wallimann, T. (2006). Cardiac system bioenergetics: metabolic basis of the Frank-Starling law. J. Physiol. (Lond.) *571*, 253–273.

Saks, V., Kaambre, T., Guzun, R., Anmann, T., Sikk, P., Schlattner, U., Wallimann, T., Aliev, M., and Vendelin, M. (2007a). The Creatine Kinase Phosphotransfer Network: Thermodynamic and Kinetic Considerations, the Impact of the Mitochondrial Outer Membrane and Modelling Approaches. In Creatine and Creatine Kinase in Health and Disease, G.S. Salomons, and M. Wyss, eds. (Springer Netherlands), pp. 27–65.

Saks, V., Monge, C., Anmann, T., and Dzeja, P.P. (2007b). Integrated and Organized Cellular Energetic Systems: Theories of Cell Energetics, Compartmentation, and Metabolic Channeling. In Molecular System Bioenergetics, V. Saks, ed. (Wiley-VCH Verlag GmbH and Co. KGaA), pp. 59–109.

Saks, V., Beraud, N., and Wallimann, T. (2008). Metabolic compartmentation - a system level property of muscle cells: real problems of diffusion in living cells. Int J Mol Sci *9*, 751–767.

Saks, V., Guzun, R., Timohhina, N., Tepp, K., Varikmaa, M., Monge, C., Beraud, N., Kaambre, T., Kuznetsov, A., Kadaja, L., et al. (2010). Structure–function relationships in feedback regulation of energy fluxes in vivo in health and disease: Mitochondrial Interactosome. Biochimica et Biophysica Acta (BBA) - Bioenergetics *1797*, 678–697.

Saks, V., Kuznetsov, A.V., Gonzalez-Granillo, M., Tepp, K., Timohhina, N., Karu-Varikmaa, M., Kaambre, T., Dos Santos, P., Boucher, F., and Guzun, R. (2012). Intracellular Energetic Units regulate metabolism in cardiac cells. J. Mol. Cell. Cardiol. *52*, 419–436.

Saks, V., Schlattner, U., Tokarska-Schlattner, M., Wallimann, T., Bagur, R., Zorman, S., Pelosse, M., Santos, P.D., Boucher, F., Kaambre, T., et al. (2013). Systems Level Regulation of Cardiac Energy Fluxes Via Metabolic Cycles: Role of Creatine, Phosphotransfer Pathways, and AMPK Signaling. In Systems Biology of Metabolic and Signaling Networks, M.A. Aon, V. Saks, and U. Schlattner, eds. (Springer Berlin Heidelberg), pp. 261–320.

Saks, V., Schlattner, U., Tokarska-Schlattner, M., Wallimann, T., Bagur, R., Zorman, S., Pelosse, M., Santos, P.D., Boucher, F., Kaambre, T., et al. (2014). Systems Level Regulation of Cardiac Energy Fluxes Via Metabolic Cycles: Role of Creatine, Phosphotransfer Pathways, and AMPK Signaling. In Systems Biology of Metabolic and Signaling Networks, M.A. Aon, V. Saks, and U. Schlattner, eds. (Springer Berlin Heidelberg), pp. 261–320.

Sato, H., Hori, M., Kitakaze, M., Iwai, K., Takashima, S., Kurihara, H., Inoue, M., and Kamada, T. (1993). Reperfusion after brief ischemia disrupts the microtubule network in canine hearts. Circ. Res. *72*, 361–375.

Sato, H., Nagai, T., Kuppuswamy, D., Narishige, T., Koide, M., Menick, D.R., and Cooper, G., 4th (1997). Microtubule stabilization in pressure overload cardiac hypertrophy. J. Cell Biol. *139*, 963–973.

Sazanov, L.A. (2015). A giant molecular proton pump: structure and mechanism of respiratory complex I. Nat. Rev. Mol. Cell Biol. *16*, 375–388.

Schäfer, E., Seelert, H., Reifschneider, N.H., Krause, F., Dencher, N.A., and Vonck, J. (2006). Architecture of active mammalian respiratory chain supercomplexes. J. Biol. Chem. *281*, 15370–

15375.

Schäfer, E., Dencher, N.A., Vonck, J., and Parcej, D.N. (2007). Three-dimensional structure of the respiratory chain supercomplex I1III2IV1 from bovine heart mitochondria. Biochemistry *46*, 12579–12585.

Schägger, H., and Pfeiffer, K. (2000). Supercomplexes in the respiratory chains of yeast and mammalian mitochondria. EMBO J. *19*, 1777–1783.

Schägger, H., and Pfeiffer, K. (2001). The Ratio of Oxidative Phosphorylation Complexes I–V in Bovine Heart Mitochondria and the Composition of Respiratory Chain Supercomplexes. J. Biol. Chem. *276*, 37861–37867.

Schägger, H., de Coo, R., Bauer, M.F., Hofmann, S., Godinot, C., and Brandt, U. (2004). Significance of respirasomes for the assembly/stability of human respiratory chain complex I. J. Biol. Chem. *279*, 36349–36353.

Schiaffino, S., and Reggiani, C. (1996). Molecular diversity of myofibrillar proteins: gene regulation and functional significance. Physiol. Rev. *76*, 371–423.

Schlattner, U., Eder, M., Dolder, M., Khuchua, Z.A., Strauss, A.W., and Wallimann, T. (2000). Divergent enzyme kinetics and structural properties of the two human mitochondrial creatine kinase isoenzymes. Biol. Chem. *381*, 1063–1070.

Schlattner, U., Gehring, F., Vernoux, N., Tokarska-Schlattner, M., Neumann, D., Marcillat, O., Vial, C., and Wallimann, T. (2004). C-terminal lysines determine phospholipid interaction of sarcomeric mitochondrial creatine kinase. J. Biol. Chem. *279*, 24334–24342.

Schlattner, U., Tokarska-Schlattner, M., and Wallimann, T. (2006). Mitochondrial creatine kinase in human health and disease. Biochim. Biophys. Acta *1762*, 164–180.

Schrödinger, E. (1992). What is Life?: With Mind and Matter and Autobiographical Sketches (Cambridge University Press).

Scorrano, L., Ashiya, M., Buttle, K., Weiler, S., Oakes, S.A., Mannella, C.A., and Korsmeyer, S.J. (2002). A distinct pathway remodels mitochondrial cristae and mobilizes cytochrome c during apoptosis. Dev. Cell *2*, 55–67.

Selivanov, V.A., Alekseev, A.E., Hodgson, D.M., Dzeja, P.P., and Terzic, A. (2004). Nucleotide-gated KATP channels integrated with creatine and adenylate kinases: amplification, tuning and sensing of energetic signals in the compartmentalized cellular environment. Mol. Cell. Biochem. *256-257*, 243–256.

Seppet, E.K., Eimre, M., Anmann, T., Seppet, E., Peet, N., Käämbre, T., Paju, K., Piirsoo, A., Kuznetsov, A.V., Vendelin, M., et al. (2005). Intracellular energetic units in healthy and diseased hearts. Exp Clin Cardiol *10*, 173–183.

Seppet, E.K., Eimre, M., Anmann, T., Seppet, E., Piirsoo, A., Peet, N., Paju, K., Guzun, R., Beraud,

N., Pelloux, S., et al. (2006). Structure-function relationships in the regulation of energy transfer between mitochondria and ATPases in cardiac cells. Exp Clin Cardiol *11*, 189–194.

Sheldon, K.L., Maldonado, E.N., Lemasters, J.J., Rostovtseva, T.K., and Bezrukov, S.M. (2011). Phosphorylation of voltage-dependent anion channel by serine/threonine kinases governs its interaction with tubulin. PLoS ONE *6*, e25539.

Sirajuddin, M., Rice, L.M., and Vale, R.D. (2014). Regulation of microtubule motors by tubulin isotypes and post-translational modifications. Nat. Cell Biol. *16*, 335–344.

Soboll, S., Brdiczka, D., Jahnke, D., Schmidt, A., Schlattner, U., Wendt, S., Wyss, M., and Wallimann, T. (1999). Octamer-dimer transitions of mitochondrial creatine kinase in heart disease. J. Mol. Cell. Cardiol. *31*, 857–866.

Di Somma, S., Di Benedetto, M.P., Salvatore, G., Agozzino, L., Ferranti, F., Esposito, S., La Dogana, P., Scarano, M.I., Caputo, G., Cotrufo, M., et al. (2004). Desmin-free cardiomyocytes and myocardial dysfunction in end stage heart failure. Eur. J. Heart Fail. *6*, 389–398.

Song, J., Midson, C., Blachly-Dyson, E., Forte, M., and Colombini, M. (1998). The sensor regions of VDAC are translocated from within the membrane to the surface during the gating processes. Biophys. J. *74*, 2926–2944.

De Sousa, E., Veksler, V., Minajeva, A., Kaasik, A., Mateo, P., Mayoux, E., Hoerter, J., Bigard, X., Serrurier, B., and Ventura-Clapier, R. (1999). Subcellular creatine kinase alterations. Implications in heart failure. Circ. Res. *85*, 68–76.

Spinazzi, M., Casarin, A., Pertegato, V., Salviati, L., and Angelini, C. (2012). Assessment of mitochondrial respiratory chain enzymatic activities on tissues and cultured cells. Nat Protoc *7*, 1235–1246.

Spindler, M., Illing, B., Horn, M., de Groot, M., Ertl, G., and Neubauer, S. (2001). Temporal fluctuations of myocardia high-energy phosphate metabolite with the cardiac cycle. Basic Res. Cardiol. *96*, 553–556.

Spindler, M., Meyer, K., Strömer, H., Leupold, A., Boehm, E., Wagner, H., and Neubauer, S. (2004). Creatine kinase-deficient hearts exhibit increased susceptibility to ischemia-reperfusion injury and impaired calcium homeostasis. Am. J. Physiol. Heart Circ. Physiol. *287*, H1039–H1045.

Srere, P.A. (2000). Macromolecular interactions: tracing the roots. Trends Biochem. Sci. *25*, 150–153.

Srivastava, D.K., and Bernhard, S.A. (1986). Metabolite transfer via enzyme-enzyme complexes. Science *234*, 1081–1086.

Starling, E.H., and Visscher, M.B. (1927). The regulation of the energy output of the heart. J. Physiol. (Lond.) *62*, 243–261.

Stiburek, L., Cesnekova, J., Kostkova, O., Fornuskova, D., Vinsova, K., Wenchich, L., Houstek,

J., and Zeman, J. (2012). YME1L controls the accumulation of respiratory chain subunits and is required for apoptotic resistance, cristae morphogenesis, and cell proliferation. Mol. Biol. Cell *23*, 1010–1023.

Stroh, A., Anderka, O., Pfeiffer, K., Yagi, T., Finel, M., Ludwig, B., and Schägger, H. (2004). Assembly of respiratory complexes I, III, and IV into NADH oxidase supercomplex stabilizes complex I in Paracoccus denitrificans. J. Biol. Chem. *279*, 5000–5007.

Suga, H. (1990). Ventricular energetics. Physiol. Rev. *70*, 247–277.

Tashiro, T., and Komiya, Y. (1989). Stable and dynamic forms of cytoskeletal proteins in slow axonal transport. J. Neurosci. *9*, 760–768.

Tepp, K., Timohhina, N., Chekulayev, V., Shevchuk, I., Kaambre, T., and Saks, V. (2010). Metabolic control analysis of integrated energy metabolism in permeabilized cardiomyocytes - experimental study. Acta Biochim. Pol. *57*, 421–430.

Tepp, K., Shevchuk, I., Chekulayev, V., Timohhina, N., Kuznetsov, A.V., Guzun, R., Saks, V., and Kaambre, T. (2011). High efficiency of energy flux controls within mitochondrial interactosome in cardiac intracellular energetic units. Biochim. Biophys. Acta *1807*, 1549–1561.

Teijido, O., Rappaport, S.M., Chamberlin, A., Noskov, S.Y., Aguilella, V.M., Rostovtseva, T.K., and Bezrukov, S.M. (2014). Acidification asymmetrically affects voltage-dependent anion channel implicating the involvement of salt bridges. J. Biol. Chem. *289*, 23670–23682.

Timohhina, N., Guzun, R., Tepp, K., Monge, C., Varikmaa, M., Vija, H., Sikk, P., Kaambre, T., Sackett, D., and Saks, V. (2009). Direct measurement of energy fluxes from mitochondria into cytoplasm in permeabilized cardiac cells in situ: some evidence for Mitochondrial Interactosome. J. Bioenerg. Biomembr. *41*, 259–275.

Toleikis, A., Dzeja, P., Praskevicius, A., and Jasaitis, A. (1979). Mitochondrial functions in ischemic myocardium. I. Proton electrochemical gradient, inner membrane permeability, calcium transport and oxidative phosphorylation in isolated mitochondria. J. Mol. Cell. Cardiol. *11*, 57–76.

Tsutsui, H., Tagawa, H., Kent, R.L., McCollam, P.L., Ishihara, K., Nagatsu, M., and Cooper, G. (1994). Role of microtubules in contractile dysfunction of hypertrophied cardiocytes. Circulation *90*, 533–555.

Turrens, J.F., Beconi, M., Barilla, J., Chavez, U.B., and McCord, J.M. (1991). Mitochondrial generation of oxygen radicals during reoxygenation of ischemic tissues. Free Radic. Res. Commun. *12-13 Pt 2*, 681–689.

Ueta, H., Ogura, R., Sugiyama, M., Kagiyama, A., and Shin, G. (1990). O2-. spin trapping on cardiac submitochondrial particles isolated from ischemic and non-ischemic myocardium. J. Mol. Cell. Cardiol. *22*, 893–899.

U. Schlattner,T. Wallimann (2004). Metabolite channeling: creatine kinase microcompartments. In Encyclopedia of Biological Chemistry, (New York, USA: Academic Press), pp. 646–651.

Vander Heiden, M.G., Chandel, N.S., Li, X.X., Schumacker, P.T., Colombini, M., and Thompson, C.B. (2000). Outer mitochondrial membrane permeability can regulate coupled respiration and cell survival. Proc Natl Acad Sci U S A *97*, 4666–4671.

Vandroux, D., Schaeffer, C., Tissier, C., Lalande, A., Bès, S., Rochette, L., and Athias, P. (2004). Microtubule alteration is an early cellular reaction to the metabolic challenge in ischemic cardiomyocytes. Mol. Cell. Biochem. *258*, 99–108.

Varanita, T., Soriano, M.E., Romanello, V., Zaglia, T., Quintana-Cabrera, R., Semenzato, M., Menabò, R., Costa, V., Civiletto, G., Pesce, P., et al. (2015). The opa1-dependent mitochondrial cristae remodeling pathway controls atrophic, apoptotic, and ischemic tissue damage. Cell Metab. *21*, 834–844.

Vasdev, S.C., Biro, G.P., Narbaitz, R., and Kako, K.J. (1980). Membrane changes induced by early myocardial ischemia in the dog. Can. J. Biochem. *58*, 1112–1119.

Vempati, U.D., Han, X., and Moraes, C.T. (2009). Lack of cytochrome c in mouse fibroblasts disrupts assembly/stability of respiratory complexes I and IV. J. Biol. Chem. *284*, 4383–4391.

Vendelin, M., Kongas, O., and Saks, V. (2000). Regulation of mitochondrial respiration in heart cells analyzed by reaction-diffusion model of energy transfer. Am. J. Physiol., Cell Physiol. *278*, C747–C764.

Vendelin, M., Eimre, M., Seppet, E., Peet, N., Andrienko, T., Lemba, M., Engelbrecht, J., Seppet, E.K., and Saks, V.A. (2004). Intracellular diffusion of adenosine phosphates is locally restricted in cardiac muscle. Mol. Cell. Biochem. *256-257*, 229–241.

Ventura-Clapier, R., Kuznetsov, A., Veksler, V., Boehm, E., and Anflous, K. (1998). Functional coupling of creatine kinases in muscles: species and tissue specificity. Mol. Cell. Biochem. *184*, 231–247.

Ventura-Clapier, R., Garnier, A., and Veksler, V. (2004). Energy metabolism in heart failure. J. Physiol. (Lond.) *555*, 1–13.

Vonck, J., and Schäfer, E. (2009). Supramolecular organization of protein complexes in the mitochondrial inner membrane. Biochim. Biophys. Acta *1793*, 117–124.

Wallimann, T., Zurbriggen, B., and Eppenberger, H.M. (1985). Separation of mitochondrial creatine kinase (MiMi-CK) from cytosolic creatine kinase isoenzymes by Cibachrome-Blue affinity chromatography. Enzyme *33*, 226–231.

Wallimann, T., Wyss, M., Brdiczka, D., Nicolay, K., and Eppenberger, H.M. (1992). Intracellular compartmentation, structure and function of creatine kinase isoenzymes in tissues with high and fluctuating energy demands: the "phosphocreatine circuit" for cellular energy homeostasis. Biochem. J. *281 (Pt 1)*, 21–40.

Wan, B., Doumen, C., Duszynski, J., Salama, G., Vary, T.C., and LaNoue, K.F. (1993). Effects of cardiac work on electrical potential gradient across mitochondrial membrane in perfused rat hearts.

Am. J. Physiol. *265*, H453–H460.

Weiss, R.G., Gerstenblith, G., and Bottomley, P.A. (2005). ATP flux through creatine kinase in the normal, stressed, and failing human heart. Proc. Natl. Acad. Sci. U.S.A. *102*, 808–813.

Wendt, S., Schlattner, U., and Wallimann, T. (2003). Differential effects of peroxynitrite on human mitochondrial creatine kinase isoenzymes. Inactivation, octamer destabilization, and identification of involved residues. J. Biol. Chem. *278*, 1125–1130.

Wikman-Coffelt, J., Sievers, R., Coffelt, R.J., and Parmley, W.W. (1983). The cardiac cycle: regulation and energy oscillations. Am. J. Physiol. *245*, H354–H362.

Wikström, M. (1989). Identification of the electron transfers in cytochrome oxidase that are coupled to proton-pumping. Nature *338*, 776–778.

Williamson, J.R., Ford, C., Illingworth, J., and Safer, B. (1976). Coordination of citric acid cycle activity with electron transport flux. Circ. Res. *38*, I39–I51.

Wisneski, J.A., Gertz, E.W., Neese, R.A., Gruenke, L.D., and Craig, J.C. (1985). Dual carbon-labeled isotope experiments using D-[6-14C] glucose and L-[1,2,3-13C3] lactate: a new approach for investigating human myocardial metabolism during ischemia. J. Am. Coll. Cardiol. *5*, 1138–1146.

Wisniewski, E., Gellerich, F.N., and Kunz, W.S. (1995). Distribution of flux control among the enzymes of mitochondrial oxidative phosphorylation in calcium-activated saponin-skinned rat musculus soleus fibers. Eur. J. Biochem. *230*, 549–554.

Wittig, I., Braun, H.-P., and Schägger, H. (2006). Blue native PAGE. Nat Protoc *1*, 418–428.

Wyss, M., Schlegel, J., James, P., Eppenberger, H.M., and Wallimann, T. (1990). Mitochondrial creatine kinase from chicken brain. Purification, biophysical characterization, and generation of heterodimeric and heterooctameric molecules with subunits of other creatine kinase isoenzymes. J. Biol. Chem. *265*, 15900–15908.

Xiao, X., Hu, Y., Quirós, P.M., Wei, Q., López-Otín, C., and Dong, Z. (2014). OMA1 mediates OPA1 proteolysis and mitochondrial fragmentation in experimental models of ischemic kidney injury. Am. J. Physiol. Renal Physiol. *306*, F1318–F1326.

Yancey, D.M., Guichard, J.L., Ahmed, M.I., Zhou, L., Murphy, M.P., Johnson, M.S., Benavides, G.A., Collawn, J., Darley-Usmar, V., and Dell'Italia, L.J. (2015). Cardiomyocyte mitochondrial oxidative stress and cytoskeletal breakdown in the heart with a primary volume overload. Am. J. Physiol. Heart Circ. Physiol. *308*, H651–H663.

Zhang, K., Li, H., and Song, Z. (2014). Membrane depolarization activates the mitochondrial protease OMA1 by stimulating self-cleavage. EMBO Rep *15*, 576–585.

Zhang, M., Mileykovskaya, E., and Dowhan, W. (2002). Gluing the respiratory chain together. Cardiolipin is required for supercomplex formation in the inner mitochondrial membrane. J. Biol.

Chem. *277*, 43553–43556.

Zhang, M., Mileykovskaya, E., and Dowhan, W. (2005). Cardiolipin Is Essential for Organization of Complexes III and IV into a Supercomplex in Intact Yeast Mitochondria. J Biol Chem *280*, 29403–29408.

Zhou, Y., Duncan, T.M., Bulygin, V.V., Hutcheon, M.L., and Cross, R.L. (1996). ATP hydrolysis by membrane-bound Escherichia coli F0F1 causes rotation of the gamma subunit relative to the beta subunits. Biochim. Biophys. Acta *1275*, 96–100.

Zimmerberg, J., and Parsegian, V.A. (1986). Polymer inaccessible volume changes during opening and closing of a voltage-dependent ionic channel. Nature *323*, 36–39.

11. Appendix: Other Contributions

Beside the three papers introduced in the result part of this manuscript, during the three years of the thesis my work have contributed to other publications with our collaborators, a review article and a book chapter.

Type: Review article

Title: Modular organization of cardiac energy metabolism: energy conversion, transfer and feedback regulation.

Authors: Guzun R, Kaambre T, Bagur R, Grichine A, Usson Y, Varikmaa M, Anmann T, Tepp K, Timohhina N, Shevchuk I, Chekulayev V, Boucher F, Dos Santos P, Schlattner U, Wallimann T, Kuznetsov AV, Dzeja P, Aliev M, Saks V.

State: Article published on January 2015 in *Acta Physiol (Oxf);* 213(1):84-106 (doi: 10.1111/apha.12287)

Abstract: To meet high cellular demands, the energy metabolism of cardiac muscles is organized by precise and coordinated functioning of intracellular energetic units (ICEUs). ICEUs represent structural and functional modules integrating multiple fluxes at sites of ATP generation in mitochondria and ATP utilization by myofibrillar, sarcoplasmic reticulum and sarcolemma ion-pump ATPases. The role of ICEUs is to enhance the efficiency of vectorial intracellular energy transfer and fine tuning of oxidative ATP synthesis maintaining stable metabolite levels to adjust to intracellular energyneeds through the dynamic system of compartmentalized phosphoryl transfer networks. One of the key elements in regulation of energy flux distribution and feedback communication is the selective permeability of mitochondrial outer membrane (MOM) which represents a bottleneck in adenine nucleotide and other energy metabolite transfer and microcompartmentalization. Based on the experimental and theoretical (mathematical modelling) arguments, we describe regulation of mitochondrial ATP synthesis within ICEUs allowing heart workload to be linearly correlated with oxygen consumption ensuring conditions of metabolic stability, signal communication and

synchronization. Particular attention was paid to the structure-function relationship in the development of ICEU, and the role of mitochondria interaction with cytoskeletal proteins, like tubulin, in theregulation of MOM permeability in response to energy metabolic signals providing regulation of mitochondrial respiration. Emphasis was given to the importance of creatine metabolism for the cardiac energy homoeostasis.

Type: Book chapter

Title: Systems Level Regulation of Cardiac Energy Fluxes Via Metabolic Cycles: Role of Creatine, Phosphoryl transfer Pathways, and AMPK Signaling

Authors: Valdur S, Schlattner U, Tokarska-Schlattner M, Wallimann T, Bagur R, Zorman S, Pelosse M, Dos Santos P, Boucher F, Kaambre T, Guzun R.

State: Book published on August 2013 in *Springer Series in Biophysics Volume 16, 2014*, pp 261-320

Abstract: Integrated mechanisms of regulation of energy metabolism at cellular, tissue, and organ levels are analyzed from a systems biology perspective. These integrated mechanisms comprise the coordinated function of three cycles of mass and energy transfer and conversion: (1) the Randle cycle of substrate supply, (2) the Krebs cycle coupled with energy transformation in mitochondrial oxidative phosphorylation, and (3) the kinase cycles of intracellular energy transfer and signal transduction for regulation of energy fluxes. These cycles are extended and partially governed by information transfer systems like those linked to protein kinase signaling. In the heart, these cycles are closely related to the Ca2+ cycle during excitation–contraction coupling. According to the view of integrated metabolic cycles, the phosphocreatine/creatine kinase system represents a most important subsystem determining the efficiency of regulation of metabolic and energy fluxes in heart, brain, and oxidative skeletal muscles. It carries about 80 % of the energy flux between mitochondria and cytoplasm in heart. The substrate uptake, respiration rate, and energy fluxes are regulated in response to workload via phosphoryl transfer pathways and Ca2+ cycling. We propose integrated network mechanisms to explain the linear relationship between myocardial oxygen consumption and heart work output under conditions of metabolic stability (metabolic aspect of Frank–Starling's law of the heart). The efficiency of energy transfer, force of contraction, and

metabolic regulation of respiration and energy fluxes depend upon the intracellular concentration of total creatine, which is decreased in heart failure. The role of creatine, creatine kinase, and adenylate kinase phosphoryl transfer and AMP-activated protein kinase (AMPK) signaling systems and their interrelationship with substrate supply and Ca2+ cycles are analyzed. Finally, an introduction to the AMPK signaling network is provided with a particular emphasis on the heart in health and disease.

Type: Research article

Title: Metabolic control analysis of respiration in human cancer tissue

Authors: Kaambre T, Chekulayev V, Shevchuk I, Tepp K, Timohhina N, Varikmaa M, Bagur R, Klepinin A, Anmann T, Koit A, Kaldma A, Guzun R, Valvere V, Saks V.

State: Article published on Junuary 2013 in *Frontiers in Physiology;* 28;4:151 (doi: 10.3389/fphys.2013.00151.)

Abstract: Bioenergetic profiling of cancer cells is of great potential because it can bring forward new and effective therapeutic strategies along with early diagnosis. Metabolic Control Analysis (MCA) is a methodology that enables quantification of the flux control exerted by different enzymatic steps in a metabolic network thus assessing their contribution to the system's function. Our main goal is to demonstrate the applicability of MCA for in situ studies of energy metabolism in human breast and colorectal cancer cells as well as in normal tissues. We seek to determine the metabolic conditions leading to energy flux redirection in cancer cells. A main result obtained is that the adenine nucleotide translocator exhibits the highest control of respiration in human breast cancer thus becoming a prospective therapeutic target. Additionally, we present evidence suggesting the existence of mitochondrial respiratory supercomplexes that may represent a way by which cancer cells avoid apoptosis. The data obtained show that MCA applied in situ can be insightful in cancer cell energetic research.

Type: Research article

Title: Mysterious Ca(2+)-independent muscular contraction: déjà vu

Authors: Kuznetsov AV, Guzun R, Boucher F, Bagur R, Kaambre T, Saks V.

State: Article published on August 2012 in *Biochemical Journal;* 1;445(3):333–6 (doi: doi: 10.1042/BJ20120439)

Abstract: The permeabilized cells and muscle fibres technique allows one to study the functional properties of mitochondria without their isolation, thus preserving all of the contacts with cellular structures, mostly the cytoskeleton, to study the whole mitochondrial population in the cell in their natural surroundings and it is increasingly being used in both experimental and clinical studies. The functional parameters (affinity for ADP in regulation of respiration) of mitochondria in permeabilized myocytes or myocardial fibres are very different from those in isolated mitochondria in vitro. In the present study, we have analysed the data showing the dependence of this parameter upon the muscle contractile state. Most remarkable is the effect of recently described Ca(2+)-independent contraction of permeabilized muscle fibres induced by elevated temperatures (30-37°C). We show that very similar strong spontaneous Ca(2+)-independent contraction can be produced by proteolytic treatment of permeabilized muscle fibres that result in a disorganization of mitochondrial arrangement, leading to a significant increase in affinity for ADP. These data show that Ca(2+)-insensitive contraction may be related to the destruction of cytoskeleton structures by intracellular proteases. Therefore the use of their inhibitors is strongly advised at the permeabilization step with careful washing of fibres or cells afterwards. A possible physiologically relevant relationship between Ca(2+)-regulated ATP-dependent contraction and mitochondrial functional parameters is also discussed.